FABRICATION AND CHARACTERIZATION OF HALLOYSITE NANOTUBES (HNTs) FILLED POLYTETRAFLUOROETHYLENE (PTFE) NANOCOMPOSITES FOR SELF-LUBRICATION APPLICATIONS

A Thesis submitted in the partial fulfillment of the requirements for the award of the degree of

DOCTOR OF PHILOSOPHY

by

GAMINI SURESH
(ROLL NO: 701109)

DEPARTMENT OF MECHANICAL ENGINEERING

NATIONAL INSTITUTE OF TECHNOLOGY

WARANGAL (T.S) INDIA 506 004

August 2017

FABRICATION AND CHARACTERIZATION OF HALLOYSITE NANOTUBES (HNTs) FILLED POLYTETRAFLUOROETHYLENE (PTFE) NANOCOMPOSITES FOR SELF-LUBRICATION APPLICATIONS

A Thesis submitted in the partial fulfillment of the requirements for the award of the degree of

DOCTOR OF PHILOSOPHY

by

GAMINI SURESH
(ROLL NO: 701109)

Under the supervision of

Dr. V. VASU

&

Dr. M. VENKATESWARA RAO

DEPARTMENT OF MECHANICAL ENGINEERING

NATIONAL INSTITUTE OF TECHNOLOGY

WARANGAL (T.S) INDIA 506 004

August 2017

Dedicated

to

- **My beloved Parents & Family**
- **All my Teachers and Professors who taught and encouraged me with positive thoughts**

NATIONAL INSTITUTE OF TECHNOLOGY
WARANGAL (T.S) INDIA 506 004

DECLARATION

This is to certify that the work presented in the thesis entitled **"Fabrication and Characterization of Halloysite Nanotubes (HNTs) Filled Polytetrafluoroethylene (PTFE) Nanocomposites for Self-Lubrication Applications"**, is a bonafide work done by me under the supervision of Dr. V. Vasu and Dr. M. Venkateswara Rao was not submitted elsewhere for the award of any degree.

I declare that this written submission represents my idea in my own words and where other's ideas or words have not been included. I have adequately cited and referenced the original sources. I also declare that I have adhered to all principles of academic honesty and integrity and have not misinterpreted or fabricated or falsified any idea/data/fact/source in my submission. I understand that any violation of the above will be a cause for disciplinary action by the Institute and can also evoke penal action from the sources which have thus not been properly cited or from whom proper permission has not taken when needed.

Date: **(Gamini Suresh)**

Place: Warangal Research Scholar,

Roll No.701109

NATIONAL INSTITUTE OF TECHNOLOGY
WARANGAL (T.S) INDIA 506 004

CERTIFICATE

This is to certify that the thesis entitled **"Fabrication and Characterization of Halloysite Nanotubes (HNTs) Filled Polytetrafluoroethylene (PTFE) Nanocomposites for Self-Lubrication Applications"**, that is being submitted by **Mr. Gamini Suresh (701109)** in partial fulfillment for the award of Doctor of Philosophy (**Ph.D)** in the Department of Mechanical Engineering, National Institute of Technology, Warangal, is a record of bonafide work carried out by him under our guidance and supervision. The results of embodied in this thesis have not been submitted to any other Universities or Institutes for the award of any degree or diploma.

Dr. V Vasu

Assistant Professor
Department of Mechanical Engineering
NIT- Warangal.

Dr. M. Venkateswara Rao
Professor
Department of Mechanical Engineering
Bapatla Engineering College - Bapatla

ACKNOWLEDGEMENTS

I take the opportunity to express my heartfelt adulation and gratitude to my supervisor, **Dr. V VASU**, Assistant Professor, Mechanical Engineering Department, National Institute of Technology Warangal for his unreserved guidance, constructive suggestions, thought provoking discussions and unabashed inspiration in nurturing this research work. It has been a benediction for me to spend many opportune moments under the guidance of the perfectionist at the acme of professionalism. The present work is a testimony to his alacrity, inspiration and ardent personal interest, taken by him during the course of this thesis work in its present form.

I would like to express my heartfelt gratitude to my supervisor, **Dr. M. VENKATESWARA RAO**, Professor, Mechanical Engineering Department, Bapatla Engineering College, Bapatla, for his unreserved guidance, constructive suggestions, thought provoking discussions and unabashed inspiration in nurturing this research work

I deeply express my heartfelt adulation and gratitude to **Dr. SURYASARATHI BOSE**, Associate Professor, Department of Materials Engineering, Indian Institute of Science., Bangalore, for timely acceptance and sanction of the project **"Investigation of surface morphology, mechanical, and thermal properties of Halloysite nanotubes filled PTFE matrix nanocomposites"** during 4th February, 2013, under UGC- Networking Resource Centre for Materials in Department of Materials Engineering., IISc., Bangalore.

I wish to sincerely thank university authorities, **Prof. G. R. C. REDDY, DIRECTOR**, National Institute of Technology, Warangal and other top officials who gave me an opportunity to carry out research work.

I also sincerely thank **Prof. P BANGARU BABU, Head**, Mechanical Engineering Department, National Institute of Technology, Warangal for his continuous support towards carrying out research work.

I also sincerely thank to **Prof. L. KRISHNANAND, Prof. C. S. P. RAO, Prof. S. SRINIVASA RAO,** former HODs, Mechanical Engineering Department, National Institute of Technology, Warangal, for their timely suggestions, support and for providing necessary department facilities and services during successful completion of research work

I wish to express my sincere and whole hearted thanks and gratitude to **Prof. C. S. P. RAO** and **Dr. T.D. GUNNESWARA RAO** (DSC members) for their kind help, encouragement and valuable suggestions for successful completion of research work.

I would like to thank **M/s Jayhind Polymers**, Sangli, Maharashtra, for taking up fabrication section.

I sincerely express my deepest gratitude to my friends **Ramesh Babu, Ranga Babu, Shiva, Sai Sudheer** and **other co-scholars** for doing timely co-operation and help in many respects during my stay at NIT Warangal.

Words are inadequate to express my thanks to all my family members, my father Sri **G. V. Ramanjaneyulu**, mother Smt. **G. Subba Lakshmi**, and brother **G. Prakash** deserve specially mention of appreciation for exhibiting patience during this long and arduous journey.

No amount of thanks is enough, finally, for my beloved wife **Segu Sriprada** who held the key to my success. Her patience and encouragement kept my motivation up. Despite all odds, she single handily and intelligently managed all family matters as well as my two kids (**G.V.S. Raghu Ram** and **G.M.S. Krishna**) along with her job.

I want to express my sincere thanks to all those who directly or indirectly helped me at various stages of this work.

Above all, I express my indebtedness to the **"LORD VENKATESWARA"** for all his blessing and kindness.

(Gamini Suresh)

ABSTRACT

PTFE is one of the best material used for fabricating bearings, seals etc., in food, textile, and automobile sectors, as it offers low coefficient of friction and high operating temperatures. But, sacrifices easily due to low tensile strength and high wear rate. A thorough literature survey was carried out in the selection of inorganic nanofiller and Halloysite nanotubes (HNTs) was chosen as the reinforcement material to disperse in Polytetrafluorethylene (PTFE) matrix, in order to enhance the mechanical and thermal tribological properties.

PTFE/HNT nanocomposites at 0 wt. % to 10 wt. % with 2 wt. % increment of HNTs were fabricated. Morphology characterization tests such as XRD and SEM images of PTFE/HNT nanocomposites samples were studied for degree of dispersion in the matrix material. Mechanical properties such as tensile strength, Young's modulus, impact strength, flexural strength and flexural modulus, and micro-hardness were examined using tensile, impact, flexural and Vickers micro-hardness tests respectively. Thermal properties for heat of fusion, melting crystallization temperature, cooling crystallization temperature, degree of crystallinity were characterized using the DSC test and properties like storage modulus, loss modulus, tan delta, glass transition temperature were studied using the DMA test. Subsequently, wear characterization through optimization process was done. For conducting wear tests after screening the material for operating parameters wt% HNT, load, speed and distance and their corresponding levels were selected to achieve the target i.e., for minimum coefficient of friction, minimum wear rate and maximum specific energy. All experiments were carried out as per the ASTM standards.

XRD results were plotted and found maximum value of degree of crystallinity as 76.34 % at 4 wt. % HNT addition and SEM results shown satisfactory dispersion of HNTs in the PTFE matrix at low wt. % HNT loading. DSC results has shown that HNT acts as a hetero nucleating agent. The HNT content in nanocomposites has helped in increasing the degree of crystallinity. The degree of crystallinity of PTFE increased from 57.83% for neat PTFE to 73.5% at 4 wt. % HNT addition. DMA results shown increase in storage modulus, loss modulus and tan delta values. Improved mechanical properties of PTFE/HNT nanocomposites showed an increase in yield tensile strength by 135% and tensile modulus by 250% at 6 wt. % HNT addition in comparison with neat PTFE. Also, an increase in the impact strength by 130% at 4 wt % loading is observed. The maximum Vickers micro-hardness value is observed for sample 'F' (10 wt. %), which is increased by 163% compared to neat PTFE. From the mechanical

analysis at higher HNT loading (i.e. >8 wt%), poor dispersion HNT was realized. Moreover, change in PTFE structure was also observed. The enhancement in mechanical properties can be attributed to increase in the degree of crystallinity.

From the wear study rubbing on steel counter face, a hybrid method was adopted and the optimum input parameters were estimated as per the designer based requirement. The wt. % HNT was about 4% from hybrid method and from RSM based on same weightage to all factors, the wt. % HNT was about 6.67%. Hence, the hybrid method suggested an optimum wt. % HNT addition to be 4 % and minimum COF, minimum SWR, and maximum EW might be obtained. From the wear study rubbing on counter face fitted with different surface roughness SiC abrasive papers, the optimum input parameters and responses of PTFE/HNT nanocomposites were predicted to be 4 wt. % of HNT addition, 20 N of load, 3.0 km of distance, 3 m/sec of sliding velocity when running against a counter surface roughness of 9.5 microns were 0.1001 and 700×10^{-6} mm^3/N-m for COF and SWR respectively. A composite desirability of the model close to 1 was obtained, which indicated the responses were reasonably optimized. From the erosion wear study, conforming to the minimization of erosive wear at desirability equal to 1, wt. % HNT addition of 5.14 %, pressure of 0.83 bar, and an impingement angle of 88.42^0 were found. The erosion wear rate corresponding to the optimum input parameters was predicted as $0.349455x10^{-5}$ g/g.

SEM analysis was also done on the fracture surfaces, wear test pin surfaces, and deposited films on the SiC abrasive papers. From the SEM micrographs of impact fracture surfaces, pull out regions were observed suggesting resistance offered by the HNT in the matrix attributed to good interfacial strength and dispersion of HNTs in the PTFE matrix material at smaller fractions of HNT (4 wt. % to 6 wt. %). SEM analysis of pin surfaces and transfer film on the abrasive paper revealed the reduction in the coefficient of friction of PTFE/HNT nanocomposites due to the deposition of transfer film. It was also observed that the strength of transfer film is found to be optimum at a surface roughness of 9.5 microns under the optimum operating conditions of input parameters.

From the present research work, it can be concluded that, a novel ‘green’ and cost effective PTFE/HNT nanocomposites were fabricated and tested. From the characterization study, it was concluded that about 4 wt. % HNT to 6 wt. % HNT addition, the material shows multi-functional properties such as improved mechanical , thermal and tribological properties due to better dispersion in the PTFE matrix material. These characteristics help in increasing

the fatigue life of PTFE/HNT nanocomposite components. Hence, the components can be fabricated with PTFE filled with Halloysite nanotubes for self-lubrication applications.

CONTENTS

ACKNOWLEDGEMENTS	**i**
ABSTRACT	**iii**
CONTENTS	**vi**
LIST OF FIGURES	**x**
LIST OF TABLES	**xvi**
NOMENCLATURE	**xvii**
Chapter 1 INTRODUCTION	**1-17**
1.1 Brief view of polymer nanocomposites (PNMCs)	2
1.2 Characterization	5
1.3 Tribology	7
1.4 Materials tribology in mechanical/machine design	8
1.4.1 Tribology of polymers and polymer nanocomposites	9
1.4.2 Different types of wear and wear mechanisms in polymers	10
1.4.3 Abrasive wear of polymers	11
1.4.4 Tribology of thermoplastic nanocomposites filled with inorganic fillers	11
1.5 Tribometer and modes of testing	12
1.6 Solid Lubricant materials and the use of Polytetrafluoroethylene (PTFE)	13
1.6.1 Methods to improve tribological behaviour of PTFE	16
1.7 Erosion wear	17
1.7.1 Erosion wear procedure	17
Chapter 2 LITERATURE SURVEY	**18-37**
2.1 Tribology: Friction, Wear, and Lubrication	18
2. 2.2 Polytetrafluoroethylene (PTFE)	19
3. 2.3 PTFE composites	22
4. 2.4 PTFE nanocomposites	23
2.5 Filler material: Halloysite nanotubes (HNTs)	25
2.6 Transfer film mechanism	27

2.7 Erosion wear 29
2.8 Design of experiments 31
2.9 Research gaps 33
2.10 Problem Definition 33
2.11 Research Objectives 34
2.12 Work Plan 35
Chapter 3 MATERIALS AND METHODS 38-60
3.1. Matrix material: Polytetrafluoroethylene (PTFE) 38
3.2 Reinforcement material: Halloysite nanotubes (HNTs) 38
3.3 Fabrication of PTFE/HNT nanocomposites 40
3.3.1 Ensemble weight calculation 40
3.3.2 Description of the apparatus 40
3.3.3 Fabrication procedure 41
3.4 Density Measurement by using Specific Gravity meter 44
3.5 Morphological study 44
3.5.1 X-ray diffraction (XRD) study 44
3.5.2 Energy Dispersive X-Ray Spectroscopy (EDX) 45
3.6 Thermal properties study 45
3.6.1 Differential Scanning Calorimetry (DSC) 45
3.6.2 Dynamic Mechanical Analysis (DMA) 46
3.7 Mechanical Property Characterization 49
3.7.1 Tensile test (ASTM D638) 49
3.7.2 Impact test (ASTM D256) 52
3.7.3 Flexural test (ASTM D 790) 54
3.7.4 Vickers's Micro-hardness test (ASTM E384) 58
3.8 Wear characterization 60
Chapter 4 RESULTS AND DISCUSSION 61-84
4.1 Morphology characterization 61
4.1.1 X-Ray Diffraction 61
4.1.2 SEM microstructure of PTFE/HNT Nanocomposites 63
4.2 Thermal properties Characterization 65

4.2.1 Differential Scanning Calorimetry (DSC) 65

4.2.2 Dynamic Mechanical Analysis 67

4.3 Mechanical property characterization 71

4.3.1 Study of tensile properties 72

4.3.2 Impact properties 75

4.3.3 Flexural properties 76

4.3.4 Vickers's micro-hardness 78

4.4 SEM microstructures of fracture surfaces 79

Chapter 5 ABRASIVE AND EROSION WEAR STUDY 85-131

PHASE –I

5.1 Abrasive Wear Characterization using Design of experiments (DOE) concept 85

5.1.1 Specific Wear Rate (SWR) 86

5.1.2 Specific Wear Energy (EW) 87

5.1.3 Coefficient of friction 88

5.2 Response Surface Methodology (RSM) 95

5.2.1 Regression Equation in Uncoded Units 96

5.2.2 Surface plots 97

5.2.3 Optimization study 98

5.3 Multi-optimization of wear input parameters by Response Surface Methodology 99

5.3.1 Analysis of Variance (ANOVA) 100

5.3.2 Regression analysis 101

5.3.3 Surface plots 102

5.3.4 Multi objective optimization of Tribological Parameters: composite desirability 104

PHASE – II

5.4 Effect of surface roughness on wear properties of PTFE/HNT nanocomposites 106

5.4.1 Specific wear rate 107

5.4.2 Response surface methodology 108

5.4.3 Contour plots of the responses COF & SWR 110

5.4.4 Regression analysis 114

5.4.5 Composite desirability of the multi-responses: COF & SWR 114
5.4.6 SEM analysis 115
PHASE – III
5.5 Erosion wear optimization of input parameters 120
5.5.1 Experiment Procedure 120
5.6 Results and Discussion 120
5.6.1 Response surface methodology (RSM) 123
5.6.2 Surface plots 124
5.7 Effect of individual input parameters (pressure and impingement angle) on erosion wear rate 127
Chapter 6 CONCLUSIONS & SCOPE OF FUTURE WORK 132-136
Conclusions 132
Scope of future work 136
Visual outcomes of the present research work 137
References 138

List of Figures

Figure No.	Title	Page No
Figure 1.1	Progress of industrial revolutions in the development of innovative products	1
Figure 1.2	(a) Classification of nanocomposites (b) Common particle reinforcement and their respective surface to volume ratios	3
Figure 1.3	Synthesis methods to disperse layered silicate into nanocomposites	5
Figure 1.4	Types of nanocomposite structures	6
Figure 1.5	Practical objectives of tribology	7
Figure 1.6	Different failures in the loss functionality of a system	9
Figure 1.7	Wear classification of polymers	11
Figure 1.8	Cohesive wear process	12
Figure 1.9	Types of friction wear assessment – modes of test rigs	13
Figure 1.10	Potential fields of applications of polymers including PTFE as self-lubricating material	15
Figure 1.11	Factors influencing the wear behaviour of polymers	16
Figure 2.1	(a) molecular structure of PTFE (b) arrangement of spherulites in PTFE	20
Figure 2.2	Microstructure of PTFE: (a) semi-crystalline band; (b) crystalline slices, separated due to shear in the disordered region; (c) hexagonal array of chains arrangement of PTFE molecules in the slice	21
Figure 2.3	Typical wear loss of virgin PTFE material with hard counterface	21
Figure 2.4	Semi-log plot of Wear rate versus friction coefficient for various solid lubricating unfilled polymers, polymer blends and polymeric composites. The lower left hand corner, a target region of ultra-low wear rate and friction coefficient is also portrayed.	25
Figure 2.5	Transmission Electron Microscope (TEM) Images of HNT particles (a) average inner and outer dimension (b) Particles have different lengths	26
Figure 2.6	Wear process in soft polymers (ploughing effect) and hard polymers (debris flakes)	28

Figure 2.7	Polymer erosion wear mechanism modes	29
Figure 2.8	Flow chart of work plan	35
Figure 3.1	Halloysite nanotubes: a) particles have different lengths; b) cluster of particles; c) a typical HNT particle	39
Figure 3.2	Pulverizer used for breaking agglomerates and mixing of the powders	41
Figure 3.3	(a)-(e) sample preparation steps (mixing, cold pressing, preforming, sintering)	42
Figure 3.4	sintering cycle: heating - holding - cooling	42
Figure 3.5	Sample preparation steps and micro-structural changes in three stages (performing, sintering (heating), and cooling)	43
Figure 3.6	PANalytical X'Pert PRO diffractometer	45
Figure 3.7	METTLER-TOLEDO (DSC 822e) setup	46
Figure 3.8	Single cantilever dynamic mode of load on the PTFE/HNT samples in DMA test	47
Figure 3.9	Perkin Elmer make Dynamic Mechanical Analysis setup	48
Figure 3.10	Test specimen	49
Figure 3.11	Moduli triangle	49
Figure 3.12	INSTRON 5967 tensile testing machine: test specimen fitted with extensometer	50
Figure 3.13	Tensile test specimen: dimensions as per ASTM standards	52
Figure 3.14	Tensile test samples of PTFE/HNT nanocomposite with varying wt. % HNT addition	52
Figure 3.15	(a) Impact Testing Machine (b) Notch cutter	53
Figure 3.16	Impact test specimen dimension used for PTFE/HNT nanocomposite samples	54
Figure 3.17	(a) Tensometer (b) three point bending test fixture	55
Figure 3.18	Three point bending test specimen along with standard dimensions	56
Figure 3.19	Vickers's Micro-hardness tester (SHIMADZU make)	58

Figure 3.20	Indentation shape on the surface after release of load	59
Figure 4.1	Calculation of degree of crystallinity of PTFE/HNT nanocomposites by integrating the area under the peaks and halos (expressed in terms of intensity units)	62
Figure 4.2	XRD spectra of PTFE/HNT nanocomposite samples: a) crystalline peaks; b) Increase in peak intensity due to wt. % HNT addition in the PTFE matrix, at $2\theta = 12.2^0$	63
Figure 4.3	SEM images of PTFE/HNT nanocomposites with 4 wt. % HNT: (a) Intercalation distribution of HNTs in the matrix; (b) Shows structure of nanocomposite	64
Figure 4.4	EDX spectrum of PTFE/HNT nanocomposite specimen with 4 wt. % of HNT	64
Figure 4.5	DSC scans of PTFE/HNT nanocomposite samples: (a) DSC heating curve and (b) cooling curve	66
Figure 4.6	DMA plots of PTFE/HNT nanocomposites: a) storage modulus and temperature; b) loss modulus and temperature; c) tan δ and temperature	69
Figure 4.7	Plots of storage modulus, loss modulus, and loss tangent for (a) neat PTFE; (b) 2 wt. % HNTs; (c) 4 wt. % HNTs; (d) 6 wt. % HNTs; (e) 8 wt. % HNTs	71
Figure 4.8	Draw stress Behaviour of PTFE/HNT Nanocomposite at 2 wt. % HNTs addition	73
Figure 4.9	Engineering stress-Engineering strain diagrams of PTFE/HNT nanocomposites	74
Figure 4.10	Effect of wt. % HNT addition on tensile strength and Young's modulus	75
Figure 4.11	Effect of wt. % HNT addition on impact energy of PTFE/HNT nanocomposites	76
Figure 4.12	Flexural stress vs flexural strain diagram	78
Figure 4.13	Effect of wt. % HNTs addition in the PTFE matrix on flexural strength and flexural modulus.	78
Figure 4.14	Effect of wt. % HNT addition on micro-hardness values of PTFE/HNT nanocomposites	79
Figure 4.15	(a) & (b) SEM image of fractured tensile specimen: at 10% HNT filled tensile specimen	80

Figure 4.16	SEM images of impact test fracture surfaces of PTFE/HNT nanocomposites: a) 2 wt.% HNT; b) 4 wt.% HNT; c) 6 wt. % HNT d)8 wt. % HNT e)10 wt. % HNT	83
Figure 5.1	(a) Pin on Disc test set up; (b) close up view of counter face disc and PTFE/HNT composite test pin	86
Figure 5.2	PTFE/HNT nanocomposite test specimens	86
Figure 5.3	Flow chart for calculation of weights	89
Figure 5.4	Preference graphs showing the suggestions of (a) Designer 1; (b) Designer 2; (c) Designer 3	90
Figure 5.5	Main effects plot for SN ratios of (a) COF (C2L1D1S1); (b) SWR (C1L1D2S2); (c) EW (C1L1D3S2)	93
Figure 5.6	Effect of interaction of factors on the value of utility index; (a) Distance and velocity; (b) Distance and load	97
Figure 5.7	Effect of interaction of factors on the value of utility index; (a) wt. % HNT and load; (b) wt. % HNT and distance	98
Figure 5.8	Optimum values of input parameters of PTFE/HNT nanocomposites at desirability, D=1	99
Figure 5.9	(a)-(e) Response surface contour plots: (a) interaction of wt. % HNT and distance on COF; (b)) interaction of wt. % HNT and speed on SWR; (c)) interaction of wt. % HNT and load on SWR; (d)) interaction of wt. % HNT and speed on EW; (e)) interaction of wt. % HNT and load on EW	104
Figure 5.10	Optimization of parameters for minimum COF and SWR & for maximum EW	105
Figure 5.11	Line sketch of POD apparatus (a) Isometric view (b) Rear view	106
Figure 5.12	Main effects plot for (a) COF; (b) SWR	109
Figure 5.13	Contour plots showing effect of the interaction of the input factors on COF: (a) wt. % HNT vs Load; (b) wt. % HNT vs Velocity; (c) wt. % HNT vs Distance; (d) wt. % HNT vs Surface roughness	111
Figure 5.14	Contour plots showing effect of the interaction of the input factors on SWR: (a) wt. % HNT vs Load; (b) wt. % HNT vs Velocity; (c) wt. % HNT vs Distance; (d) wt. % HNT vs Surface roughness	112
Figure 5.15	Composite desirability plot for multi-objective optimization of COF and SWR	114
Figure 5.16	Scanning Electron Microscope images of test pin surfaces using operating conditions: abraded against 25.8 μm SiC paper, to an	118

	abrading distance of 2 km against a normal load of 20 N at 3 m/s sliding velocity: a) Pure PTFE; b) 4 wt. % HNT addition; c) 6 wt. % HNT addition; d) 8 wt. % addition	
Figure 5.17	Scanning Electron Microscope images of transfer film deposited on the counter face, at operating conditions: abraded against 25.8 μm SiC paper, to an abrading distance of 2 km against a normal load of 20 N and at 3 m/s sliding velocity: (a) for 4 wt. % HNT addition in the PTFE matrix; (b) for 6 wt. % HNT addition in the PTFE matrix	119
Figure 5.18	Air jet erosion test set up (MAGNUM make): 1. Hopper section; 2. Conveyor belt section; 3. Mixing chamber section; 4. Specimen holder section; 5. Collecting chamber; 6. Reciprocation air compressor	121
Figure 5.19	Plot of externally studentized residuals and normal probability	124
Figure 5.20	Surface plots depicts the interaction of the input factors on erosion wear rate: (a) wt.% HNT Vs Impingement angle; (b) Pressure Vs Impingement angle	125
Figure 5.21	Response optimizer plot of the PTFE/HNT nanocomposites, depicts the optimum input factors at Desirability = 1	125
Figure 5.22	Specimen holder orientations: (a) $\theta = 90^0$ (b) $\theta = 60^0$ (c) $\theta = 45^0$ (d) $\theta = 30^0$	126
Figure 5.23	Crater shape of wear at different angle of impingements: (a) $\theta = 90^0$ (b) $\theta = 60^0$ (c) $\theta = 45^0$ (d) $\theta = 30^0$, for nano-filler addition of 8% by weight of HNT addition and at 1.5 bar pressure.	126
Figure 5.24	Crater shape on the nanocomposites after test for angle of impingement, **$\theta = 90^0$:** (a) at pressure, p =0.5 bar; (b) at pressure, p = 1 bar; (c) at pressure, p =1.5 bar	127
Figure 5.25	Effect of increase in pressure on erosion wear rate for different wt.% addition in the PTFE matrix, at an impingement angle, 30^0	128
Figure 5.26	Effect of increase in pressure on erosion wear rate for different wt.% addition in the PTFE matrix, at an impingement angle, 60^0	128
Figure 5.27	Effect of increase in pressure on erosion wear rate for different wt.% addition in the PTFE matrix, at an impingement angle, 45^0	129
Figure 5.28	Effect of increase in pressure on erosion wear rate for different wt.% addition in the PTFE matrix, at an impingement angle, 90^0	129

Figure 5.29	Effect of increase in pressure on erosion wear rate of PTFE/HNT nanocomposites for different impingement angles and at a pressure of 0.5 bar	130
Figure 5.30	Effect of increase in pressure on erosion wear rate of PTFE/HNT nanocomposites for different impingement angles and at a pressure of 1 bar	130
Figure 5.31	Effect of increase in pressure on erosion wear rate of PTFE/HNT nanocomposites for different impingement angles and at a pressure of 1.5 bar	131
Figure 6.1	Validation of wear results of PTFE/HNT nanocomposites	135

List of Tables

Table No	Title	Page No
Table 1.1	Different types of polymer and its wear behaviour	10
Table. 1.2	Typical test geometries for friction and wear testing	13
Table 2.1	Erosion wear study by some researchers on polymer composites	31
Table.3.1	Proportions of PTFE and HNTs for making sheets	40
Table. 4.1	XRD results of PTFE/HNT nanocomposites	61
Table 4.2	DSC results of PTFE/HNT nanocomposites	65
Table. 4.3	Effect of wt. % HNT addition on Tensile strength and Young's modulus	73
Table. 4.4	Effect of wt. % HNT reinforcement on impact strength of PTFE nanocomposites	76
Table. 4.5	Effect of wt. % HNT reinforcement on Flexural and micro-hardness properties of the nanocomposites	77
Table.4.6	Effect of wt. % HNT addition on micro-hardness values of PTFE/HNT nanocomposites	79
Table. 5.1	Design variables (factors) and levels	85
Table. 5.2	Experimental runs and responses	88
Table. 5.3	Calculation of factors A_i	94
Table. 5.4	Input factors and utility index values (U) for each run	95
Table. 5.5	Analysis of Variance (ANOVA) of utility values	96
Table. 5.6	ANOVA of the input factors and their interactions for quadratic model of the responses COF, SWR, and EW	100
Table. 5.6 (a)	Comparison of optimum input parameters for Hybrid method and RSM	105
Table 5.7	Factors and Levels	107
Table 5.8	Taguchi L27 orthogonal array of experimental runs	107
Table.5.9	ANOVA and model summary for COF and SWR	109
Table.5.10	R-squared values of the model Summary for COF and SWR	109
Table 5.11	Control factors and levels	120
Table 5.12	Erosion wear rate for the experimental runs	122
Table 5.13	ANOVA for Response Surface Quadratic model response erosion wear rate	123

Nomenclature

PTFE	Polytetrafluoroethylene
HNT	Halloysite nanotubes
XRD	X-ray Diffraction
DSC	Differential Scanning Calorimetry
DMA	Dynamic Mechanical Analysis
COF	Coefficient of Friction
SWR	Specific Wear Rate, mm^3/N-m
EW	Specific Wear Energy, MJ/g
n	Order of diffraction = 1,
λ	Wave length of the characteristic X-ray = 1.24 Å
d_{hkl}	Interplanar spacing of crystal planes = d-spacing
θ	X-ray incidence angle (Bragg angle)
X_c	Degree or % crystallinity, a.u.
ΔH_f	Heat of melt endotherm
ΔH_{100f}	Theoretical heat of fusion
T_c	Cooling crystallization temperature, ^{0}C
T_m	Heating crystallization temperature, ^{0}C
w_t	wt. % of HNT in the matrix
E’	Storage modulus, MPa
E”	Loss, modulus, MPa
E*	Complex dynamic modulus, MPa
$Tan\ \delta$	Loss tangent, δ= phase angle of response
σ_y	Yield tensile stress, MPa
Δl	Change in length
ε	Normal strain
E	Young’s modulus, GPa
R	rate of crosshead motion, mm/min
Z	rate of straining of the outer fiber, mm/mm/min
P	load at a given point on the load-deflection curve, N
L	support span, mm,
b	width of specimen tested, mm
d	depth of specimen tested, mm

P_y	load at a given point on the load-deflection curve, N
σ_f	Stress in the outer fibres at mid-point, MPa
σ_{fs}	Flexure stress, MPa
ε_f	strain in the outer surface, mm/mm
E_B	Modulus of elasticity in bending, MPa
m	slope of the tangent of the load-deflection curve, N/mm
HV	Force applied/ surface area of the permanent impression
P	Applied load, gf
D_m	*M*ean diagonal length of the indentation, micrometres
V	Mean velocity, m/s
W	Applied load, N
μ	Friction coefficient due to constant loading
Δm	Mass loss, g
ρ	Density of PTFE/HNT nanocomposite, gm/cc
D	Sliding distance, m
PG_n	Adjacency matrix
n	Number of individuals
D^n	Dominance matrix
RDP	Relative degree of performance
RIR	Relative importance rating
Wm	Weights of performance
m	No. of users
W_{COF}	Weight coefficient of friction
W_{SWR}	Weight of specific wear rate
W_{EW}	Weight of specific wear energy
S/N	Signal to Noise ratio
P_{COF}	Preference scale for coefficient of friction
P_{SWR}	Preference scale for specific wear rate
P_{EW}	Preference scale for specific wear energy
X_i	Value of attribute response
X_i'	Minimum acceptable value of response
U	Non dimensional utility index value
RSM	Response Surface Methodology

CHAPTER - 1

INTRODUCTION

The technological progress in any field is directly related to the development of different innovative materials. Figure 1.1 shows the chronological advancements in the industrial revolution. The progress in material technologies always opens a new arena for industrial revolutions and is the clear evidence for making complex range products into simple and viable to the common man as shown in Fig 1.1. Many countries give the primary emphasis on the research and development of innovative materials by encouraging new research projects, including the Ministry of Human Resources Development (MHRD) of India.

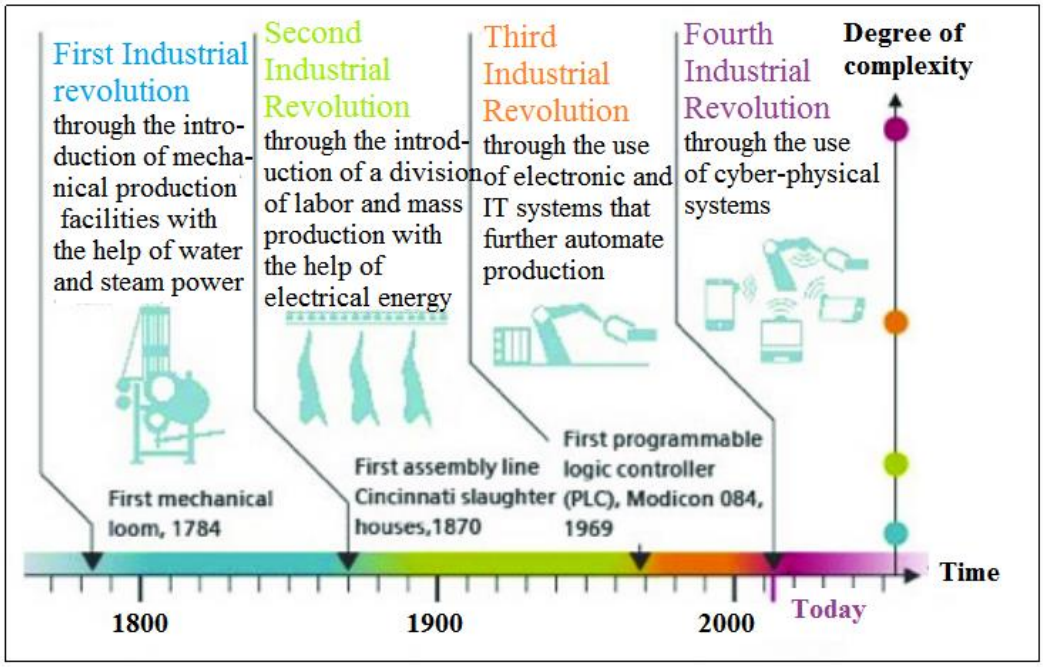

Figure 1.1 Progress of industrial revolutions in the development of innovative products

In the present scenario of industrial products, all high-density material (metals) products gradually replaced by low-density material products like polymers. But, to increase the applicability of polymers, the weak polymers are reinforced with micron size or nano-sized fillers and hence the evolution of composites and nanocomposites came into the picture. A nanocomposite product is one in which the filler material has at least one characteristic dimension (diameter or thickness) in less than 100 nm in contrast to the micron-sized filler. Also, a nanocomposite component/product implies that the filler is at nanoscale not the dimensions of the product are at Nano size [1]. Nanocomposites have been gaining great interest in academia as well as industrial fields due to its tailored functional properties. Especially, the

use of nanocomposites embraced in mechanical engineering due to several reasons, like low unit cost, ease of fabrication, high strength to weight ratio, inherent tribological characteristics etc. The research carried out in the development of moderate to high performance materials specifically in polymer nanocomposites from academia is being converted into the real-time fabrication of products in bulk quantities for a variety of applications from industries. For instance, the first nanocomposite product (N6/MMT nanocomposites) was an engine cover-belt developed for its automotive industry by Toyota Research Centre [2], claimed that significantly improved mechanical properties and increase moisture resistance. Also, several commercial nanocomposite products made by different companies were also successfully put into use.

Nylon6/66 fuel system components
ABS flame retardant computer and monitor housings
Nylon6 automotive parts like Mitsubishi engine cover
Food packaging
Butyl rubber/Nanoclay coating on Tennis balls
PU bladder for athletic shoes
Tribological applications like
    Gears
    Bearings/bearing cages
    Artificial human joint bearing surfaces
    Automobile brake pads

The research on polymer nanocomposites broadly encompasses many areas like electronics and computing, data storage, communications, aerospace and sporting materials, health and medicine, energy, environmental, air-craft structures, transportation and defence applications [3].

1.1 Brief view of polymer nanocomposites (PNMCs)

In this section, it is discussed briefly about types of nanofiller, the effect of surface treatment of nanofiller, processing and morphological characterization of the polymer nanocomposites. Nanocomposites classified into metal matrix nanocomposites, polymer matrix nanocomposites, or ceramic matrix nanocomposites, as shown in Fig. 1.2 (a). In all the cases the filler may be an organic/inorganic filler that exists with one characteristic dimension on the nanoscale (i.e., ~100

nm). The shape of nanofiller exists in nano particulate (nano Al2o3, ZnO), nano fibres (nano-glass fibre, CNTs, HNTs), and nano-platelets (Montmorillonite clay, kaolin) as shown in Fig. 1.2 (b) [4].

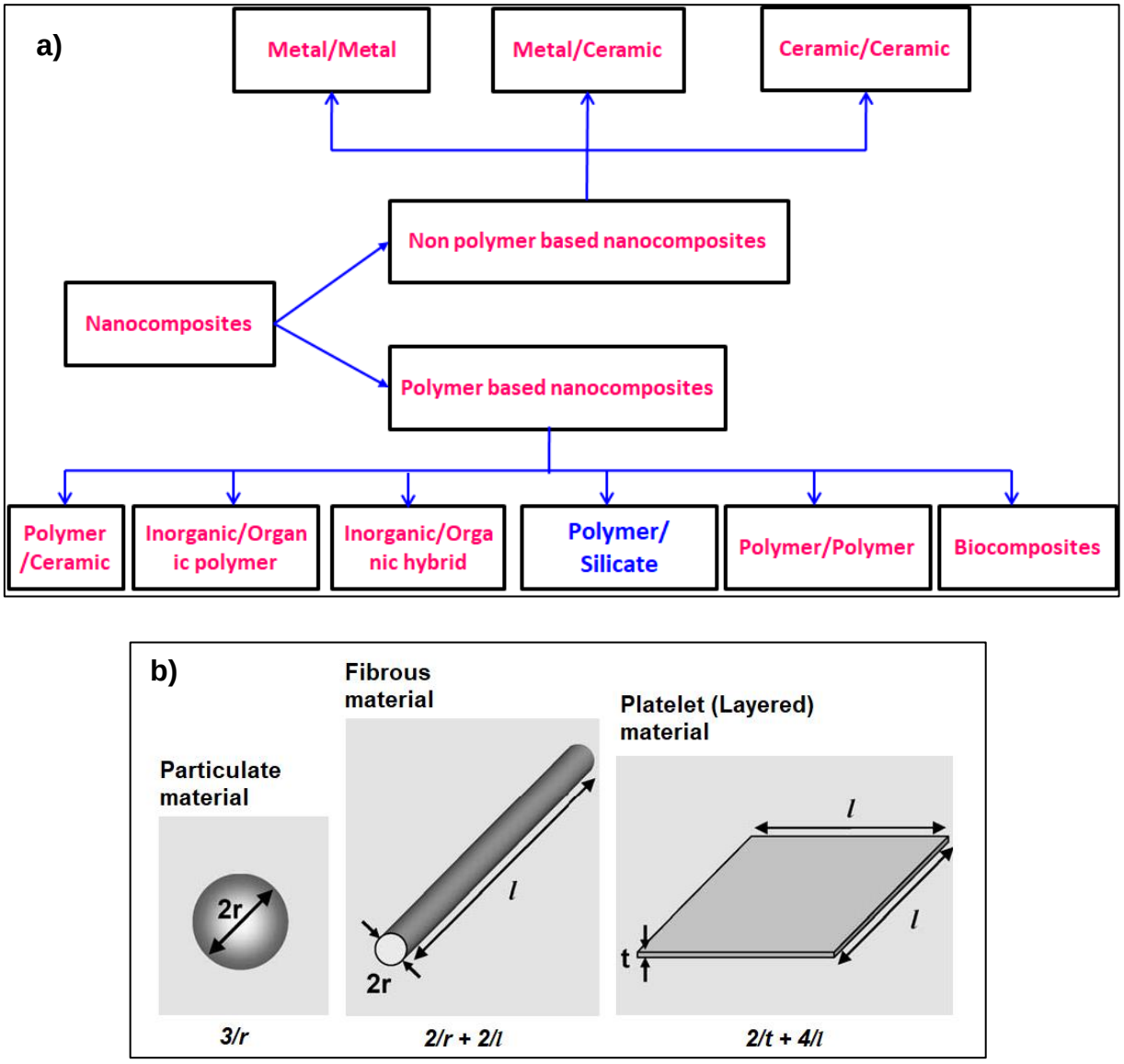

Figure 1.2 (a) Classification of nanocomposites; & (b) Common particle reinforcement and their respective surface to volume ratios [5]

Processing and characterization of nanocomposites

After the selection of a particular matrix and nanofiller combination for a specific application, the next challenge is to select a proper synthesis method to obtain nanocomposites. There are three common methods used to disperse nanofiller in the polymer matrix (thermo-set/ thermoplastic/ elastomer) to produce polymer nanocomposites. They are

Melt compounding/intercalation

In-situ polymerization

Solvent method.

High shear mixing, pressing and sintering

In melt compounding/intercalation of the nanofiller into a polymer melt is done simultaneously when the polymer is being processed through a screw extruder (single/twin) and injection moulder. Injection moulding along with screw extruder has several stages. They are plasticity stage, melting stage, and homogenizing stage. Accordingly, the screw barrel contains different temperature zones along the screw barrel. The nanoparticles will be introduced into the polymer melt during melting stage, as the mixture is passing through the homogenizing stage the dispersion of the nanoparticles will be done and the barrel length provided under this section relatively longer than other two sections. At the end of the screw barrel, the inlet to the injection moulding machine is connected. During injection of the melt the screw acts as a ram and transfer the polymer melt rapidly from the reservoir into the mould cavity and subsequently, the mould is cooled and the product is ejected. The shape of the mould cavity may be made as any desired shape. The rotation of the screw provides the necessary shear force in completing the cycle. The nanofiller (clay) is introduced into the melt polymer using shear forces helps in obtaining exfoliated structure [6]. In In-situ polymerization process, the nanofiller is added directly to the liquid monomer (selected polymer matrix material) during the polymerization step. High shear mixing, pressing and sintering method is used when melt intercalation is not suitable for materials like PTFE, whose viscosity increases abruptly at high temperatures. In this case, both polymer matrix and nanofiller are mixed thoroughly by using a high-speed pulverizer (jet milling) which is meant for breaking agglomerates. Subsequently, pressing and sintering of the compaction is followed for the final production of nanocomposites. In solution method, the nanofillers are added to the selected polymer solution by using solvents like toluene, chloroform and acetonitrile to integrate the polymer and nanofiller molecules[7]. Since the use of solvents is not eco-friendly, the first three methods are widely preferred in the production of polymer nanocomposites [8]. Figure 1.3 depicts the varieties of synthesis method to disperse the filler material in the matrix material.

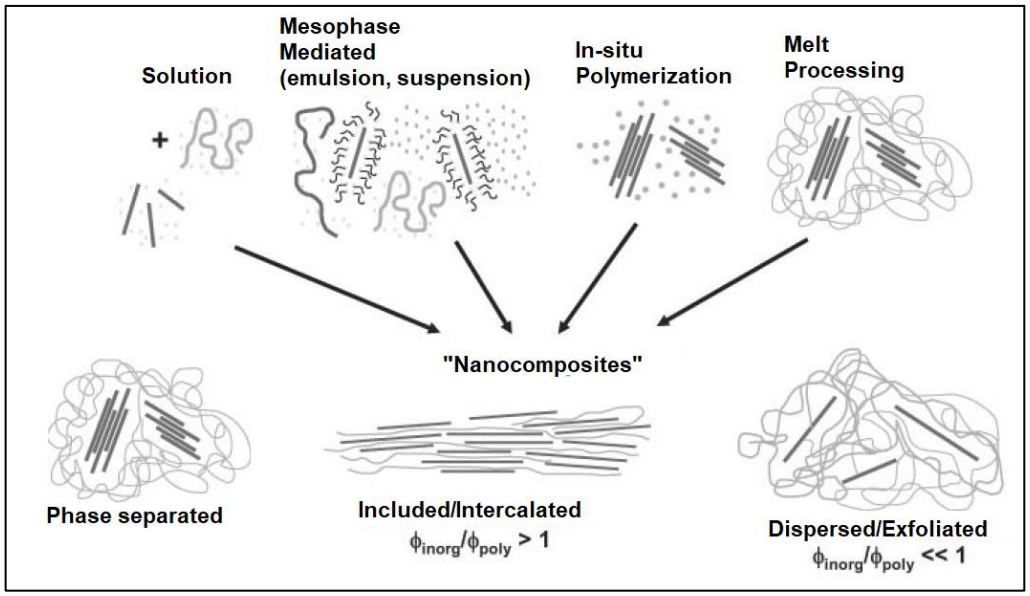

Figure 1.3 Synthesis methods to disperse layered silicate into nanocomposites

1.2 Characterization

The variation in properties is highly influenced by the size scale of its component phases and degree of mixing between the two phases. Hence, depending on the type of filler/matrix combinations, a method of fabrication result possibly three types of structures as shown in Fig. 1.4. They are

- Phase separated (like micro-composites)
- Intercalated
- Exfoliated

For instance, when a polymer matrix is filled with Nano silicate platelets the three structures are explained as follows: When the matrix is unable to penetrate between the nano silicate platelets, a phase separated structure is obtained, and the properties lie in the same range of those for conventional composites. In an intercalated structure, where a single extended polymer chain can penetrate between the nano silicate platelets, a well-ordered multilayer structure with alternate matrix and Nano platelets is obtained. When the nano silicate platelets are completely and uniformly dispersed in the polymer matrix, an exfoliated structure is obtained [9]. In each case, the resulting properties are obviously different and better improved properties enhanced in the exfoliated structure. Hence, one of the main areas in the development of nanocomposites is how to get an exfoliated structure. Achieving the exfoliated structure is very difficult, as nanoparticles form agglomerates during mixing in polymer melts. Therefore,

the degree of dispersion of nanofiller in the matrix plays a crucial role in obtaining improved functional properties. Without proper dispersion, i.e. a poorly dispersed nanofiller even may diminish the values of mechanical properties [10], [11]. Additionally, if the surface of nanofiller is modified, a good dispersion and adhesion at the interface will be achieved.

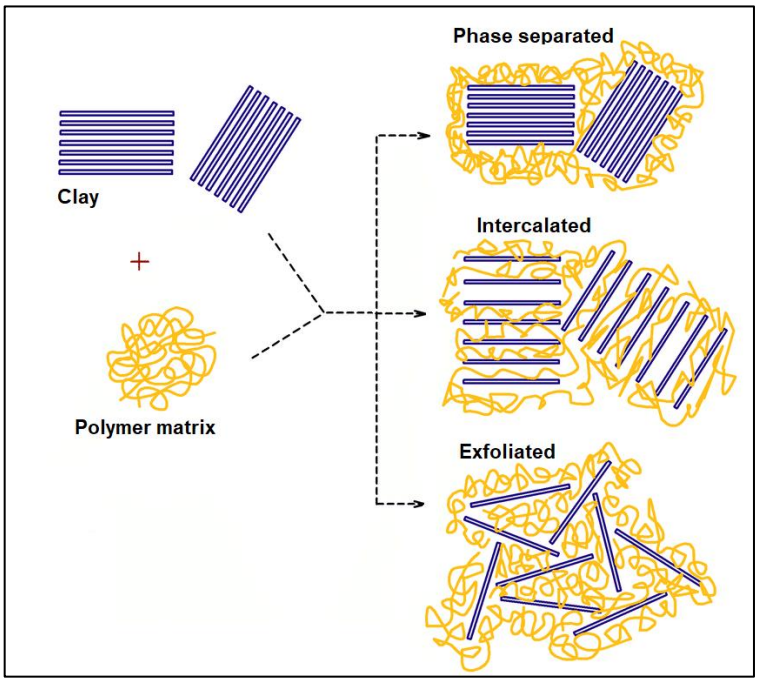

Figure 1.4 Types of nanocomposite structures [9]

The interface properties like, delamination resistance, fatigue, inter-laminar shear strength and corrosion resistance etc. will then be improved. There are usually two types of surface treatment namely surface modification by chemical reaction and surface modification by non-reactive modifier. In the first type of surface modification develops a chemical reaction between the inorganic filler and polymer matrix to improve the adhesion. A hydrophobic surface can be obtained by the use of two reagents such as an alkyl saline coupling agent and another is an alcohol [12]–[14]. In the second type of surface modification which is by the use of non-reactive modifier. A nonreactive modifier generally reduces the interaction between the filler particle interfaces and there by reduces the agglomeration during mixing. A widely used non-reactive type of surface modifier is stearic acid. If added in matrix materials which reduces the melt viscosity and thereby increase in dispersion capability [15]

Numerous characterization techniques are available to understand various physical, chemical, and morphological properties of PMNCs. The commonly used techniques are Wide Angle X-ray Diffraction (WAXD), Scanning Electron Microscope (SEM), and Transmission Electron Microscope (TEM). These techniques provide images of associated surface details of

the combined nanofiller and matrix interfaces at micro to nano level. Also, Scanning Probe Microscope (SPM) and Scanning Tunnelling Microscope (STM) are also widely used to characterize the surface structural information at atomic level [16]. Raman spectroscopy has also evidenced a useful investigation of material with carbon-based properties[17].

1.3 Tribology

Tribology includes the science and technology of interacting surfaces characteristics. They include friction, wear and lubrication. The term 'tribology' was first coined by Prof. H. Peter Jost in 1966, in a report submitted to UK department of education and science. It deals with the technology of lubrication, control of friction and prevention of wear of surfaces having relative motion under load. The work of tribology engineer is mainly interdisciplinary, connecting mechanics, thermodynamics, and materials science, physics, chemistry, and including a huge, multifarious and entangled area of machine design, reliability, and performance where relative motion between surfaces involved [18]. While, the main objective of tribology is to regulate the magnitudes of frictional force i.e., either to reduce the friction for lubrication applications or increase the friction in case of anti-skid applications (Figure 1.5).

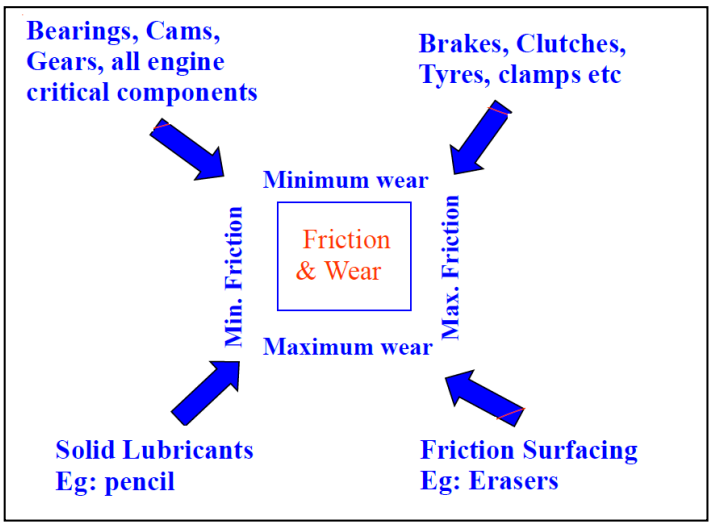

Figure 1.5 Practical objectives of tribology [19]

Tribology of polymer nanocomposites refers to the study of effect of nanofiller addition on friction and wear properties under different operating conditions. Selected Nanofiller are added in order to improve the wear resistance of polymers since they possess long polymer chains with less Vander Walls energy without affecting or even reducing the friction coefficient. The early works led in this area was mainly reflect in improving the tribological parameters with

the addition of novel filler into the polymer matrix. It is a continuous quest of new nanocomposites, they contribute to the less wear rate[20].

The coefficient of friction is defined as the ratio of applied load to the normal reaction from the surface. Since in tribology, the components are in relative motion, here the term coefficient of friction is nothing but kinetic coefficient of friction, simply called as coefficient of friction (COF). Wear is nothing but loss of material due to friction, when a soft material is forced to rub against hard counter surface. The rate at which the material is losing the mass from the base material is known as wear rate, expressed in mm^3. The amount of wear rate per unit applied load and distance travelled is termed as specific wear rate, expressed in $mm^3/N\text{-}m$. The amount of frictional work spent in removing unit material from the base surface is known as specific wear energy, expressed in *J/g* [21].

1.4 Materials tribology in mechanical/machine design

A typical machine or mechanical system is made from assemblies and sub-assemblies. The individual parts connected together such that to make a sub-assembly and led to final assembly. The interfaces of the component with the neighbour component obviously form either higher pair or lower pair. These pairs can be of sliding pairs or rolling pairs (tribological components), are in relative motion and transmit loads. Whenever two components are in relative motion, at the interfaces, wear of the components occurs due to friction and improper lubrication. Hence, for successful functioning of components, at these surfaces of mechanical systems low friction and low wear is desirable. Since, the inherent tribological characteristic, wear is vital in the successful utilization of the end product for longer periods of life. In a mechanical system design, a designer tries to optimize a design, accuracy of the properties of materials become vital during the design process. The design process is even more intensive while designing tribological components as wear rate and coefficient of friction are not properties of material. The tribological behaviour of materials is therefore depends on many parameters like: material couple, contact geometry, external normal load, contact pressures, relative sliding speed, material surface topology and roughness, operating temperature, chemical interactions, sliding direction (unidirectional, reciprocating, or random) etc. The tribological design even requires more attention in case of the mechanical assemblies have to work in multiple environments like air and submerged fluids, terrestrial and space environments, cryogenic environments etc., [22].

1.4.1 Tribology of polymers and polymer nanocomposites

Wear is a material response to the external motivation and can be mechanical or chemical in nature. It involves progressive loss of materials, due to relative motion between the surface and a contacting surface. It was observed that, failure of the component s is due to reduction in wear life, which the main factor to damage the system functionality. Several researchers worked in improving the wear resistance of polymer components by incorporating varieties of nanofiller. But, very few researchers contributed towards the development of eco-friendly polymer nanocomposites [23]. Since eco-friendly polymer nanocomposites contribute to green tribology. The term green tribology means, saving materials, energy, and improving the quality of environmental life. i.e., reducing the waste and extending the life of components. For example, in the area of tribology, green tribology demands on the development of biomimetic composites, self-lubricating and recyclable materials etc. The life of Industrial components mainly depends up on its reliability and successful service. It is termed as loss of function of a system. The loss of functionality of a system relies on the successful functionality of individual components. Several aspects they lead loss in functionality of a system/component is as follows:

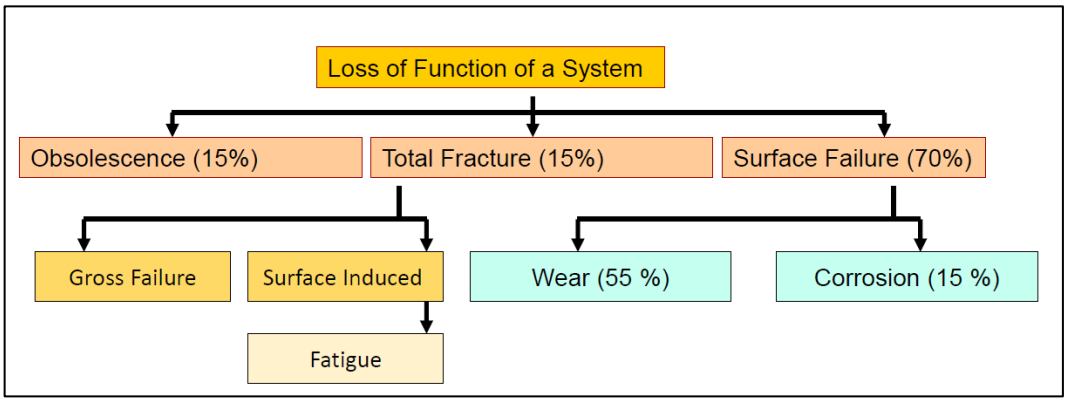

Figure 1.6 Different failures in the loss functionality of a system [24]

Obsolescence 15% → Discontinuation of the usage due to old design concepts followed.

Total Fracture 15%→ Gross failure and surface induced failure→ surface induced one is due to fatigue of component/system

Surface failure 70% → Wear 55% or corrosion 15%

The effect of wear on the reliability of industrial components is acknowledged widely and the cost of wear has also been accepted to be high (Figure 1.6). It is assessed that around 33% of the world's energy resources in current use indicate as friction many forms. This

communicates to an astonishing loss of potential power for the present automated society. The reason for research in tribology is naturally the minimization and disposal of pointless waste at all levels of engineering applications where the rubbing of surfaces is included [23].

1.4.2 Different types of wear and wear mechanisms in polymers

In case of solid lubrication (dry lubrication) system the material under two body wear mechanism, during the service of polymer components depends on several parameters like: normal load, sliding speed, sliding distance, temperature, surface finish, type of contact, hardness toughness, melting point, thermal conductivity, as shown in Fig. 1.7. In case of polymer composite systems filler wt. % addition, and the characteristics of filler such as size, shape, hardness etc. Hence, in the present context associated with materials, the type of wear mechanism depends up on the type of polymer material, blend, composite or nanocomposite of thermoset, thermoplastic, or elastomeric matrix materials. The wear mechanism in these types of materials is discussed in Table. 1.1, and its corresponding mode of wear when running against metallic counter face and counter face fitted with abrasive paper.

Table 1.1 Different types of polymer and its wear behaviour [25]

Material	**Examples**	**Wear on abrasive paper**		**Wear on metal counter surface**	
		Contact conditions	**Type of wear**	**Contact conditions**	**Type of wear**
Rigid	Polystyrene, PMMA, Thermosetting resins	Plastic	cutting	plastic-partly elastic	cutting and partly fatigue
Elastic	Filled rubbers, polyamides	Plastic partly elastic	cutting and partly tearing or fatigue	elastic-partly plastic	Tearing and fatigue and partly cutting
Highly elastic	Rubbers	Elastic-partly plastic	tearing	elastic	tearing and fatigue
Plastic-elastic	PVC, PTFE	Plastic	cutting	plastic-elastic	cutting, tearing, and fatigue

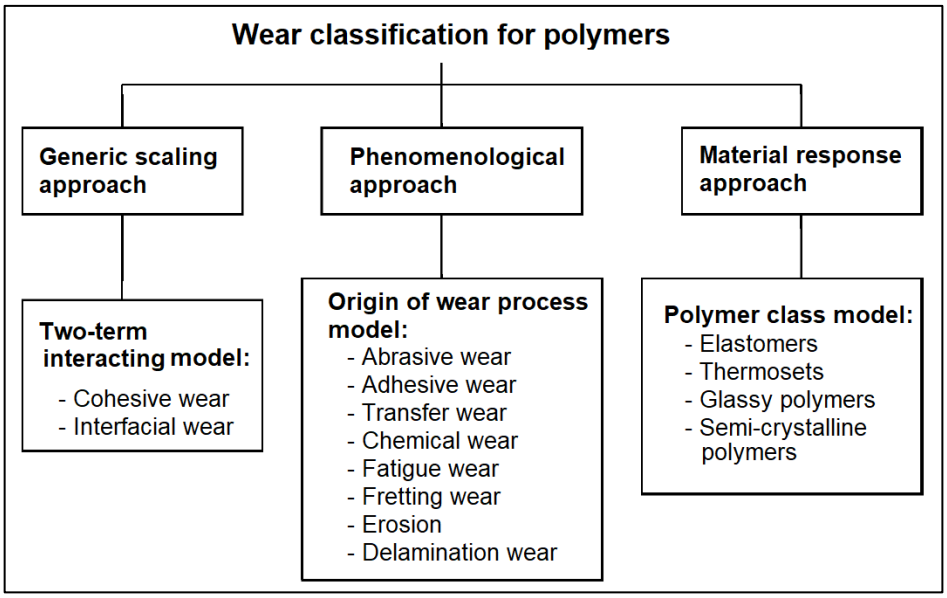

Figure 1.7 Wear classification of polymers [26]

Two-term model of the wear processes. The difference between interfacial and cohesive wear processes occurs from the point of deformation in the softer material (usually polymer) by a rigid, non-dissipative, asperity of the counter-face. For interfacial wear the frictional energy is dissipated mainly by adhesive interact ions while for cohesive wear the energy is dissipated by adhesive and abrasive (subsurface) interactions as depicted in Fig. 1.8. In the present work the emphasis made mainly on abrasive wear and erosive wear of nanocomposites.

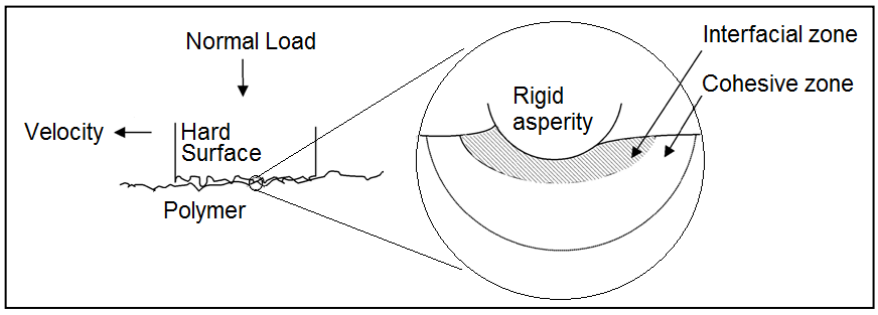

Figure 1.8 Cohesive wear process [27]

1.4.3 Abrasive wear of polymers

1.4.4 Tribology of thermoplastic nanocomposites filled with inorganic fillers

Thermoplastic material is widely used for several tribological applications. Polymer nanocomposites fabricated by the use of inorganic fillers into polymer matrix had shown better properties even without surface modification but by the use of reduced dimensions of fillers. It

means the fetching in the desired properties are governed by the size and shape of the nanofiller which is incorporated into the matrix facilitates the good bonding strength [28]. It is proposed that with decreasing filler dimensions or increasing filler content a significant improve in the contact area between the filler and matrix, and in turn it would greatly and effectively improve the transfer of the load between the fillers and the polymer matrix. The inorganic nano-fillers, ranging from 1 to 50 nm, were successfully incorporated into the polymeric matrix to strengthen and improve the ductile polymer to be more stiff and resistant for abrasion [29]. The inclusion of the ceramic nano-filler into the more ductile and low thermal resistant polymer can substantially improve its stiffness and thermal stability [30]. The nano-sized silica or alumina particles without any chemical modification were incorporated into the PEEK polymer. The addition of reduced size alumina particles greatly reduced the agglomeration cluster density and improved dispersion of filler in the PEEK matrix [31].

1.5 Tribometer and modes of testing

The main purpose of friction and wear tester is to provide experimental simulation of the wear parameters under predefined operating conditions. Because, the wear and friction are very much sensitive to operating parameters such as temperature, load or weather conditions of surrounding environment as discussed in table 1.2. Hence, it is vital to have an experimental setup where many of these parameters can precisely be controlled and observed. Also, precise measurement of these parameters cannot be done with classic industrial equipment. Therefore, careful design and fabrication of the experimental setup are essential to develop as per the international standards. The recent technological development in the area of tribology of materials also helped in manufacturing the advanced tribometers for the tribological researches.

A group of tribometers are available to assess the tribological performance of different materials. Hence, it is important to select the required type of tribometer along with the mode in order to conduct the wear runs. Selection of a particular friction tester depends upon the type of geometry between the friction pair, type of loading, type of contact and the corresponding type of motion. Table 1.2 describes the aforementioned parameters for selecting a particular wear and friction tester. Figure 1.9 depicts the types of test modes available for the wear assessment

Table. 1.2 Typical test geometries for friction and wear testing [32]

Geometry		Face/Edge loading	Type of contact	Type of motion
1	Pin-on-disc	Face loaded	point/conformal	uunidirectional sliding, oscillating
2	Pin-on-flat	Reciprocating	point/conformal	Reciprocating sliding
3	Pin-on-cylinder	Edge loaded	point/conformal	unidirectional sliding, oscillating
4	Thrust washers	face loaded	conformal	unidirectional sliding, oscillating
5	Pin-into-bushing		conformal	unidirectional sliding, oscillating
6	Flat-on-cylinder	edge loaded	Line	unidirectional sliding, oscillating
7	Crossed cylinders		Elliptical	unidirectional sliding, oscillating
8	Four balls		Point	unidirectional sliding

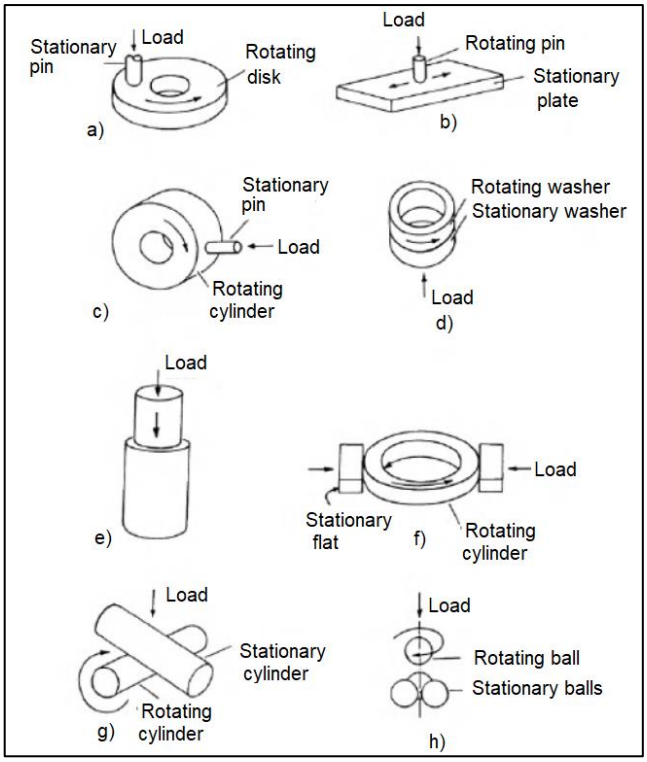

Figure 1.9 Types of friction wear assessment – modes of test rigs [32], [33]

1.6 Solid Lubricant materials and the use of Polytetrafluoroethylene (PTFE)

Fluid lubrication require pumps, seals and filtration systems to keep the contacting surfaces out of lubrication. So the main drawback of fluid lubrication system is smaller operating temperature range in which they operate and leakage issues, environmental pollution upon disposal etc. Under these circumstances, solid lubricant is an excellent opportunity and provide

many added benefits like a broad operating temperature range, low coefficient of friction value, new environmental capabilities, the lubricant remains in contact and is self-replenish, can be applied as a coating. Figure 1.10 depicted the potential applications of polymer materials.

The major downfall of polymers is rapid wear rate, finite life time, wear debris generation. Hence lot of focus by researchers is going on in reducing the unwanted effects and increasing favourable effects. i.e., increased life span, reduced wear rate, reduced debris generation, reduced or less effect on friction coefficient of friction. Materials with low shear strength metals such as gold, silver, lead, lamellar solids such as MoS_2, talc, boric acid, graphite, can be used as self-lubricants. The reason for high wear rate for these materials is low shear strength and low interaction energy between lamellar layers. Diamond like carbon coatings show extremely low friction and wear under dry and vacuum conditions.

Polymers and polymeric composites are another option as solid lubricant material. Common high performance polymers are Polyether ether ketone (PEEK), Polyamide imide (PAI), Polyimide (PI), Polytetrafluorethylene (PTFE). PEEK, PI, or PAI have desirable mechanical and thermal properties with moderate wear behaviour but have high coefficient of friction values. On the other hand, PTFE and similar fluoropolymers have low friction coefficient but suffer from poor wear. Using wt. % addition of micron sized or nano sized fillers the wear rate can be reduced. PTFE is one of the most promising self-lubricating and superior performance industrial polymer invented by Dr. Roy J. Plunket at DU Pont's laboratory, US, on 6th April 1938. The structure of PTFE is a long chain consists of stable and strong Carbon-Fluorine bonds and the molecules possesses very low coefficient of friction, outstanding chemical resistance, high thermal resistance.

Characteristics of PTFE:

Self-sacrificing during wear between surface
Offers resistance to chemical exposure
Hydrophobic surface
Offers thermal and electrical insulation
Good operating temperature limits
Low coefficient of friction
Dry running capability
High surface speeds
Resistance to weathering

High impact strength

Applications of unfilled PTFE (Fig. 1.10)

Sealing rings in ball valves and globe valves

Sealants

Transportation of food products, oils, paints, acids, alkaline solutions, gases and solvents

Gaskets, washers, well-drilling parts

Pharmaceutical, beverage, food and cosmetics industries use virgin PTFE for making conveyor belts, slides, guide rails, ovens etc., as PTFE meets the FDA regulations.

Insulation of high voltage cables

Linings of electrical heating elements such as protective covering for micro-electronics and electroplating

Coverings for medical appliances

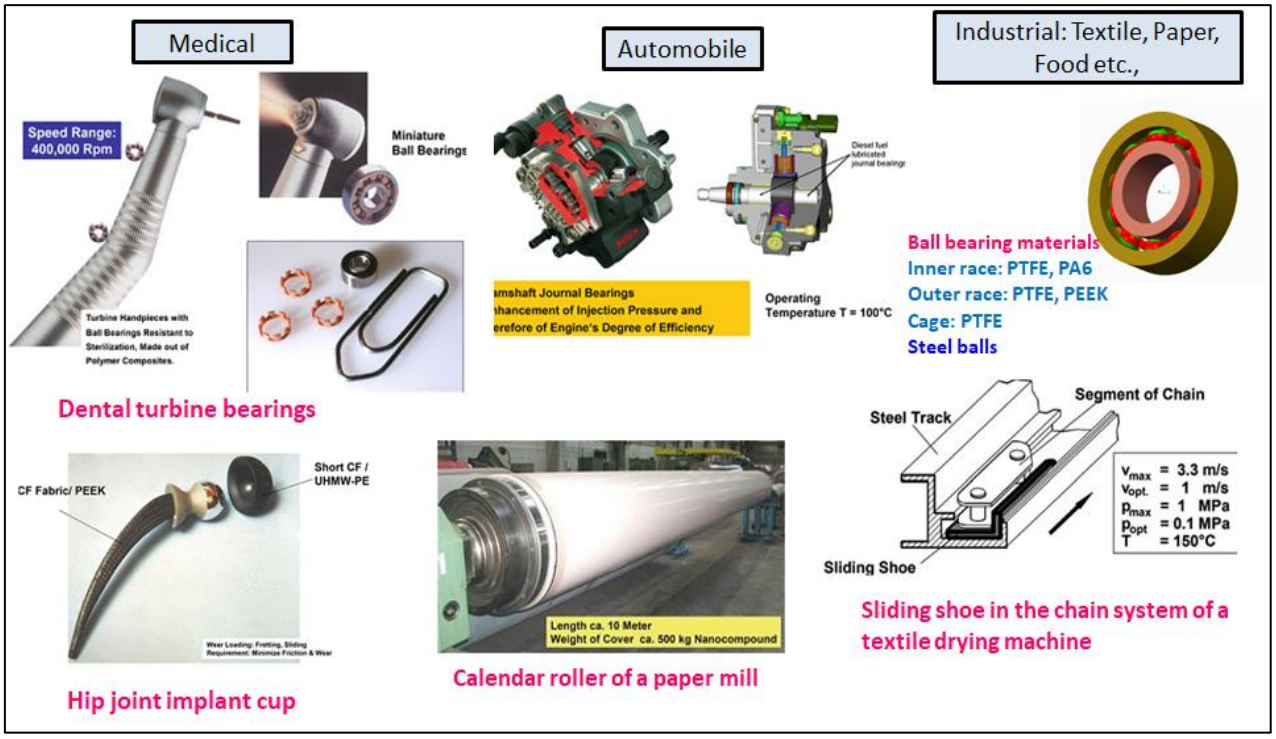

Figure 1.10 Potential fields of applications of polymers including PTFE as self-lubricating material [34]

Limitations of unfilled PTFE

Inferior mechanical properties

Poor thermal conductivity

Cold shear flow of the molecules due to pressure near contact surface

1.6.1 Methods to improve tribological behaviour of PTFE

In order to overcome the limitations mentioned, the wear resistance of PTFE over a range of operating temperatures, operational loads and the overall tribological performance, a specialized tribosystem is required in addition to the material property enhancement. Coming to material properties such as % crystallinity, glass transition temperature, mechanical properties, molecular weight, orientation, hardness, and surface energy are factors that have been shown to influence both the friction and wear behaviour of pristine polymers under different experimental parameters. While for a tribosystem: loading characteristics, the counterpart material, operating temperature, presence of lubricants etc. play a major role for the active wear mechanism and subsequently for the overall wear performance as shown in Fig. 1.11.

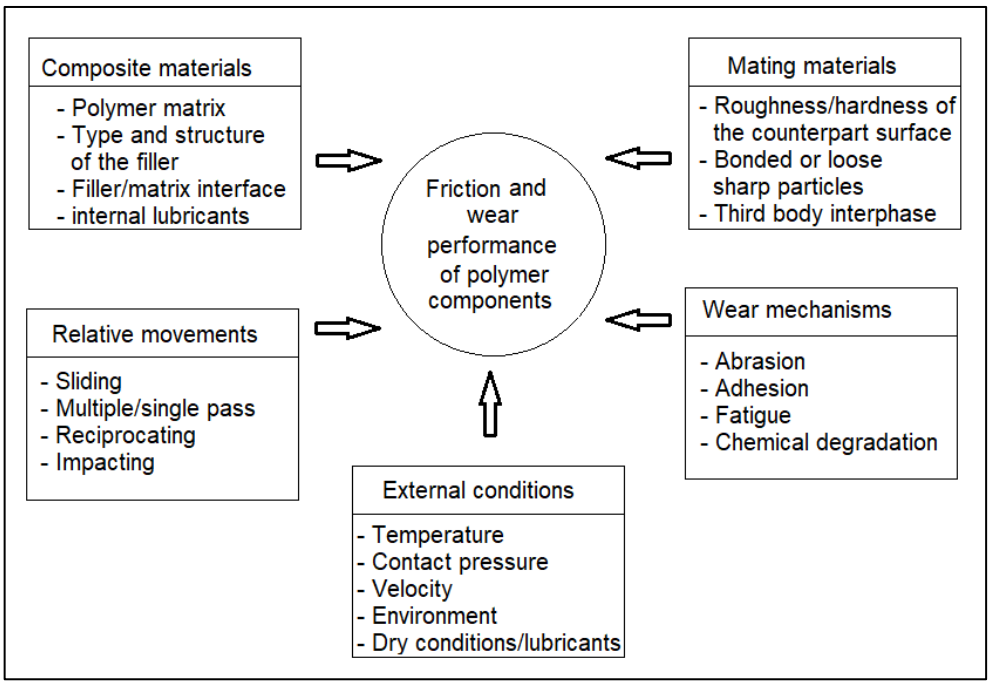

Figure 1.11 Factors influencing the wear behaviour of polymers [35]

Applications of present day frequently require a more specific modification of the tribological properties to meet the demands. Accordingly many researchers had put continuous efforts in search of new fillers to improve the sliding performance of pristine polymers. However, the developments are still ongoing to interlace with other fields of applications for extreme operating conditions. In detail the literature survey on PTFE, PTFE composites and PTFE nanocomposites were discussed in chapter 2

1.7 Erosion wear

Solid particle erosion wear in polymers: Solid particle erosion is the loss of material from the surface, results from repeated collision of accelerated particles. The erosion wear also occurs, whenever, hard solid particles are entrained in fluid medium impinging on a counter surface at considerable velocity. In both the cases, particles can be accelerated or decelerated, and change their directions of motion by the action of fluid. The solid particle erosion is a useful process in some cases like, sand blasting and water jet cutting, but the wear process is not desirable in many other engineering systems, like steam and jet turbines, pipelines and valves carrying chemicals/solid matter, and FBC systems. The motivation for study and understanding erosion wear mechanism might be reduced life times, failures of mechanical components utilized in erosive environments such as, pipelines carrying sand slurry, petroleum refinery, turbine blades, nozzles, fire tube/water tube boilers.

1.7.1 Erosion wear procedure

Erosion and local removal of material in the matrix rich zones: The erosions wear resistance is mainly depends on the erosion characteristics of matrix material, since the impact of solid particles is first exposed to the matrix material. Hence, the toughness of exposed matrix rich zone directly affected for the erosion mechanism. In case of thermosets, the matrix erodes in brittle manner. Whereas, in case of thermoplastics, the matrix is uniformly ridged and cratered with local material removal in the zone is revealed. Erosion in the fibre zones associated with breakage of fibers: The effect of fibre reinforcement has some significance in the erosion wear process, as fiber material, fiber content, fibre geometry and its orientation affects the erosion magnitude. The damage is characterized by the separation and detachment of broken fibres from the matrix. The material with the strongest interface strength showed the highest wear resistance. The inclusion of brittle fibres produce lower erosion rates compared to unfilled thermoplastics [36].

Erosion of the interface zones between the fibres and the adjacent matrix: as the next erosion affected zone is weak interface between fibers and the matrix. This is the next weakest zone which is exposed to the impacting media. Highest interface strength can be observed if the surface of the fibres were modified by some special treatment. Thus the bonding strength at the interface increases due to surface modification and hence the increased wear resistance at the interface. This phenomenon helps even in the matrix rich zones and delay in the wear can be observed [37].

CHAPTER – 2

LITERATURE SURVEY

The chapter discusses about the literature review, it describes clearly about the necessity of solid lubrication for several industrial applications, Literature related to PTFE as a solid lubricant, necessity of filler addition to the PTFE matrix material, conclusions from PTFE composites, conclusions from PTFE nanocomposites, HNT as a filler material, HNT filled polymer nanocomposites, problem identification, problem definition from research gap, and motivation for the current work.

2.1 Tribology: Friction, Wear, and Lubrication

Tribology is defined as science and technology that mainly deals with friction, lubrication, and wear. Friction is inevitable characteristic between the moving parts or components of machinery in industries. This is controlled by the thin surface layers of bodies in dynamic contact. Therefore it is always desirable to have less value of friction coefficient and that leads to minimum losses and torque requirement. The study of friction in polymers is mainly emphasized on two main elements i.e., adhesion and deformation [27]. Wear is the dislodging of mass lumps from the weak material when is set to slide against hard counter-surface. Abrasion, adhesion, and fatigue wear are common types of wear of polymers[38]. The basis for wear process is as follows: The basic mechanism of friction of polymers in the highly elastic state over smooth surfaces is adhesion. The changes in surface layer arise from mechanical stresses, temperature and chemical reactions. Polymers are generally more sensitive to these factors due to their specific structure and mechanical behaviour. The local temperature at the interface may be substantially higher than that of environment, and may also be enhanced at the asperity contacts by transient flashes or hot spots. The temperature exerts an influence on wear of polymers. In practice, less number of polymers are available for sliding against steel at higher operating temperatures. Friedrich et al, [39] fabricated composites with different fillers like PTFE particles, short glass, carbon and aramid fibres in the matrix of PEEK, and studied the friction and wear properties of high temperature resistant polymers,. They found any fibre orientations of carbon fibres in the PEEK matrix give better wear resistance than the arbitrary orientation of glass fibres, and aramid fibres.

In many materials, wear is closely related to friction and lubrication. Varieties of materials were developed with different film coatings and strengthening mechanisms of soft polymer

phase loaded with micro and nano-reinforcements to combat wear and friction. The reinforcement in the matrix material would improve wear resistance at the cost of slight increase in friction coefficient. In recent years, several new solid lubricant materials have been developed to achieve better lubricity and longer wear life in challenging tribological applications [40].

2.2 Polytetrafluoroethylene (PTFE)

PTFE is one of the most promising solid lubricant material to possess all desirable characteristics and replaces many metals in wear and friction aspect. But it highly suffers from low wear resistance rather low coefficient of friction. PTFE is viscoelastic in nature and as a result, its friction, wear and lubrication properties are functions of both sliding velocity and operating temperature. PTFE is a linear chain, non-cross linked, semi-crystalline polymer with smooth molecular contour consisting of 20,000 to 2, 00,000 repeating units of TFE $-(C_2F_2C_2F_2)-_n$. The fluorine encasement of the carbon backbone provides high chemical inertness, while its smooth profile provides low friction sliding [41].

PTFE also has a wide operating temperature range (269 ^{0}C – 227 ^{0}C) and a very low vapour pressure (low out gassing) making it a viable material for solid lubrication in space craft applications. The molecular structure of PTFE is shown in Fig.2.1 (a) and in Fig.2.1 (b) the details of the typical spherulite arrangement in the structure is shown. An increase in coefficient of friction of PTFE material was observed, at reduced operating temperatures or increased sliding velocities [42]. In their work, for applications at speeds less than 10 mm/s a low coefficient of friction value (0.03-0.1) and a moderate specific wear resistance (10^{-5}mm^3/N-m) was registered. Makinson et al. [43] found that, when the sliding velocity was increased to above 10 mm/s at room temperature, a changeover from mild to high wear (10^{-5}–10^{-3} mm^3/N-m) along with increased friction coefficient. They also hypothesized that at speeds <10mm/s and temperatures >30 ^{0}C shearing occurs in the amorphous regions (regions at the interface of neighbouring crystalline portions) and formed lamellar type of debris on the counter surface [6,7, 8]. Also, they observed an increase in the shear stress compared to the shear stress under original conditions of material (low friction and moderate wear) in case of sintered PTFE material. The stress required to cause failure at the boundaries between crystalline regions of the material, at increased speeds and decreased temperatures. They concluded that this leads to larger debris and increased wear rates.

.

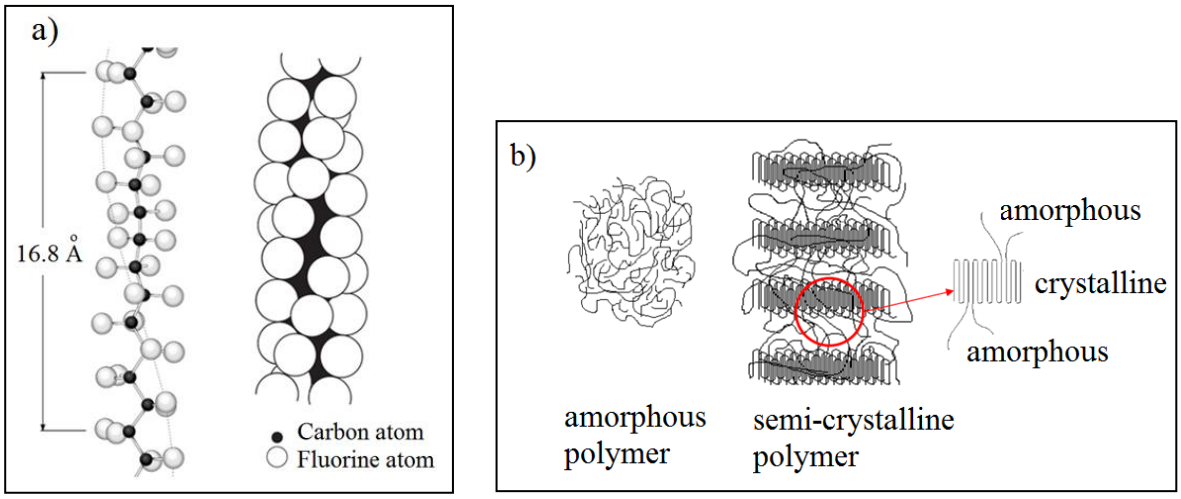

Figure 2.1 a) molecular structure of PTFE [41] and b) arrangement of spherulites in PTFE

PTFE powder does not actually liquefy at its melt temperature ~340^{0}C, due to its extremely high molecular weight i.e., the melt viscosity increases with increase in temperature [44]. Consequently, the bulk PTFE powder must be consolidated by other than usual melt flow processing techniques like screw extrusion. Press-sinter methods are commonly employed, where the PTFE powder was cold pressed into a mould pressure of 10MPa or above, subsequently sintered above the melting point, maintained few hours of holding time and slowly cooled to room temperature. The typical shapes of moulds used are in the form of rod or sheet and the final shape of the part can be obtained by machining these rods or sheets. PTFE composites may be shaped by simply blending the particles of filler into the PTFE matrix powder before pressing.

The molecular structure of sintered PTFE is shown in Fig. 2.2. The chains organize parallel each another with their axes lying within the plane of thin crystalline wedges or slices, with tangled regions separating slices as they pile to form bands. The hypothesized crystalline slices appear to have thickness in the range 20-30 nm [45], along the length of these bands observed upon fracture surfaces. Figure 2.3, depicts the gradual wear loss mechanism of virgin PTFE material.

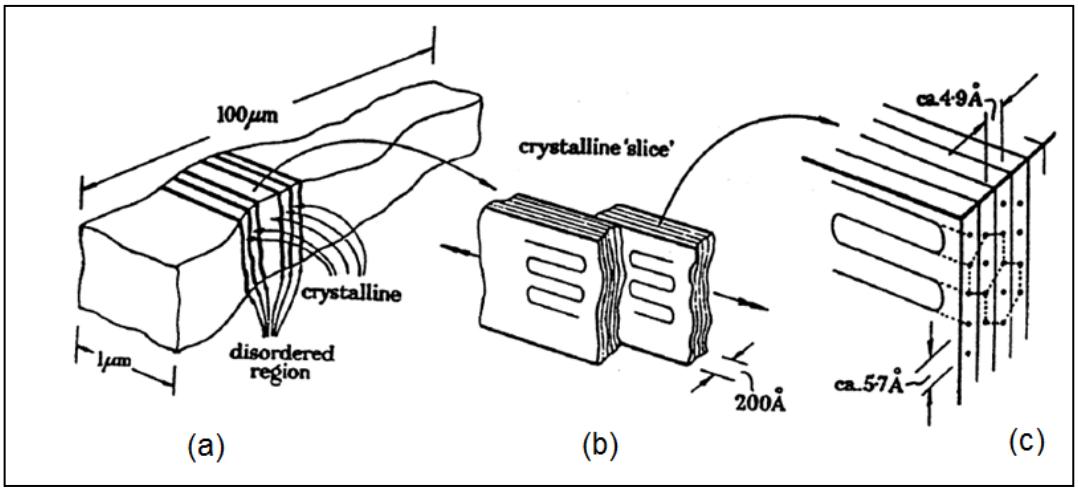

Figure 2.2 Microstructure of PTFE: (a) semi-crystalline band; (b) crystalline slices, separated due to shear in the disordered region; (c) hexagonal array of chains arrangement of PTFE molecules in the slice [45].

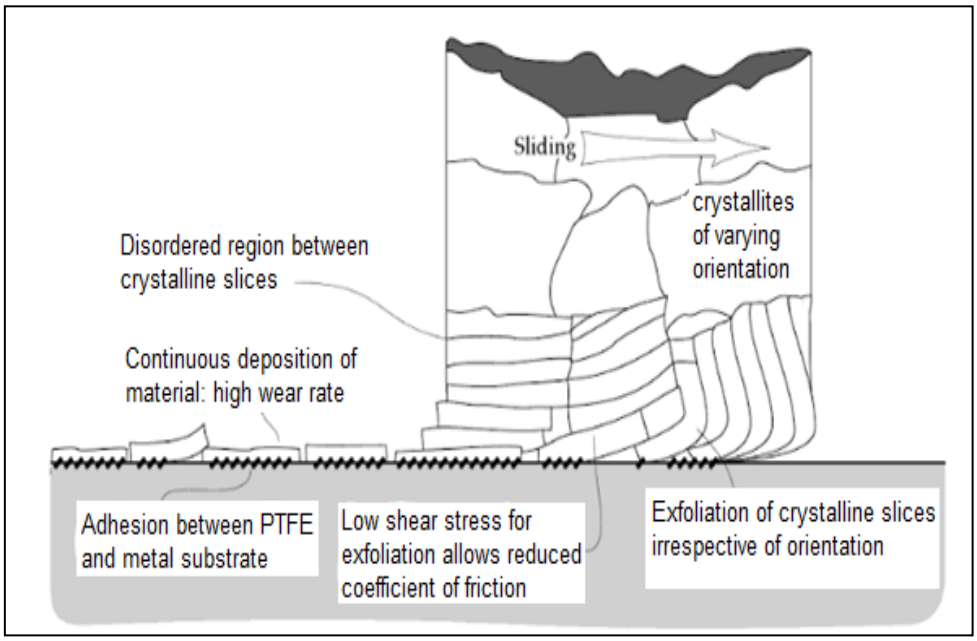

Figure 2.3 typical wear loss of virgin PTFE material with hard counterface [46]

Blanchet and Kennedy [47] observed from their study of transition wear behaviour speed at different temperatures at increased temperatures the wear rate transition speed is also increased. The transition of severe wear occurred at COF=0.1 was observed from wear rate 'k' versus COF graph plots at different temperatures. These results were in good agreement with the work of Makinson and Tabor [43] and suggested that severe wear transition was a response to the shear stress at the interface, as shear stress is a function of COF and thus the COF is dependent on both speed and temperature. Moreover, in search of reasons for causing severe wear rates they also studied several microtomed samples (perpendicular to the direction of

wear) after mild and severe wear test. When observed severe wear samples, some cracks were found to propagate in the direction of sliding under a layer of worked material at subsurface depth consistent with observed debris thickness. On the other hand no such cracks were found in mild wear samples. They explained the reasons as follows: the defects in the sintered material act as crack initiator, when speeds are low, the kinetic friction coefficient at the tribo-interface is low and the static friction coefficient is just sufficient to support the PTFE interface for the surface tractions. Whereas, when the sliding speed increases the kinetic friction coefficient at the tribo-interface increases and exceeds the static COF (~0.1) at the PTFE/PTFE crack interfaces, the crack tips must support surface tractions. Eventually, this leads to a progressive delamination wear process. Due to this severe wear of PTFE at high speeds and operating temperatures it has precluded its use as pristine PTFE in many applications and motivates the use of reinforcement to overcome the onset of severe wear.

2.3 PTFE composites

In the previous topic it is discussed the necessity of filler addition in PTFE matrix material. For the last few years, micro fillers were incorporated and up to 100X wear reduction was observed. The following graph shows the reduction of wear rate with filler wt. % addition in few PTFE composites found in the literature. In spite of being tested with different testers, methods, pressures, speeds and fillers, there was a regular trend of reduced wear rate with increased filler wt. % up to 50 wt. % was noticed. The reasons for wear reduction due to filler addition were discussed in the coming section.

Lancaster [48] suggested that the inclusion of hard wear resistant fillers with a high aspect ratio resulted the reduced wear of PTFE composite and increased support to the load due to a thin film formation. Especially when metal fillers were added, the transferred fragments of metal fillers on the counterface, had some adhesion interaction with the remaining filler particles of the slider. Moreover the metal fillers on the counterface form as ‘hot spots’ acts as catalyst for the chemical reaction between PTFE matrix and the filler establishes a strong thin film on the counterface and there by the reduction in the wear was observed.

Tanaka et al. [42], prepared PTFE composites with fibers, particulate and lamellar types of fillers. The tribological behaviour of PTFE composites was studied under a constant load and at different sliding speeds. They observed that friction is independent of type of filler added to neat PTFE and concluded that fibre and particle type fillers were more effective than solid

lubricant lamellar and other hard fillers in the contribution of preventing large scale destruction of long structure of PTFE material near friction surface. In their work they also noticed that, the effect of shape and size of the filler on the friction and wear behaviour of PTFE material.

Bahadur and Tabor [23], carried out experiments, using polar graphite, Pb_3O_4, MoS_2 and CuS fillers in different proportions included in PTFE slider, rubbing against flat counterface of glass and mild steel, which were finished by grinding, abrading using 600 grade emery paper and lapping. They recorded the following observations: Graphite filler inclusion reduced the wear rate of PTFE by about 100 X and increased the coefficient of friction by ~30%. CuS filler inclusion provided 100X reduction in wear rate with no increase the coefficient of friction.

2.4 PTFE nanocomposites

In the previous section from the literature it was revealed that, PTFE micro-composites were loaded with more than 20% (by volume) filler in order to make it as wear resistant. But the subsequent problem with high % of filler loadings is that, the hard and wear-resistant fillers cause abrasion to the counterface and spoils the surface roughness. Hence, nanofillers might be the other option to use as reinforcement. The main advantage with nanoparticles is its size scale, on par with counterface asperities and therefore has potential as wear-resistant, nonabrasive fillers. Also, the improvement in the properties can be achieved with low wt.% addition of fillers (<10%). From the literature, in various other polymeric systems, low filler fractions of nanoparticles have resulted in appreciable improvements in mechanical properties and thermal properties [31], [49], [50].

Collective researches showed that the addition of low amount of organic and inorganic nanofillers can render superior improvement of functional properties. In this regard carbonaceous nanoparticles such as graphene sheets (GS) and carbon nanotubes (CNTs) have gained great deal of interest as a functional filler for polymer-based nanocomposites. In recent study, Graphene nano platelets (GNPs) was used as reinforcement in polydimethylsiloxane (PDMS) silicone elastomers and the effect of concentration of GNPs on ultimate properties of composites was studied [51]. From the study, useful mechanical and thermal properties were analyzed through Infrared mechanical responses at different pre-strain values.

The improved properties of the composites witnessed several varieties of applications like photo-responsive coating material for many MEMS devices, optomechanical memory, adaptive skin smart material, temperature sensitive strain gauge etc. An optimum increase in mechanical properties such as Young's modulus, photomechanical induced stresses in the composite material at different pre-strain levels was realized at 2 wt. % GNPs addition. The addition of

graphitic nano-carbons such as single layer graphene and graphene nano platelets (SLGs and GNPs) as reinforcement played an important role in enhancing several mechanical properties through improved load transfer from the work of Xu et al [52]. During their preliminary studies, they developed advanced PDMS composites containing SLGs and GNPs for robotic actuator applications. The remarkable enhancement in load transfer and mechanical properties was observed for PDMS composites containing 1 wt. % exfoliated graphene and it was ascertained with the help of strain induced Raman band shift. Due to the band shift in tension and compression modes, a considerable increase in mechanical properties such as elastic modulus of PDMS (about 42%), toughness (about 39%), damping capability (about 673%), and strain energy density (about 43%) was reported. It was also observed that the orientation of the GNP and SLG flakes in PDMS matrix influences the damping and frictional properties in longitudinal and transverse loading [53]. The synergistic effect of multi-wall carbon nanotubes (MWNTs) and SLGs towards load transfer and enhanced mechanical properties was studied in PDMS matrix. The significant improvement in the load transfer as well as mechanical properties was obtained with total 1 wt% addition of MWNTs and SLGs in the matrix material [52].

The extensive studies by Burris et al [54]–[56] showed a prominent improvement in mechanical and tribological properties of PTFE composites with organic and inorganic nanofillers compared to micron sized fillers due to its large aspect ratio. Further, they consolidated the work of previous authors and defined the target direction for high performance materials as shown in Fig. 2.4. The tribological parameters such as friction and wear plotted on a semi-log plot and classified as per the specific wear rate magnitude of PTFE blends, composites, and nanocomposites. From the Fig. 2.4, the circles enclosed with letters were the design points, the work of previous authors, and represent the specific wear rate and coefficient of friction. The classification described these materials into low performance, medium performance, and high performance materials suitable for several tribological applications.

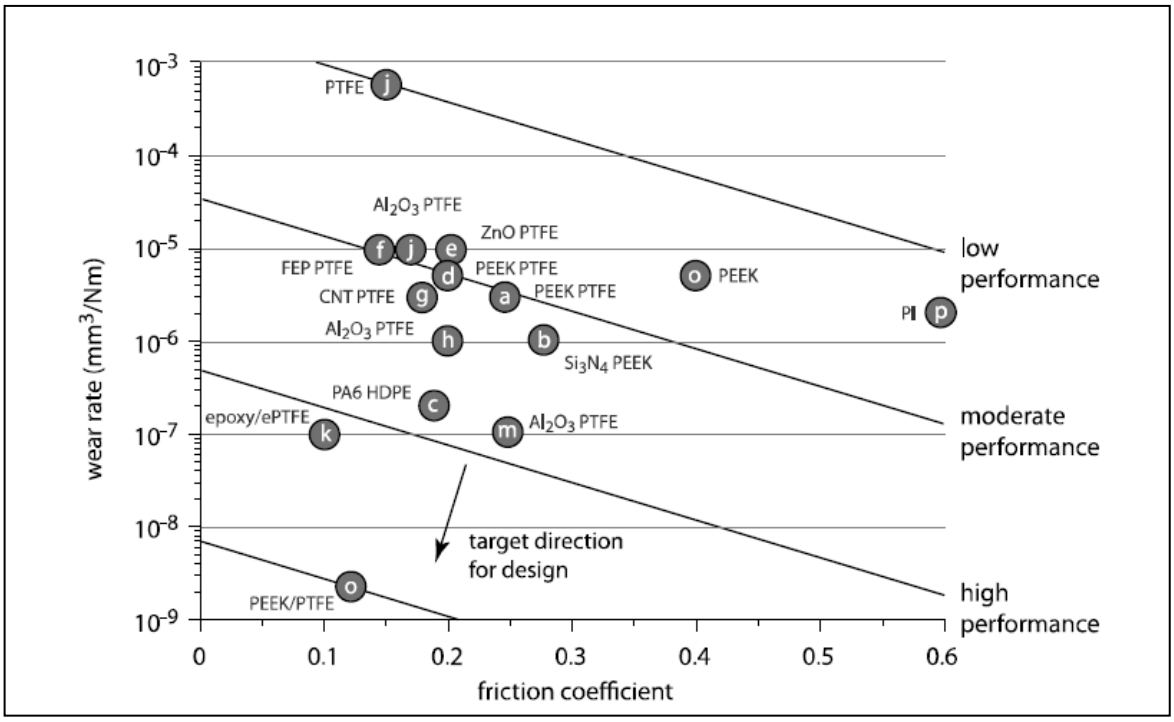

Figure 2.4 Semi-log plot of Wear rate versus friction coefficient for various solid lubricating unfilled polymers, polymer blends and polymeric composites. The lower left hand corner, a target region of ultra-low wear rate and friction coefficient is also portrayed. [54]

Conte et al [57] has observed that combination of soft and hard phases influenced the coefficient of friction, self-lubricating and load carrying properties of PTFE composites as compared to pure PTFE and proved that mateirals . The studies by Feng et al [58] showed an enhanced tribo-performance with the dispersion of surface modified ZnO nanoparticles in PTFE matrix. Improved mechanical, wear and electrical properties were reported in single walled carbon nanotube (SWNT)/PTFE composites [50]. Optimum performance in tensile properties of GF/PTFE composites was found at 0.3 wt% of surface modified glass fibers by using rare earth surface modifier (LaCl3) [59].

2.5 Filler material: Halloysite nanotubes (HNTs)

HNTs are a kind of natural occurring clay minerals with nanotubular structures, usually being extracted from mines. HNTs are attracting the focus of researchers as a reinforcement material due to its hollow tubular structure similar to carbon nanotubes (CNTs) with good aspect ratio. The clay mineral was first identified and reported by Berthier in 1826, as a dioctahedral clay mineral of kaolin group [60]. The chemical formula for a typical HNT can be expressed as $Al_2Si_2O_5(OH)_4 \cdot nH_2O$, with n equals 0 and 2, representing dehydrated and hydrated HNTs, respectively. Lots of deposits of HNTs have found in countries such as, France,

Belgium, China, and New Zealand. HNTs adopt other than tubular morphologies like spheroidal and plate like particles under varying crystallization conditions. Of these tubular morphology is the most common and useable for several applications. Initially, HNTs reported its application in biomedical use as controlled release of drugs, since the lumens of HNT can be loaded with drugs and other chemicals [61]. For engineering applications, HNTs found its place as corrosion inhibitor loaded within the lumen, when doped with specialized coatings for surface protection [62]. In the field of material science applications, owing to its several advantages like high L/D ratio, low density, ready to disperse easily without any surface modification, HNTs have attracted as a promising reinforcement filler for thermoplastics for improving functional properties. Many researchers reported that increased mechanical, thermal, and tribological properties were observed with the incorporation of HNTs as filler [61], [63]–[67]. Fig.2.5 (a) & (b) shows the TEM images of Halloysite nanotubes particles supplied by the manufacturer. Fig.2.5 (a) shows the average inner and outer dimensions of tube structure whereas Fig.2.5 (b) shows the lengthwise dimensions of the nanotubes. The length of nanotubes play some dominant role in improving the mechanical properties such as tensile, impact, flexural, and micro-hardness and thermal properties like improved heat capacity, process of crystallization, degree of crystallinity etc.,

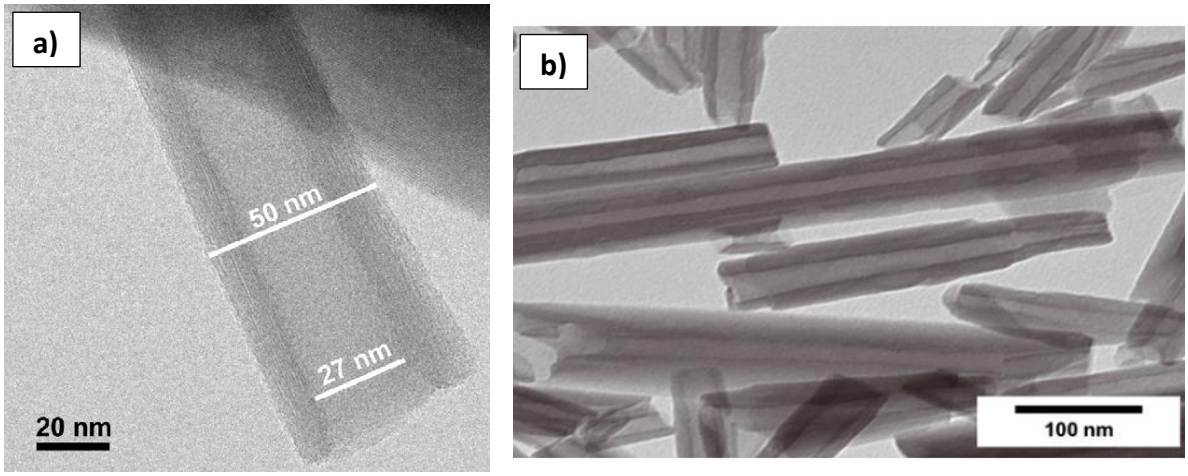

Figure 2.5 Transmission Electron Microscope (TEM) Images of HNT particles (a) average inner and outer dimensions; (b) Particles have different lengths {source: NaturalNano Inc., USA [63]}

A survey on the natural mineral Halloysite nanotubes (HNTs) being used as filler for thermoplastic, thermoset, and elastomer polymers, was reported by Rawtani et al [61]. Halloysite nanotubes have alternate alumino silicate layers with alumino layers located inside the HNTs and most of outer layers are siloxane. The HNTs are usually hydrophobic in nature

due to low content of hydroxyl groups on their surface compared to other nanoclays and nanosilica. Therefore, HNTs can be easily dispersed in non-polar polymers like PP, ABS, PTFE etc, using shear mixers [67]–[69]. Also in case of CNTs, owing to π–π interactions, the dispersion in polymer matrices is complex [70]. On the other hand, HNTs have very less inter-tube relations due to less hydroxyl groups and also the presence of siloxane makes the inter-tube interaction relatively weak and promotes exfoliated dispersion in the polymer matrix [68]. In addition, it possess high aspect ratio and cost effectiveness compared to single or multiwalled carbon nanotubes. HNTs have emerged in its usability as filler in comparison to other nanofillers for polymer-based nanocomposites. This is in comparison to the effect of fillers like talc, mica and various other aluminum silicates used to improve functional properties of several polymers [28], [71]. Consequently, modified HNTs were dispersed in the several polymer matrices such thermoset/thermoplastic/elastomers [15], [67], [72]–[77] and improved functional properties were found. Moreover, the recent trend in developing 'green tribological' materials has been motivated in the preparation of PTFE/HNT nanocomposites as PTFE is recyclable and HNTs are naturally available materials. In the present context, green tribology means saving energy, improving the environment and the quality of life [78].

2.6 Transfer film mechanism

Coming to transfer film characteristics, filled polymers produced a uniform and articulate film on the steel surface compared to unfilled PTFE. The changes in size and shape of the worn debris of filled PTFE and their bonding to the counter surface with less shear stress during sliding caused smear film. The increase in the wear resistance or reduction in wear debris can be quantified directly with the strength of transfer film. Especially, when sliding on hard counter surfaces, the established film that fills the asperities of the counter surface and grows gradually its thickness with further sliding distances. The optimum thickness of the formed film begins as a PTFE/over laying PTFE pair and hence the tribological behaviour of PTFE becomes very insensitive to the counter surface roughness or composition. Transfer film formation on the hard counter surface occurs due to weakening of current layer from the slider end, since adhesive force from the counter surface dominates the cohesive force between the layers. Repeated stress cycles at the interface are the main reason in forming the film. For unfilled polymers, transfer can be beneficial or detrimental to the wear process, depending upon the topography generated.

Figure 2.6 shows certain results from this type of experiment and it may be noted that transfer causes increased wear with the brittle polymers and reduced wear for the more ductile

ones. It is reasonable to suppose that transferred fragments from the ductile materials are readily deformed during repeated contacts and generate a surface which is smoother than the original metal. The localized asperity stresses are therefore reduced, and in turn the magnitude of the rate of wear. Various zone presented in the Fig. 2.6 were explained as follows: I. Initiation of contact between the surfaces. II. Running-in wear process where the soft polymer molecules are gradually transferred to the hard counter surface as a third body. III. Steady state wear process where the wear and friction phenomena are influenced mainly by shear and adhesive properties of the transfer film [27]

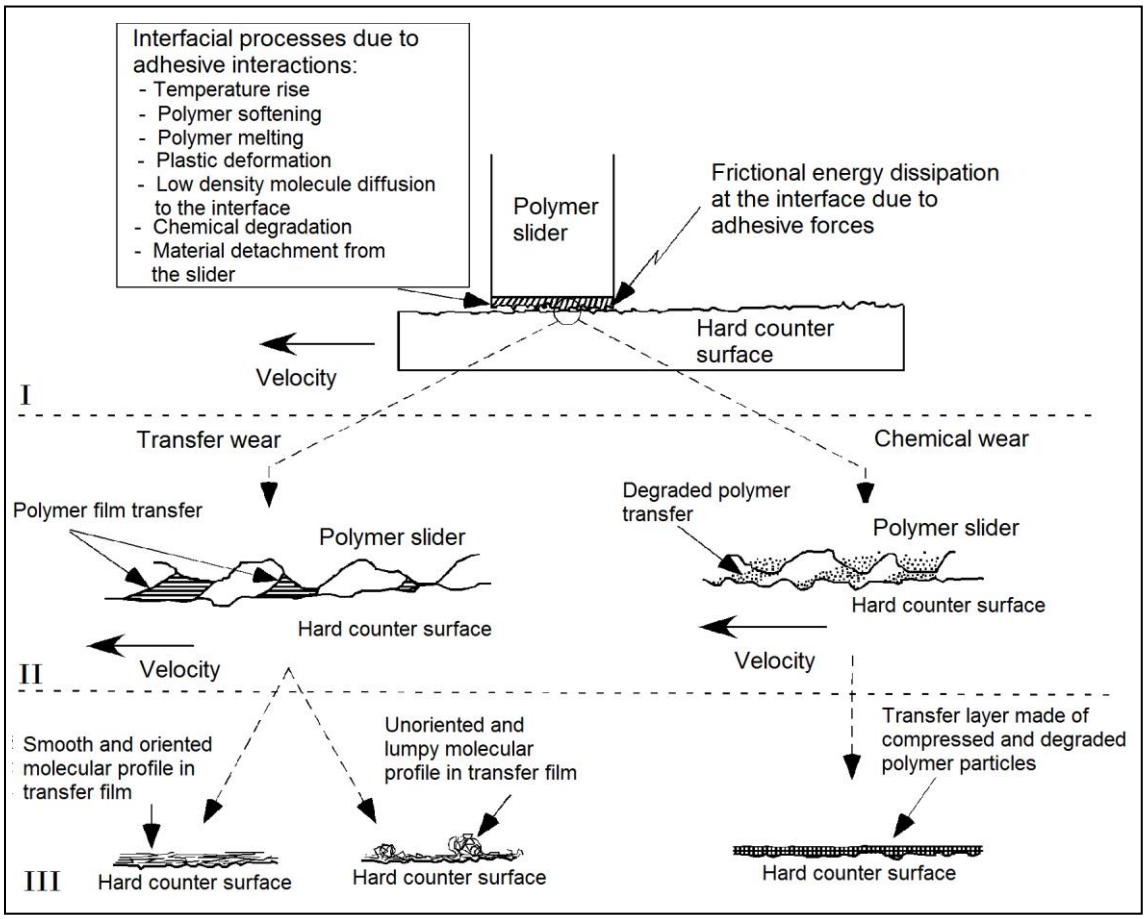

Figure 2.6 wear process in soft polymers (ploughing effect) and hard polymers (debris flakes) [27]

Gong et al., found that the wear rate of PTFE was independent of chemical bonding with the counterface, and concluded that cohesive failure within the PTFE must govern its wear rate. Blanchet et al. [47], had similar findings with XPS analysis of PTFE and PTFE composites in dry sliding, and concluded that the wear reducing role of the filler is to slow primary removal

of material from the bulk by arresting crack propagation rather than slowing secondary removal of material from the counterface via increased transfer film adhesion.

2.7 Erosion wear

Solid particle erosion wear is one among the other wear modes, occurs when hard solid particles entrained in a fluid and impinging the target surface at different angles. It involves the gradual loss of material of the target surface when exposed to the dusty environments encounters in many industrial applications. This results change in functional properties and life of the components. In general there are several applications of components which are made of polymer composites working in sandy environments; situations like pipelines carrying sand, slurries in petroleum refining, helicopter rotor blades, pump impeller blades etc., If proper measures not taken to overcome the loss of material; the component cost due to wear failure will be increased because of replacement frequency. Hence many researchers worked, in order to improve the resistance to rain and sand erosion of reinforced polymers [79], [80]. The erosion wear rate is a dynamic process and governed by several operating factors like, striking velocity, angle of impingement, shape and size of erodent, erodent discharge rate, erodent material properties, and target material properties [81].

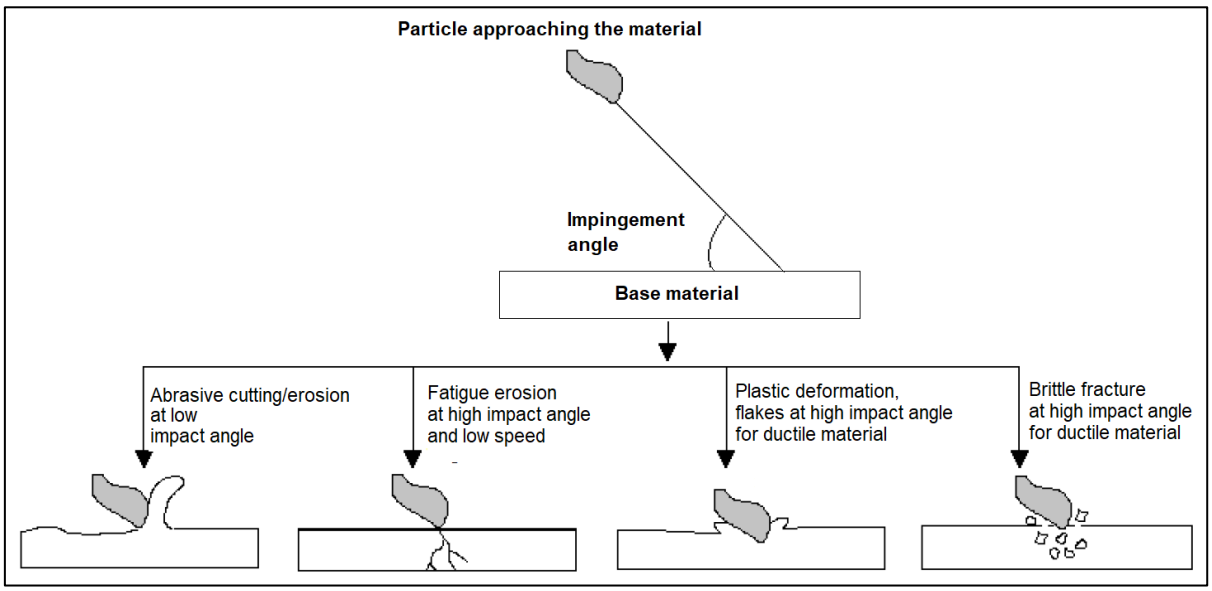

Figure 2.7 Polymer erosion wear mechanism modes[82]

Erosion wear mechanism

From the literature, it is known that the amount of erosion wear rate of various types of polymer matrix composites are depends upon by the amount, type, orientation and properties of the reinforcement on the one hand and by the type and properties of the matrix and its adhesion to the fibers/fillers on the other. Next to that the experimental conditions (impact angle, erodent velocity, erodent shape, erodent flux rate, etc.) have a great influence on the erosive response of the target materials. Two erosion modes are namely brittle and ductile erosion are found. The erosion wear rate (E_{wr}) of them is mainly depends on impact angle. For ductile materials E_{wr} goes through a maximum at impact angles, at about15^0–30^0. For brittle materials E_{wr} continuously increases and reaches maximum at about 90^0[83]. Solid particle erosion includes cutting, impact and fatigue processes. The local energy concentration of the erodent on the impacted surface is crucial for the erosive wear. During the impact at first the top layer consists of both matrix and reinforcement will be eroded by the cutting action and next new layer will be exposed and so on, as it is a gradual removal of material from the target surface. Also the fracture begins at the breakage of the weakest interface between the filler and matrix. Figure 2.4 depicts different types of erosion wear mechanism in brittle and ductile materials.

PTFE material for erosion environment

Polytetrafluoroethylene (PTFE) is one of the iconic thermoplastic material offers a broad range operating temperatures and are used for several applications include bearing pads and compressor piston seals, oven conveyor belts for food industry, and architectural protective coverings which are exposed to rain and sand erosion [84]. A very little literature was available on PTFE and its composites in erosion wear area. The matrix material, PTFE is a semi-crystalline, high temperature resistant material and can be reusable, but suffers from low wear and inferior mechanical properties. In order to strengthen and increase the usability with the addition of fillers/nanofillers are generally used. Halloysite nanotubes (HNTs) are naturally and abundantly available filler material at relatively low cost. A conventional method of processing of the PTFE nanocomposites in bulk is also another favourable aspect in choosing the matrix material. Design of high performance nanocomposites is highly essential to increase the wear strength, decrease the replacement costs and there by diminishes the environmental pollution and many health issues. Hence, in the current paper the work is carried out on the complex material made of PTFE and HNTs filled nanocomposites.

Table 2.1 Erosion wear study by some researchers on polymer composites

Material Tested	**Test Conditions**	**Erodent Type, Shape & Size used**	**Ref.**
Polyimide composites based on Quartz polybutadiene, glass cloth epoxy and quartz	V=42m/s, a = 30°, 45°, 60°, 75°, 90°	Natural sea sand, slightly rounded, 210-297 μm	[85]
Bismaleimide (BMI) matrix and reinforced with graphite fibre	V=20, 40, 60 m/s a = 30°, 90°	Alumina oxide particles, angular, 63, 130 and 390 μm	[86]
Bismaleimide (BMI) matrix	V=60 m/s, a = 90°	Alumina oxide particles, angular, 42, 63, 143, 390 μm	[87]
Polypropylene matrix and reinforced with discontinuous short, long glass fiber and continuous unidirectional glass fiber	V=70m/s a = 30°, 60°, 90°	Corundum particles, angular, 60-120 μm	[88]
Ultra-high molecular weight polyethylene (UHMWPE)	V=10,20,40,70, 100 m/s a =15°, 30°, 45°, 60°, 75° and 90°	Coal powder, silicon dioxide, angular, 60-70 mesh size	[89]
Glass Fiber reinforced with granite filled with unsaturated ophthalic polyester resin	V= 32, 43, 54, 65m/s a= 45°, 60°, 75°, 90°	silica sand 200 μm, 300 μm, 400μm, 500 μm	[90]
Polyetheretherketone (PEEK) matrix filled with aligned carbon fiber	V= 61, 97.5, 152.4m/s a =15°, 30°, 45°, 60°, 90° T= 210c and 2600c	10 μm Arizona road dust, 100 μm sieved runway sand	[91]
Unsaturated polyester resin filled with micro and nanofillers	V= 97.8, 128, 152m/s a =15°, 30°, 45°, 60°, 75° and 90°	Alumina sand, 11.5μm	[92]

2.8 Design of experiments

For evaluating optimum input parameters of tribological responses response surface methodology is adopted. Response surface methodology (RSM) is a combination of statistical experimental design, regression modelling and optimization. Several authors worked on optimization of cutting tool input parameters was accomplished by using DOE techniques in

production field. Due to its simplicity of the methodology, the RSM was adopted in polymer material science area for optimizing the operating input parameters in order to find better mechanical properties of composites/nanocomposites. Chow[13] worked on the flexural properties for epoxy/organo-montmorillonite (OMMT) nanocomposites. RSM was used to find process variable of in-situ polymerization those affect the flexural properties. They found that the speed of mechanical stirrer, post-curing time and post-curing temperature were influencing the flexural modulus and flexural yield stress of epoxy/4 wt. % OMMT nanocomposites. Chakradhar et al. [93] studied the optimization of mechanical properties of MMT clay filled epoxy/polyester nanocomposites. The objective of their work was the nanocomposites which offer low cost, high strength and eco-friendly in nature. Ghasemi et al. [94] studied the optimization of processing parameters of elastomer/clay nanocomposites. Erdem et al. [95] utilized and found best input parameters in the preparation of polystyrene/MMT nanocomposites.

Many studies have reported using RSM to evaluate the effect of input parameters on the tribological properties of composites materials.In the work of Kumaresh Babu et al. [96] the two-body abrasive wear behavior of Glass–Epoxy (G–E) composites, the addition of Titanium carbide (TiC) as a secondary reinforcement using different operating conditions with 400 grit water proof Silicon Carbide (SiC) abrasive paper. Box- Behnken design was adopted to get the significant factors and their interactions, influencing the weight loss of the composites. They found that highest wear resistance of G-E composite was achieved by the addition of 2wt. % TiC in particulate form. Rajmohan et al., investigated the modeling and optimization of tribological parameters on PEEK reinforced glass fiber composites. In their work the weight percentage of glass fibre content as a categorical factor. An experimental plan of four-factor D-optimal design based on the RSM was employed to carry out the experimental study. The regression model for the responses has been obtained a model adequacy of 95% confidence level. The optimization results indicated PEEK/30 GF composite were preferred to minimize the specific wear rate and coefficient of friction [97]. Ojha et. al. [98], utilized RSM for optimization of input parameters such as fiber concentration, applied load and sliding velocity for abrasive wear of Rice Husk ceramic Reinforced Epoxy Composites. They conducted experiments using full factorial design on pin-on-disc type wear testing machine, against 400 grit size abrasive paper. A second order polynomial model was developed for the prediction of wear loss. The adequacy of the developed model was verified by using analysis of variance (ANOVA) at 95% confidence level and found an acceptable deviation of 7.438%

2.9 Research gaps

The PTFE nanocomposites containing HNTs are not well established in the literature. Therefore, in this study, we have made an attempt to design PTFE nanocomposites containing HNTs as a functional fillers and their thermal and mechanical performance was systematically studied. The remarkable enhancement in the mechanical performance of PTFE nanocomposites containing HNT was realized over neat PTFE. Hence, this study provides critical insights in the designing of PTFE nanocomposites containing HNT with enhanced mechanical performance. From the literature the following points were extracted and the problem has been identified.

1. Most of the work reported on fluoropolymer nanocomposites with different fillers with a target of increasing wear resistance for self-lubrication applications. Also, from the literature it was shown that, decrease in wear rate occurred at the cost of marginal increase in the coefficient of friction. For longer service operations the increase in friction value is not desirable. Only few researchers reported on the mechanical properties of fluoropolymers filled with inorganic fillers.
2. There are many techniques available for mixing of nanofiller in the fluoropolymer matrix material for better dispersion of nanofiller was discussed in literature. The sophisticated blending techniques used for mixing of powders were not commercially viable for the selected application.
3. The effect of filler addition on tribological study for different counter surface roughness values was not actively reported.
4. Most of work was reported on the study of erosion wear characteristics of epoxy based nanocomposites and on thermoplastic nanocomposites.
5. The existing multi-response optimization techniques like Response surface methodology, Taguchi Grey-based techniques are complex and equal weightage to all responses in the optimization process, but not as per the designer requisites. A new hybrid technique to be proposed considering priority based weightage to all responses.

2.10 Problem Definition

A novel ‘green’ PTFE nanocomposites reinforced with HNT has to be fabricate for self-lubricating applications such that it will have multi-functional properties such as high mechanical , thermal, and tribological properties and cost effective as well.

2.11 Research Objectives

1. To fabricate PTFE nanocomposites by dispersing different weight fractions of HNT using high speed pulverizer, cold pressing, followed by sintering cycle (heating and cooling).
2. To study the morphology characterization of the PTFE nanocomposites using XRD and SEM.
3. To study the mechanical behaviour of the PTFE nanocomposites: Tensile test, Flexural test, impact test, and micro-hardness test.
4. To study thermal behaviour of the PTFE nanocomposites subjected to thermal and combined mechanical and thermal loads using Differential Scanning Calorimetry (DSC), Dynamic mechanical analysis (DMA).
5. To study abrasive wear of PTFE nanocomposites, when running against steel counter surface and when running against counter surface fitted with several SiC abrasive grade papers. Erosion wear study of PTFE nanocomposites, when the target surface is hit by accelerated erodent particles.

2.12 Work Plan

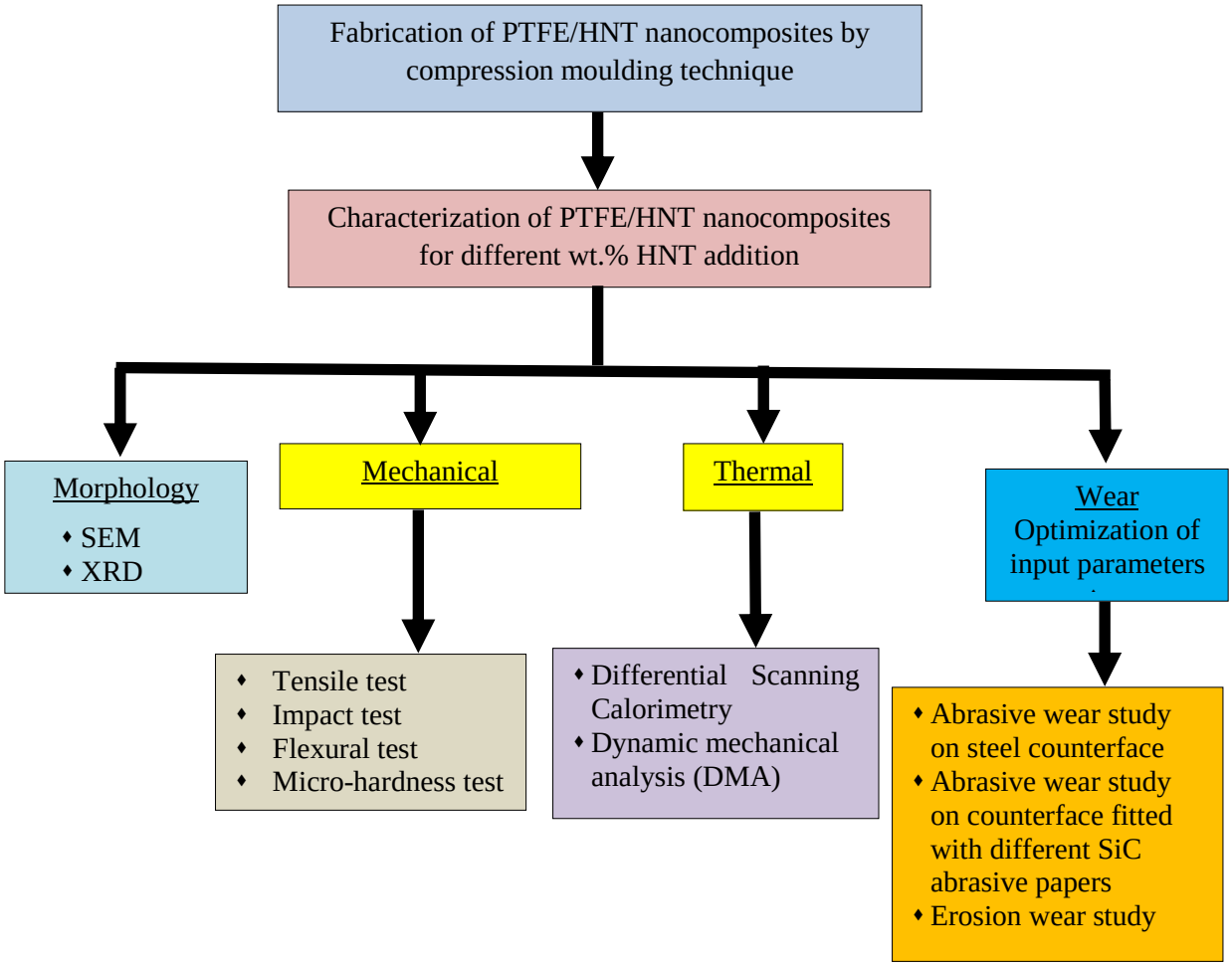

Figure 2.8 Flow chart of work plan

Plan of work

Chapter 3 discusses about the experimental methods used like fabrication of PTFE/HNT nanocomposites, morphology characterization of the PTFE nanocomposites, mechanical property characterization, and thermal property characterization. Compression moulding technique was adopted in the fabrication of nanocomposites. PTFE/HNT nanocomposites were fabricated in the form of sheet of size 300 mmx300 mm x 3.2 mm thickness. Samples were cut from the sheets as per ASTM standard of respective test. X-Ray Diffraction was carried out for the determination of amount of HNT addition in terms of intensity values. Mass density of PTFE/HNT samples was also determined by using density measurement experimental setup. Followed by mechanical properties characterization was carried out from tensile test, flexural

test, impact test, and hardness test. The thermal properties characterization was also carried out from Differential Scanning Calorimetry and Dynamic Mechanical Analysis and several thermal properties were studied.

Chapter 4 discusses about the results and discussion on characterization of PTFE/HNT nanocomposites. Mechanical properties were estimated from tensile test, flexural test, impact test, and hardness test. UTM was utilized and test data was extracted for all samples. Tensile properties such as, yield tensile strength, ultimate tensile strength, Young's modulus, were estimated from the tension test data. A Tensometer was utilized and properties flexural modulus, bending strength were calculated from three point bending flexural test. Instron make impact tester was used and amount of energy absorbed by each sample and thus impact strength was determined from Izod impact test. Notches were cut on the impact test specimens as per ASTM standard by using Instron make notch cutter. Vickers-micro hardness tester was used and hardness of each nanocomposite was estimated in terms of hardness number and converted to MPa. The chapter also discusses about the thermal properties characterization. The characterization is highly essential as the improvement in the properties of nanocomposites were directly related to the changes in thermal and dynamic mechanical properties as well. Thermal related properties like glass transition temperature, melting temperature, crystallization temperature, degree of crystallinity and dynamic mechanical properties like storage modulus, loss modulus, and tan delta were studied. For thermal properties, Differential Scanning Calorimetry (DSC) test and for dynamic mechanical properties, dynamic mechanical analysis (DMA) test were performed. In the chapter the tests procedure, about operating conditions in experimentation part, and the addition of wt. % HNT addition in the PTFE matrix were also discussed under results and discussion.

Chapter 5 discusses wear properties characterization. The ultimate utilization of any PTFE/ filled PTFE components are meant for wear applications. The backbone chapter of the present work was divided into three phases. Phase I deals with multi response optimization of input parameters using a sandwich method. Phase II deals with optimization of input factors for multi-response optimization corresponding to various counter surface roughness values. In this case the counterface is covered with different grades of abrasive papers. Phase III deals with optimization of erosion wear properties of the nanocomposites were studied when the material is struck by a jet of air filled with abrasive particles like sand, at different pressures. In all the

three cases design of experiments concept was utilized in estimating optimum input parameters for minimum wear rate, minimum friction, and minimum erosion wear loss. To enhance the wear resistance of pristine PTFE filler addition is must. Since it was observed from literature, the inclusion of fillers boosts the wear resistance of PTFE. Selection of filler material should be such that it should have less influence on the coefficient of friction while improving its wear resistance or reducing wear rate. Operating parameters like applied load, speed, distance of travel are highly affected by the filler wt. %HNT addition. While, the input factors for erosion wear are different than abrasive wear and are discussed in the third section. In the study the parameters were optimized for objectives namely: minimization of coefficient of friction, minimization of specific wear resistance, and maximization of specific wear energy. The input factors considered for the study were: wt. % HNT, Load, Speed, and Distance. The focus was mainly given on multi-response optimization of input factors by selecting three levels for each input factor. During the process of optimization a sandwich based method (graph theory based utilization approach – Taguchi - Response surface methodology) was followed. These results were validated through RSM and satisfactory optimized input parameters were obtained.

Chapter 6 presents conclusions and scope for future work. The chapter wise end findings of the work were discussed. Also explored the future scope of the work in order to continue research for the selected material combinations to serve the society in a better manner through technological research and development.

CHAPTER - 3
MATERIALS & METHODS

3.1. Matrix material: Polytetrafluoroethylene (PTFE)

PTFE is a white colour thermoplastic crystalline polymer with a density of 2.2 g/cm3. Its T_g and T_m are −20 and 321 °C; respectively. Due to the robust nature of molecular bonds in its structure; PTFE is highly resistive to UV radiation and most of the chemicals except alkali metals and elemental fluorine. It retains these properties over a very wide range of temperatures. The matrix material was selected of INOFLON 640 (moulding grade) for wear applications and procured from Gujarat Fluorocarbons Limited, India.

The properties of the matrix material were as follows:

- Particle size = 20 microns
- Mould shrinkage = 4-5 %
- Specific gravity = 2.14-2.17
- Melting point = 327 ^{0}C- 342 ^{0}C
- Tensile strength at break = 30 MPa
- Elongation at break = 350 %.

3.2 Reinforcement material: Halloysite nanotubes (HNTs)

The selected Halloysite nanotubes (HNTs) filler material was procured from Natural nano Inc., USA. Halloysite powder, as received was suspended in acetone for few hours and dried. The SEM microstructure of the dried HNTs were captured and shown in Fig. 3.1 (a) – (c). Fig. 3.1 (a) & (b) shows the HNTs on 1 micron scale, and 300 nm scale, whereas Fig. 3.1 (c) shows a typical nanoparticle with few microns extended length. The average outer and inner diameters of HNT particles were 30 nm, 50 nm respectively from SEM microstructure.

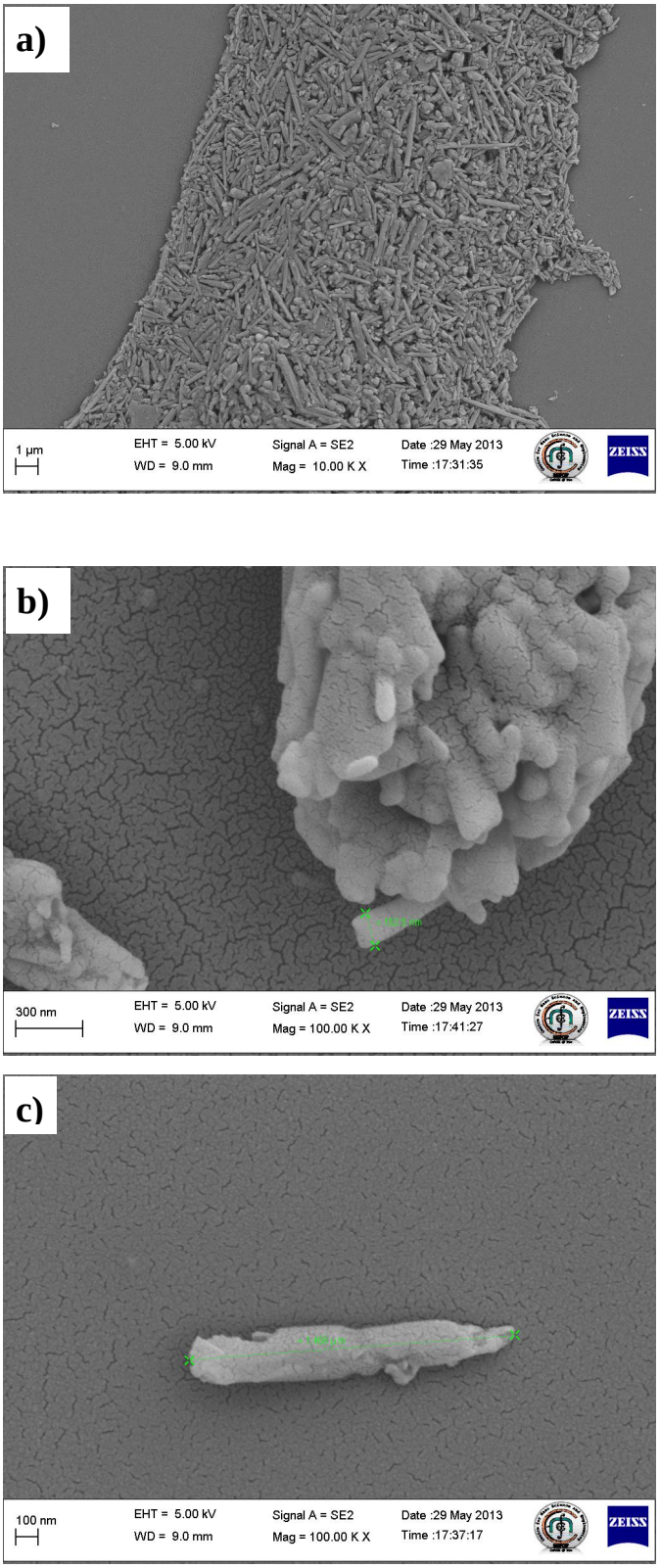

Figure 3.1 Halloysite nanotubes: a) particles have different lengths; b) cluster of particles; c) a typical HNT particle

3.3 Fabrication of PTFE/HNT nanocomposites

3.3.1 Ensemble weight calculation

Ensemble is the mixture of both matrix and filler in powder form. The weight of the ensembles were calculated based on the mould size (Table 3.1). The selected mould size was being 300 mm x 300 mm x 3.2 mm and the density of PTFE material was taken as 2.21 gm/cc.

Table.3.1 Proportions of PTFE and HNTs for making sheets

HNT (wt%)	PTFE material (wt.%)	PTFE material (g)	HNT (g)	Total weight of ensemble (g)
0	100	630	0	630
2	98	617.4	12.6	630
4	96	604.8	25.2	630
6	94	592.2	37.8	630
8	92	579.6	50.4	630
10	90	567	63	630

3.3.2 Description of the apparatus

The pulverizer consists of a high speed rotor as shown in Fig.3.2. The function of the pulverizer is to break the lumps or mix the combined material fed into it. The speed of the rotor is about 10,000 rpm. The material was fed at the top. The agglomerates of PTFE were then broken into fine powder by the high shear action of the rotor. The electronic balance was used for measuring ensemble powders has 0.001g accuracy. The hydraulic press employed for compressing the ensemble in the mould. The sintering oven employed for drying the green products of PTFE or its composites. The PTFE/HNT nanocomposites were prepared at JAYHIND Polymers, Sangli, Maharashtra under the supervision of the author. The heating and cooling cycles for different PTFE grades can be set with the help of programmable PID controller. The heating or cooling operations of the PTFE/PTFE nanocomposite samples were done under nitrogen controlled atmosphere. The maximum operating temperature is about 500 ^{0}C with +/– 1 ^{0}C error.

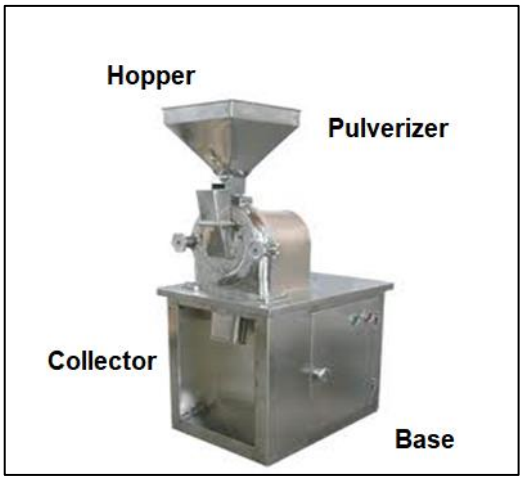

Figure 3.2. Pulverizer used for breaking agglomerates and mixing of the powders

3.3.3 Fabrication procedure

Compression moulding technique followed by sintering is employed for fabricating the PTFE nanocomposite samples (Fig. 3.3 (a)-(e)). At high temperatures the melt creep viscosity of PTFE material is so high and is not suitable for processing it through melt intercalation or injection moulding technique[99]. The PTFE nanocomposite sheets were fabricated in sheets of size 300 mm x 300 mm x 3.2 mm. The sheets were made with 2 wt. % - 10 wt. % and were designated as samples 'A' - 'F'. These were fabricated by following the sequence of steps: (i) production of preforms, (ii) breathing, (iii) sintering, (iv) cooling, and (v) cleaning. The properties of a sample mainly depends up on the following process parameters: preforming pressure, dwell time, sintering time and temperature and the cooling rate. The 'preform' is a compacted sheet/sample, which is made by pressing the premixed ensemble in the mould. An operating pressure of 14 MPa is applied for about 20 min. and later the sheets were ejected out of the mould. The preforms were kept for about 12 h at room temperature as a breathing period in order to relieve any entrapped air or moisture. Subsequently, they were sintered in an electrical furnace as per heating and cooling sintering cycle as shown in Fig. 3.4, for about 8 h hold time at 365^0 C. The preforms were heated to a temperature above the crystalline melting point of the resin during the sintering cycle. The cooling cycle is used to control the crystallinity of the sample. The process was repeated for all the compositions of PTFE nanocomposite samples. Finally, after diagnosing the samples for defects like sintering cracks, bending of sheets, the blur edges of each sample was cleaned by wiping with a medium grade abrasive paper. Later, the specimens were cut from these samples for characterization as per ASTM standards for different tests.

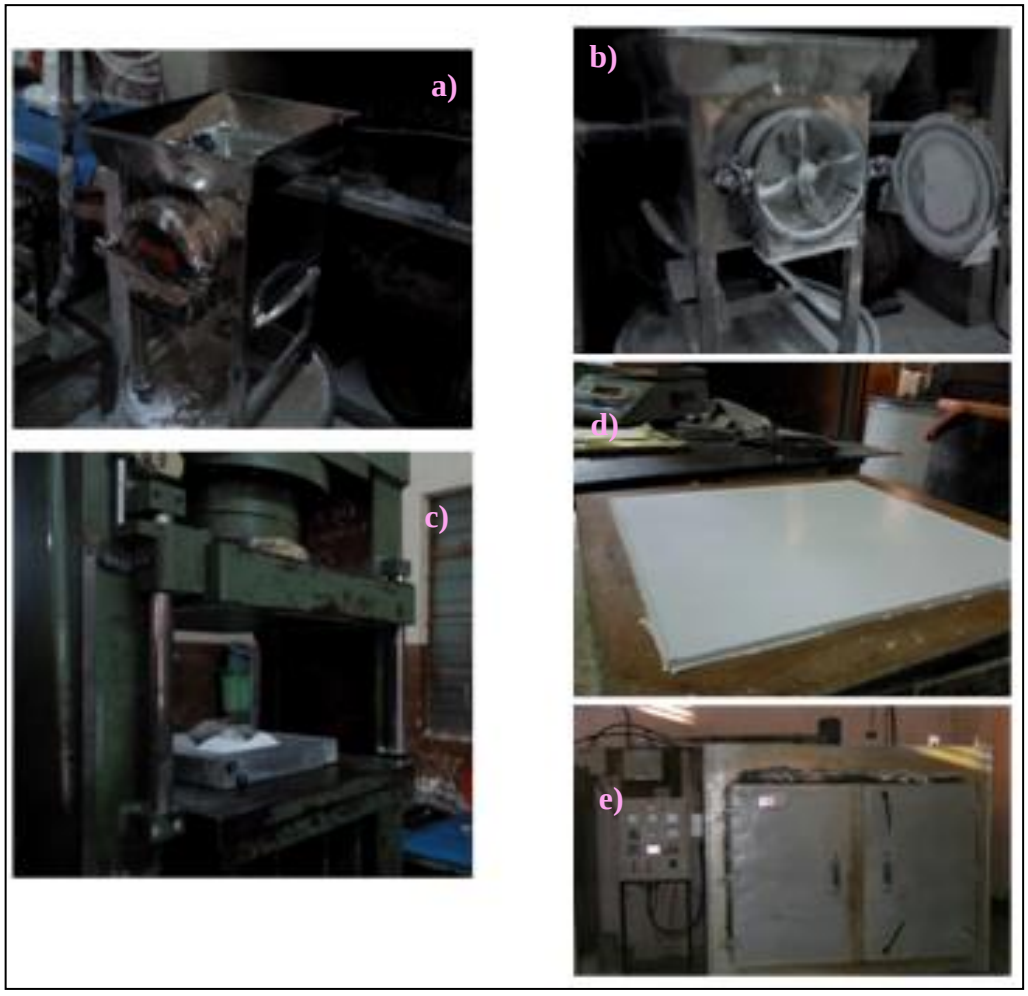

Figure 3.3 (a)-(e) sample preparation steps (mixing, cold pressing, preforming, sintering)

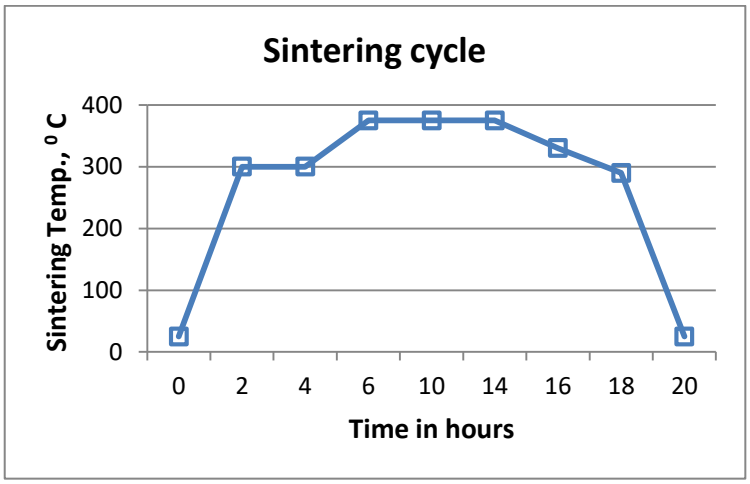

Figure 3.4 sintering cycle: heating - holding - cooling

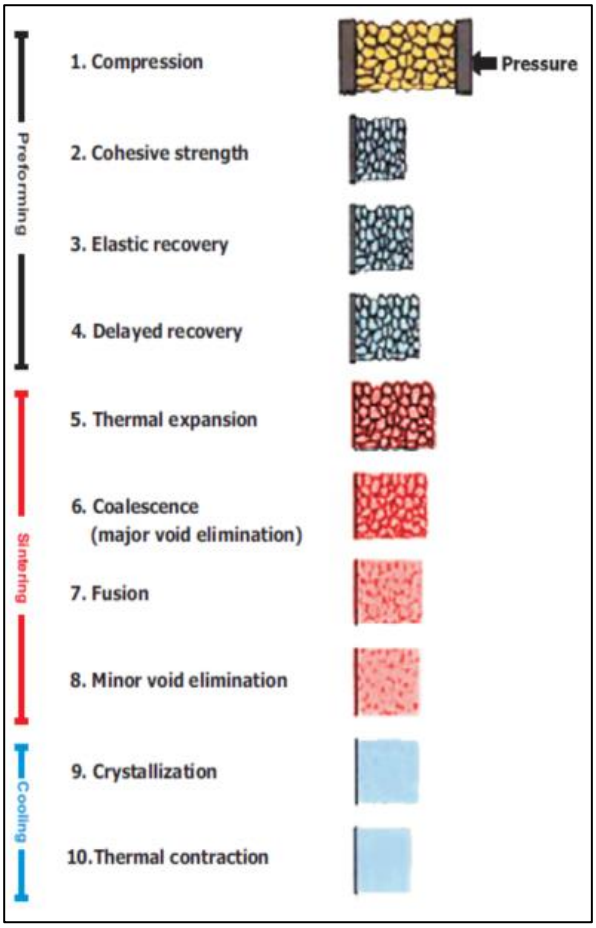

Figure 3.5 Sample preparation steps and micro-structural changes in three stages (performing, sintering (heating), and cooling)

While fabrication of the PTFE/HNT nanocomposite samples the structural changes were briefly depicted in Fig. 3.5. Stages 1-4 shows delayed recovery after compression or compaction of the powders in the mould. The green stock with good cohesive strength which was removed from the mould was left in still air for 24 hours helps in escaping the entrapped air. The sintering process was initiated in the oven and was programmed as per the manufacturer's catalogue. In the oven as the temperature was increasing gradually, at first thermal expansion in the sample occurs and later melting and mixing take place at hold temperature (360^0 C) and also eliminates if any voids at the interfaces (Stages 5-8). As the temperature decreases during cooling, crystallization starts simultaneously at different locations of reinforcement. After reaching to room temperature thermal contraction of the samples take place. Finally, the samples were designated as follows: A: 0 wt.% HNT; B: 2 wt.% HNT; C: 4 wt.% HNT; D: 6 wt.% HNT; E: 8 wt.% HNT; F: 10 wt.% HNT.

3.4 Density Measurement by using Specific Gravity meter

An electronic specific gravity meter (KUDALE INSTRUMENTS) was used to measure the specific gravity of PTFE/HNT nanocomposite samples. ASTM D 792-98 standard is used for specific gravity and density measurement of PTFE/HNT nanocomposites.

Description of the apparatus

The apparatus can measure specific gravities ranging from 0.9 to 25 and has a least count of 0.0001 is used. The Digital Read-Out (DRO) display shows directly the specific gravity of the sample. It consists of Cast Iron structure along with a beaker holder to mount the specimen to be tested. Because of hydrophobic nature of PTFE and PTFE/HNT nanocomposites, the specific gravity of PTFE/HNT nanocomposite samples were measured by using solid sample testing in 'water option' [100]. The procedure to calculate the specific gravity and density measurements were done based on [101].

3.5 Morphological study

X-Ray Diffraction and Energy Dispersive X-Ray Spectroscopy were carried out for the determination of amount of HNT addition in terms of intensity values as follows:

3.5.1 X-ray diffraction (XRD) study

XRD technique was used to study the crystal structure of materials. It produces a diffraction pattern, in the form of sharp peaks and amorphous regions result in broad halos that reveal arrangement of reinforcement particles in the matrix material. The diffraction pattern of polymers usually contains a combination of both. The degree of crystallinity of nanocomposites can be estimated by integrating the relative intensities of the peaks and halos [102]. Figure 3.6 shows a PANalytical X'Pert PRO diffractometer. The working principle of Goniometer is, it collects the intensity value of the sample which was counted in arbitrary units by the counter corresponding to the rotation of sample (2θ), while it was being struck by the X-ray beam in the chamber [103]. The XRD patterns for the nanocomposite samples ('A' – 'F'), were scanned from 10^0 to 50^0; in steps of 0.02^0, and integration time of 0.5 s.

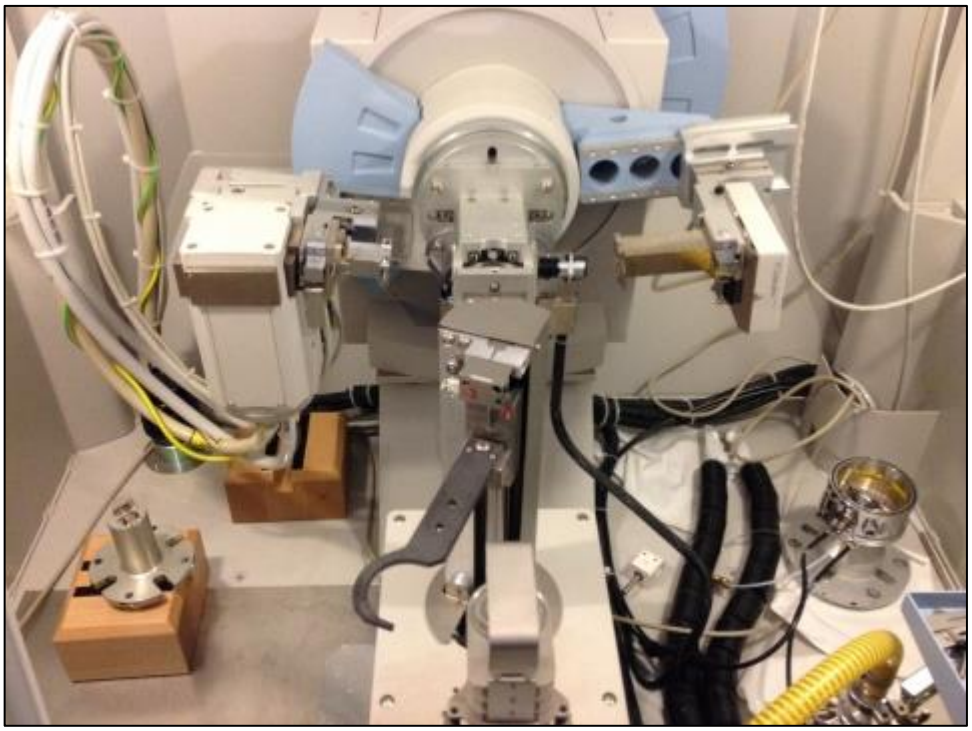

Figure 3.6 PANalytical X'Pert PRO diffractometer

3.5.2 Energy Dispersive X-Ray Spectroscopy (EDX)

EDX system is an attachment to Scanning Electron Microscope instruments (SEM), where the imaging capability of the microscope identifies the specimen of interest. SEM provides detailed high resolution images of the sample by rastering a focussed electron beam across the surface and detecting secondary or backscattered electron signal. Thus, by measuring the amounts of energy present in the X-rays being released by a specimen during electron beam bombardment, the identity of the atom from which the X-rays was emitted can be established.

3.6 Thermal properties study

The change in mechanical and other properties of any composites mainly depends on degree of crystallinity of the material. DSC and DMA tests were conducted on all the specimens. The degree of crystallinity of the PTFE/HNT nanocomposites was estimated based on the procedure described by Chan et. al. [104]

3.6.1 Differential Scanning Calorimetry (DSC)

METTLER-TOLEDO Differential Scanning Calorimeter (DSC 822e) with STAR e software was used for measuring the thermal transitions of PTFE/HNT nanocomposites. It can estimate the glass transition temperature, melting point of a PTFE nanocomposites by measuring the heat flow difference between the sample and reference. Differences in heat flow arise when a

sample absorbs or releases heat due to thermal effects such as melting, crystallization, chemical reactions, and polymorphic transitions. Fig. 3.7 shows the DSC test set up used for conducting the test.

Figure 3.7 METTLER-TOLEDO (DSC 822e) setup

The heat of fusion *(mJ/mg)* of the nanocomposites is estimated by measuring the area of heating peaks. The degree of crystallinity or % crystallinity denoted by $\% X_c$, is defined as:

$$\% X_c = \frac{Area\ of\ the\ melt\ endotherm, (\Delta H_f)}{Theoritical\ heat\ of\ fusion, (\Delta H_{100f})}$$

For semi-crystalline polymers without filler, the degree of crystallinity can be calculated by using equation (3.1).

$$\% X_c = \frac{\Delta H_f}{\Delta H_{100f}} \times 100 \tag{3.1}$$

For different wt.% addition of HNT in the matrix material, the % Crystallinity can be estimated by using equation (3.2)[105].

$$\% X_c = \frac{\Delta H_f}{\Delta H_{100f}(1 - w_t)} \times 100 \tag{3.2}$$

Where, ΔH_f = area of the melt endotherm in J/g; ΔH_{100f} = heat of fusion for a 100% crystalline PTFE sample; w_t = wt% of HNT. Assuming the crystallinity of pure PTFE matrix material is 83 J/g [5].

3.6.2 Dynamic Mechanical Analysis (DMA)

Many materials, including polymers, behave both like an elastic solid and a viscous fluid, thus the term viscoelastic. DMA differs from other mechanical testing devices in two important

ways. First, simple tensile test devices focus only on the elastic component of the material. In many applications, the inelastic, or viscous component, is critical as it determines properties such as impact resistance. Second, tensile test devices work predominantly outside the linear viscoelastic range. Whereas DMA works mainly in the linear viscoelastic range and is therefore more sensitive to the structure. DMA measures the viscoelastic properties using either transient or dynamic oscillatory tests [106]. The most common test is the dynamic oscillatory test, where a sinusoidal stress is applied to the material and a sinusoidal strain is measured. Hence, by using DMA, properties such as, the storage modulus and loss modulus of polymers/composites can be investigated under the action of dynamic oscillatory (sinusoidal type) loads [107].

The response of the polymer is dependent on both temperature and time. The storage modulus is a measure of stiffness whereas loss modulus is a measure of degree of damping present in the system. The phase difference known as phase lag, between the two sine waves is then measured. The phase lag will be zero degrees for purely elastic materials and 90 degrees for purely viscous materials. Polymers will exhibit an intermediate phase difference [108]. Due to the application of sinusoidal loads, the elastic modulus exhibited by the material decreases over a period of time because of the molecular rearrangement in an attempt to minimize localized stresses. The method is also useful for characterizing the glass transition temperatures of polymer materials. DMA can identify small transition regions that are beyond the vicinity of DSC.

Figure 3.8 Perkin Elmer make Dynamic Mechanical Analysis setup

A Perkin Elmer DMA 7e was used to investigate the dynamic mechanical properties of PTFE/HNT nanocomposites. The parameters, E', the storage modulus is the elastic component and related to the samples stiffness. E", the loss modulus, is the viscous component and is related to the samples ability to dissipate mechanical energy through molecular motion. The tangent of phase difference, or Tan delta, is another common parameter that provides information on the relationship between the elastic and inelastic component. Figure 3.8 shows Perkin Elmer, USA, DMA set-up used for testing the PTFE/HNT nanocomposite samples.

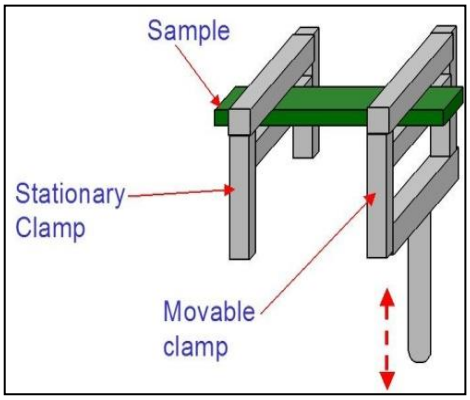

Figure 3.9 Single cantilever dynamic mode of load on the PTFE/HNT samples in DMA test

Test Description

The viscoelasticity of the PTFE/HNT nanocomposite samples were measured by DMA (ASTM D7028 - 07(2015)). The samples are deformed periodically at a frequency of 1Hz over a varying temperature from 30^0 C to 200^0 C with oscillation amplitude of 15µm, which is in the linear viscoelastic regime. The measurements were done by using a single cantilever test clamp as shown in Fig. 3.9, which is more suitable for thermoplastic materials.

Test parameters

Clamp used: single cantilever

Operation mode: multi-stress/strain mode (Dynamic mode)

Frequency: constant frequency = 1 Hz

Temperature ramp input = 3^0 C/ min

Temperature range= room temperature to 250 ^{0}C

The specimens were cut to the required length with rectangular cross section (63.00 mm×13 mm×3.26 mm), as shown in Fig. 3.10. Before conducting the test, the section dimensions were measured with Vernier and micrometre and were recorded.

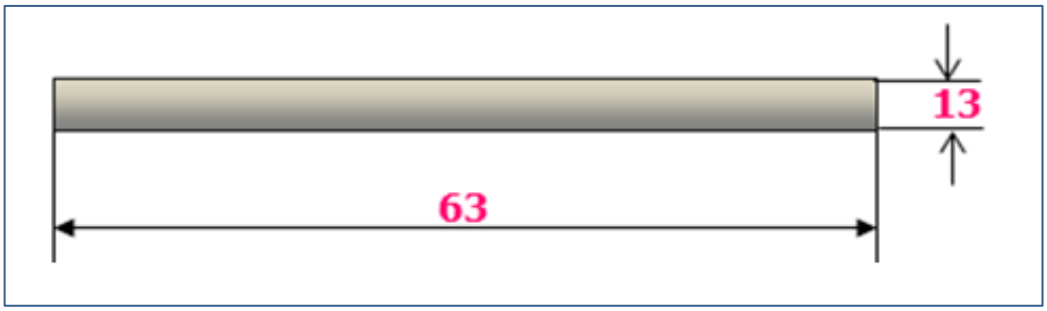

Figure 3.10 Test specimen

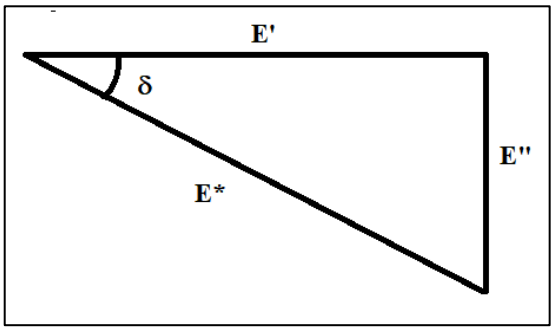

Figure 3.11 Moduli triangle

From figure 3.11:

Storage modulus is the energy stored elastically during deformation

$$E' = E^* \times cos\ \delta \tag{3.3}$$

Loss modulus is the energy loss during deformation,

$$E^{"} = E^* \times sin\ \delta \tag{3.4}$$

where, E^* = Complex dynamic modulus $= E' + i\ E"$

Loss tangent or loss factor is a measure of damping of the material and it shows the ability of material to dissipate the energy

$$Tan\ \delta = \frac{E"}{E'} \tag{3.5}$$

The values of storage modulus, loss modulus and tan delta are calculated by equations (3.3) - (3.5). Figure 3.11 shows the relation between the storage modulus and loss modulus with phase angle ' δ'

3.7 Mechanical Property Characterization

Mechanical properties were estimated from tensile test, flexural test, impact test, and hardness test as per ASTM standards. Three to five samples were used and the results were

averaged. UTM was utilized and test data was extracted for all samples. Tensile properties such as, yield tensile strength, ultimate tensile strength, Young's modulus, were estimated from the tension test data.

3.7.1 Tensile test (ASTM D638)

The tensile test method is used to determine tensile properties such as yield tensile strength, break tensile strength, and Young's modulus of PTFE/HNT nanocomposites when tested under defined standard conditions like laboratory room temperature, humidity, testing machine speed and environment conditions of testing. Tensile properties may provide useful data for newly developed materials for design purpose. However, because of the high degree of sensitivity exhibited by PTFE nanocomposites to rate of straining and environmental conditions, data obtained by this test method cannot be applicable for applications involving load-time scales.

Figure 3.12 INSTRON 5967 tensile testing machine: test specimen fitted with extensometer

Specifications:

Model –INSTRON 5967

Maximum Load capacity: 30 kN

Speed range: 0.001 mm/min to 1000 mm/min

Total crosshead travel: 1140 mm

Vertical test space: 1212 mm

Column spacing: 418 mm

Footprint dimensions: 163 cm height x 78 cm base width x 73 cm base depth

Measurement accuracy: ± 0.5% of reading

Data acquisition rate: up to 2.5 kHz

Test description

Mechanical characterization was conducted using the Instron 5967 as shown in Fig.3.12. Samples for mechanical testing are created using the standard processing procedures outlined in the standard ASTM D 638 of type I for many types of plastics. Following compression moulding, the PTFE/HNT nanocomposite samples are machined to the shape by using high speed fine sawing machine for consistent sample dimensions. The sample is gripped and the pulling force can only be achieved through friction at the clamp interface. The tensile ASTM D 638 specimen dimensions were shown in Fig. 3.13. The final dimensions provide a factor of safety of two to ensure that the clamp does not slip during the test. The corners of the dog bone are relieved such that the shape provides a well-defined tensile section in the centre of the sample where strain can occur without significant stress concentration. The tensile test was carried out on all formulations of PTFE/HNT nanocomposite samples (Figure 3.14). The values of stresses and strains can be calculated from equations (3.6) and (3.7)

The calculations of these quantities are as follows,

$$\sigma = \frac{F}{h \times w} \tag{3.6}$$

$$\varepsilon = \frac{l - l_0}{l_0} = \frac{\Delta l}{l_0} \tag{3.7}$$

where, σ is the stress, F is the axial force, h is the sample height, w is the sample width, ε is the engineering strain, l is the length during loading and l_0 is the original sample length.

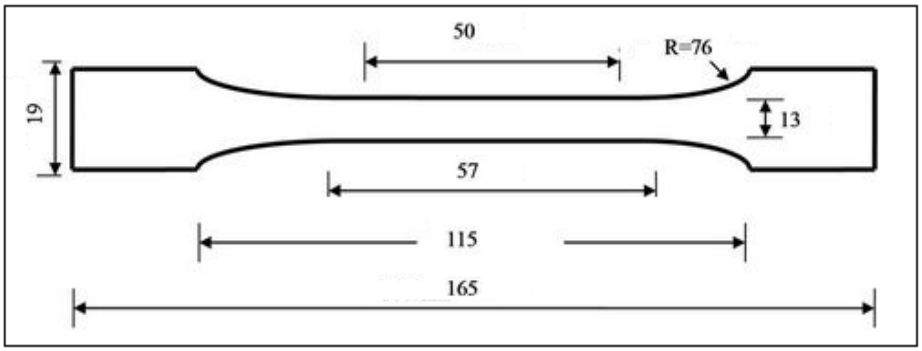

Figure 3.13 Tensile test specimen: dimensions as per ASTM standards

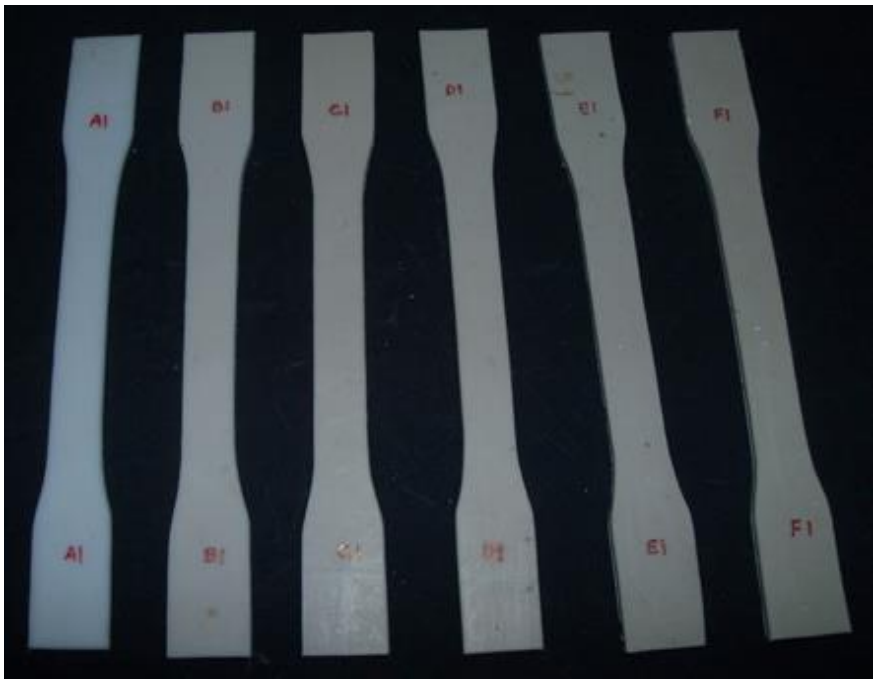

Figure 3.14 Tensile test samples of PTFE/HNT nanocomposite with varying wt. % HNT addition

3.7.2 Impact test (ASTM D256)

Impact tests are used in studying the toughness of material. A material's toughness is a factor of its ability to absorb energy during plastic deformation. Ductile materials have high toughness as a result of the large amount of plastic deformation that they can endure. The impact value of a material can also change with temperature. Generally, at lower temperatures, the impact energy of a material is decreased due to ductile to brittle transition. Also, parameters like size of the specimen, defects or imperfections in the material, will greatly affect the impact energy. The available test methods are Izod, and Charpy methods. For testing plastics or its nanocomposites Izod test was selected as polymers absorb moderate energy.

Apparatus Description

Instron make pendulum type tester was used to measure the impact energy absorbed by PTFE nanocomposites samples (Figure 3.15 (a)). The machine is a table top type mounted on a rigid frame. The pendulum was mounted on bearings allowed to swing freely with negligible friction and it may be of simple or compound pendulum type. The effective length of the pendulum is about 0.4 m, one end is mounted on to the bearings and other end is provided with a striker. The striker of the pendulum is made of hardened steel and has some provision to fix the weight. The position of the pendulum holding and releasing mechanism is held at a height of 610 mm and produce a velocity of the striker at the moment of impact is about 3.5 m/s.

Figure 3.15 (a) Impact Testing Machine; (b) Notch cutter

Impact tester specifications:

Model no: 7614.000 - Ceast (Italy)

Hammer capacity: 0.5J to 50 J

Fixture: Charpy, Izod

Angular encoder resolution:0.05”

Braking system: Hammer disc brake system

Cryobox: conditioning of specimens for sub-zero tests

cooling system: liquid nitrogen

Temperature range: ambient to – 60^0 C

High resolution data acquisition system

There are four types of failure, when a specimen is tested for impact strength.

1. C: completer break – the specimen breaks completely and separates into two pieces.
2. H: hinge break – an incomplete break, the free part above the notch bends with less than 90^0 included angle while the lower fixed part remains vertical.
3. P: partial break – an incomplete break, with 90% of distance from the notch is fractured
4. NB: non-break - an incomplete break, with less than 90% of distance from the notch is fractured

Since the PTFE samples are more ductile in nature, the sample do not fail under sudden impact load. So, all the samples were prepared with notches. A standard INSTRON notch cutter (Figure 3.15 (b)) was utilized and standard notches were cut on each sample as shown in Fig. 3.16.

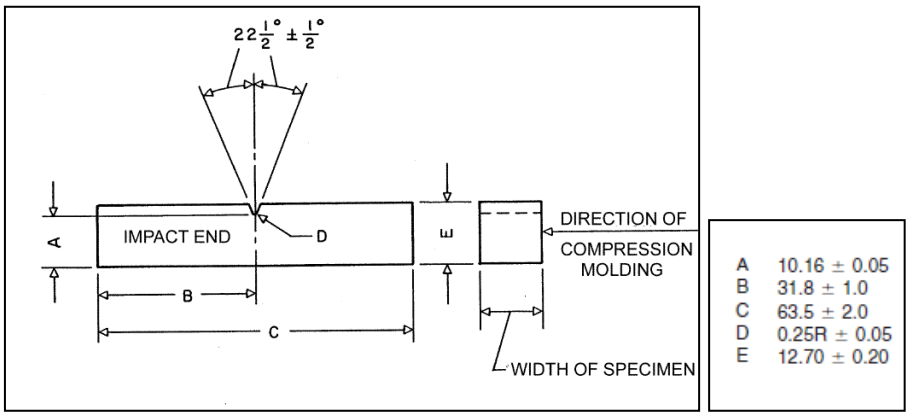

Figure 3.16 Impact test specimen dimension used for PTFE/HNT nanocomposite samples

The force signal during impact will be acquired through a strain-gauge circuit, which is located inside the striker body. The deformation coming on the striker during impact will be read by a suitable data acquisition system as an electric signal, which is further transformed into a force value.

3.7.3 Flexural test (ASTM D 790)

Flexure test method determines the flexural properties (including flexural stress, flexural strength, flexural strain, modulus of elasticity, and load/deflection behaviour) of PTFE/HNT nanocomposites. The test method utilize a three-point loading system applied to a simply

supported beam i.e., the bar rests on two supports and is loaded by means of a loading nose midway between the supports as shown in Fig. 3.17 (b).

Apparatus Description

The flexural properties were studied by conducting three point bending test on a Tensometer (see Figure 3.17 (a)). The ASTM D 790 flexure test specimen was made of rectangular cross section with dimensions as shown in Fig. 3.18, was loaded by means of a loading nose midway between the supports. A special fixture was used for the purpose and tests are conducted on a Tensometer. Since the specimen do not rupture in the outer surface and hence according to the test procedure a maximum strain of 5.0 % is considered as failure point. The test was stopped once the maximum value of strain is reached.

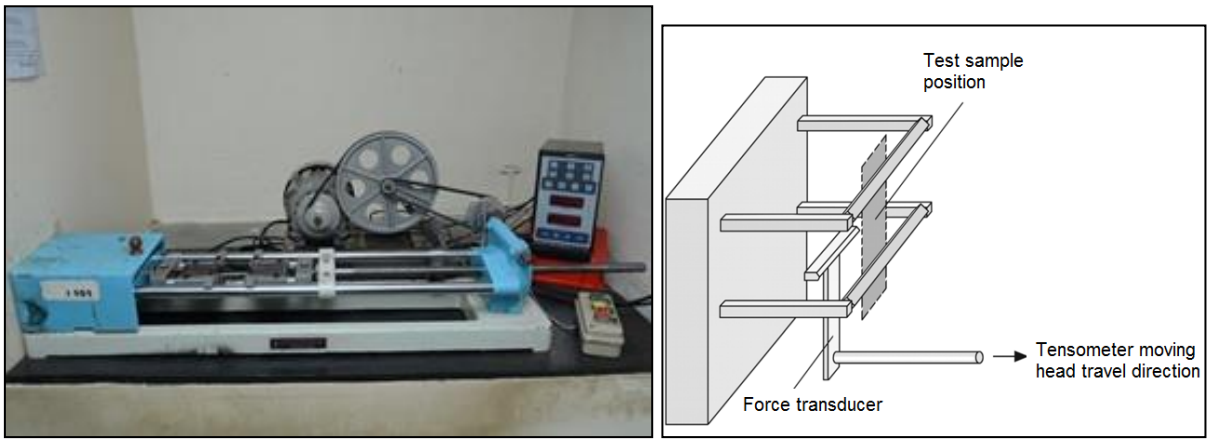

Figure 3.17 (a) Tensometer; (b) three point bending test fixture

Test parameters:

Speed of Testing: speed of testing considered for the test is at a rate of crosshead movement of 0.1 mm/mm/min.

Force application: Force applied to the specimen and resulting specimen deflection reaches a strain of 0.05 mm/mm. The predetermined value of deflection is considered as the failure criterion, as the PTFE /HNT nanocomposites are highly flexible and do not fail under the load.

Deflection Measurement: Specimen deflection at the common centre of the loading span is measured by a properly calibrated device. The device has an electronic controller that increments the load on the specimen automatically by some initial settings. The display controller displays continuously the readings of deflection in ‘mm’ and applied load in ‘N’.

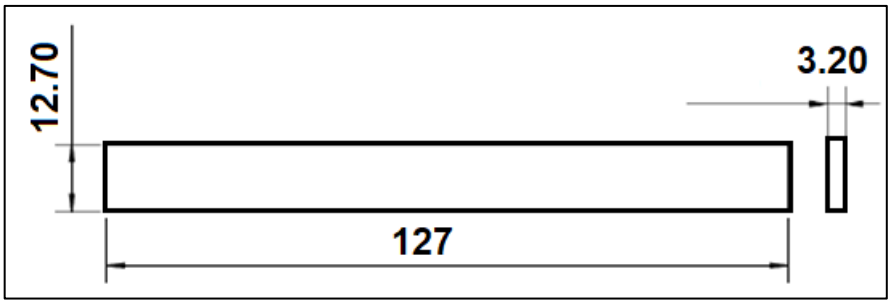

Figure 3.18 Three point bending test specimen along with standard dimensions

The rate of crosshead motion is calculated by using equation (3.8) and the machine is set to run for the calculated rate of crosshead motion.

$$R = \frac{ZL^2}{6d} \tag{3.8}$$

where,

R = rate of crosshead motion, mm/min,

L = support span, mm,

d = depth of specimen, mm, and

Z = rate of straining of the outer fiber, mm/mm/min ,

Z = 0.01

Flexural Stress (sf) While calculating the flexural stress the same hypothesis of homogeneous elastic material is used for all PTFE nanocomposites specimens. For a simply supported beam loaded at the midpoint, the maximum stress in the outer surface of the test specimen occurs at the midpoint. This stress can be calculated for any point on the load-deflection curve by using equation (3.9)

$$\sigma_f = \frac{3PL}{2bd^2} \tag{3.9}$$

where

σ_f = stress in the outer fibres at mid-point, MPa,

P = load at a given point on the load-deflection curve, N,

L = support span, mm,

b = width of specimen tested, mm, and

d = depth of specimen tested, mm.

Flexural strength is defined as maximum flexural stress sustained by the test specimen during a bending test. Since PTFE/PTFE nanocomposites do not break at strains of up to 5 % may give a load deflection curve that shows a point at which the load does not increase with an increase in strain, that is, a yield point. The flexural strength can be calculated for these materials by letting P of equation (3.4) equal to the corresponding load value at yield point (P_y). Flexural strength of the nanocomposites is calculated by using equation (3.10)

$$\sigma_{fs} = \frac{3\,P_y L}{2bd^2} \tag{3.10}$$

where

σ_{fs} = Flexure stress, MPa,

P_y = load at a given point on the load-deflection curve, N,

L = support span, mm,

b = width of specimen tested, mm, and

d = depth of specimen tested, mm.

Flexural Strain is defined as nominal fractional change in the length of an element of the outer surface of the test specimen at mid-span, where the maximum strain occurs. It may be calculated for any deflection using Equation (3.11)

$$\varepsilon_f = \frac{6Dd}{L^2} \tag{3.11}$$

ε_f= strain in the outer surface, mm/mm,

D = maximum deflection of the centre of the beam, mm,

L = support span, mm, and

d = depth/thickness, mm.

Modulus of Elasticity (Tangent Modulus of Elasticity): It is defined as the ratio, within the elastic limit, of stress to corresponding strain. It is calculated by drawing a tangent to the steepest initial straight-line portion of the load-deflection curve and using Equation (3.12)

$$E_B = \frac{L^3 m}{4bd^3}$$

(3.12)

where,

E_B = modulus of elasticity in bending, MPa,

L = support span, mm,

b = width of specimen tested, mm,

d = depth of specimen tested, mm, and

m = slope of the tangent to the initial straight-line portion of the load-deflection curve, N/mm

3.7.4 Vickers's Micro-hardness test (ASTM E384)

Hardness, although empirical in nature, can be correlated to tensile strength for many materials, and is also an indicator of wear resistance, toughness and ductility. In this test method, a hardness number is determined based on the formation of a very small indentation by application of a relatively low force. The size of the indentation is measured using a light microscope equipped with a filar type eyepiece. It is assumed that elastic recovery does not occur when the indenter is removed after the loading cycle, that is, it is assumed that the indentation retains the shape of the indenter after the force is removed. The indenter shall contact the specimen at a velocity between 15 and 70 μm/s.

Figure 3.19 Vickers's Micro-hardness tester (SHIMADZU make)

Specifications:

- Model : HMV-G20S (E,230V)
- Test modes: Vicker's, Knoop, Brinell, and Triangular Pyramid Indentation Tests
- Test input controls: the test force and indentation duration time
- Pre-set forces range: 98.1 mN to 19.6 N (9 values)
- A 40x objective lens for indentation size measurement
- Electromagnetic force control
- Multi turret
- Indenter type: Dual Indenters and lens
- Load resolution:9.81 mN

Apparatus Description

The micro-hardness test was conducted on all PTFE/HNT nanocomposite samples by using Vickers microhardness tester as shown in Fig. 3.19. The indenter of the tester is of square based pyramidal shaped diamond type and the face of the diamond makes an angle of 136^0 with horizontal. In the Vickers micro-hardness test, a force of about 100 g is applied gradually, without impact, and held in position for 10 to 15 seconds. After removing the force, both diagonals were measured (see Fig. 3.20) and the average is used to calculate the Vicker's Hardness (HV) number (equation (3.13)).

HV= force applied/ surface area of the permanent impression

And simplified as

$$HV = \frac{1854.4 \times P}{d^2} \tag{3.13}$$

where, *P*= applied load, gf

D= mean diagonal length of the indentation, micrometres

From the above equation, it is understood that the hardness value depends up on the size of diagonal.

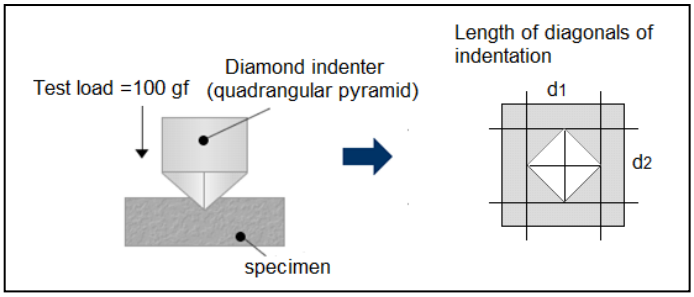

Figure 3.20 Indentation shape on the surface after release of load

3.8 Wear characterization

The eventual utilization of PTFE/HNT nanocomposites are intended for dry lubrication applications. The wear chapter of the present work was divided into three phases. First phase deals with multi response optimization of input parameters using a sandwich method based on Graph Theory Matrix Approach (GTMA). Second phase deals with optimization of input factors for multi-response optimization corresponding to various counter surface roughness values. In this case the counter face is covered with different grades of SiC abrasive papers. Third phase deals with erosion wear. The erosion wear properties of the nanocomposites are studied when the material is struck by a jet of air filled with abrasive particles like sand at different pressures. In all the three phases, design of experiments concept is utilized in estimating optimum input parameters for minimum wear rate, minimum friction, and minimum erosion wear loss. To enhance the wear resistance of pristine PTFE filler addition is must. Since it was observed from literature, the inclusion of fillers boosts the wear resistance of PTFE. Selection of filler material should be such that it should have less influence on the coefficient of friction while improving its wear resistance or reducing wear rate. Operating parameters like applied load, speed, distance of travel are highly affected by the filler wt. % addition. While, the input factors for erosion wear are different than abrasive wear and are discussed in the third phase. The wear analysis of PTFE/HNT nanocomposites were discussed in Chapter 5.

CHAPTER - 4

RESULTS AND DISCUSSION

4.1 Morphology characterization

Morphology characterization of PTFE/HNT nanocomposite samples were conducted in order to know the morphological structure, inter laminar spacing, degree of crystallinity, and the level of dispersion of HNTs in the PTFE matrix. The properties were studied by conducting XRD, and SEM on the samples.

4.1.1 X-Ray Diffraction

X-ray diffraction curves of the studied samples were characterized by diffraction peaks of crystalline structures of PTFE matrix and nanofillers as well as regions of amorphous halo (Fig.3.11 (a) & (b)). Table 4.1 shows the estimated parameters like d-spacing and degree of crystallinity for PTFE Nanocomposite with wt.% of HNT ranging from 0-10%, in which d-spacing was estimated by using Bragg's equation (4.1) and degree of crystallinity was estimated from Fig. 4.1.

$$n\lambda = 2\, d_{hkl}\, \sin\theta \tag{4.1}$$

where, n = order of diffraction = 1,

λ = wave length of the characteristic X-ray = 1.24 Å

d_{hkl} = interplanar spacing of crystal planes = d-spacing

θ = X-ray incidence angle (Bragg angle)

Table. 4.1 XRD results of PTFE/HNT nanocomposites

PTFE nano-composite	peak position [2Theta]	Intensity (counts)	d-spacing Å	Degree of crystallinity	Density gm/cc
A- 0%	-	-	-	51.55%	2.210
B – 2%	12.38	1826	7.14	70.37%	2.243
C – 4%	12.31	1979	7.18	76.34%	2.257
D – 6%	12.31	2182	7.18	70.98%	2.259
E – 8%	12.27	2451	7.21	75.77%	2.262
F – 10%	12.31	2487	7.18	76.16%	2.265

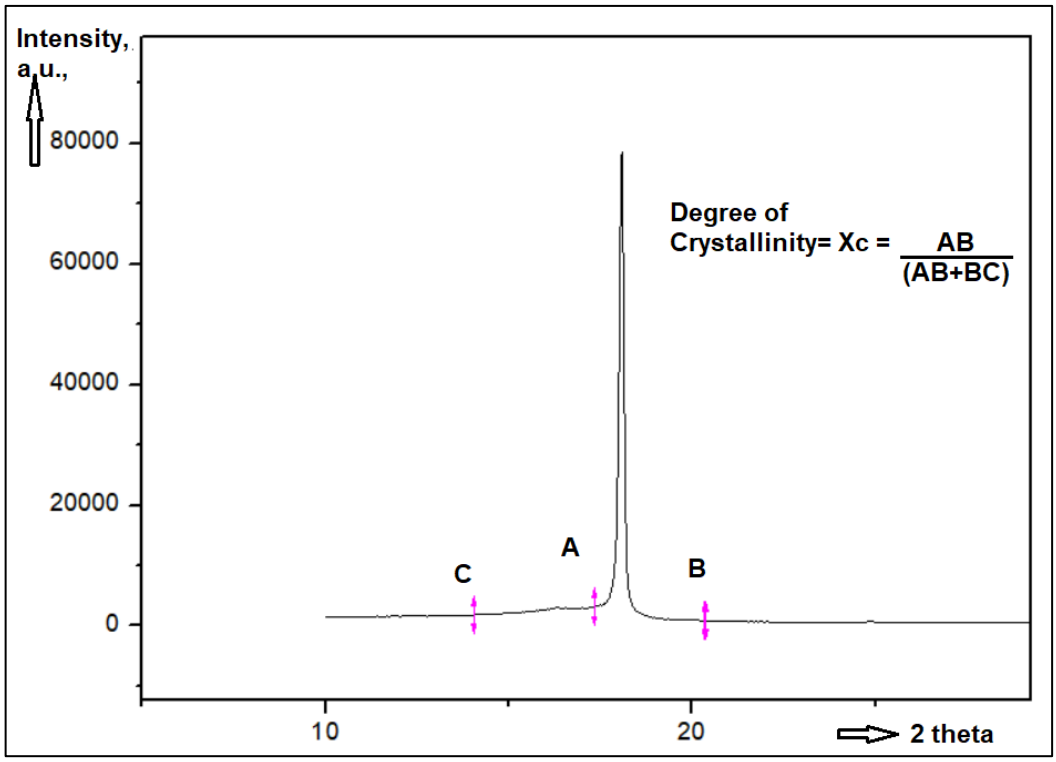

Figure 4.1 Calculation of degree of crystallinity of PTFE/HNT nanocomposites by integrating the area under the peaks and halos (expressed in terms of intensity units)

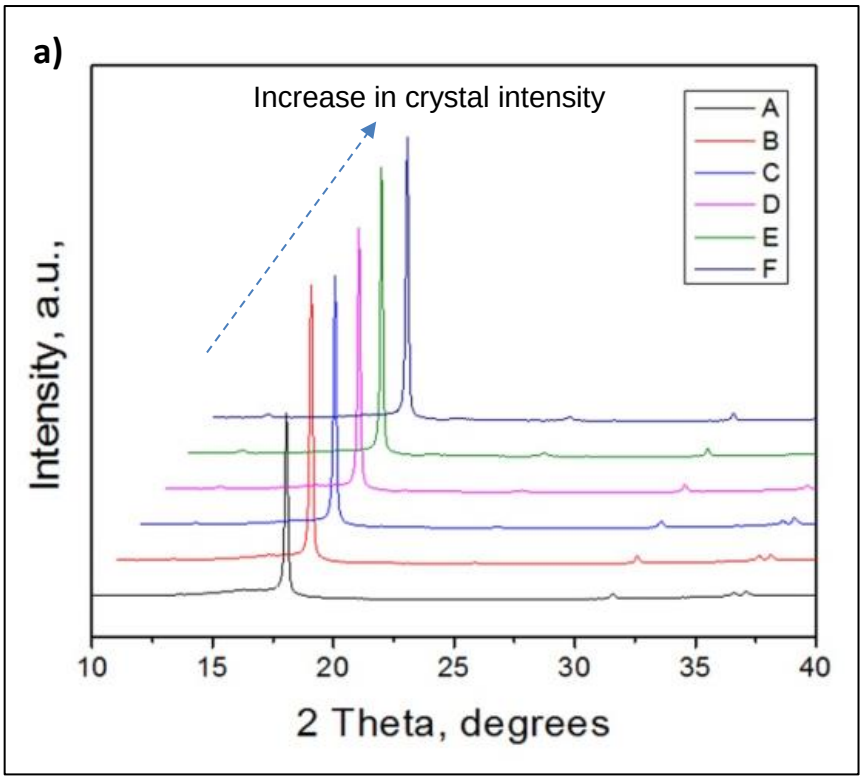

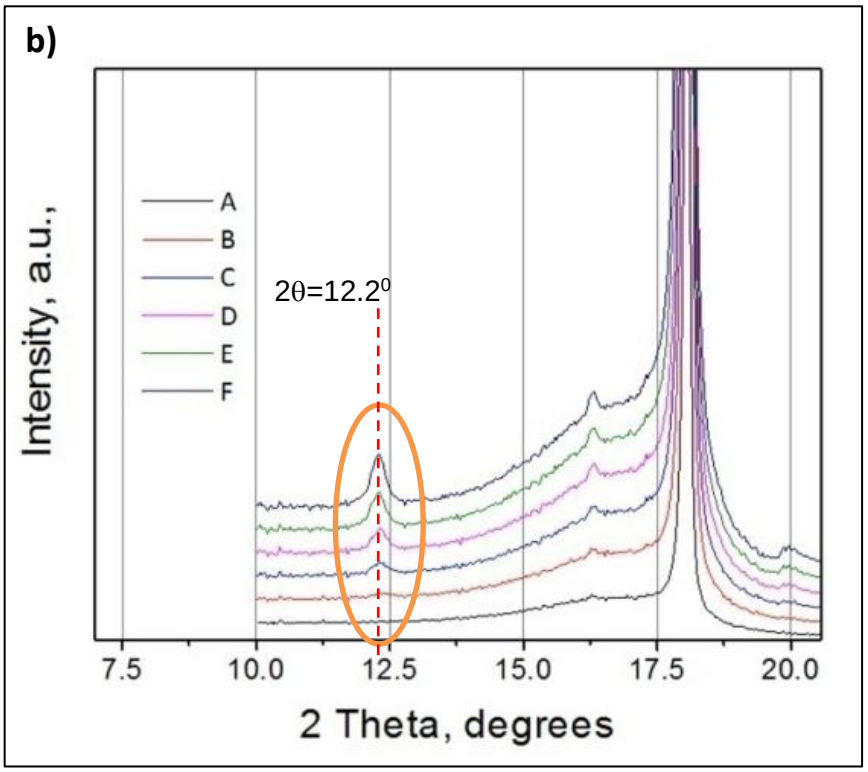

Figure 4.2 XRD spectra of PTFE/HNT nanocomposite samples: a) crystalline peaks; b) Increase in peak intensity due to wt. % HNT addition in the PTFE matrix, at $2\theta = 12.2^0$

From the XRD plots shown in Fig. 4.1, an in increase in the crystalline intensity was observed with the addition of wt.% HNT in the PTFE matrix. Also, from Fig. 4.2, a new peak was generated due to the presence of wt. % of HNT in the PTFE matrix at $2\ \theta$ of 12.2^0.

4.1.2 SEM microstructure of PTFE/HNT Nanocomposites

The uniform dispersion of HNT nanofiller in PTFE matrix can be seen from SEM microstructures (see Figure 4.3 (a)). The type of dispersion in the PTFE matrix material resulted was an intercalation type whereas, the SEM plot (Fig. 4.3 (b)) depicts different lengths of HNTs. Further, the data generated by EDX analysis consist of spectra showing peaks corresponding to the elements making up the true composition of the sample being analysed. In Fig. 4.4, the spectrum shows a PTFE/HNT nanocomposites sample at 4 wt. % of HNT. The elements presented in the spectra were carbon (C) and fluorine (F) associated with PTFE matrix material, Aluminium (Al) and Silicon (Si), elements of Halloysite nanotubes and gold (Au) refers to gold sputtering coating on the sample.

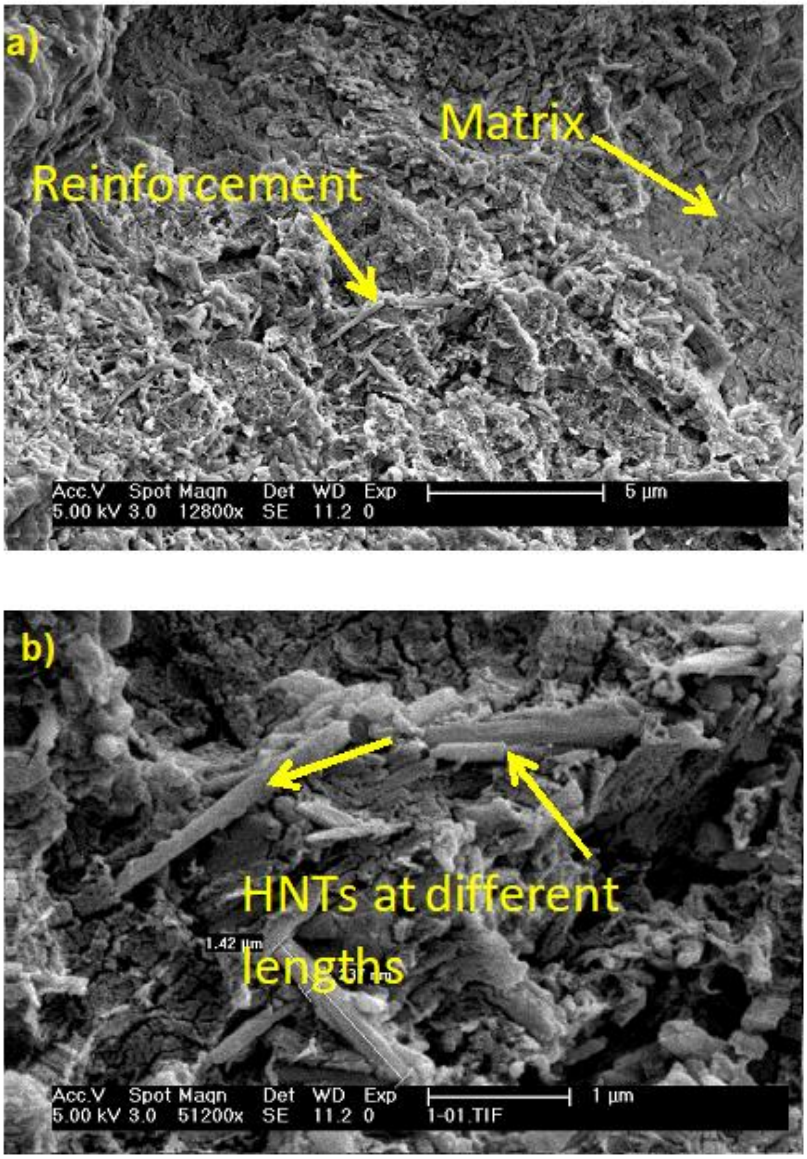

Figure 4.3 SEM images of PTFE/HNT nanocomposites with 4 wt. % HNT: (a) Intercalation distribution of HNTs in the matrix; (b) Shows structure of nanocomposite

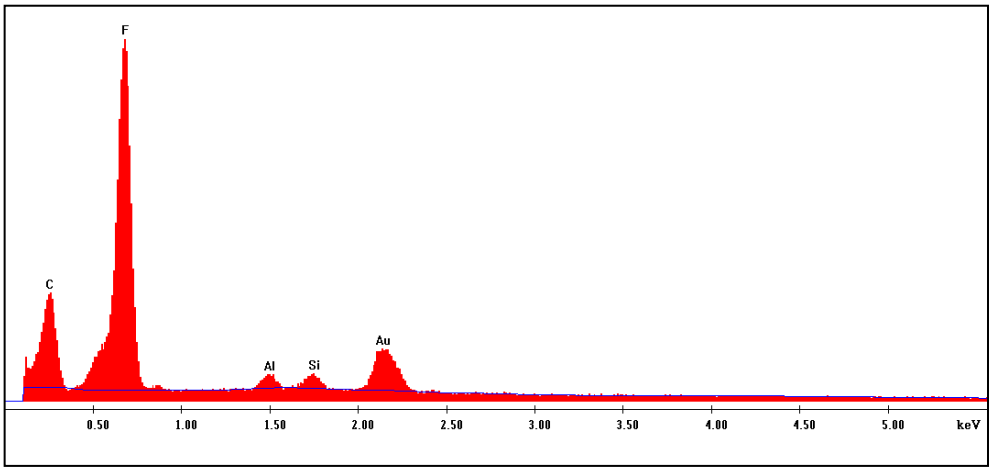

Figure 4.4 EDX spectrum of PTFE/HNT nanocomposite specimen with 4 wt. % of HNT

4.2 Thermal properties Characterization

The characterization is highly essential as the improvement in the properties of nanocomposites were directly related to the changes in thermal and dynamic mechanical properties as well. Thermal related properties like glass transition temperature, melting temperature, crystallization temperature, degree of crystallinity and dynamic mechanical properties like storage modulus, loss modulus, and tan delta were studied. For thermal properties, Differential Scanning Calorimetry (DSC) test and for dynamic mechanical properties, dynamic mechanical analysis (DMA) test were performed. In the chapter the tests procedure, about operating conditions in experimentation part, and the addition of wt. % HNT addition in the PTFE matrix were also discussed under results and discussion.

4.2.1 Differential Scanning Calorimetry (DSC)

Thermal properties like heating and cooling crystallization temperatures, degree of crystallinity for PTFE/HNT nanocomposite samples were shown in table 4.2 The degree of crystallinity of samples ('A' – 'F') with different wt.% of HNT was calculated by considering ΔH_{100f} equal to 83 J/g [57]. From the Table 4.2, neat PTFE depicted degree of crystallinity of 57.83% and PTFE with 10 wt. % HNT loading manifested in maximum degree of crystallinity of 74.7%. The increase in degree of crystallinity, which was a function of heat absorption capacity, leads to enhanced functional properties. Enhanced degree of crystallinity could be attributed to concentration of wt. % HNT and promotes nucleation process simultaneously at several locations of PTFE/HNT interfaces during cooling of the PTFE/HNT nanocomposites.

Table 4.2 DSC results of PTFE/HNT nanocomposites

PTFE/HNT Nanocomposite	Enthalpy (J/g) and degree of Crystallinity		Cooling crystallization temperatures, ^{0}C			Heating crystallization temperatures, ^{0}C		
	ΔH_f	% X_c	$T_{c1,}$	T_c	T_{c2}	T_{m1}	T_m	T_{m2}
A- 0 wt. % HNT	-31.0	57.83	319	310	295	322	333	342
B- 2 wt. % HNT	-33.1	63.85	318	308	296	324	336	349
C- 4 wt. % HNT	-34.6	73.5	318	307	292	322	337	350
D- 6 wt. % HNT	-35.1	65.06	319	311	298	322	332	344
E- 8 wt. % HNT	-36.3	72.28	319	308	292	322	337	357
F- 10 wt. %HNT	-42.2	74.7	319	312	297	322	334	346

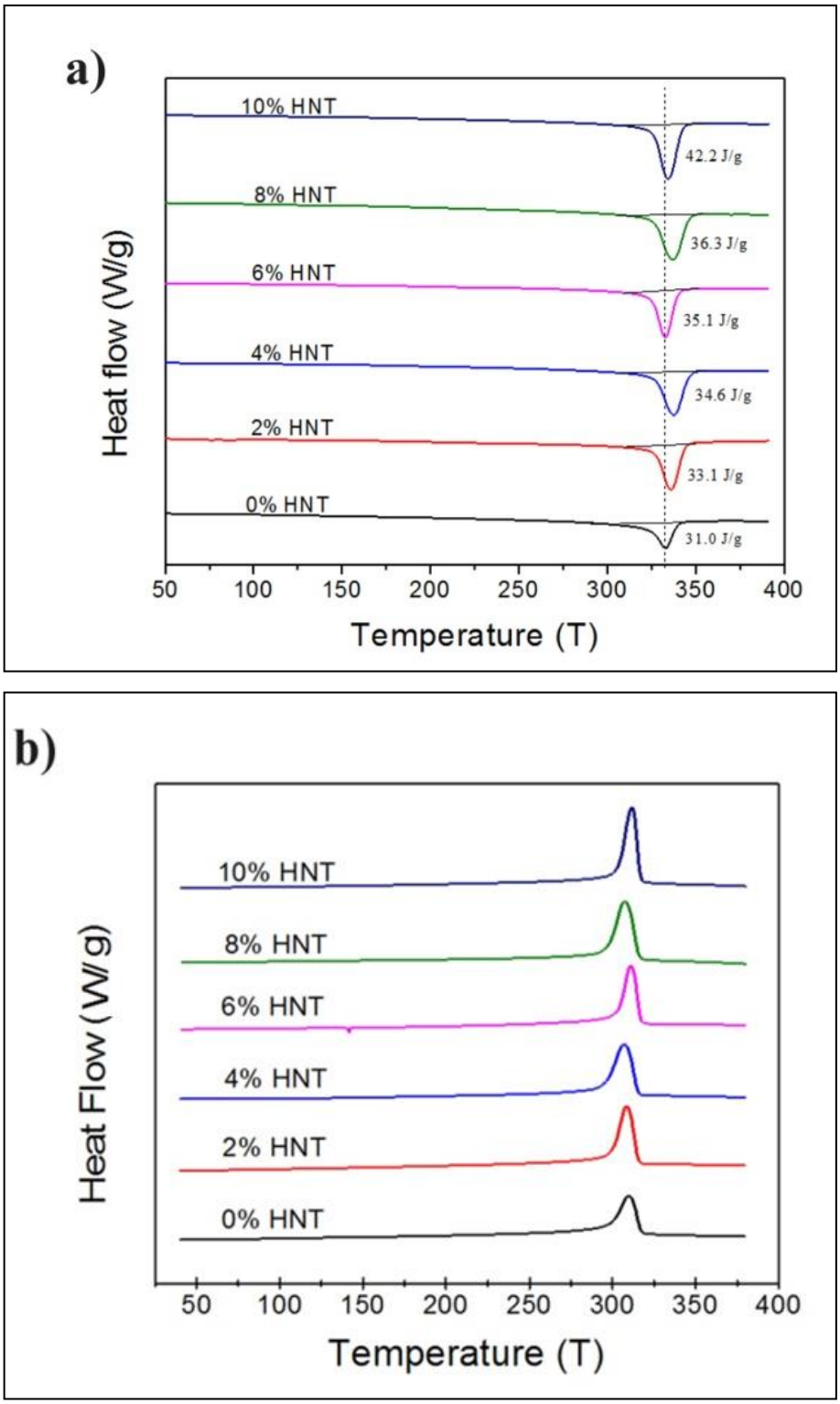

Figure 4.5 DSC scans of PTFE/HNT nanocomposite samples: (a) DSC heating curve and (b) cooling curve

Heating and cooling thermo-grams were shown in Fig. 4.5 (a) & (b) whereas Fig. 4.5 (c) portrayed the effect of wt. % HNT addition on the heat capacity of the PTFE/HNT nanocomposites. PTFE nanocomposites showed no indication of any additional reaction

between the HNT filler and the PTFE matrix in the given temperature range and some apparent variation in the position of transition melting peak. From Fig. 4.5 (a), a shift of melting peak is observed. A similar trend was reported by Prashantha et. al. [73]. From the heating thermograms (Fig. 4.5 (a)) of PTFE/HNT nanocomposites, it was observed that the melting point temperatures of specimens (B, C, E, F) are slightly affected compared to the neat PTFE. In these specimens, a new crystal structure might be promoted at the surface of HNT. However, in case of specimen D, the melting temperature was unaffected by the incorporation of HNT. From cooling thermograms of PTFE nanocomposites (Fig. 4.5 (b)), in case of specimen B, C, and E, the hindering type of crystallization and for specimens D and F heterogeneous crystallization was observed. In case of heterogeneous crystallization, the nucleation will be initiated by the HNT filler, whereas in hindering type of crystallization the nucleation would be initiated by the PTFE matrix region. In addition, the reduced size of PTFE/HNT nanocomposite crystallites were observed for nanocomposite as compared to neat PTFE. [109].

4.2.2 Dynamic Mechanical Analysis

DMA test was carried out on all the PTFE/HNT nanocomposite samples and the thermo mechanical behaviour of the samples were studied. The variation in the storage modulus (E´, which is the measure of elastically stored energy) and the tangent of the phase angle were analyzed as a function of temperature. The variation in tan delta is an indicative to the molecular movement and phase transitions of the PTFE/HNT nanocomposite.

The variation of storage modulus and loss modulus as a function of temperature (Figure 4.6 (a) –Figure 4.6 (b)) shows that the moduli of the PTFE/HNT nanocomposite increases as a function of %HNT loading. The tan δ plot (Figure 4.6 (c)) suggests the possibility of a relaxation present around the room temperature which corresponds to the β relaxation of the PTFE polymer. This phenomenon was due to the change from the 13-CF_2 unit helical conformation to 15-CF_2 unit helical conformation. The storage modulus shown a steady decrease with the temperature whereas the tan δ plot shown a peak maxima at around 120^0 C correspond to α-glass transition. The tan delta value corresponds to the loss factor of the PTFE polymer and was related to the energy dissipated by the sample. The shape and intensity of the tan δ peak was an indication on the crystallinity of PTFE. The DSC results were also shown an increase in the crystallinity of the PTFE/HNT nanocomposite samples. The decrease in tan δ associated with the glass transition corresponds to the increase in the storage modulus and decrease in loss modulus of

the material. This behaviour was due to the addition of HNTs improved the capability of the material to dissipate energy with an enhanced loss modulus.

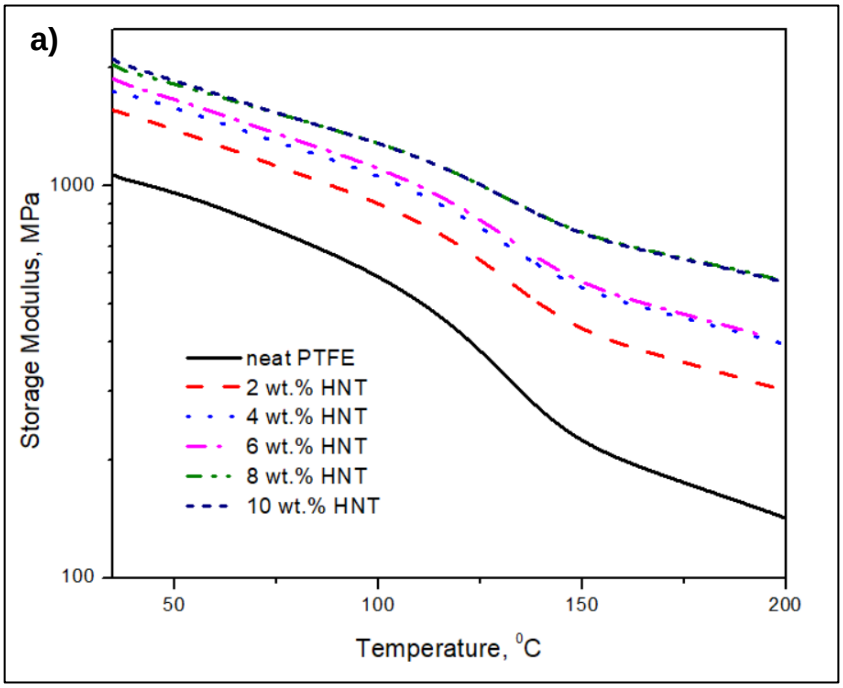

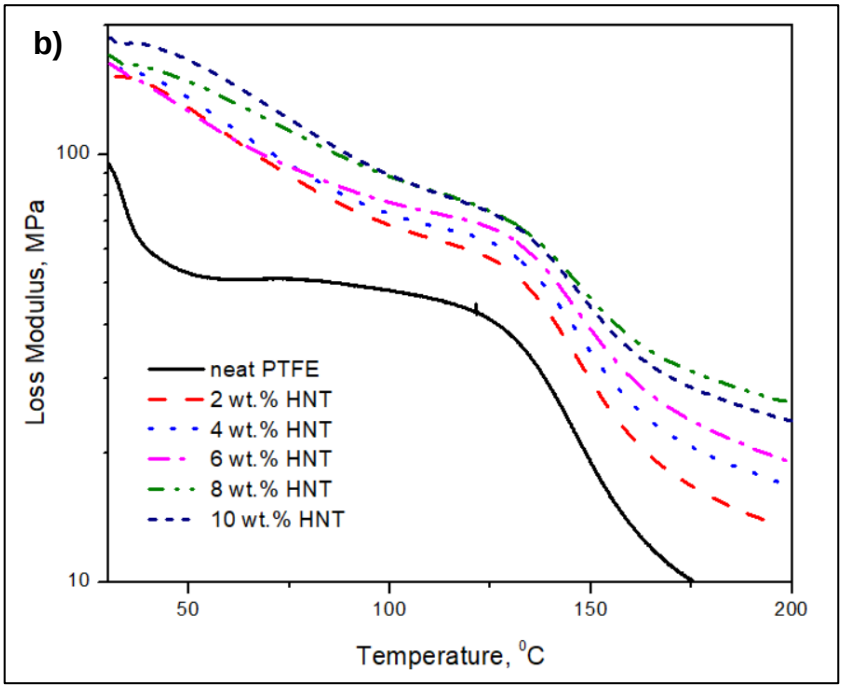

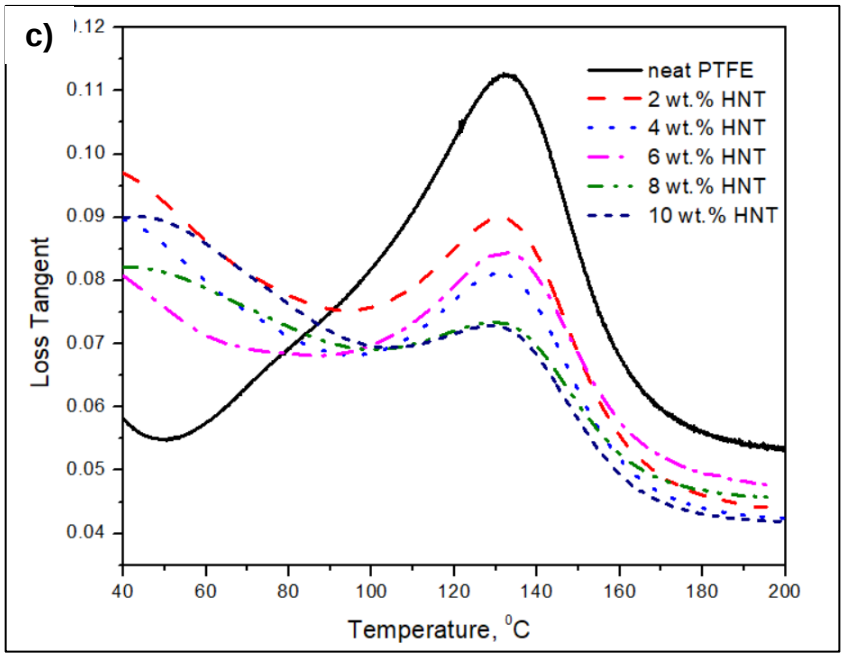

Figure 4.6 DMA plots of PTFE/HNT nanocomposites: a) storage modulus and temperature; b) loss modulus and temperature; c) tan δ and temperature

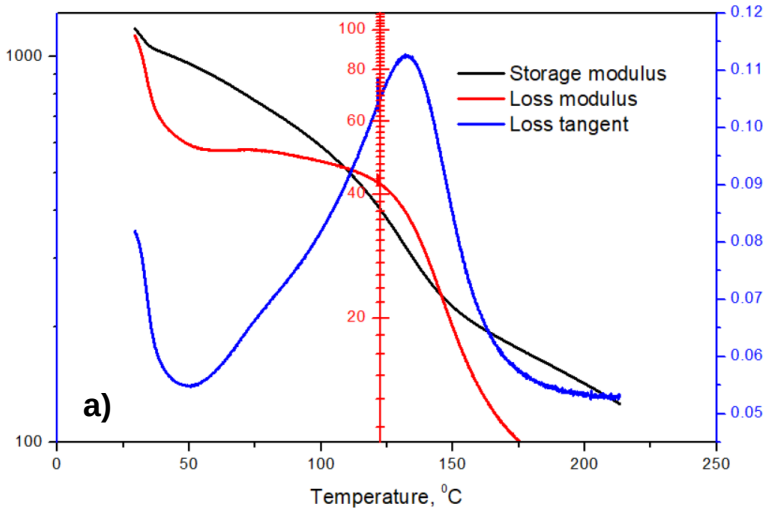

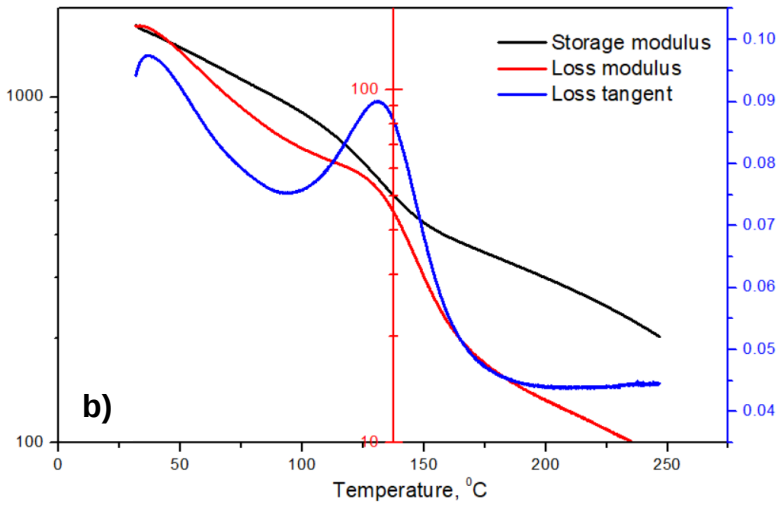
Storage modulus
Loss modulus
Loss tangent
b)
Temperature, °C

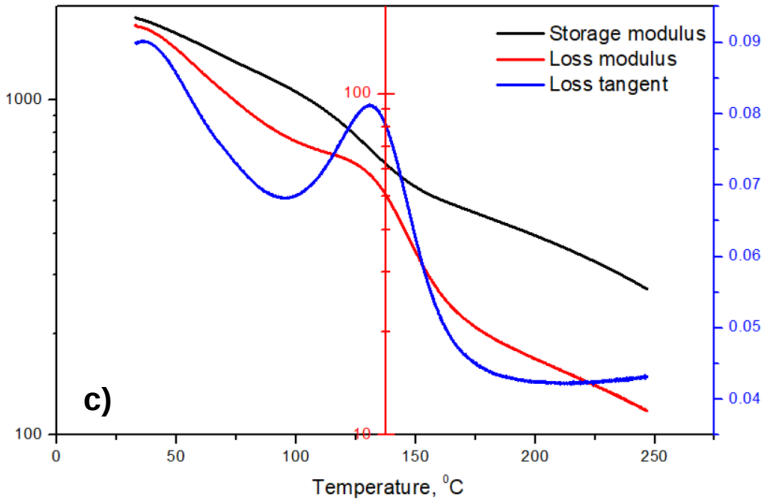
Storage modulus
Loss modulus
Loss tangent
c)
Temperature, °C

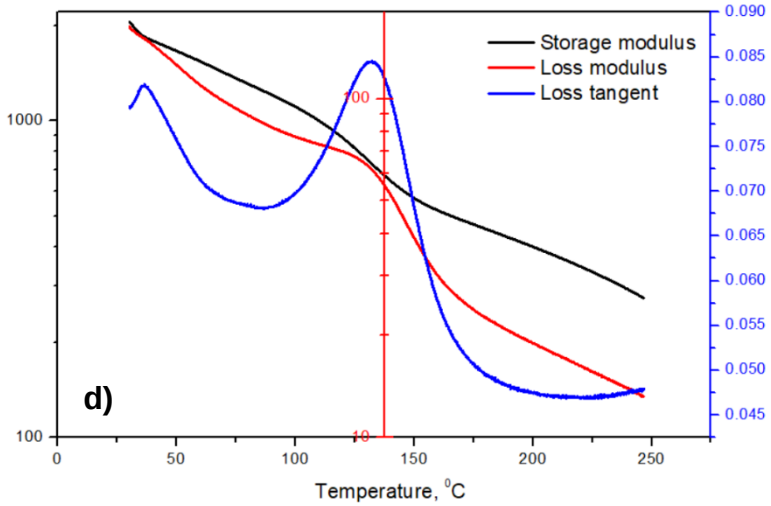
Storage modulus
Loss modulus
Loss tangent
d)
Temperature, °C

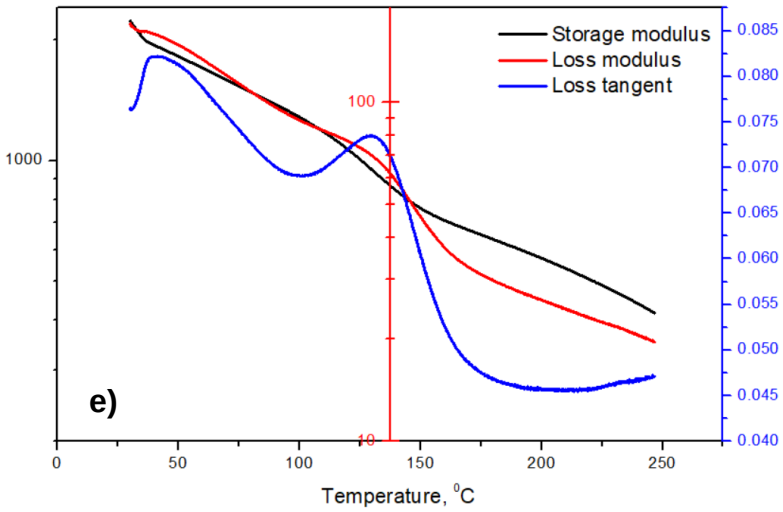

Figure 4.7 Plots of storage modulus, loss modulus, and loss tangent for (a) neat PTFE; (b) 2 wt. % HNTs; (c) 4 wt. % HNTs; (d) 6 wt. % HNTs; (e) 8 wt. % HNTs

As the specimens were heated gradually from room temperature through its glass transition temperature, the modulus values were increased whereas the loss tangent peaks were reduced (Figs. 4.7 (b) – (e)) compared to neat PTFE samples. The increase in loss tangent or loss modulus after glass transition temperature for the PTFE/HNT nanocomposite samples were attributed as the ductile to brittle transition of the nanocomposite samples took place. This was due to reduced PTFE chain movement with increased wt. % HNT addition as well as higher viscosities of PTFE material at elevated temperatures [110]. The wt. % HNTs addition at 2% to 10 % indicated the reduced second order transition temperatures when compared to neat PTFE sample and shifting of glass transition temperatures was also shown in Fig. 4.7 (b) – (e).

4.3 Mechanical property characterization

Mechanical properties were estimated from tensile test, flexural test, impact test, and hardness test. UTM was utilized and test data was extracted for all samples. Tensile properties such as, yield tensile strength, ultimate tensile strength, Young's modulus, were estimated from the tension test data. A Tensometer was utilized and properties flexural modulus, bending strength were calculated from three point bending flexural test. Instron make impact tester was used and amount of energy absorbed by each sample and thus impact strength was determined from Izod impact test. Notches were cut on the impact test specimens as per ASTM standard by using Instron make notch cutter. Vickers-micro hardness tester was used and hardness of each nanocomposite was estimated in terms of hardness number and converted to MPa.

4.3.1 Study of tensile properties

During tension test, the structural changes in the PTFE nanocomposite material, in particular at 2 wt. % HNT addition in the PTFE matrix was shown in Fig.4.8. As the applied load was increased the specimen elongates. The elongation was observed to be low compared to neat PTFE, as the HNTs addition increased the resistance and restricted the elongation. The increased resistance can be attributed to increased yield tensile strength. The different stages of the failure of PTFE/HNT nanocomposite during tensile test were shown on the Fig. 4.8. Hence, for proper dispersion of HNTs in the PTFE matrix, at the interfaces of HNTs and PTFE, some crazes would be formed due to applied load and the size of the craze further increase with the increased applied load, resulted early cracks and failure of the sample occurred.

Figure 4.9 shows the stress-strain diagrams of PTFE/HNT nanocomposites with wt. % of 0%, 2%,4%, 6%, 8%, and 10 % HNT (specimens 'A' to' F'). The values of yield tensile strength and Young's modulus are calculated for each curve and are presented in Table 4.3. The increase in wt% of HNT addition resulted in an increase in yield tensile strength and a decrease in ultimate tensile strength was observed. The yield tensile strength and Young's modulus were improved by 135% and 250% respectively. A similar trend was observed by Yan et. al. [111], from the tensile properties of PTFE/nano-EG composites reinforced with nanoparticles. During the test it was noticed that, specimen 'A' (neat PTFE) deforms steadily and reaches yield point and later due to strain hardening, an increase in the applied load was observed and breaks at about 400% strain. For Specimen 'B' &'D' shows some initial resistance, reaches yield point and was elongated uniformly through the gauge length till fracture. A flat plateau indicates constant elongation and no substantial strain hardening which was observed from the (see Fig. 4.9

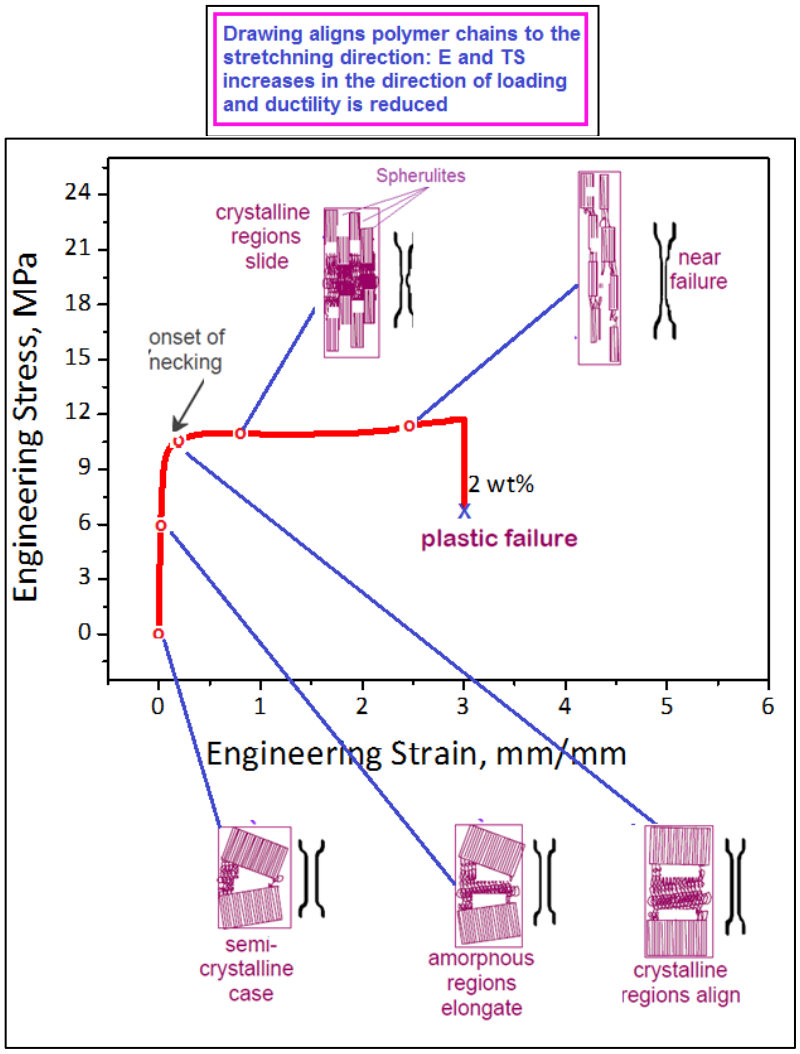

Figure 4.8 Draw stress Behaviour of PTFE/HNT Nanocomposite at 2 wt. % HNTs addition

Table 4.3 Effect of wt. % HNT addition on Tensile strength and Young's modulus

Composition %HNT by weight	Tensile strength (MPa)	Std. deviation	Young's modulus (MPa)	Std. deviation
A- 0%	8.82	±0.4	245.54	±14.19
B – 2%	10.45	±0.39	415.59	±6.67
C – 4%	10.43	±0.32	521.06	±26.92
D – 6%	10.65	±0.26	477.11	±19.62
E – 8%	10.35	±0.51	566.36	±23.62
F – 10%	11.52	±0.54	607.80	±30.94

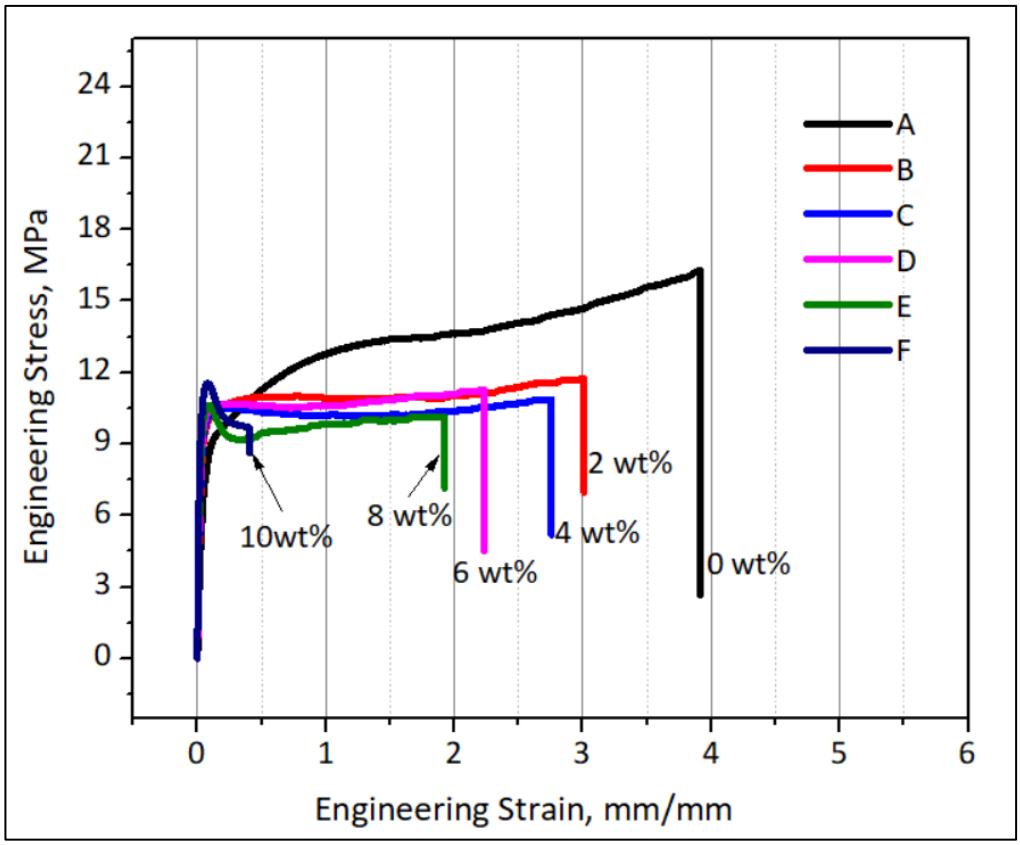

Figure 4.9 Engineering stress-Engineering strain diagrams of PTFE/HNT nanocomposites

For sample C, a drop in stress after yield point was observed, which may be due to the formation of gaps in crazes of PTFE around HNT particles. For samples E and F, an appreciable decrease in the applied load was observed after the yield point which is mainly due to poor dispersion of HNTs in the PTFE matrix. The ultimate tensile strength and percentage elongation for all wt% of HNT were significantly reduced in comparison to neat PTFE. The ultimate tensile strength was decreased from 16.48 MPa for neat PTFE to 9.72 MPa at 10 wt. % of HNT, and percentage elongation was decreased from 392% for net PTFE to 48% at 10 wt. % of HNT. Further, from Fig. 4.10, the increase in the Young's modulus and yield tensile strength occurs as a function of HNT filler content in the PTFE matrix. The addition of hard filler in soft matrix can increase the Young's modulus as well as bulk hardness of the PTFE nanocomposites. Quasi-brittle behaviour was observed in the specimens 'E' & 'F', i.e. after 6 wt. % of HNTs addition. A similar behaviour in the tensile properties of polypropylene/halloysite composites was observed from the work of Ning et. al. [112] This behaviour is due to development of more interfaces in the PTFE nanocomposites with increasing HNT filler content. Further, it was observed that, due to poor dispersion and agglomerates in specimens E & F causes less interface or bonding strength which initiates early cracks. Evidently, which contribute less elongation

near break point as clearly seen in Fig. 4.9. The optimum values of tensile strength and Young's modulus could be taken at 4 wt. % HNT since the increase in the wt. % addition was also tend to increase the agglomerate density in the nanocomposites and thus increase in brittleness of the nanocomposites which was undesirable in the view of tribological aspect.

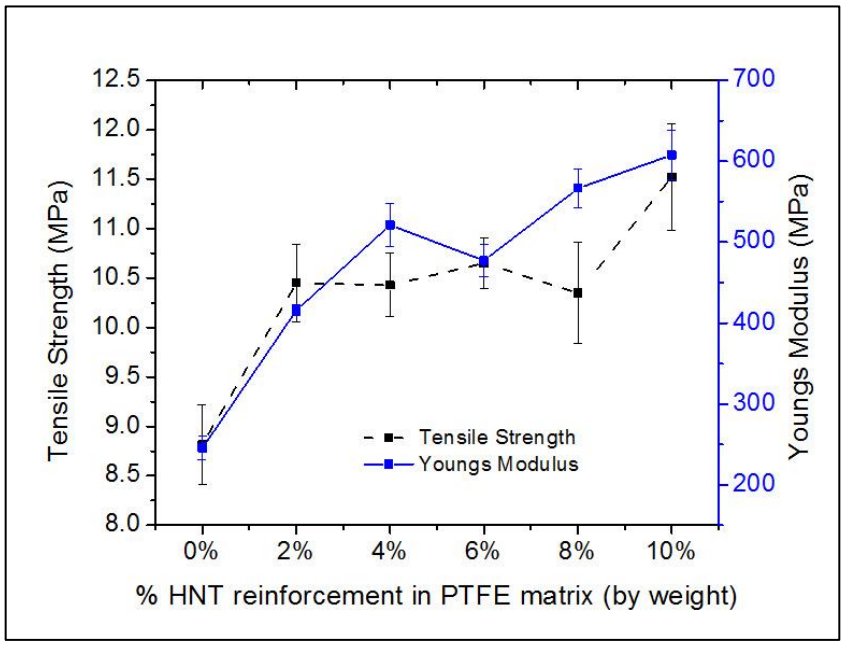

Figure 4.10 Effect of wt. % HNT addition on tensile strength and Young's modulus

4.3.2 Impact properties

Impact strength is the ability of the material to resist the fracture under stress applied at high speed. The specimens are deformed within a short time and therefore exposed to high strain rates. The effect of wt% HNTs addition on impact strength of PTFE nanocomposite are shown in Table 4.4. Figure 4.11 shows the increase in of impact strength corresponding to 4wt% of HNT loading causes an increase in the energy absorbing capacity. The increase in the energy absorption of the PTFE nanocomposites can be attributed as a function of dispersion of HNTs filler in the PTFE matrix material and % crystallinity of the nanocomposites. The observed impact properties were in well correlation with % crystallinity (see Table 4.5). When small quantities of HNTs were added to the PTFE matrix material the impact resistance to fracture was increased and found a maximum value of 13.47 kJ/m^2 at 4 wt. % of HNT addition. The decrease in impact strength was observed after 4% might be due to mixing time of powders, less resistance near the interfaces due to agglomerates, and slight decrease in the % crystallinity of the PTFE nanocomposites.

Table. 4.4 Effect of HNT reinforcement on impact strength of PTFE nanocomposites

HNT addition (by weight)	Impact strength (J/m^2)	Std. Deviation
0%	10.97	±1.03
2%	11.88	±0.97
4%	13.47	±0.65
6%	11.38	±0.65
8%	11.89	±0.72
10%	12.98	±0.31

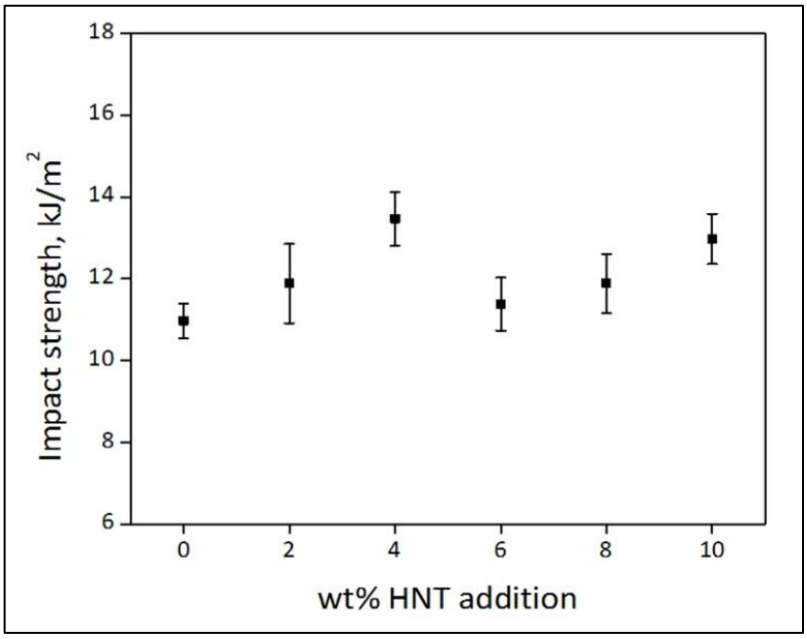

Figure 4.11 Effect of wt. % HNT addition on impact energy of PTFE/HNT nanocomposites

4.3.3 Flexural properties

Flexural strength is the ability of the material to withstand bending forces applied perpendicular to its longitudinal axis. The stresses induced due to the flexural load are a combination of compressive and tensile stresses. Flexural properties were calculated in terms of the maximum stress and strain that occur at the outside surface of the PTFE/HNT nanocomposite test specimens. Many polymers do not break under flexural even after a large deflection that makes determination of the ultimate flexural strength [113] and same behaviour was observed with the present PTFE/HNT nanocomposites specimens. In such cases, to report flexural yield strength, when the maximum strain in the outer fibre of the specimen has reached five percent. Flexural properties of all wt. % HNT addition in the PTFE matrix were reported in Table 4.5.

Table. 4.5 Effect of wt. % HNT reinforcement on Flexural and micro-hardness properties of the nanocomposites

PTFE nanocomposite (wt. %. HNT)	Flexural strength (Mpa)	Flexural Modulus (Gpa)
A- 0%	26.35	0.0875
B- 2%	33.91	0.1320
C- 4%	47.44	0.1567
D- 6%	46.98	0.1875
E- 8%	49.70	0.2112
F- 10%	48.83	0.2250

The effect of wt. % HNT on the flexural properties of PTFE/HNT Nanocomposites was shown in Fig. 4.12. As the wt. % of HNT addition in the PTFE matrix material was increased from 0 wt. % to 4 wt. % an appreciable increase in the flexural strength PTFE/HNT nanocomposites was observed due to the good interfacial bonding between the matrix and reinforcement materials. A similar kind of response was reported by Yong X. Gan. [114], from flexure tests on CNTs/epoxy advanced material. And, beyond 4 wt.% the increase in the flexural strength was quite minimum due to the formation of agglomerates of HNT and subsequent reduction in interfacial bonding due to the formation of micro-cracks between the PTFE matrix and HNT reinforcement. It seems that adding HNTs leads to an improvement in the flexural properties i.e., bending strength and flexural Young's modulus of PTFE as shown in Fig. 4.13, the percentage increase is about 44.45% for bending strength and 44% for bending modulus at 4 wt. % addition. Reinforcement by HNTs at 4 wt.% seem to be an optimal value as flexural properties tend to reach a flatland above this value. At 6 wt.% a small reduction in the flexural strength which may be due to the fact that overfilling of HNTs tips to clustering of nanotubes. These micron sized clustered masses in the PTFE matrix are in micron-sizes and forming as weak zones and failure starter points. Similar remarks were reported by Liu et al.[115], for Halloysite filled epoxy nanocomposites and Prashantha et al. [64] for HNTs filled in masterbatch Polypropylene.

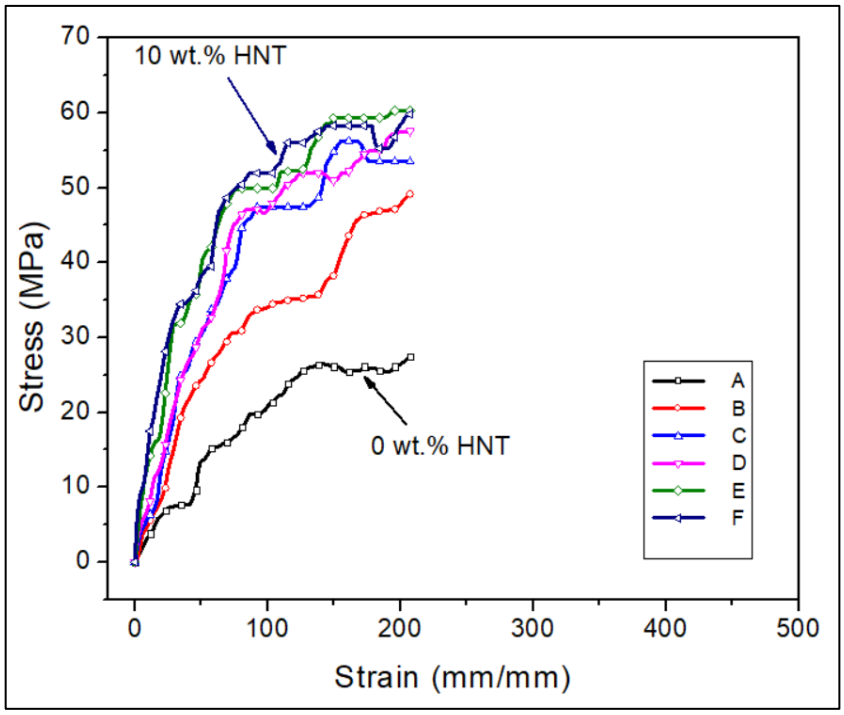

Figure 4.12 Flexural stress vs flexural strain diagram

.

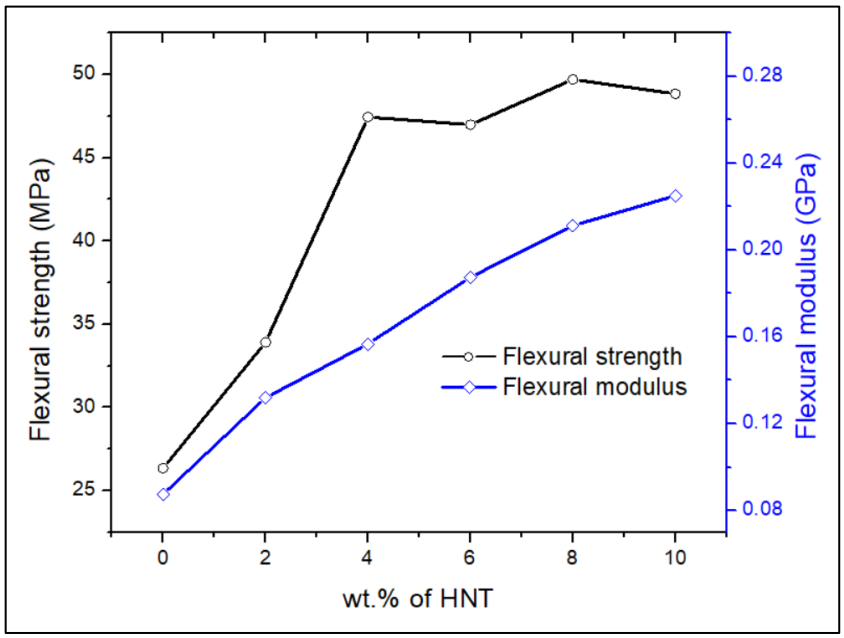

Figure 4.13 Effect of wt. % HNTs addition in the PTFE matrix on flexural strength and flexural modulus.

4.3.4 Vicker's micro-hardness

Vickers micro-hardness values of the PTFE/HNT nanocomposite specimens were presented in Table 4.6 and were average of three readings, for each nanocomposite sample. The increase in the hardness was observed due to increase in the wt% of HNTs addition in the PTFE matrix.

The increase in these values is due to the dispersion of hard HNT filler in the soft PTFE matrix. The micro-hardness value for neat PTFE, was 23.07 MPa, increased to 37.61 MPa for sample 'F'. The increase in micro hardness values indicated that the wt. % HNT addition above 4 %, introduced quasi-brittle nature of PTFE/HNT nanocomposites. As discussed, in section 4.3.1, the brittle nature was also revealed by the increase in micro hardness values. Also, the increased hardness can be attributed to the high surface energy of HNT agglomerates formation and high aspect ratio as well.

Table.4.6 Effect of wt. % HNT addition on micro-hardness values of PTFE/HNT nanocomposites

PTFE nanocomposite (wt. %. HNT)	**Average Vickers micro-hardness value (MPa)**
A- 0%	23.07
B- 2%	25.72
C- 4%	29.20
D- 6%	25.63
E- 8%	35.90
F- 10%	37.61

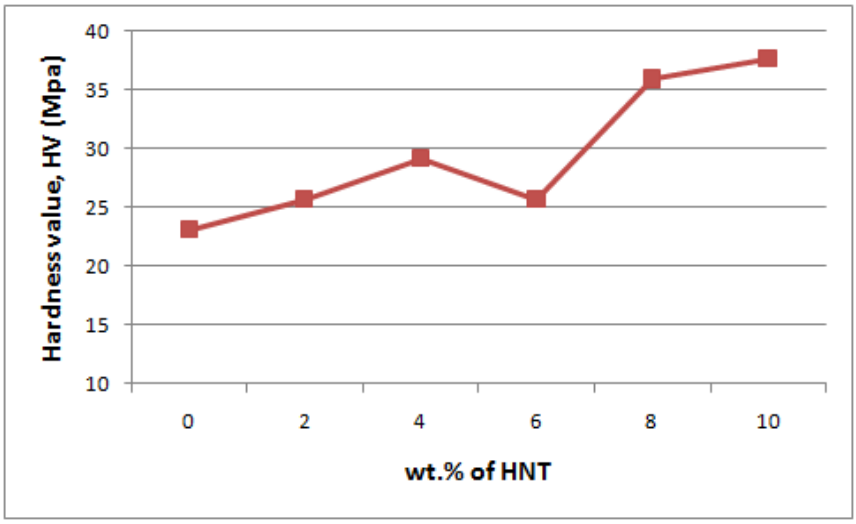

Figure 4.14 Effect of wt. % HNT addition on micro-hardness values of PTFE/HNT nanocomposites

4.4 SEM microstructures of fracture surfaces

Figure 4.15 (a) – (b) shows the tensile fracture surfaces of PTFE/HNT nanocomposites at 10 wt. % of HNTs addition. Fig. 4.16 (a) – (e) shows the fracture surfaces of PTFE nanocomposites under impact failure at different wt. % of HNTs addition. The addition of HNTs into the PTFE matrix material produces heterogeneous type of structure. The addition of HNTs with low wt.

% seems better dispersion from the impact fracture surfaces (see Fig. 4.16 (a) & (b)). The smaller pull out regions from these images indicated the intercalation type of structure. As the wt. % addition increased beyond 6 wt. %, due to increased cluster formation the dispersion of reinforcement in the PTFE matrix material was affected. It was revealed from the SEM microstructures that the larger pull out regions on the fracture surfaces.

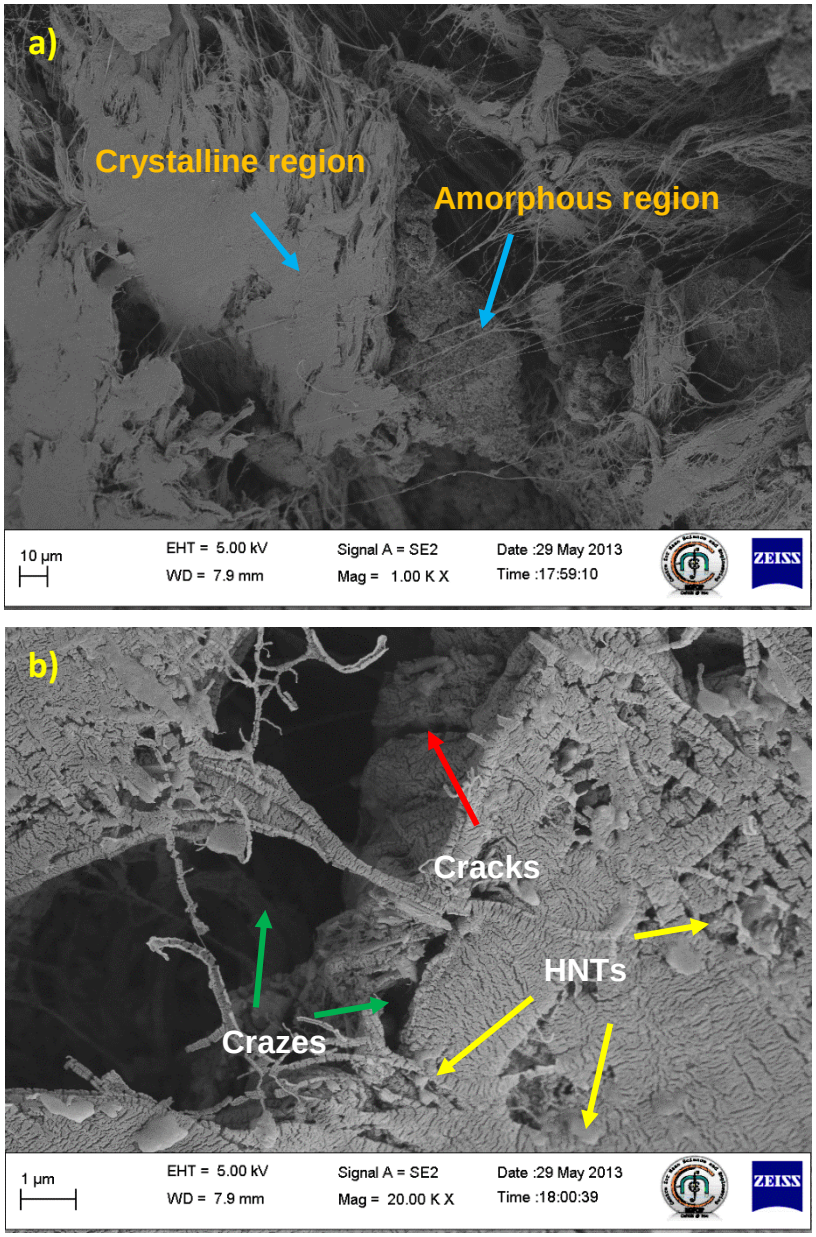

Figure 4.15 (a) & (b) SEM image of fractured tensile specimen: at 10% HNT filled tensile specimen

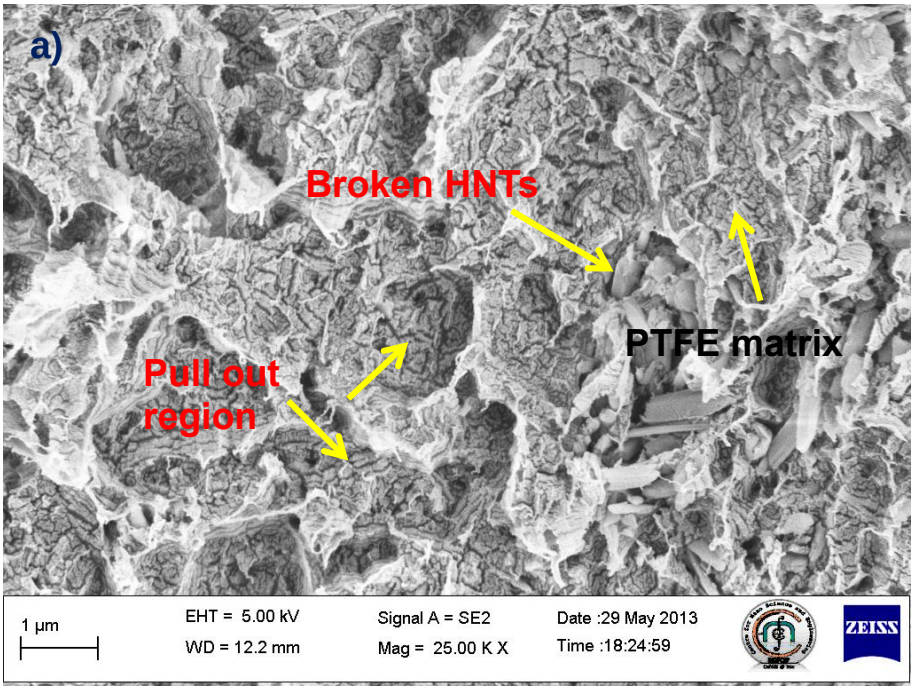
a)
Broken HNTs
PTFE matrix
Pull out region
1 µm
EHT = 5.00 kV
WD = 12.2 mm
Signal A = SE2
Mag = 25.00 K X
Date :29 May 2013
Time :18:24:59
ZEISS

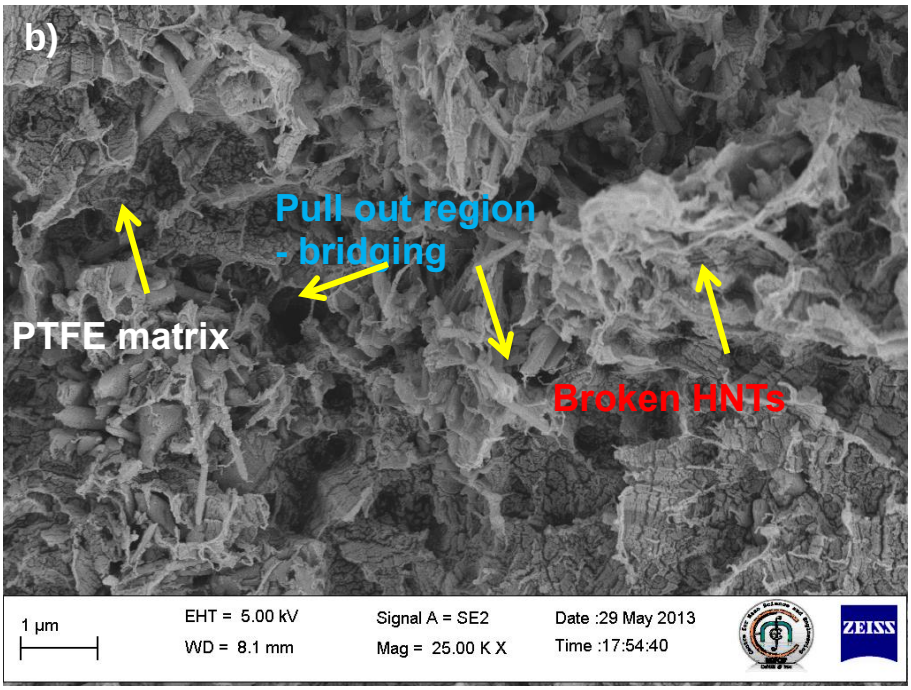
b)
Pull out region - bridging
PTFE matrix
Broken HNTs
1 µm
EHT = 5.00 kV
WD = 8.1 mm
Signal A = SE2
Mag = 25.00 K X
Date :29 May 2013
Time :17:54:40
ZEISS

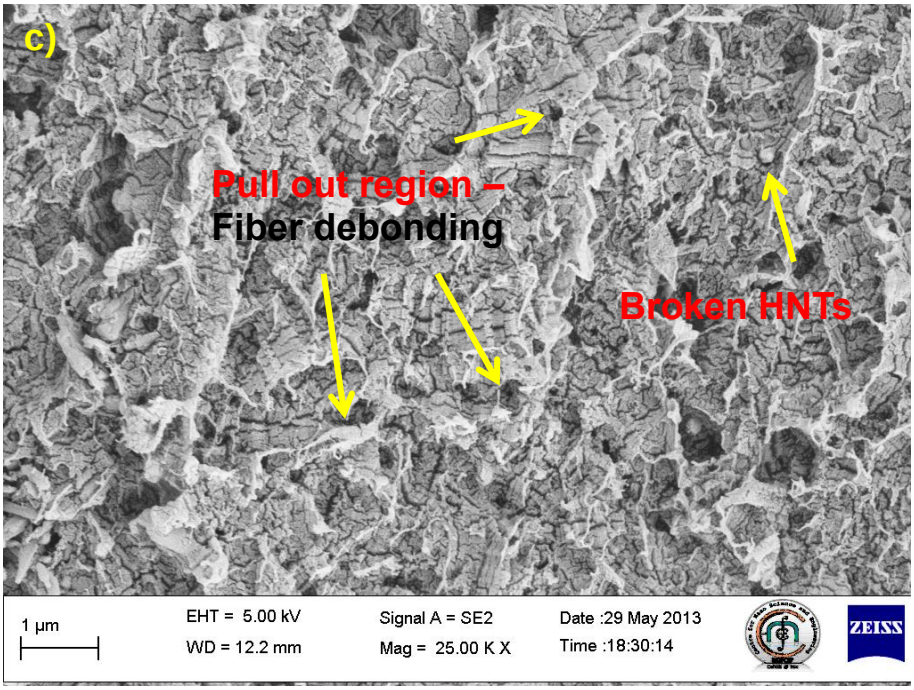
c)
Pull out region –
Fiber debonding
Broken HNTs
1 µm
EHT = 5.00 kV
WD = 12.2 mm
Signal A = SE2
Mag = 25.00 K X
Date :29 May 2013
Time :18:30:14
ZEISS

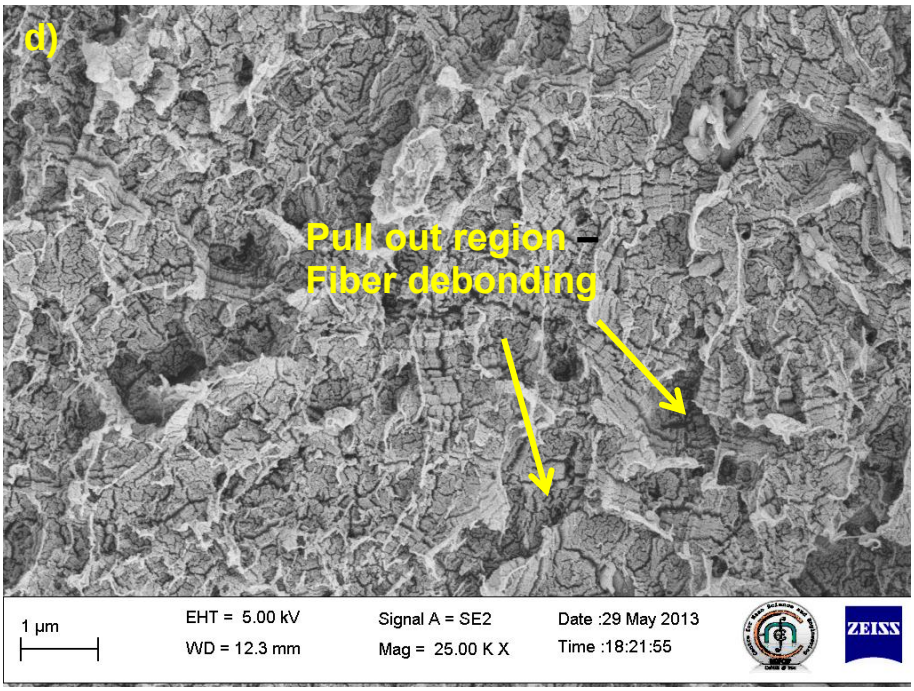
d)
Pull out region –
Fiber debonding
1 µm
EHT = 5.00 kV
WD = 12.3 mm
Signal A = SE2
Mag = 25.00 K X
Date :29 May 2013
Time :18:21:55
ZEISS

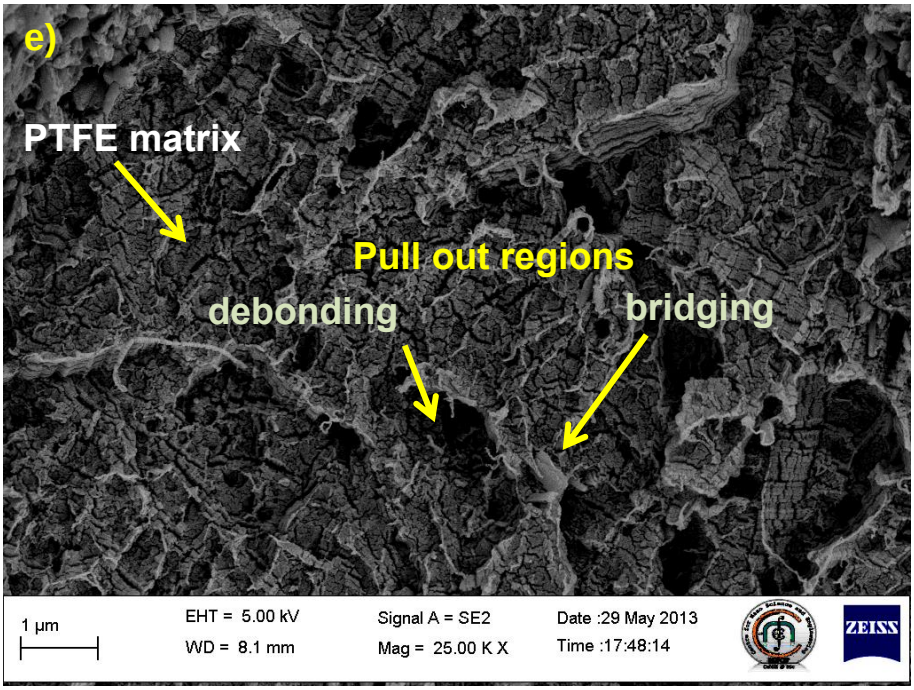

Figure 4.16 SEM images of impact test fracture surfaces of PTFE/HNT nanocomposites: a) 2 wt.% HNT; b) 4 wt.% HNT; c) 6 wt. % HNT d)8 wt. % HNT e)10 wt. % HNT

In Table 4.4, it was observed that, increased impact strength of the PTFE/HNT nanocomposite samples due to wt. % HNT addition. The impact test specimens were deformed within a short time and therefore exposed to high strain rates during the test. The increase in impact strength can be attributed to the fact that, the HNT filler related energy dissipation mechanisms, such as Halloysite nanotubes debonding, pull out, bridging and fracture, induced plastic deformation of the PTFE matrix before failure. The pull out regions were also shown on SEM micrographs (Figure 4.16 (a) – (e)). Bridging and fibre fracture were likely to occur as a consequence of HNTs with lengths longer than the critical value for effective reinforcement, while debonding and Halloysite nanotubes pull out were expected to occur as the result of a set of HNT with length shorter than the critical value. The 'pulled out' effect was displayed in the form of arbitrary shaped gaps on the SEM microstructures. The gap density and its size were different and revealed the quality of dispersion of HNT in the matrix material. The increase in the energy absorption of the nanocomposites can also be attributed as the function of dispersion of HNTs filler in the PTFE matrix material and degree of crystallinity of the nanocomposites.

The improved dispersion of HNTs in PTFE matrix was revealed by the fact that silicon content on the surface of Halloysite decreases their surface free energy and hinders

nanotube/nanotube interaction, thereby separating the aggregates during the mixing process and produces better interfaces between the matrix and reinforcement materials.

The increase in tensile and impact properties of the PTFE/HNT nanocomposites were explained as follows: The increase in the toughness of PTFE/HNT nanocomposites compared to pure PTFE could be attributed that bridging/pull-out/breaking of nanotubes in the matrix material. At low wt. % loading of HNTs with better dispersion offers good resistance to impact loads. On the contrary, more wt. % loading largely affected the ductile nature of neat PTFE matrix material. The reinforcement material acts as a barrier for the mobility of the PTFE matrix chains, thus limiting the ductile deformation (Fig. 4.12 (c)). A similar behaviour was also reported by Naffakh et. al. [116], for thermoplastic polymer nanocomposites filled with inorganic fullerene-like nanoparticles and inorganic nanotubes.

CHAPTER -5

Abrasive and erosion wear study

PHASE –I

5.1 Abrasive Wear Characterization using Design of experiments (DOE) concept

Design of experiments is a powerful tool for analysing the influence of control variables on responses. Experiments were designed according to Taguchi method so that effect of the parameters could be studied with minimum possible number of experiments [117]. In the present work, Taguchi *L27*orthogonal experimental plan for four factors with three levels was used as shown in Table 1. Multi-Response optimization of tribological parameters of PTFE /HNT filled nanocomposites were performed by using a novel hybrid technique based on Graph Theory Matrix Approach. The technique consists of usage of Taguchi method, utility approach [118] and response surface methodology. The procedure was described as follows:

1. Design of experiments by using Taguchi L27 orthogonal array
2. Conducting the experimental runs on POD apparatus.
3. Calculation of response variables
4. Calculation of utility index
5. Optimization of utility index by using response surface methodology

Table. 5.1 Design variables (factors) and levels

Factors	**Units**	**Levels**		
		1	**2**	**3**
Composition: Comp	(%HNT by wt.)	4	6	8
Load: L	(N)	5	10	15
Distance: D	(km)	2	3.5	5
Velocity: S	(ms-1)	1	2	3

A pin-on-disc wear tester was used to investigate the dry sliding wear and friction characteristics of the PTFE/HNT nanocomposites as per ASTMG 99-95 standard. Figure 5.1 (a) shows the setup of the POD apparatus and Figure 5.1 (b) shows a typical arrangement of POD specimen holder. The sample pin was fixed in a holder and was set to run on a counter disc made of hardened EN31 steel (58-62 HRC and 1.6 Ra) counter surface at different operating conditions. All runs were conducted at a track radius of 50 mm on counter disc surface of POD apparatus. The samples were cleaned by using acetone to remove debris adhered on sample before and after the test and were weighed on a precise balance to measure the mass of worn material.

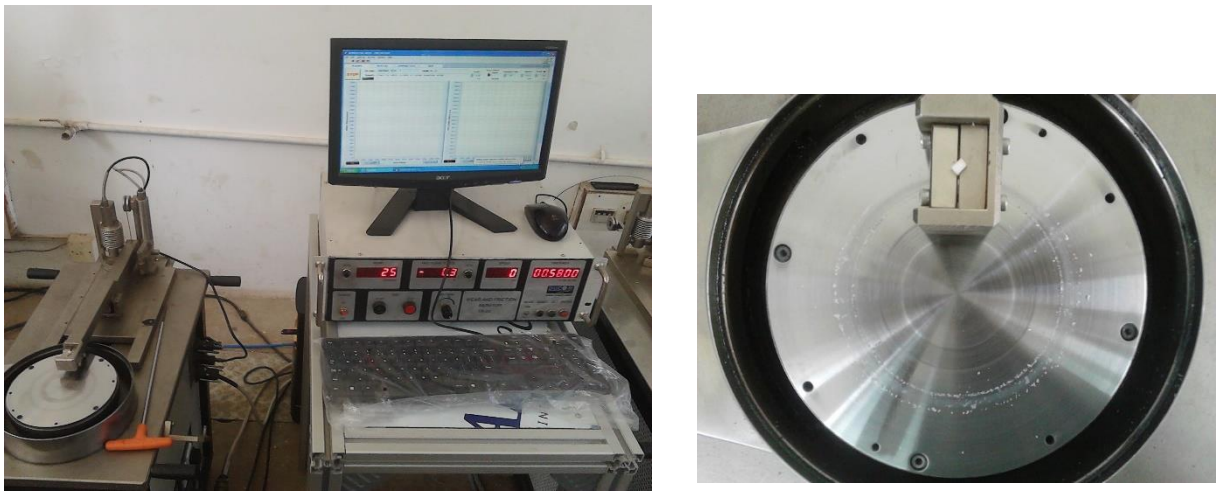

Figure 5.1 (a) Pin on Disc test set up; (b) close up view of counter face disc and PTFE/HNT composite test pin

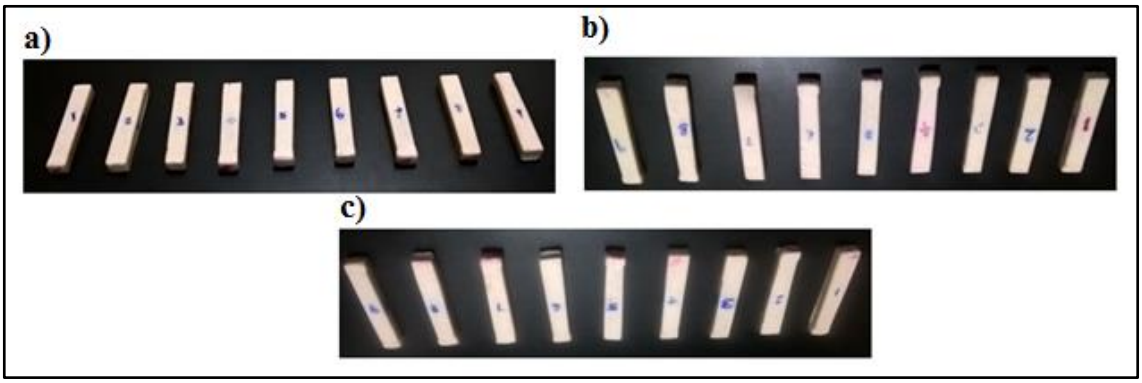

Figure 5.2 PTFE/HNT nanocomposite test specimens

5.1.1 Specific Wear Rate (SWR)

The dry sliding wear tests were performed on PTFE-HNT nanocomposites with 4%, 6%, and 8% HNT additions by POD apparatus. Each experiment was performed as per the DOE plan. A total of 27 runs were conducted on 27 specimens. The responses for all experimental runs were shown in Table 3. The coefficient of friction was taken from the display at the end of each test. The specific wear rate was calculated by using the relation (5.1).

$$Specific\ Wear\ Rate\ (SWR) = \frac{Loss\ in\ volume\ due\ to\ wear}{Load\ X\ Distance}$$

$$SWR = \frac{mass\ dislodged\ (\Delta m)}{Density\ (\rho) X\ Load(W) X\ Distance(D)} \qquad (5.1)$$

Where, Δm =mass dislodged, g; ρ =density, gm/mm^3; W=Load, N; D=distance, m

5.1.2 Specific Wear Energy (EW)

Specific wear Energy was defined as the ratio of frictional energy consumed at the interface and mass dislodged due to wear. In a tribo system the active surface and counter surface form a closed contact under the application of normal load. The hypothesis taken in the wear process is that, the active surface was composed of different parallel layers (friction stack theory [119]) represent the possible locations of frictional energy dissipation zones. The frictional contact under the application of load results molecular motion, deformation and loosening of layer from the active surface and forms an oil less film. The new layer will then be exposed to the counter surface and the process repeats. Each layer consists of matrix and nanofiller. The nanofiller adds strength to the matrix material and hence to the transfer film. Specific wear energy explains an important concept about the tribological characteristics and considers both coefficient of friction and wear rate. In the work of Conte at al. [120] time dependant friction coefficient for PTFE composites [120], the specific wear energy was estimated for non-conservative frictional variable loading by equation (5.2). Composites with high EW are said to have high wear resistance, since the amount of frictional work spent to remove per 'g' of mass loss is more hence for materials to be more wear resistant the higher EW values are preferred.

$$EW = \frac{Amount\ of\ frictional\ work\ spent,\ J}{mass\ dislodged,\ g}$$

$$EW = \frac{v\,W\ \int_{t_1}^{t_2} \mu(t)dt}{\Delta m} J\ /g \tag{5.2}$$

Where, v=mean velocity, m/s; W= applied load, N; $\mu(t)$= time dependant friction coefficient due to variable loading; Δm= mass loss, g. In the present work, the coefficient of friction was assumed to be constant throughout the test span and the specific wear energy for PTFE/HNT nanocomposites was estimated by equation (3).

$$EW = \frac{v\,W\mu\,t}{\Delta m} J\ /g \tag{5.3}$$

Where, v=mean velocity, m/s; W= applied load, N; μ= friction coefficient due to constant loading; Δm= mass loss, g.

5.1.3 Coefficient of friction

The values of coefficient of friction for the samples during the test were taken from the data controller. These values would be calculated based on normal load applied, since the coefficient of friction is defined as the ratio of frictional force and applied load.

Table. 5.2 Experimental runs and responses

Run	Input Factors				Mass loss, g	COF	Specific Wear Rate, $\times 10^{-5}$ mm^3 /N m	Specific Wear energy, MJ/ g
	Compo-sition, wt. %HNT	Load, N	Distance, km	Velocity, m/s				
1	4	5	2.0	1	0.00400	0.132	17.7	0.28
2	4	5	3.5	1	0.00924	0.143	23.4	0.27
3	4	5	5.0	1	0.01054	0.221	18.7	0.52
4	4	10	2.0	3	0.00700	0.178	15.5	0.51
5	4	10	3.5	3	0.01060	0.202	13.4	0.67
6	4	10	5.0	3	0.01125	0.202	9.97	0.90
7	4	15	2.0	2	0.00539	0.162	7.96	0.90
8	4	15	3.5	2	0.01157	0.193	9.76	0.88
9	4	15	5.0	2	0.01325	0.218	7.83	1.23
10	6	5	2.0	2	0.00198	0.136	8.76	0.69
11	6	5	3.5	2	0.00304	0.186	7.69	1.07
12	6	5	5.0	2	0.00635	0.186	11.2	0.73
13	6	10	2.0	1	0.01692	0.146	37.5	0.17
14	6	10	3.5	1	0.01735	0.166	21.9	0.33
15	6	10	5.0	1	0.04910	0.184	43.5	0.19
16	6	15	2.0	3	0.01860	0.195	27.4	0.31
17	6	15	3.5	3	0.05046	0.203	42.5	0.21
18	6	15	5.0	3	0.06430	0.221	38.0	0.26
19	8	5	2.0	3	0.00312	0.152	13.8	0.49
20	8	5	3.5	3	0.00583	0.173	14.7	0.52
21	8	5	5.0	3	0.00712	0.205	12.6	0.72
22	8	10	2.0	2	0.01800	0.188	39.8	0.21
23	8	10	3.5	2	0.02010	0.191	25.4	0.33
24	8	10	5.0	2	0.05140	0.196	45.4	0.19
25	8	15	2.0	1	0.02109	0.170	31.1	0.24
26	8	15	3.5	1	0.03047	0.189	25.7	0.33
27	8	15	5.0	1	0.05460	0.193	32.2	0.27

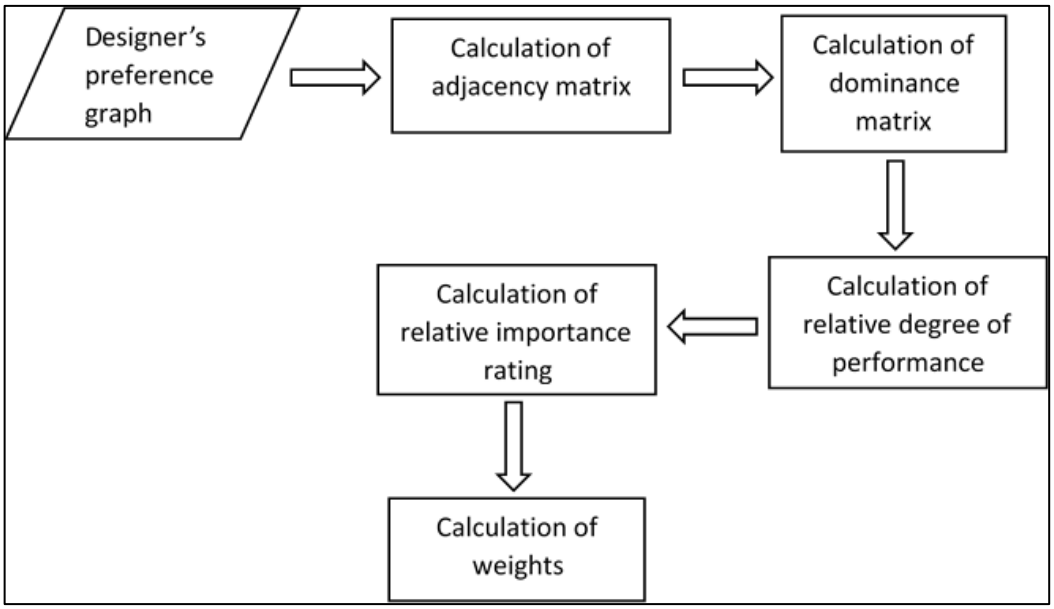

Figure 5.3 Flow chart for calculation of weights

Calculation of utility index (U)

Calculation of weights

The sequence of steps followed for calculating the weights of utility method as shown in Figure 5.3. A mathematical model is constructed from the preference graphs is discussed in the flow chart [118].

Preference graphs (PG)

The opinions of three different users are considered for the present study. The responses namely: coefficient of friction (COF), specific wear rate (SWR), and wear specific energy (EW) are represented. The opinion of first designer suggests COF is more important requirement followed by SWR and EW. The second designer suggests COF in comparison to SWR and EW. The third designer emphasizes that COF and SWR are more important than EW. The key consideration is that, the relationship of EW with the other two responses is not clearly known. The preference graphs are constructed using these individual suggestions and are shown in Figure 5.4 (a)-(c).

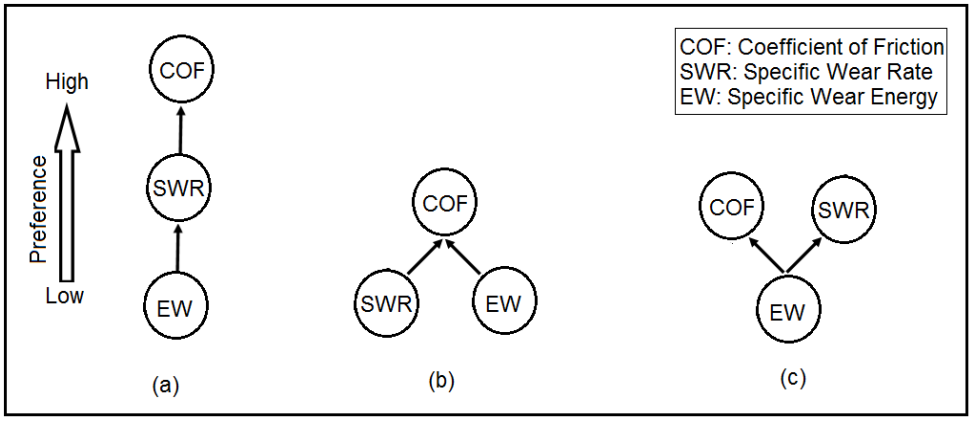

Figure 5.4 Preference graphs showing the suggestions of (a) Designer 1; (b) Designer 2; (c) Designer 3

Adjacency matrix

The adjacency matrix is constructed according to preference graph as shown below:

$$PG_n = [pg_{ij}]_{MxM} \quad (i,j = 1,2, ..., m,..., M) \tag{5.4}$$

Where n is the number of individuals, M is the number of characteristics and pg_{ij} gives the dominances of i over j in an M×M.

$$PG_1 = \begin{bmatrix} \text{COF} & \text{SWR} & \text{EW} \\ 0 & 1 & 0 \\ 0 & 0 & 1 \\ 0 & 0 & 0 \end{bmatrix} \begin{matrix} \text{COF} \\ \text{SWR} \\ \text{EW} \end{matrix} \qquad PG_2 = \begin{bmatrix} 0 & 1 & 1 \\ 0 & 0 & 0 \\ 0 & 0 & 0 \end{bmatrix} \qquad PG_3 = \begin{bmatrix} 0 & 0 & 1 \\ 0 & 0 & 1 \\ 0 & 0 & 0 \end{bmatrix}$$

Dominance matrix

The dominance matrix identifies more preferred performance characteristic among the characteristics. The dominance matrix is calculated as follows:

$$D^n = PG_n^1 + PG_n^2 + PG_n^3 + \ldots\ldots\ldots + PG_n^{M-1} \tag{5.5}$$

The dominance matrix is calculated using the equation (2), where m value is taken as 3 then:

$$D^1 = PG_1^1 + PG_1^2 + PG_1^3 \tag{5.6}$$

Also

$$d_m^n = \sum_{j=1}^{M} pg_{ij} \tag{5.7}$$

$$D^1 = \begin{bmatrix} 0 & 1 & 1 \\ 0 & 0 & 1 \\ 0 & 0 & 0 \end{bmatrix} \qquad D^2 = \begin{bmatrix} 0 & 1 & 1 \\ 0 & 0 & 0 \\ 0 & 0 & 0 \end{bmatrix} \qquad D^3 \begin{bmatrix} 0 & 0 & 1 \\ 0 & 0 & 1 \\ 0 & 0 & 0 \end{bmatrix}$$

Relative degree of performance (RDP):

The RDP and RIR are calculated using equation 6 and 7 as follows:

$$rdp_m^n = \frac{1 + d_m^n}{Max_{m=1....M} 1 + d_m^n} \tag{5.8}$$

RDP for the four dominance matrices are calculated in the form vector as follows:

RDP_1 = [1.0 0.66 0.33]

RDP_2 = [1.0 0.33 0.33]

RDP_3 = [1.0 1.0 0.5]

Relative importance rating (RIR):

$$RIR_m = \frac{\sum_{n=1}^{N} rdp_m^n}{Max_{m=1....M} \sum_{n=1}^{N} rdp_m^n} \tag{5.9}$$

$Max_{m=1....M} \sum_{n=1}^{N} rdp_m^n$ = 1+1+1=3. It is the sum of individual relative degrees of performance. RIR values of COF, SWR, and EW are given in the vector form as follows:

$$\text{RIR} = \left[\frac{3}{3} \quad \frac{1.99}{3} \quad \frac{1.16}{3}\right] = [1.0 \quad 0.663 \quad 0.387]$$

Weights

Weights of performance characteristics are calculated as follows:

$$W_m = \frac{rir_m}{\sum_{m=1}^{M} rir_m} \tag{5.10}$$

Hence, $W_{COF,}$ W_{SWR}, and W_{EW} are the weights for COF, SWR, and EW respectively and they are calculated as 0.487, 0.323, and 0.189 respectively. That means 48.7% weightage is given for COF, 32.3% weightage is given for SWR, and 18.9% weightage is given for EW i.e., weight factors are not distributed equally as in case of RSM or Grey based Taguchi methods (i.e., 0.33,0.33, 0.33). Hence the distributed weights are calculated as per the preference of the designer's choice.

Preference scale construction

Taguchi method is used to predict optimal value of the three responses separately. The experimental data of the performance characteristics shown in the Tables 3 are analyzed with smaller-the-best characteristic using equation (11) and larger the best (12) process parameters are optimized individually. Using the optimum input parameters, the responses are predicted. The Table 5.3 shows optimum process parameters, their corresponding predicted responses and maximum acceptable levels.

Smaller the best

$$S/N = -10\ log\left[\frac{1}{n}\sum_{k=1}^{n} y_k^2\right] \tag{5.11}$$

Larger the best

$$S/N = -10\ log\left[\frac{1}{n}\sum_{k=1}^{n} \frac{1}{y_k^2}\right] \tag{5.12}$$

Preference scale is required to be determined for all the responses in order to calculate utility factor of the four responses. Equation (12) is used to determine the preference scale using predicted optimal value and minimum acceptable level of the responses. The *P* value is chosen as 9 based on the acceptable levels [118].

$$P = A \times log\frac{X'}{X_i'} \tag{5.13}$$

where X_i is the value of attribute response, X_i' is the minimum acceptable value of response and A is the constant, y = experiment data, k=k^{th} experiment, and n is the number of experiments.

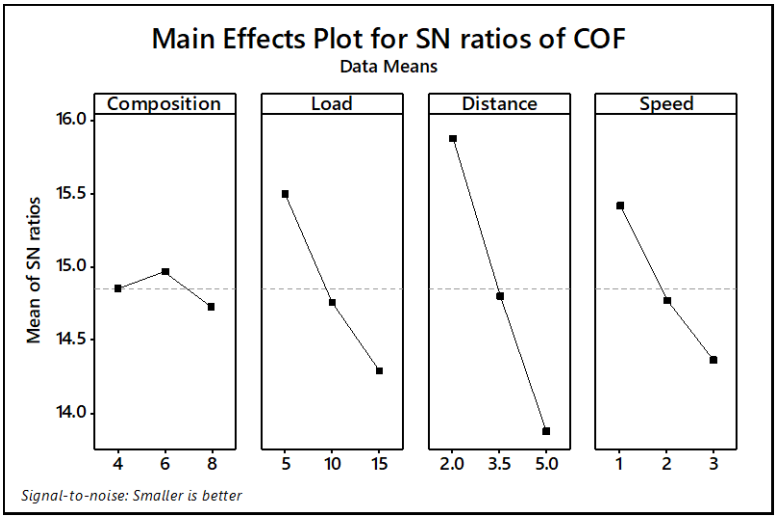

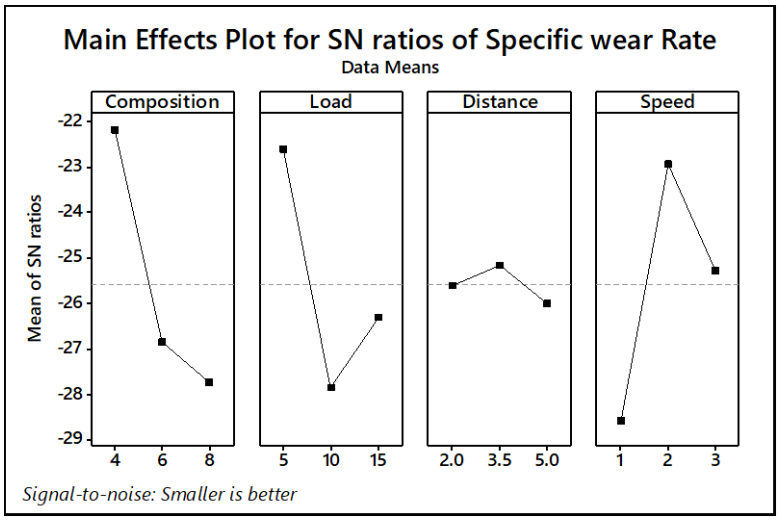

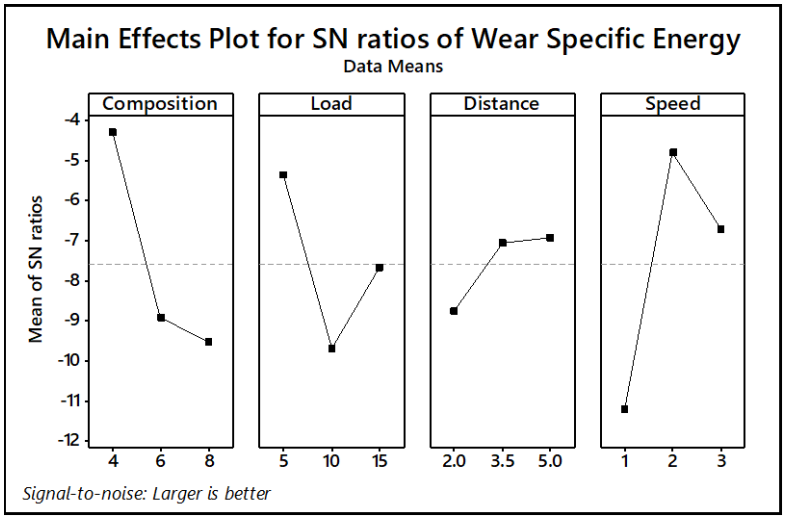

Figure 5.5 Main effects plot for SN ratios of (a) COF (C2L1D1S1); (b) SWR (C1L1D2S2); (c) EW (C1L1D3S2)

The X_i values in table 3 are estimated corresponding to the input parameter shown in main effects plot Fig.3 by using design of experiments package.

Table. 5.3 Calculation of factors A_i

Response	**Optimal input settings**	**Response value, X_i**	**Maximum acceptable value of response, X'_i**	$\boldsymbol{A_i = \frac{9}{log\,(\frac{X_i}{X'_i})}}$
COF	C2L1D1S1	0.124926	0.3	-44.09
SWR	C1L1D2S2	0.507407	9.95	5.885
EW	C1L1D3S2	1.00407	1.8	-35.5

Utility values

Utility values of three responses for the four reading or passes are calculated using the following equation:

$$U(n,Y) = P_{COF}(n,Y) \times W_{COF} + P_{SWR}(n,Y) \times W_{SWR} + P_{EW}(n,Y) \times W_{EW} \quad (5.14)$$

Where,

Preference scale for the coefficient of friction (COF):

$$P_{COF} = -44.09\ log\frac{X_{COF}}{0.3} \quad (5.15)$$

Preference scale for specific wear rate (SWR):

$$P_{SWR} = +5.885\ log\frac{X_{SWR}}{9.95} \quad (5.16)$$

Preference scale for amplitude of specific wear energy (EW):

$$P_{EW} = -35.5\ log\frac{X_{EW}}{1.8} \quad (5.17)$$

Table. 5.4 Input factors and utility index values (U) for each run

Run	Composition, %HNT	Load, N	Distance, km	Speed, ms-1	Utility index, U
1	4	5	2.0	1	13.57
2	4	5	3.5	1	13.16
3	4	5	5.0	1	07.00
4	4	10	2.0	3	08.92
5	4	10	3.5	3	06.83
6	4	10	5.0	3	05.72
7	4	15	2.0	2	07.60
8	4	15	3.5	2	06.20
9	4	15	5.0	2	03.90
10	6	5	2.0	2	10.09
11	6	5	3.5	2	05.78
12	6	5	5.0	2	07.20
13	6	10	2.0	1	14.71
14	6	10	3.5	1	11.13
15	6	10	5.0	1	12.34
16	6	15	2.0	3	09.99
17	6	15	3.5	3	11.11
18	6	15	5.0	3	09.61
19	8	5	2.0	3	10.42
20	8	5	3.5	3	09.09
21	8	5	5.0	3	06.43
22	8	10	2.0	2	11.78
23	8	10	3.5	2	09.94
24	8	10	5.0	2	11.79
25	8	15	2.0	1	12.12
26	8	15	3.5	1	10.05
27	8	15	5.0	1	10.62

5.2 Response Surface Methodology (RSM)

RSM is a statistical and mathematical modelling technique used to establish relation between input and output variables. This process is used to predict output variables and optimize input variables [121], [122]. In RSM, the quantitative relationship between input and output variables [122] is presented in equation (5.18):

$$y = f(x_1, x_2, x_3, \ldots\ldots, x_n) \pm e_r$$

(5.18)

where 'y' is desired response and 'f' is the response function, dependent variable and x_1, x_2, x_3, …..,x_n independent variables and 'e_r' is the fitting error. The RSM is used to identify the significant process variables on coefficient of friction and specific wear rate. Two factor interactions on the coefficient of friction and specific wear rate is investigated with the RSM.

Optimization of utility index by using response surface methodology

Table. 5.5 Analysis of Variance (ANOVA) of utility values

Source	Degrees of Freedom	P-Value
Model	13	**0.001**
Linear	4	0.001
wt.% HNT	1	**0.005**
Load	1	**0.036**
Distance	1	**0.001**
Velocity	1	0.222
Square	4	0.008
wt.% HNT × wt.% HNT	1	0.083
Load × Load	1	**0.003**
Distance × Distance	1	0.481
Velocity × Velocity	1	0.139
2-Way Interaction	5	0.020
wt.% HNT × Load	1	**0.015**
wt.% HNT ×Distance	1	0.113
wt.% HNT × Velocity	1	**0.003**
Load × Distance	1	0.118
Distance × Velocity	1	0.554

5.2.1 Regression Equation in Uncoded Units

Equation (5.19), provides the effect of main effects and its interactions on the utility index 'U' value. For any other combination of input factors by using equation (5.19), the value of utility index can be calculated.

Utility Value = 30.48 - 1.19 wt.% HNT + 0.742 Load - 4.69 Velocity - 12.04 Distance
- 0.261 wt.% HNT × wt.% HNT - 0.0956 Load × Load + 0.179 Velocity × Velocity
+ 1.007 Distance ×Distance + 0.1792 wt.% HNT × Load + 0.222 wt.% HNT ×
Velocity + 1.146 wt.% HNT × Distance + 0.0874 Load × Velocity
+ 0.159 Velocity × Distance

(5.19)

5.2.2 Surface plots

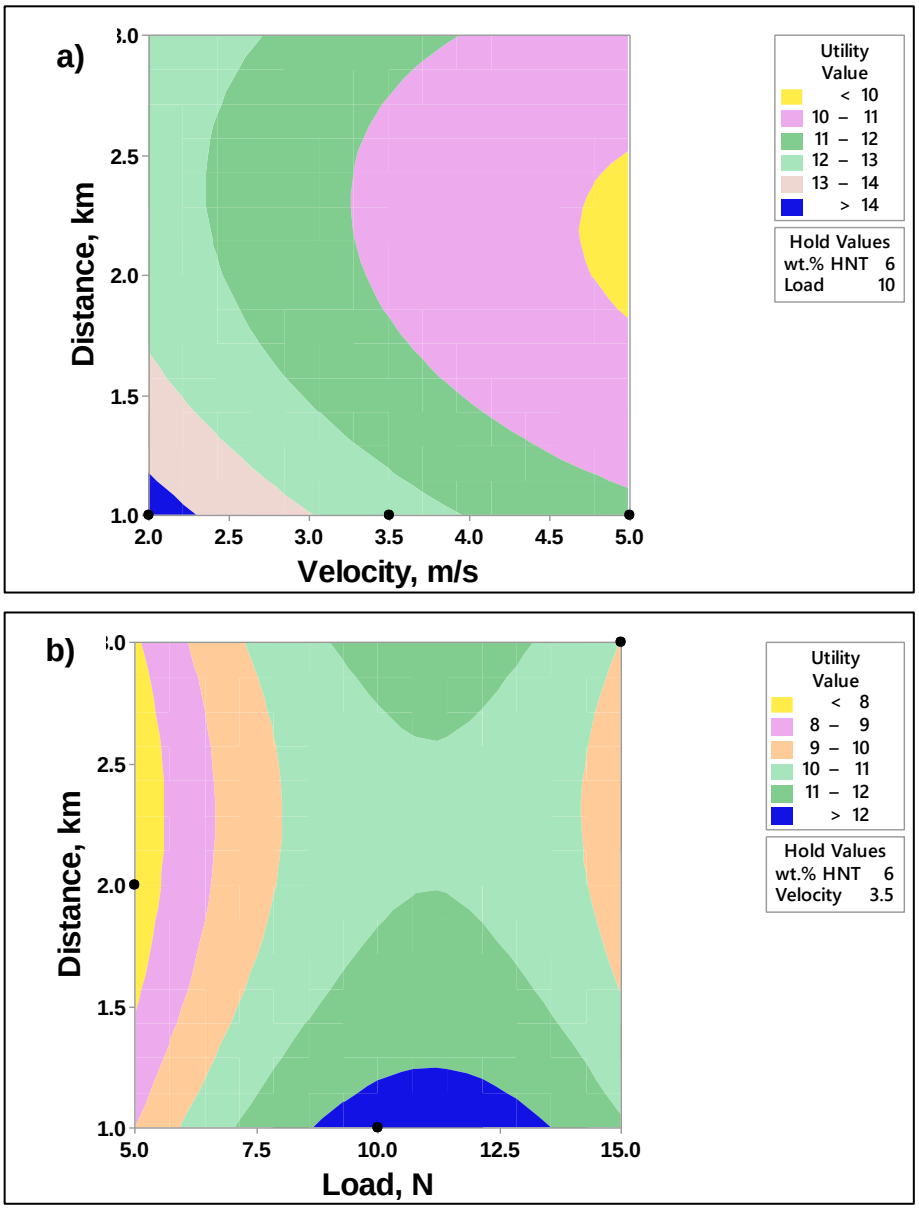

Figure 5.6 Effect of interaction of factors on the value of utility index; (a) Distance and velocity; (b) Distance and load

The effect of interaction of input factors on utility index values at the respective hold values were shown in Fig. 5.6 (a) & (b). From Fig. 5.6 (a), the utilization of the product for maximum utility was found at 2 m/s velocity and at moderate sliding distance corresponding to hold values of 6 wt. % HNT and 10 N Load. Similarly, from Fig. 5.6 (b) at 2 km distance and 11.8 N load higher values of utility index were seen corresponding to hold values of 6 wt. % HNT and at velocity of 3.5 m/s.

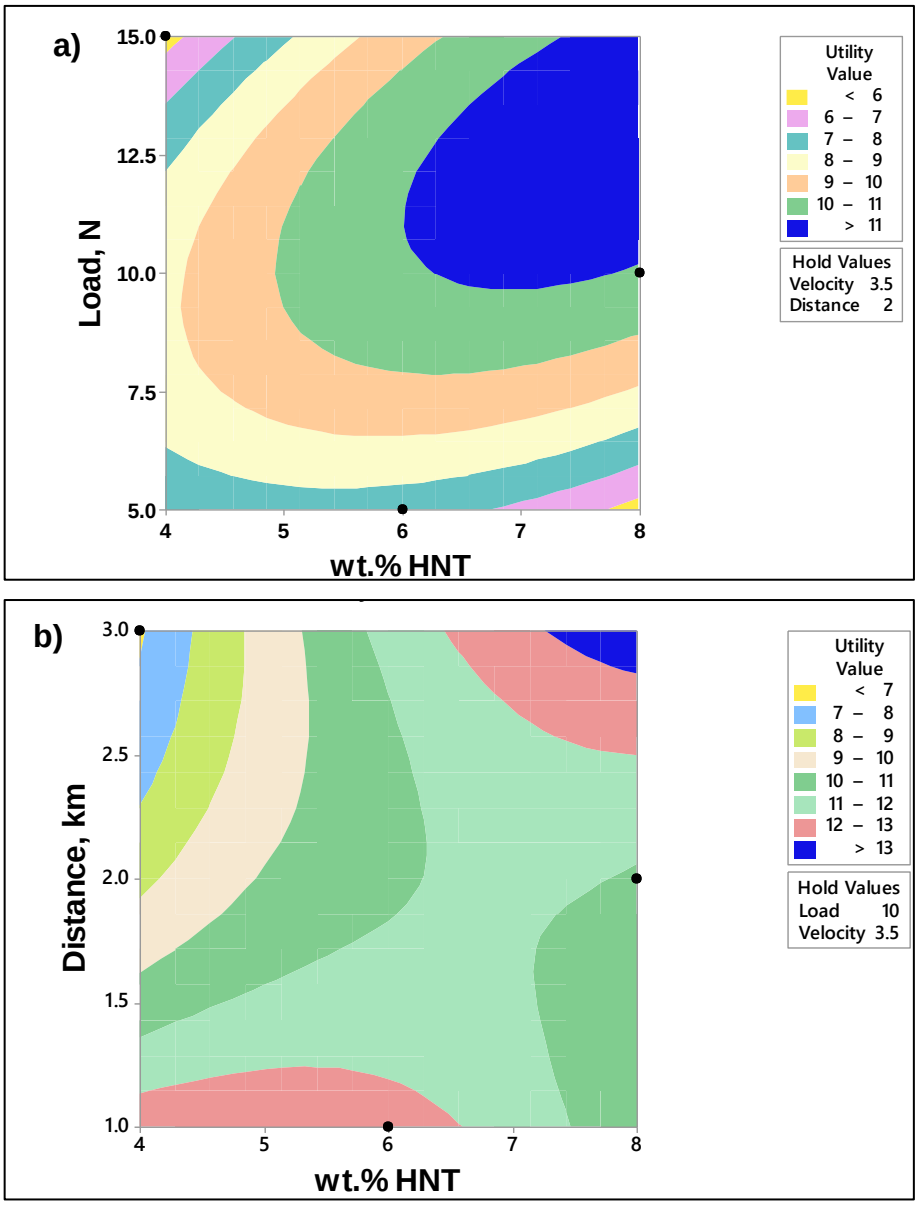

Figure 5.7 Effect of interaction of factors on the value of utility index; (a) wt. % HNT and load; (b) wt. % HNT and distance

The effect of interaction of input factors on utility index values at the respective hold values were shown in Fig. 5.7 (a) & (b). From Fig. 5.7 (a), at about 7 wt. % HNT and 12 N normal load the utility has shown maximum value. From Fig. 5.7 (b), at > 7 wt. % and 3 m/s sliding velocity the utility value was found to be maximum

5.2.3 Optimization study

Desirability value corresponding to maximum utilization, the optimum values were found: At D=1: 4% composition, 8.5354 N load, 2.0 km distance and at a velocity of 1.0 m/s as shown

in Fig. 5.8; The value of utility index observed to be 15.5066 and was within 95% confidence interval (13.01 to 17.99).

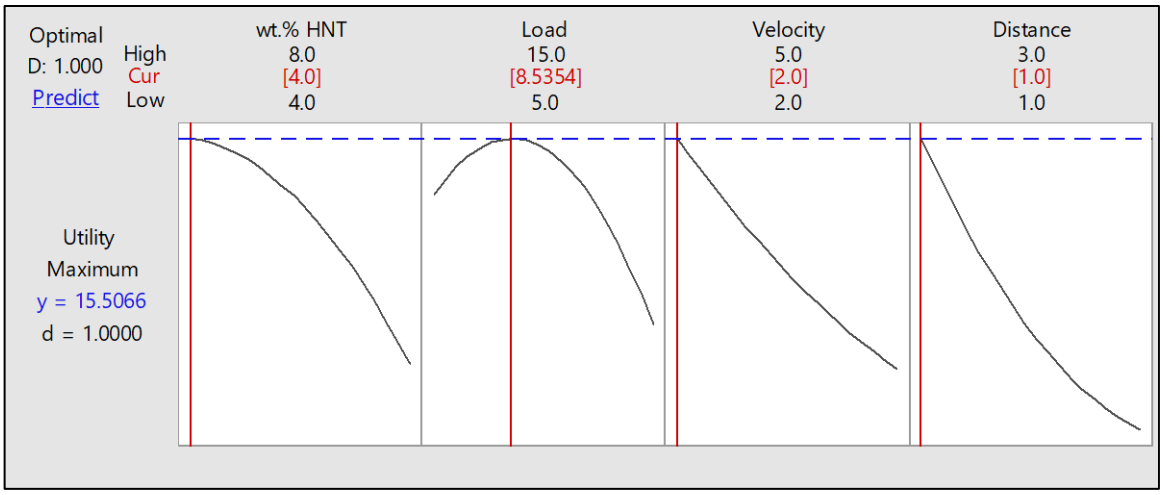

Figure 5.8 Optimum values of input parameters of PTFE/HNT nanocomposites at desirability, D=1

5.3 Multi-optimization of wear input parameters by Response Surface Methodology

In this study, the multi responses COF, SWR, and EW were optimized by using RSM. In the analysis, the experimental runs and the corresponding estimated responses were already tabulated in Table 5.2. During the analysis, quadratic models were developed among responses and process parameters using design of experiments software. The quadratic models were used to predict these responses. RSM is a statistical and mathematical modelling technique used to establish relation between input and output variables and is used to identify the significant process variables on tribological parameters.

The process was used to predict output variables and optimize input variables [121], [122]. In RSM, the quantitative relationship between input and output variables was presented in equation (5.20):

$$y = f(x_1, x_2, x_3, \dots\dots, x_n) \pm e_r \tag{5.20}$$

where 'y' is desired response and 'f' is the response function, dependent variable and x_1, x_2, x_3, …..,x_n independent variables and 'e_r' is the fitting error.

5.3.1 Analysis of Variance (ANOVA)

The model should be responsive enough to the selected input parameters. The insignificant input parameters are screened out, and those are not considered in the model formation. A quantitative evaluation of each parameter's effect on the total model variance can be carried out using analysis of variance (ANOVA) method. The equation (5.21) is used to find F- test value.

$$F_A = \frac{SS_R/k}{SS_E/(n-k-1)} \tag{5.21}$$

Where F_A denotes F test value of a particular input parameter 'A'. SS_E and SS_R are the sum of squares due to the model and residual error respectively, n is the number of samples used in the design procedure. If F_A exceeds a selected value, the input parameter 'A' is said to be significant with respect to the responses [123].

Table. 5.6 ANOVA of the input factors and their interactions for quadratic model of the responses COF, SWR, and EW

Source	**DF**	**COF P-Value**	**SWR P-Value**	**EW P-Value**
Model	13	**0.001**	**0.001**	**0.000**
Linear	4	0.000	0.000	0.000
wt.% HNT	1	0.916	**0.001**	**0.000**
Load, N	1	**0.006**	**0.000**	**0.001**
Distance, km	1	**0.000**	0.490	**0.043**
Speed, m/s	1	**0.004**	0.277	0.281
Square	4	0.735	0.002	0.001
wt.% HNT x wt.% HNT	1	0.534	**0.038**	0.124
Load x Load	1	0.510	**0.000**	**0.000**
Distance x Distance	1	0.944	0.321	0.669
Speed x Speed	1	0.274	0.955	**0.043**
2-Way Interaction	5	0.123	0.011	0.001
wt.% HNT x Load	1	0.128	**0.002**	**0.000**
wt.% HNT x Distance	1	0.086	0.664	0.127
wt.% HNT x Speed	1	0.407	**0.001**	**0.000**
Load x Distance	1	0.080	0.690	0.658
Distance x Speed	1	0.323	0.856	0.537

In this study, the experimental results were analysed with ANOVA and it performed at confidence level of 95%. The ANOVA calculates F value, the Probability > F (p-value) and the values indicate statistical significance of the model. The terms which are having p-value less than 0.05 indicate that they are significant [124]. Table 5.6 shows the ANOVA values of the three responses and whose p-values of model were less than 0.05 and the model was significant.

Also for the factors load, speed, & distance and interactions of composition and distance & load and distance are having p-value of <0.05 and highlighted as shown in Table 5.6. For response variable COF, the interactions exist but were found to be less significant. Whereas, for response variables SWR and EW, the wt. % HNT addition ensured interactions with load and speed. Based on the p-value, the developed model was considered to be significant on the responses.

5.3.2 Regression analysis

The correlation between the tribological parameters was obtained as follows by using regression technique. Empirical or regression equations (5.22) - (5.24) for the responses COF, SWR, and EW of the PTFE/HNT nanocomposites were presented.

$$\begin{aligned} COF = {} & 0.0545 - 0.0173\ wt.\%\ HNT + 0.00356\ Load + 0.0439\ Distance \\ & + 0.0370\ Speed + 0.00086\ wt.\%\ HNT \times wt.\%\ HNT - 0.000169\ Load \times Load \\ & - 0.00017\ Distance \times Distance - 0.00711\ Speed \times Speed + 0.001011\ wt. \\ & \%\ HNT \times Load - 0.00236\ wt.\%\ HNT \times Distance + 0.00267\ wt.\%\ HNT \times Speed \\ & - 0.000967\ Load \times Distance - 0.00261\ Distance \times Speed \end{aligned} \tag{5.22}$$

$$\begin{aligned} SWR, (x10^{-6}\ mm3/N\text{-}m) = {} & 44.4 - 4.81\ wt.\%\ HNT + 7.08\ Load - 10.17\ Distance - \\ & 38.3\ Speed - 1.555\ wt.\%\ HNT \times wt.\%\ HNT - 0.614\ Load \times Load + 1.24\ Distance \times \\ & Distance + 0.18\ Speed \times Speed + 1.208\ wt.\ \%\ HNT \times Load + 0.282\ wt.\%\ HNT \times \\ & Distance + 6.82\ wt.\%\ HNT \times Speed + 0.104\ Load \times Distance - 0.24\ Distance \times Speed \end{aligned} \tag{5.23}$$

$$\begin{aligned} EW, MJ/g = {} & -1.655 + 0.365\ wt.\%\ HNT - 0.0966\ Load + 0.227\ Distance \\ & + 1.379\ Speed + 0.0214\ wt.\%\ HNT \times wt.\%\ HNT + 0.01278\ Load \times Load \\ & - 0.0101\ Distance \times Distance - 0.1344\ Speed \times Speed - 0.03167\ wt. \\ & \%\ HNT \times Load - 0.0200\ wt.\%\ HNT \times Distance - 0.1572\ wt.\%\ HNT \times Speed \\ & - 0.00222\ Load \times Distance + 0.0156\ Distance \times Speed \end{aligned} \tag{5.24}$$

The interaction between the factors were found in equations (5.22) – (5.24). The positive value of the coefficients suggests that the response variable (COF or SWR or EW) of material increases with their associated variables. Whereas the negative value of the coefficients

suggests that the response variable (COF or SWR or EW) of the material will decrease with the increase in associated variables.

5.3.3 Surface plots

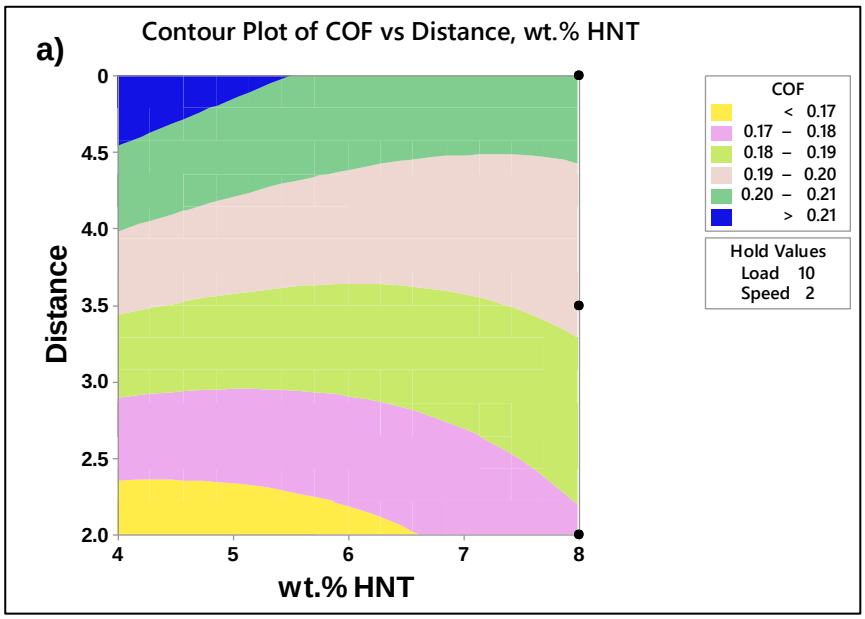

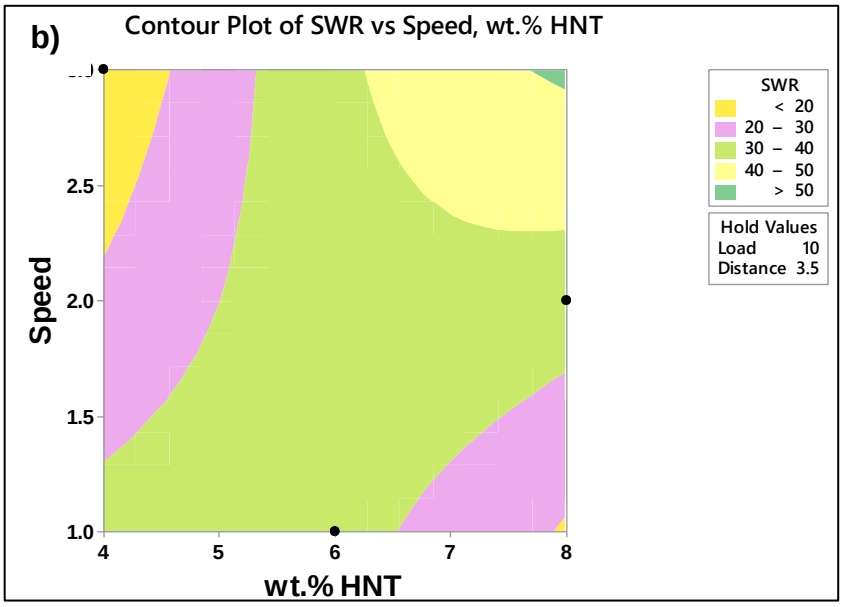

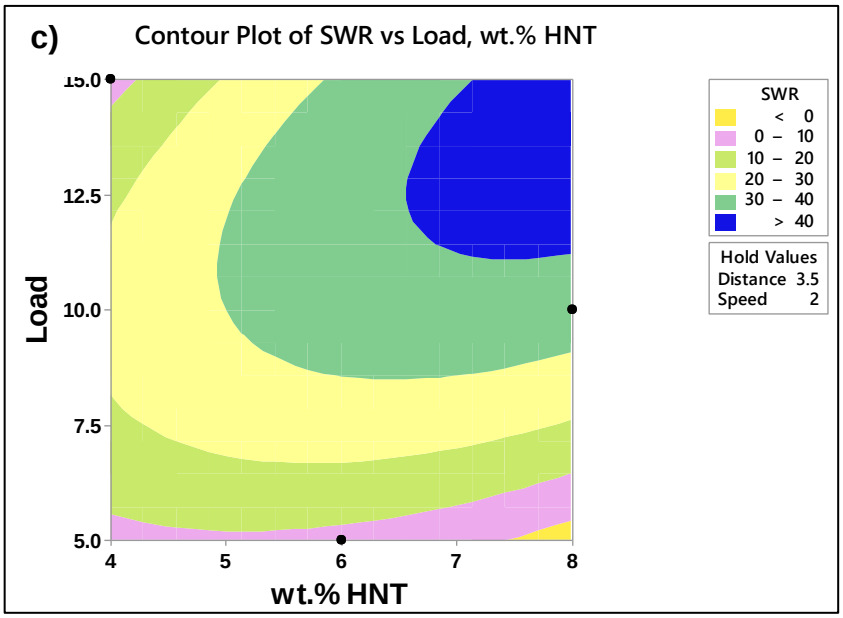
c)
Contour Plot of SWR vs Load, wt.% HNT
Load
wt.% HNT
15.0
12.5
10.0
7.5
5.0
4
5
6
7
8
SWR
< 0
0 – 10
10 – 20
20 – 30
30 – 40
> 40
Hold Values
Distance 3.5
Speed 2

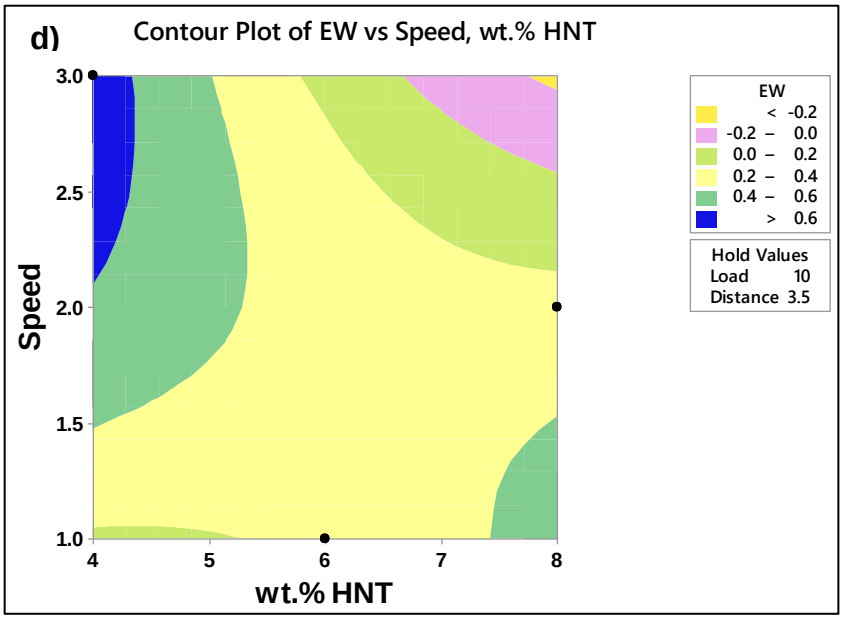
d)
Contour Plot of EW vs Speed, wt.% HNT
Speed
wt.% HNT
3.0
2.5
2.0
1.5
1.0
4
5
6
7
8
EW
< -0.2
-0.2 – 0.0
0.0 – 0.2
0.2 – 0.4
0.4 – 0.6
> 0.6
Hold Values
Load 10
Distance 3.5

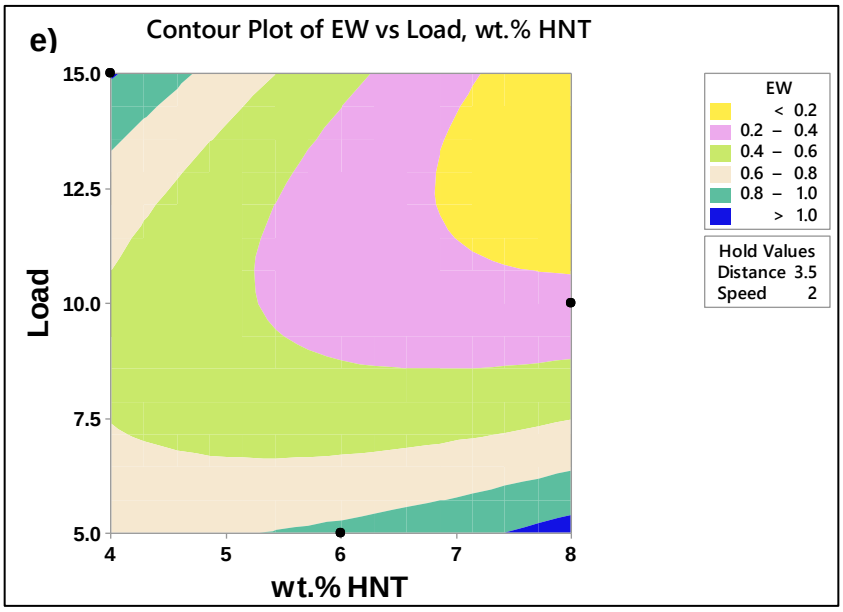

Figure 5.9 (a)-(e) Response surface contour plots: (a) interaction of wt. % HNT and distance on COF; (b) interaction of wt. % HNT and speed on SWR; (c) interaction of wt. % HNT and load on SWR; (d) interaction of wt. % HNT and speed on EW; (e) interaction of wt. % HNT and load on EW

5.3.4 Multi objective optimization of Tribological Parameters: composite desirability

Optimization using desirability function is introduced in 1980 by Derringer and Suich [125] for optimization of cutting parameters. This method works based on the reduced gradient algorithm, which starts with multiple solutions and finally obtains the maximum value of the desirability to determine the optimal solution. It uses desirability (d value) scale which ranges from 0 to 1, if d value is 0 or close to 0 then the response is completely unaccepted and if the d value is 1 or close to 1 then the response is accepted. In the present work, by using response surface methodology the responses optimized were specific wear energy (EW), specific wear rate (SWR), and coefficient of friction (COF). The composite desirability for multi-objective optimization of the responses was found to be 0.9272 as shown in Fig. 5.10. The composite desirability was found by using response optimizer tool in RSM. The corresponding optimum input parameters were found for minimum COF (0.144) and SWR (22.053×10^{-6} mm^3/N-m) while for maximum EW (0.503 MJ/g) as 6.67 wt. % of composition, 7.4242 N of load, 2.0 km of distance and 1.5051 m/sec of velocity. Since the composite desirability was close to 1, which indicates that the responses were reasonably optimized.

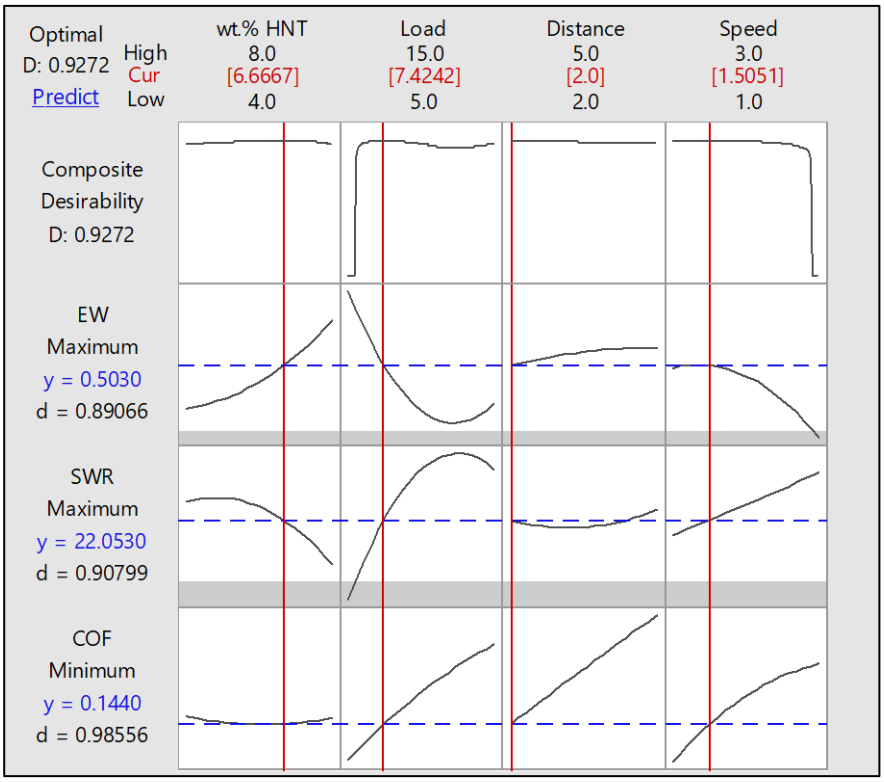

Figure 5.10 Optimization of parameters for minimum COF and SWR & for maximum EW

The optimum input parameters from the hybrid method and RSM were shown in Table 5.6 (a). From hybrid method, the optimum input parameters were found to be, 4.0 wt.% HNT, 8.5354 N load, 2.0 km sliding distance, and at a sliding velocity of 1.0 m/s, an utility index value of 15.5066 was obtained corresponding to maximum utilization of the product. Whereas from RSM, the optimum input parameters found to be 6.67 wt. % HNT, a normal load of 7.4242 N, a sliding distance of 2.0 km, and sliding velocity of 1.5051 m/s. The multi responses COF, SWR, and EW were found to be 0.144, 22.053x10^{-6}mm3/N-m, and 0.5030 MJ/g respectively. This means that, from hybrid method as per designer based requirement the value of wt. % HNT was about 4% and from RSM based on same weightage to all factors, the wt. % HNT was about 6.67%. Hence, the hybrid method suggested optimum wt. % HNT addition to be 4 % and minimum COF, minimum SWR, and maximum EW might be obtained. Also, at 4 wt. % HNT addition in the PTFE matrix, better mechanical and thermal properties were found.

Table 5.6 (a) Comparison of optimum input parameters for Hybrid method and RSM

Input parameter	Designer based Hybrid method: at desirability = 1.0	Response Surface Methodology: at Desirability = 0.9272
Wt. % HNT	4.0	6.67
Load, N	8.5354	7.4242

Distance, km	2.0	2.0
Speed/ Velocity, m/s	1.0	1.5051
Output parameter	Utility index = 15.5066	COF= 0.144; SWR=22.053x10^{-6}mm3/N-m; EW= 0.5030 MJ/g

PHASE – II

5.4 Effect of surface roughness on wear properties of PTFE/HNT nanocomposites

The specimens for POD test are cut from the sheets. The cross-section of the specimen was rectangular (3 mm x 3.5mm) and length of the pin was 20 mm. All experiments are conducted on pin on disc apparatus as per the ASTM G99 standard. A typical Pin on Disc set up used for the experimentation is shown in Figure 5.11. In this study, five parameters are selected as control factors, and each parameter was designed to have three levels, denoted 1, 2, and 3 (Table 5.7). The experimental design was according to an L27 array based on Taguchi method to investigate the relation between the process parameters and response factor. Minitab 16 software was used for optimization and graphical analysis of obtained data.

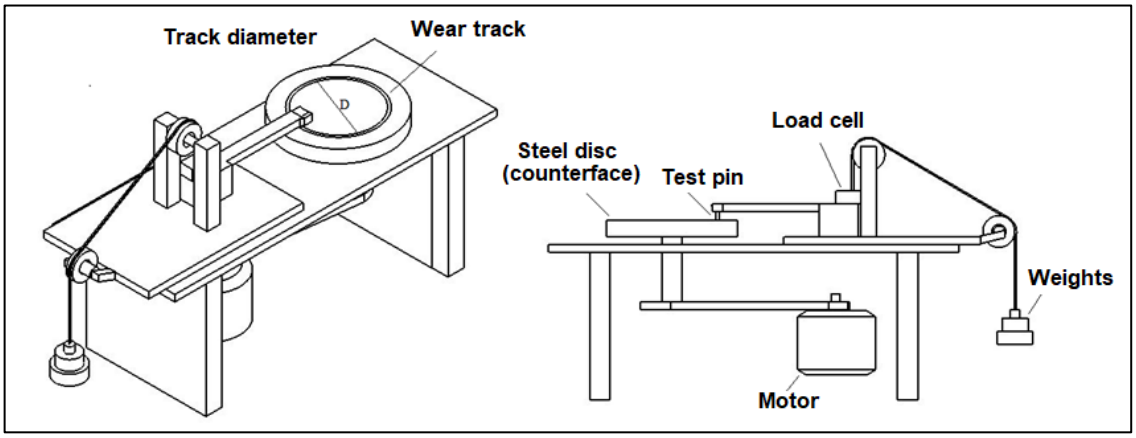

Figure 5.11 Line sketch of POD apparatus (a) Isometric view (b) Rear view

Table 5.7 Factors and Levels

Input factor	Levels		
	1	2	3
A: Filler, % HNT	4	6	8
B: Normal Load, N	5	10	20
C: Sliding Velocity, m/s	3	4	5
D: Sliding distance, m	1000	2000	3000
E: SiC abrasive paper roughness, microns	18.3	25.8	9.5

Emery papers of different grades P600, P1000, P2000 are used. P600 offers an average roughness of 25.8 micrometres while P1000 and P2000 offer 18.3 and 9.5 micrometres respectively. The values of surface roughness are obtained from the standard ISO charts.

5.4.1 Specific wear rate

The experiments are done and the results of the responses are tabulated and given Table 5.8. The coefficient of friction is calculated by taking the ratio of frictional force and applied load. The specific wear rate is calculated by using Archard's equation (5.25).

$$Specific\ Wear\ Rate = \frac{\Delta m}{\rho l f_n} \quad \text{mm3/N} - \text{m} \tag{5.25}$$

where, Δm is mass loss in gm;

ρ is density of the nanocomposite material in gm/mm^3;

l is the distance travel in m;

f_n is the normal load applied in N.

The density values of 4%, 6%, and 8% HNT by weight are experimentally estimated as: 2.257 gm/cc; 2.259 gm/cc; and 2.262 gm/cc as discussed in chapter 3

Table 5.8 Taguchi L27 orthogonal array of experimental runs

Experimental run	**A**	**B**	**C**	**D**	**E**	**SWR (mm3/N-m)**		COF	
	(%HNT)	**(N)**	**(m/s)**	**(m)**	**(µm)**	**Experimental**	**Predicted**	**Experimental**	**Predicted**
1	4	5	3	1000	18.3	0.00327	0.00309	0.4	0.403
2	4	5	4	2000	25.8	0.003514	0.00348	0.4	0.384
3	4	5	5	3000	9.5	0.003096	0.00326	0.2	0.246
4	4	10	3	2000	9.5	0.001491	0.00159	0.3	0.280
5	4	10	4	3000	18.3	0.00173	0.00158	0.3	0.262

6	4	10	5	1000	25.8	0.002349	0.00237	0.3	0.283
7	4	20	3	3000	25.8	0.000961	0.00109	0.125	0.138
8	4	20	4	1000	9.5	0.001095	0.00105	0.15	0.165
9	4	20	5	2000	18.3	0.001218	0.00116	0.15	0.163
10	6	5	3	1000	18.3	0.002813	0.00295	0.5	0.528
11	6	5	4	2000	25.8	0.003073	0.00329	0.4	0.495
12	6	5	5	3000	9.5	0.003289	0.00315	0.4	0.362
13	6	10	3	2000	9.5	0.001555	0.00151	0.4	0.395
14	6	10	4	3000	18.3	0.001639	0.00143	0.4	0.362
15	6	10	5	1000	25.8	0.002148	0.00218	0.4	0.362
16	6	20	3	3000	25.8	0.001003	0.00092	0.2	0.204
17	6	20	4	1000	9.5	0.000865	0.00097	0.25	0.228
18	6	20	5	2000	18.3	0.001078	0.00103	0.2	0.212
19	8	5	3	1000	18.3	0.002812	0.00285	0.6	0.568
20	8	5	4	2000	25.8	0.003338	0.00314	0.6	0.521
21	8	5	5	3000	9.5	0.003127	0.00309	0.4	0.391
22	8	10	3	2000	9.5	0.001547	0.00147	0.4	0.424
23	8	10	4	3000	18.3	0.000977	0.00133	0.3	0.375
24	8	10	5	1000	25.8	0.002104	0.00203	0.3	0.355
25	8	20	3	3000	25.8	0.000855	0.00079	0.2	0.183
26	8	20	4	1000	9.5	0.00101	0.00094	0.2	0.206
27	8	20	5	2000	18.3	0.000836	0.00093	0.2	0.174

5.4.2 Response surface methodology

The main effect plots for responses COF and SWR were shown in Fig. 5.12 (a) & (b). The model summary for the developed model was shown in Table 5.9. The P-value of the model for both the responses was < 0.05, which indicates a valid model. The R-squared values of the model for the optimization process were shown in Table 5.10.

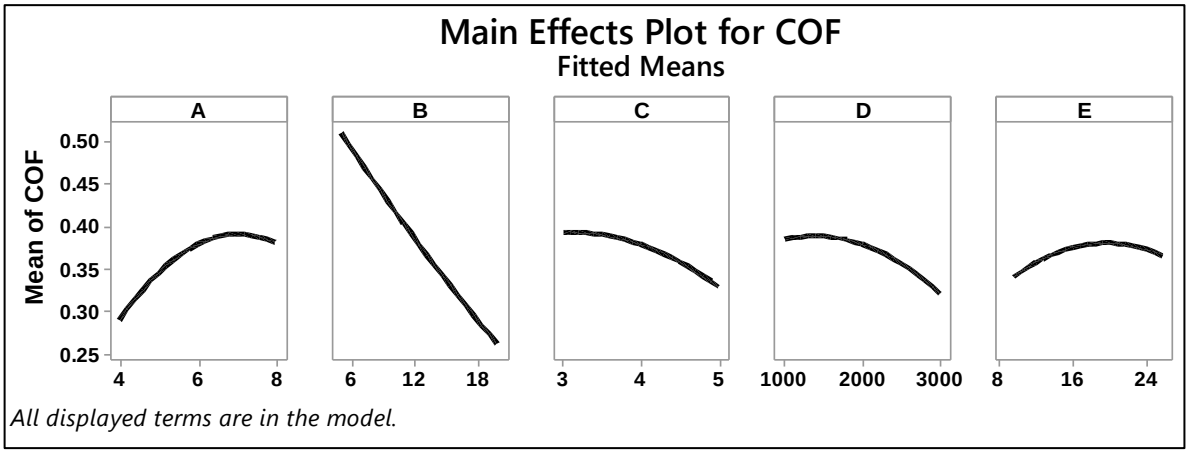

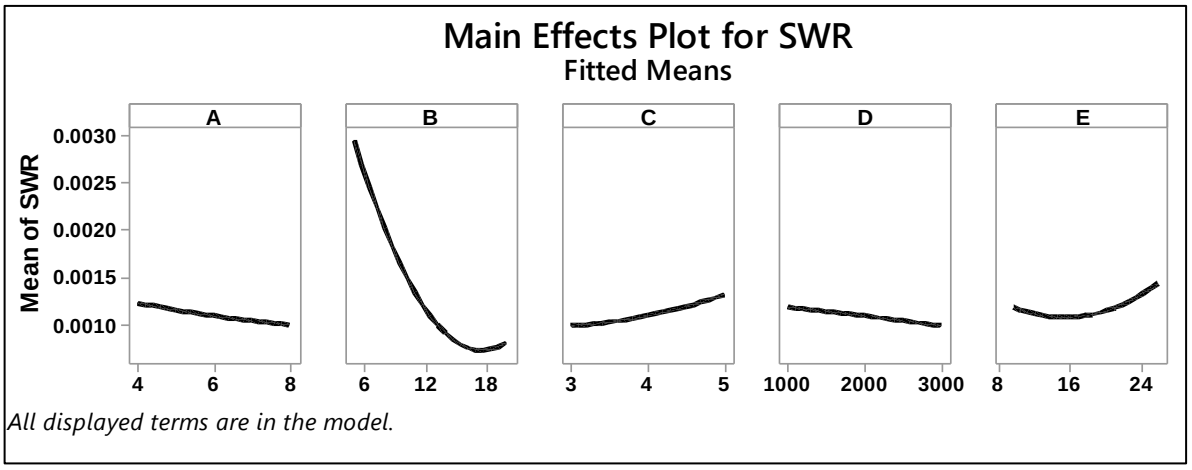

1

Figure 5.12 Main effects plot for (a) COF; (b) SWR

Table.5.9 ANOVA and model summary for COF and SWR

Source	**COF** P-Value	**SWR** P-Value
Model	0.000	0.000
Linear	0.000	0.000
A	0.005	0.030
B	0.000	0.000
C	0.033	0.004
D	0.033	0.053
E	0.363	0.019
Square	0.306	0.000
A*A	0.085	0.784
B*B	0.786	0.000
C*C	0.446	0.473
D*D	0.272	0.915
E*E	0.290	0.021

Table.5.10 R-squared values of the model Summary for COF and SWR

Response	R-Squared	R-Squared (adjusted)	R-Squared (predicted)
COF	91.34%	81.24%	56.65%
SWR	98.04%	95.75%	89.45%

5.4.3 Contour plots of the responses COF & SWR

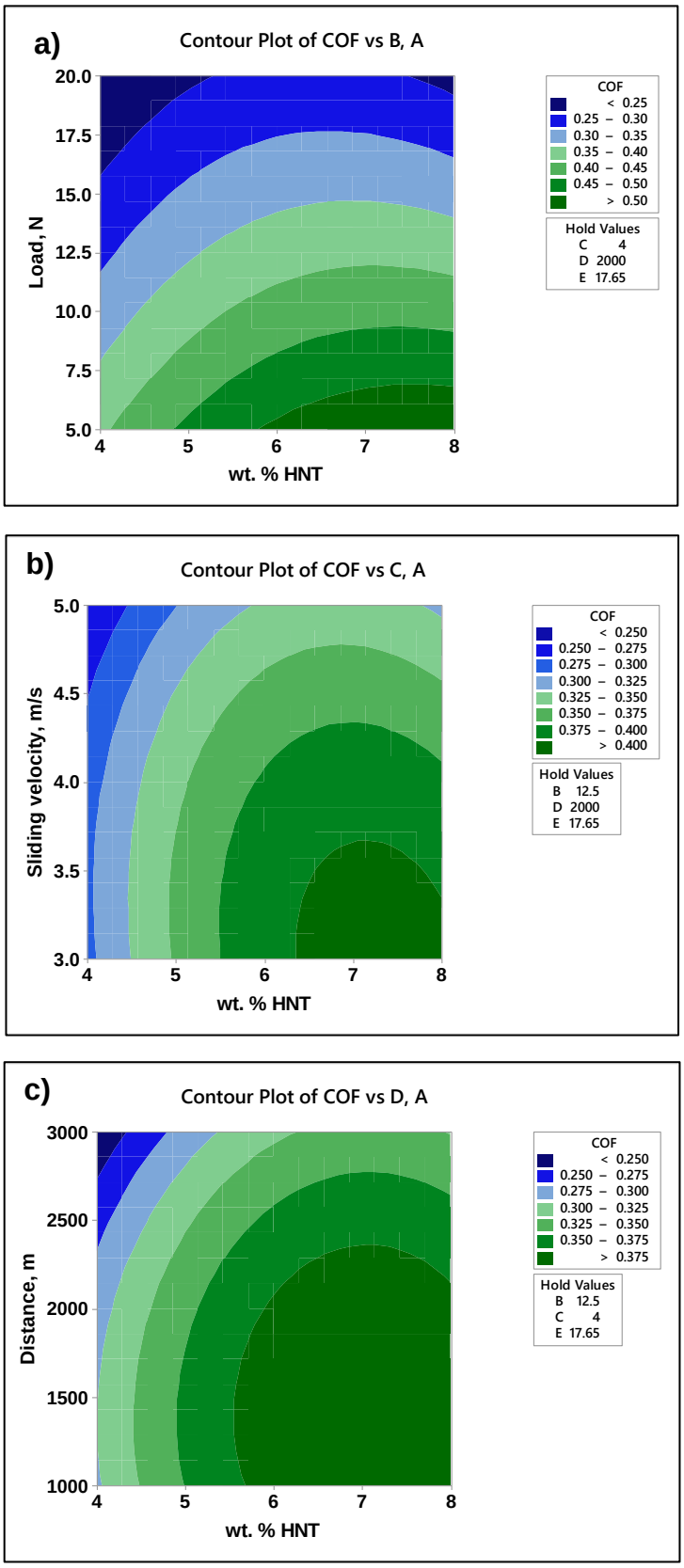

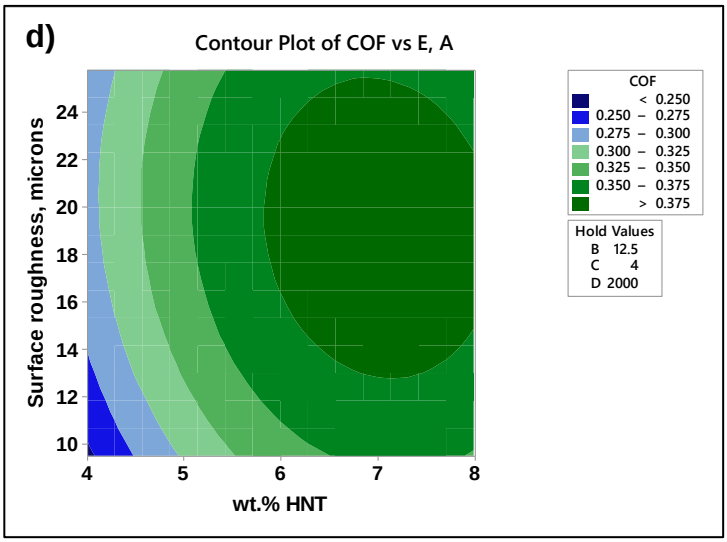

Figure 5.13 Contour plots showing effect of the interaction of the input factors on COF: (a) wt. % HNT vs Load; (b) wt. % HNT vs Velocity; (c) wt. % HNT vs Distance; (d) wt. % HNT vs Surface roughness

The contour plots from the RSM analysis for the coefficient of friction were shown from Fig. 5.13 (a)-(d). The plots show the effect of interaction of input parameters on the response coefficient of friction. From Fig. 5.13 (a), the inverse relationship between the factors was found i.e. at high loads and with low wt. % HNT addition the COF decreases and at low loads and with high wt. % HNT addition the COF increases. A gradual variation of the COF under these conditions can be observed from the plot Fig. 5.13 (a). From Fig. 5.13 (b), at lower sliding velocities and with increase in the wt. % addition, a sudden change in the COF was observed and with increase in sliding velocities at different wt. % addition the change in COF was found to be sensitive. From Fig. 5.13 (c), at lower sliding distance the value of COF was high and was found low at low wt. % addition. Finally, from Fig 5.13 (d), it can be seen that the increase of wt. % HNT and courter surface roughness caused the non-proportional increase of COF of PTFE/HNT nanocomposites.

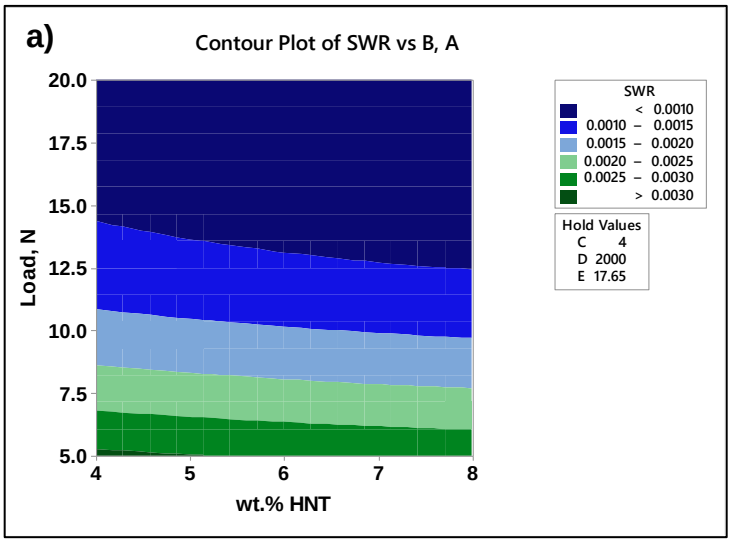
a)
Contour Plot of SWR vs B, A
Load, N
wt.% HNT
SWR
< 0.0010
0.0010 – 0.0015
0.0015 – 0.0020
0.0020 – 0.0025
0.0025 – 0.0030
> 0.0030
Hold Values
C 4
D 2000
E 17.65

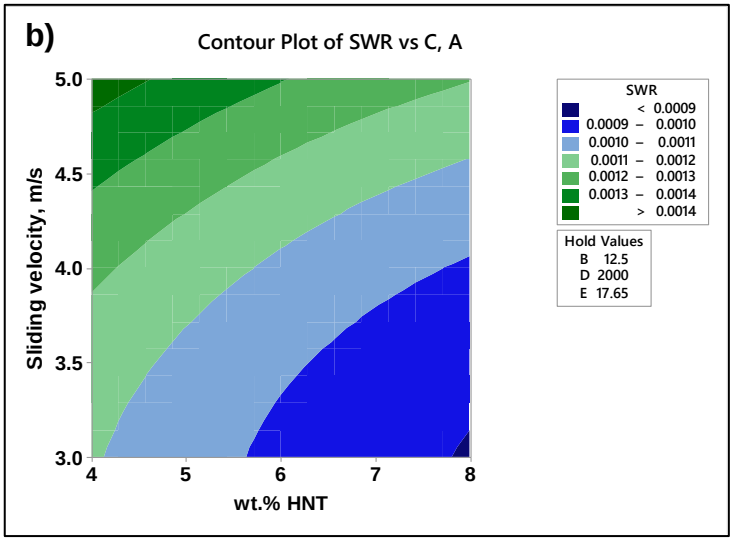
b)
Contour Plot of SWR vs C, A
Sliding velocity, m/s
wt.% HNT
SWR
< 0.0009
0.0009 – 0.0010
0.0010 – 0.0011
0.0011 – 0.0012
0.0012 – 0.0013
0.0013 – 0.0014
> 0.0014
Hold Values
B 12.5
D 2000
E 17.65

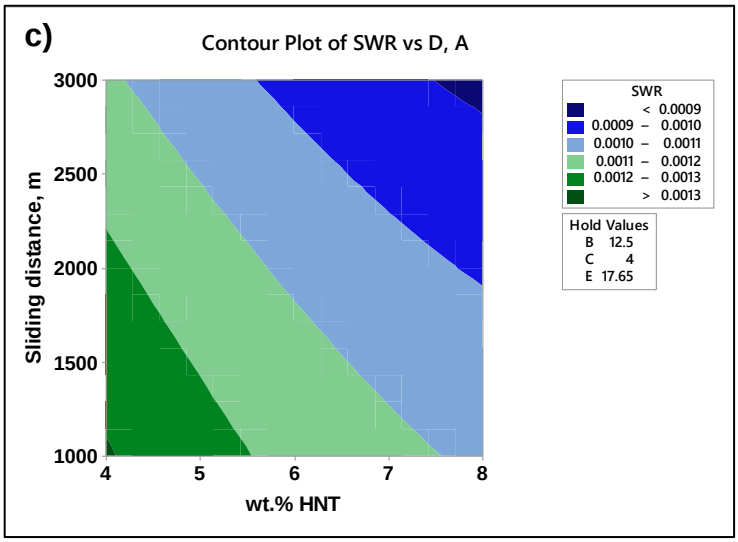
c)
Contour Plot of SWR vs D, A
Sliding distance, m
wt.% HNT
SWR
< 0.0009
0.0009 – 0.0010
0.0010 – 0.0011
0.0011 – 0.0012
0.0012 – 0.0013
> 0.0013
Hold Values
B 12.5
C 4
E 17.65

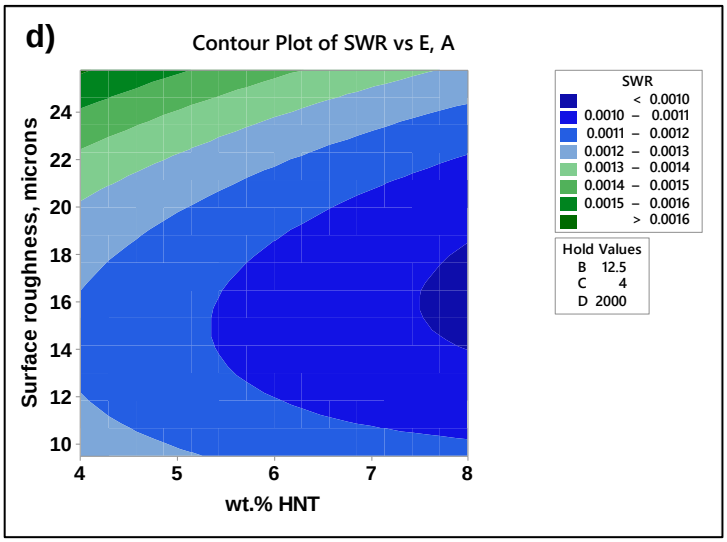

Figure 5.14 contour plots showing effect of the interaction of the input factors on SWR: (a) wt. % HNT vs Load; (b) wt. % HNT vs Velocity; (c) wt. % HNT vs Distance; (d) wt. % HNT vs Surface roughness

The contour plots from the RSM analysis for the specific wear rate were shown from Fig. 5.14 (a)-(d), while maintaining their relevant other input parameters as constant. The plots shown the effect of interaction of input parameters on the response specific wear rate. From Fig. 5.14 (a), the wear rate was predicted to be constant and independent of wt. % HNT addition in the PTFE matrix. Higher wear rates were seen from the Fig. 5.14 (a) at low load conditions, since at low load the PTFE nanocomposite sample surface was directly exposed to the counter face surface roughness but after establishment and deposition of transfer film the wear rate was reduced [126]–[128]. At this stage of running the COF also shown less value as the slider was now running on the transfer film. The aspect was also revealed at moderate addition of HNTs maintained the film strength, as shown in the SEM microstructure (see Figure 5.17 (a)). It can be seen from Fig 5.14 (b) that, at low sliding velocities and with increase of wt. % HNT caused decreased wear rate of PTFE/HNT nanocomposites. On the other hand sliding distance shown an inverse effect on specific wear rate of PTFE/HNT nanocomposites as shown in Fig. 5.14 (c). The surface plot was plotted at holding values of other three parameters, i.e., at 12.5 N load, 4 m/s sliding velocity, and 2000 m sliding distance. From Fig. 5.14 (d), the effect on wt. % addition and counter surface roughness on SWR shown an increase in it. As the wt. % HNT addition increases from 4 % to 8 % and increase in the surface roughness from 9.5 microns to 25.8 microns, the SWR was first reduced at 9.5 microns counter surface roughness and then increased SWR was noticed at 25.8 microns counter surface roughness.

5.4.4 Regression analysis

$$COF = -0.570 + 0.2019\ A - 0.0081\ B + 0.144\ C + 0.000067\ D + 0.0175\ E - 0.01076\ A*A + 0.000130\ B*B - 0.0181\ C*C - 0.000000\ D*D - 0.000385\ E*E - 0.00193\ A*B - 0.00521\ A*C + 0.000001\ A*D - 0.000400\ A*E \quad (5.25)$$

$$SWR = 0.00644 - 0.000060\ A - 0.000498\ B - 0.000290\ C - 0.000000\ D - 0.000081\ E + 0.000006\ A*A + 0.000014\ B*B + 0.000059\ C*C - 0.000000\ D*D + 0.000003\ E*E + 0.000001\ A*B - 0.000004\ A*C - 0.000000\ A*D - 0.000003\ A*E \quad (5.26)$$

The positive coefficients of the input factors increases the response variable whereas the negative coefficients of the factors influence the reduction in the response variables COF and SWR.

5.4.5 Composite desirability of the multi-responses: COF & SWR

The composite desirability for multi-objective optimization of the responses was found to be 1 as shown in Fig. 5.15. From the Fig. 5.15, the optimum input parameters and responses of PTFE/HNT nanocomposites for the abrasive wear study were predicted to be 4 wt. % of HNT

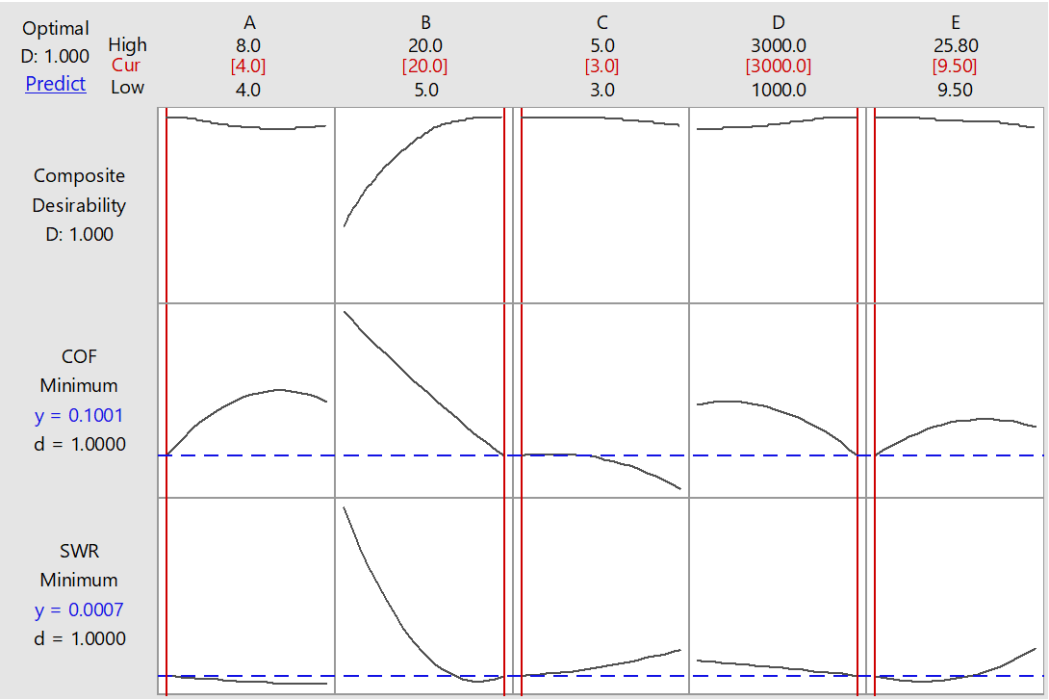

Figure 5.15 Composite desirability plot for multi-objective optimization of COF and SWR

addition, 20 N of load, 3.0 km of distance, 3 m/sec of sliding velocity when running against a counter surface roughness of 9.5 microns were 0.1001 and 700×10^{-6} mm^3/N-m for COF and

SWR respectively. Since the composite desirability was close to 1, which indicated the responses were reasonably optimized.

5.4.6 SEM analysis of PTFE/HNT nanocomposite pin surface and wear tracks

SEM microstructure had shown in Fig. 5.16 (a) – (d), the regions of localized wear along the sliding direction. High magnification observations indicated the presence of sharp, irregularly shaped particles on the wear tracks. Examinations also revealed a slight percentage of silica on the wear track surface owing its presence to the use of SiC abrasive paper.

The depth of cut is more for pin made of 4% HNT than for pin made of 8 %. The wear surface of pure PTFE is characterized by loose crystalline bands .This strongly suggests that the crystalline bands of PTFE are easily pulled out during the process of tearing. The worn surface of PTFE is very rough, displaying plucked and ploughed marks indicative of adhesive wear and ploughing as shown in Fig. 5.16 (a). The size of the plucked marks seen were increase with the increase in applied normal load and surface roughness of the SiC abrasive papers. The worn surface of PTFE sample made of 4 wt. % HNT addition, indicates the ploughed marks without plucked marks and therefore the addition of nanofiller increased the wear resistance of the PTFE nanocomposites. This indicates under the specified operating conditions the HNTs surrounded by the PTFE matrix material presents the strong interfacial adhesion between them. The debonded HNTs from the matrix were ruptured during the wear process due the cutting edges of the SiC abrasive paper. The deposition of these particles along the track can be seen in the Fig. 5.16 (b). The effect of surface roughness on this group had much influence on the wear loss and coefficient of friction.

The worn surface of PTFE sample made of 6 wt. % HNT addition, as illustrated in Fig. 5.16 (c) when abraded against 9.5 μm SiC abrasive paper to a sliding distance of 2 km. The abrasive cutting edges contacts in the wear process and removes the matrix material in the form of debris. Few of this debris deposits the space between SiC abrasives and rest are merged to the abrasive cutting edges. The grooves formed and their geometric intensities are much lesser than the grooves formed at 4 wt. % HNTs addition. The high volume wear debris adhered to the SiC abrasive particles. This is due to the reduction in the asperities height of the abrasive paper. When it comes to sample 8% for operating conditions (see Fig. 5.16 (d)), the fibrils formed due to the ploughing and cutting action of the abrasive particles and are fractured at the HNTs and PTFE matrix interface. This causes the thickness of layer surrounded by the matrix and finally

results in reduction of cross section proceeding to separation from the matrix material. At the same time the sharp asperities of SiC abrasives wears out and eventually reduces the wear rate from the material [129].

Figure 5.17 (a) and (b) depicts the transfer film deposition on the SiC abrasive paper. During the specified period of test trail, in the PTFE soft matrix the hard HNT filler is deposited uniformly and there by maintained the film thickness. The accumulation further reduced due to the reduced efficiency of the abrasive cutting edges as well as the adhesive strength gained by the HNTs addition. The increase in the coefficient of friction with increase in wt. % HNT content indicates the rubbing action between the PTFE nanocomposite sample surface and the counter face was initially more but after the formation transfer film it is predicted a slight decrement in the value of the friction. For longer sliding distances a reduction in the wear rate was observed. From the DOE analysis the responses corresponding to the optimum values of input parameters had shown these effects.

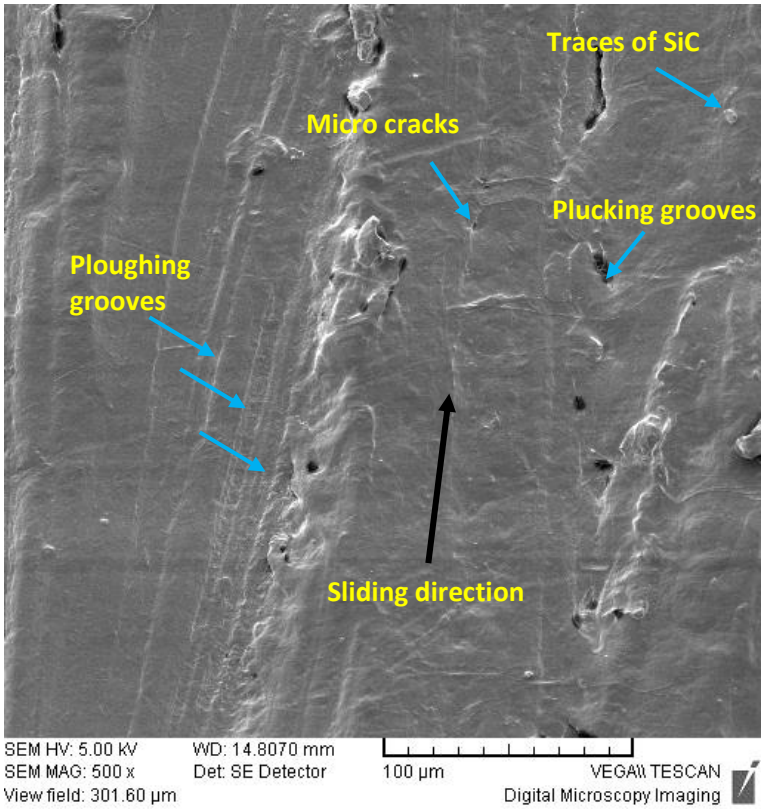
Traces of SiC
Micro cracks
Plucking grooves
Ploughing grooves
Sliding direction
SEM HV: 5.00 kV
SEM MAG: 500 x
View field: 301.60 µm
WD: 14.8070 mm
Det: SE Detector
100 µm
VEGA\\ TESCAN
Digital Microscopy Imaging

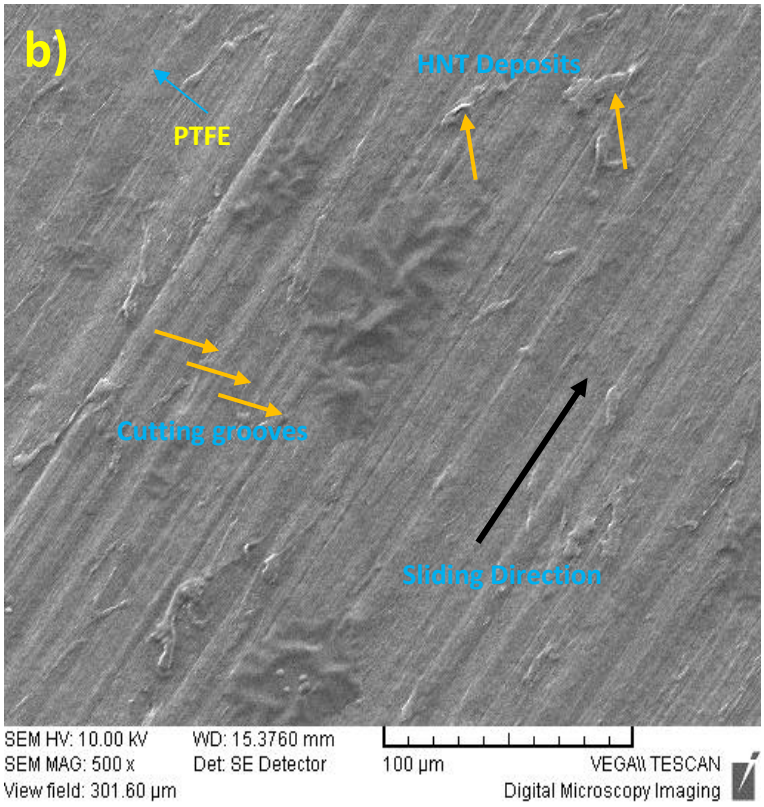
b)
PTFE
HNT Deposits
Cutting grooves
Sliding Direction
SEM HV: 10.00 kV
SEM MAG: 500 x
View field: 301.60 µm
WD: 15.3760 mm
Det: SE Detector
100 µm
VEGA\\ TESCAN
Digital Microscopy Imaging

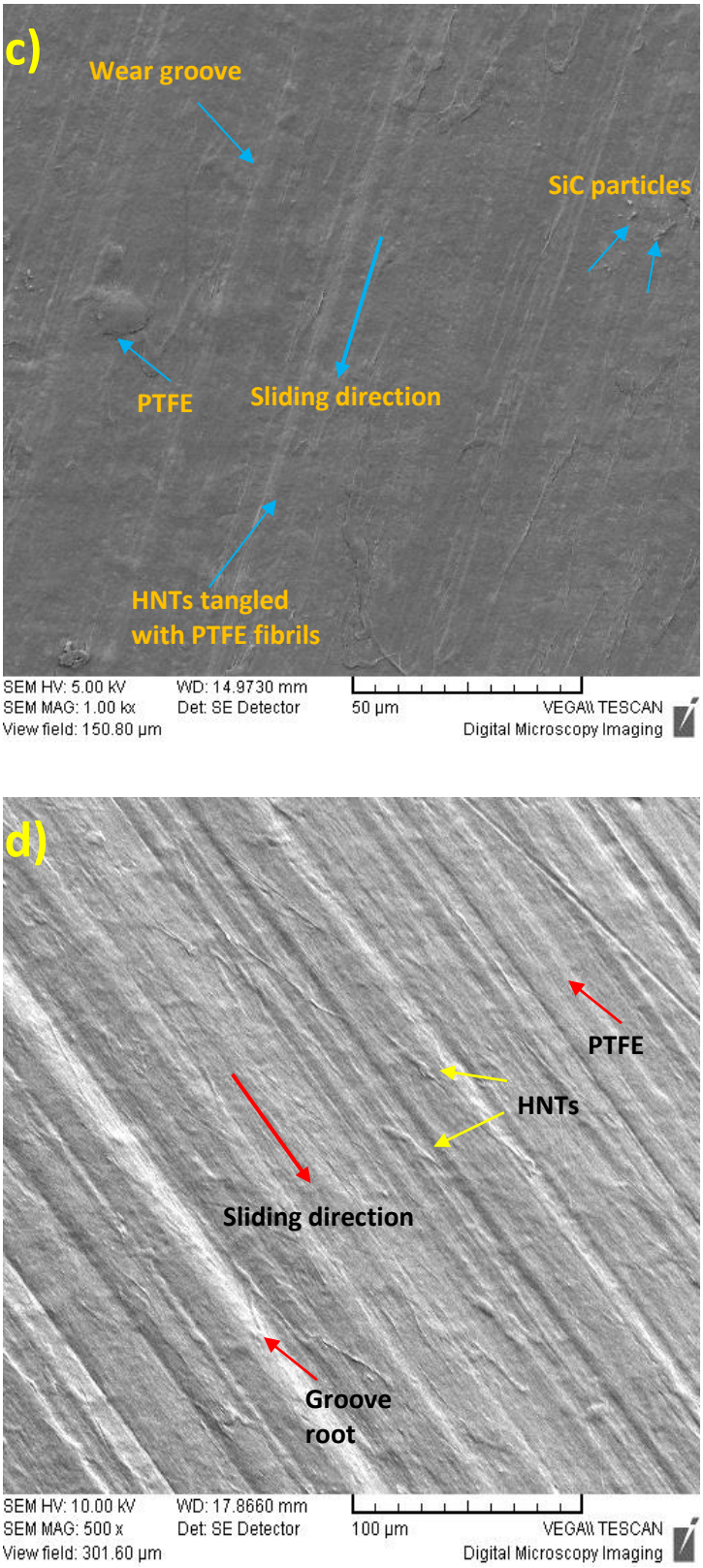

Figure 5.16 Scanning Electron Microscope images of test pin surfaces using operating conditions: abraded against 25.8 µm SiC paper, to an abrading distance of 2 km against a normal load of 20 N at 3 m/s sliding velocity: a) Pure PTFE; b) 4 wt. % HNT addition; c) 6 wt. % HNT addition; d) 8 wt. % addition

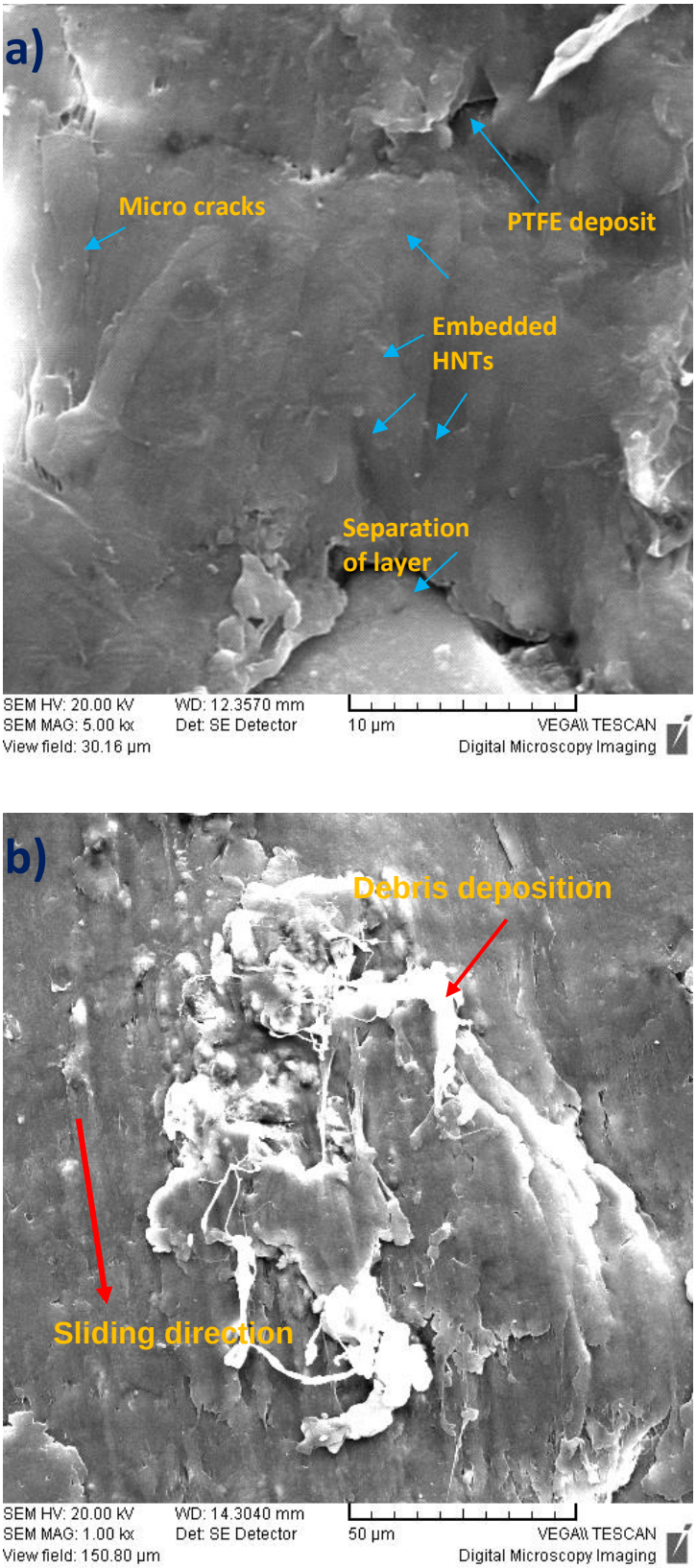

Figure 5.17 Scanning Electron Microscope images of transfer film deposited on the counter face, at operating conditions: abraded against 25.8 µm SiC paper, to an abrading distance of 2 km against a normal load of 20 N and at 3 m/s sliding velocity: (a) for 4 wt. % HNT addition in the PTFE matrix; (b) for 6 wt. % HNT addition in the PTFE matrix

PHASE – III

5.5 Erosion wear optimization of input parameters

In the erosion field the design of experiments technique was adopted by many researchers to find the optimum operating conditions to give minimum erosion wear rate [130]. Response Surface Methodology (RSM) approach was employed to find the optimum input parameters for minimization of the erosion wear rate. The experiments were planned by using customized response surface method option. The control factors with the corresponding levels were selected as shown in Table 5.11. A full factorial design consists of total 36 experimental runs were planned.

Table 5.11 Control factors and levels

Control parameter	Levels			
	1	2	3	4
Filler, wt. % HNT	4	6	8	
Pressure, bar	0.5	1	1.5	
Impingement angle, degrees	30	45	60	90

5.5.1 Experiment Procedure

The erosive wear tests (ASTM G76-83 standards) were conducted on a standard air jet erosion test rig as shown in Fig.5.18. The erodent particles selected as silica sand (40-100 microns size) and were accelerated by compressed air, exiting from a tungsten carbide nozzle (length 63 mm, diameter 1.5 mm). The accelerated particles finally hit the target surface which was away from nozzle centre by 10 mm. The measurements were done according to procedure described by Smith et. al. [131]. The velocity of the particles was determined as 86 m/s, 101 m/s, and 119 m/s at 0.5 bar, 1bar, and 1.5 bar respectively, by using the double disc method [132]. All the specimens were tested in the chamber at room temperature.

5.6 Results and Discussion

The mass loss of the samples after erosion test (Δm) was measured through a precision balance with 0.0001 g accuracy. Finally, the erosion wear rate was estimated by using the equation (5.26). The results were presented in Table 5.12.

$$Erosion\ wear\ rate, E_{wr} = \frac{\Delta m}{M}$$

(5.26)

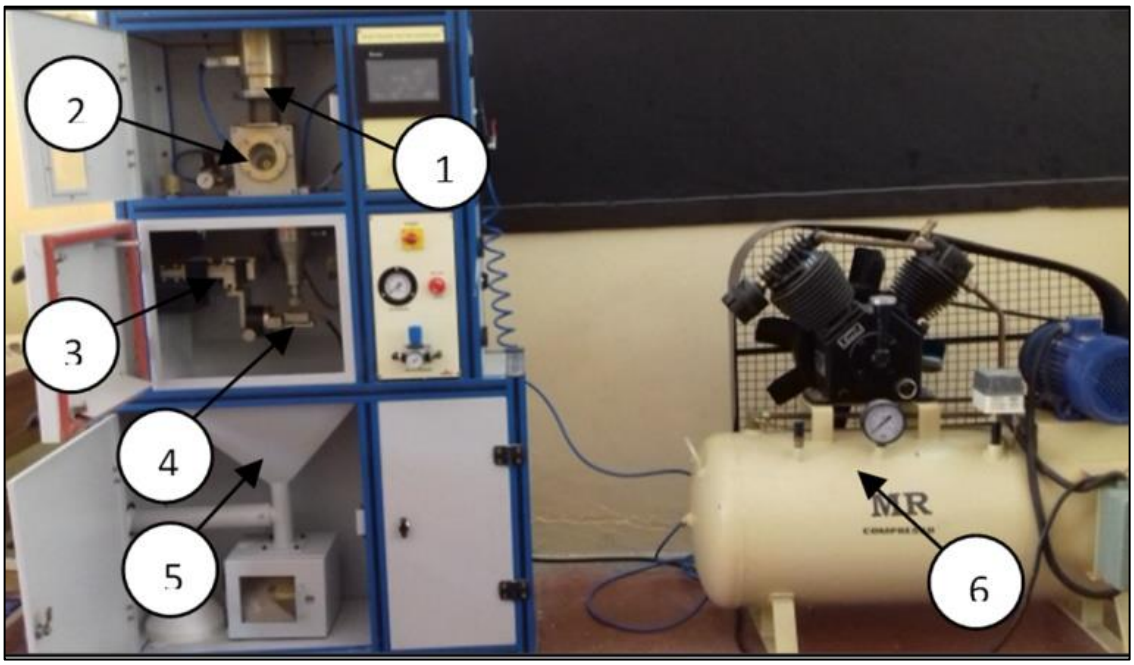

Figure 5.18 Air jet erosion test set up (MAGNUM make): 1. Hopper section; 2. Conveyor belt section; 3. Mixing chamber section; 4. Specimen holder section; 5. Collecting chamber; 6. Reciprocation air compressor

Specifications of Magnum make air jet erosion tester

Fluid – Air

Temperature – ambient

Pressure – 6 bar max.

Velocity – up to 300 m/s

Flow rate – up to 100 lpm

Nozzle – Tungsten Carbide

Particle:

Temperature – ambient

Velocity – up to 100 m/s

Feed rate – 0.5 to 10 gm/min

Specimen:

Size – 25 mmx25 mm max. & thickness 3 – 5 mm max.

Temperature 400 ^{0}C

Nozzle size – 1.5 mm diameter

Adjustment in X, Y, Z and tilt of specimen from 0 – 90 ^{0} (continuously variable)

Double disc arrangement for particle velocity measurement

Erodent collection after testing in fully enclosed removable enclosure

Table 5.12 Erosion wear rate for the experimental runs

Run	Filler, %HNT	Pressure, bar	Impingement angle,θ^0	m_1, g	m_2, g	E_{wr} x 10^{-5}, (g/g)
1	4	0.5	30	4.5329	4.5320	4.3689
2	4	0.5	45	4.2850	4.2842	3.8835
3	4	0.5	60	4.5318	4.5312	2.9126
4	4	0.5	90	4.2858	4.2850	3.8835
5	4	1.0	30	4.2742	4.2704	18.4466
6	4	1.0	45	4.4386	4.4343	20.8738
7	4	1.0	60	4.2704	4.2677	13.1068
8	4	1.0	90	4.4388	4.4386	0.9708
9	4	1.5	30	4.1422	4.1332	43.6893
10	4	1.5	45	4.3882	4.3792	43.6893
11	4	1.5	60	4.1332	4.1272	29.1262
12	4	1.5	90	4.4719	4.4706	6.3107
13	6	0.5	30	4.2863	4.2853	4.8544
14	6	0.5	45	4.2590	4.2577	6.3107
15	6	0.5	60	4.2853	4.2846	3.3981
16	6	0.5	90	4.2591	4.2590	0.4854
17	6	1.0	30	4.2948	4.2905	20.8738
18	6	1.0	45	4.4143	4.4100	20.8738
19	6	1.0	60	4.2905	4.2873	15.5340
20	6	1.0	90	4.4393	4.4389	1.9417
21	6	1.5	30	4.5017	4.4917	48.5437
22	6	1.5	45	4.3248	4.3151	47.0874
23	6	1.5	60	4.4917	4.4845	34.9515
24	6	1.5	90	4.3264	4.3248	7.7670
25	8	0.5	30	4.3599	4.3588	5.3398
26	8	0.5	45	4.4288	4.4273	7.2815
27	8	0.5	60	4.3588	4.3581	3.3981
28	8	0.5	90	4.4286	4.4285	0.4854
29	8	1.0	30	4.3236	4.3180	27.1845
30	8	1.0	45	4.4175	4.4128	22.8155
31	8	1.0	60	4.3180	4.3148	15.5340
32	8	1.0	90	4.4179	4.4177	0.9710
33	8	1.5	30	4.3605	4.3468	66.5049
34	8	1.5	45	4.4120	4.4003	56.7961
35	8	1.5	60	4.3468	4.3390	37.8641
36	8	1.5	90	4.4131	4.4121	4.8544

5.6.1 Response surface methodology (RSM)

Table 5.13, shows a valid model obtained from ANOVA. Factors A, B, C, and their interactions AB, BC, CA, and self-interactions B^2 and C^2 are found to be significant. The residual values plotted in normal plot of residuals followed the normality assumption, since all the residual points were scattered almost along the straight line as shown in Fig. 5.19. Hence, the experimental values and predicted values of erosion wear rates followed close to each other. A regression equation (5.27) in the form of mathematical model is obtained from the software and can be used to calculate any intermediate values of input factors. R-Squared value indicates the possible usage and validity of the model. R-squared and adjusted R-Squared values generated by the model were 98.06 and 97.39 respectively.

$$\begin{aligned} \textit{Erosion wear rate} = {} & \textit{-32.10567 - 0.47386} \times \textit{wt.\% HNT} + \textit{19.71217} \times \textit{Pressure} + \textit{1.11139} \times \\ & \textit{Angle} + \textit{2.60923} \times \textit{wt.\% HNT} \times \textit{Pressure} - \textit{0.050008} \times \textit{wt.\% HNT} \times \\ & \textit{Angle} - \textit{0.74958} \times \textit{Pressure} \times \textit{Angle} + \textit{0.15675} \times \textit{wt.\% HNT}^2 + \textit{19.25565} \\ & \times \textit{Pressure}^2 - \textit{3.90638E-003} \times \textit{Angle}^2 \end{aligned} \tag{5.27}$$

Table 5.13 ANOVA for Response Surface Quadratic model of response erosion wear rate

Source	Sum of Squares	dof	Mean Square	F Value	p-value Prob> F
Model	1.14E-06	9	1.27E-07	145.98	< 0.0001
A	9.63E-09	1	9.63E-09	11.11	0.0026
B	4.87E-07	1	4.87E-07	561.98	0.0001
C	2.89E-07	1	2.89E-07	333.71	0.0001
AB	1.09E-08	1	1.09E-08	12.56	0.0015
AC	1.18E-08	1	1.18E-08	13.63	0.001
BC	1.66E-07	1	1.66E-07	191.33	0.0001
A^2	3.15E-10	1	3.15E-10	0.36	0.5522
B^2	1.85E-08	1	1.85E-08	21.38	0.0001
C^2	8.74E-09	1	8.74E-09	10.08	0.0038

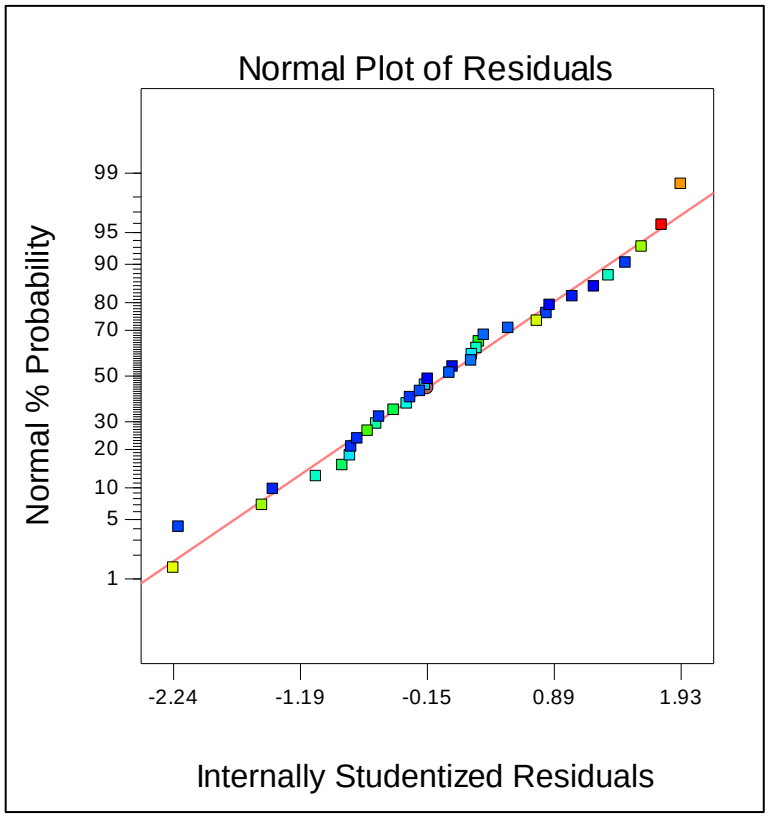

Figure 5.19 Plot of externally studentized residuals and normal probability

5.6.2 Surface plots

Significant interaction factors have considerable effect on the erosion rate is shown in Fig.5.20 in terms of surface representation. From the plots Fig. 5.20 (a) with increasing filler %HNT (A) and pressure (B), slightly low variation in the wear rate is found.

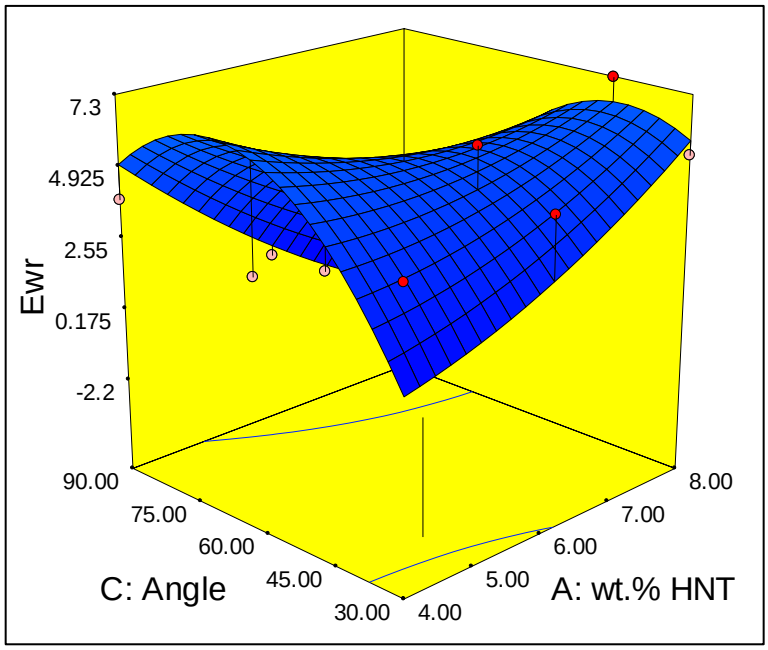

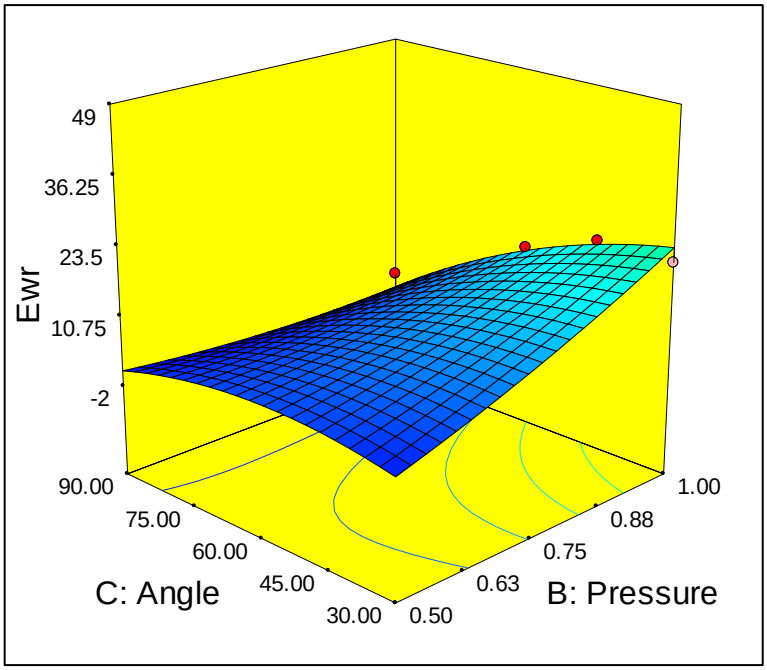

Figure 5.20 Surface plots depicts the interaction of the input factors on erosion wear rate: (a) wt.% HNT Vs Impingement angle; (b) Pressure Vs Impingement angle

The optimum input factors found from the analysis were 5.14 wt. % HNT addition, pressure, 0.83 bar, and an impingement angle 88.42^0. The Desirability was found to be l and hence the input factors were believed to be optimized. Erosion wear rate corresponding to the optimum input parameters was predicted as 0.349455×10^{-5} g/g, as shown in Fig. 5.21.

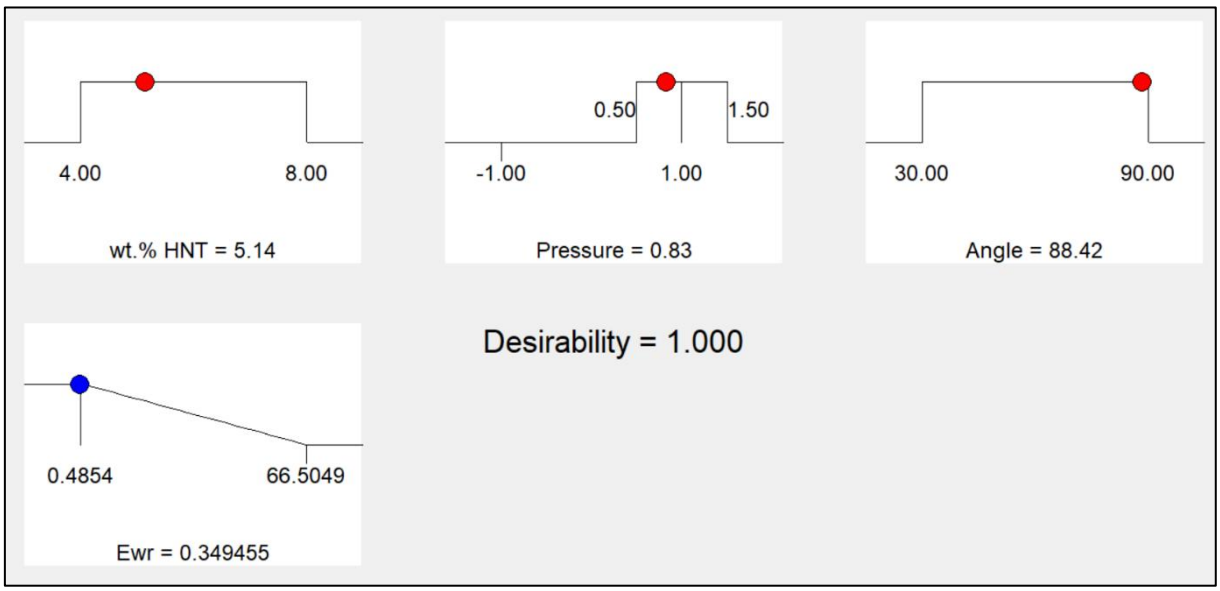

Figure 5.21 Response optimizer plot of the PTFE/HNT nanocomposites, depicts the optimum input factors at Desirability = 1

The impingement angles on the target surface were displayed in Fig. 5.22. Figure 5.23 shows the crater shape on the erosion samples at a stand-off distance of10 mm with gradual transition of circular shape to elliptical shape with increase in the impingement angle.

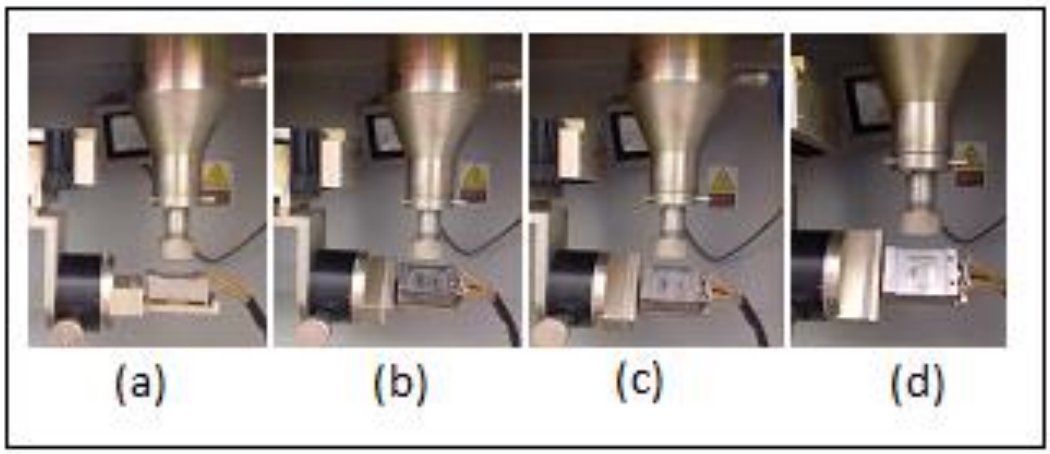

Figure 5.22 Specimen holder orientations: (a) $\theta = 90^0$ (b) $\theta = 60^0$ (c) $\theta = 45^0$ (d) $\theta = 30^0$

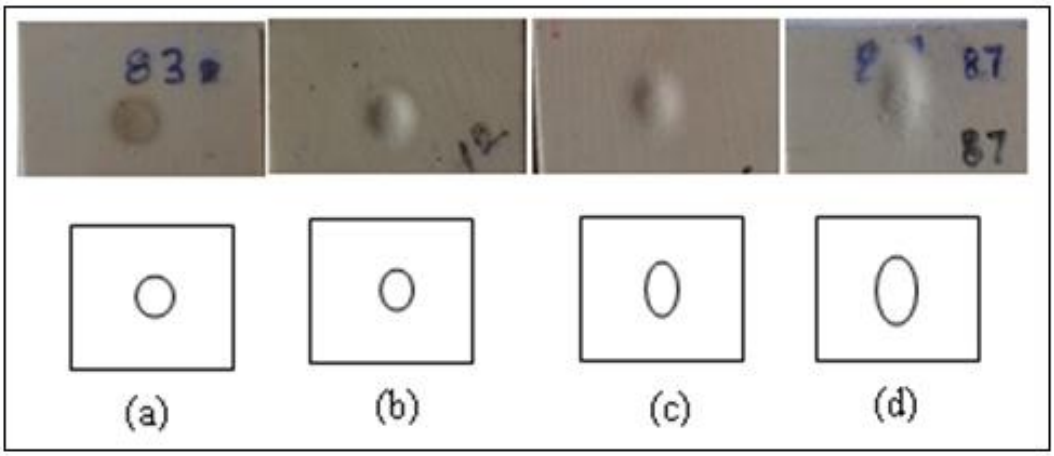

Figure 5.23 Crater shape of wear at different angle of impingements: (a) $\theta = 90^0$ (b) $\theta = 60^0$ (c) $\theta = 45^0$ (d) $\theta = 30^0$, for nano-filler addition of 8% by weight of HNT addition and at 1.5 bar pressure.

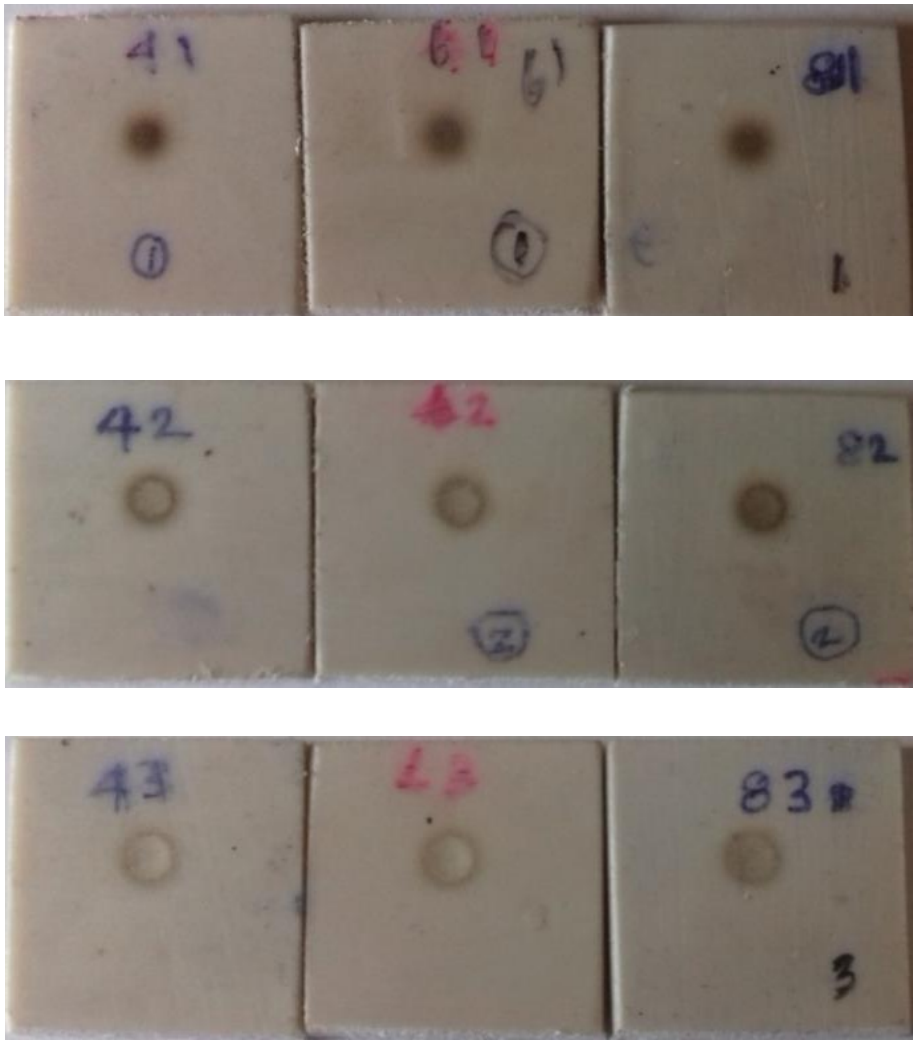

Figure 5.24 Crater shape on the nanocomposites after test for angle of impingement, **$\theta = 90^0$:** (a) at pressure, p =0.5 bar; (b) at pressure, p = 1 bar; (c) at pressure, p =1.5 bar

5.7 Effect of individual input parameters (pressure and impingement angle) on erosion wear rate

Figure 5.25 – Figure 5.28 shows the effect of pressure of air that accelerates the solid erodent particles on the erosion rate at different impingement angles. Since the PTFE matrix material is highly ductile in nature, relatively high erosion wear rates are found corresponding to low impingement angles (30^0 - 45^0). And gradual decrease in the wear rate was also found when impingement angle reaches 90^0. From the Figure 5.29 – Figure 5.31, at high pressure and low impact angles an increase in the wear rate was found due to micro cutting of erodent particles on the surface revealing the ductile nature of the nanocomposites for all wt. %HNT inclusions.

wt. % HNT	0.5 bar	1 bar	1.5 bar
4%	4.36893E-05	0.000184	0.000437
6%	4.85437E-05	0.000209	0.000485
8%	5.33981E-05	0.000272	0.000665

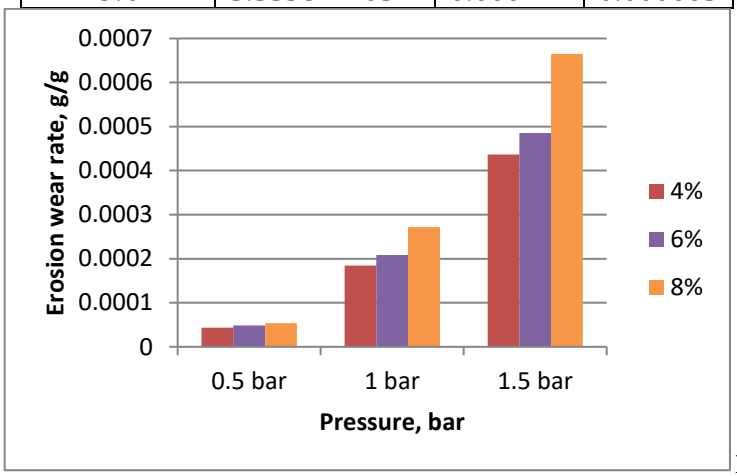

1

Figure 5.25 Effect of increase in pressure on erosion wear rate for different wt.% addition in the PTFE matrix, at an impingement angle, 30^0

	0.5 bar	1 bar	1.5 bar
4%	2.91262E-05	0.000131	0.000291
6%	3.39806E-05	0.000155	0.00035
8%	3.39806E-05	0.000155	0.000379

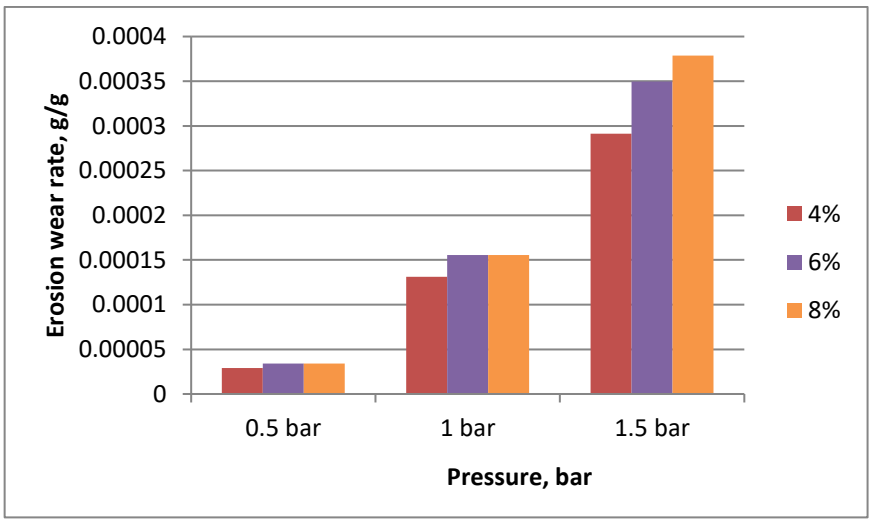

Figure 5.26 Effect of increase in pressure on erosion wear rate for different wt.% addition in the PTFE matrix, at an impingement angle, 60^0

	0.5 bar	1 bar	1.5 bar
4%	3.8835E-05	0.000209	0.000437
6%	6.31068E-05	0.000209	0.000471
8%	7.28155E-05	0.000228	0.000568

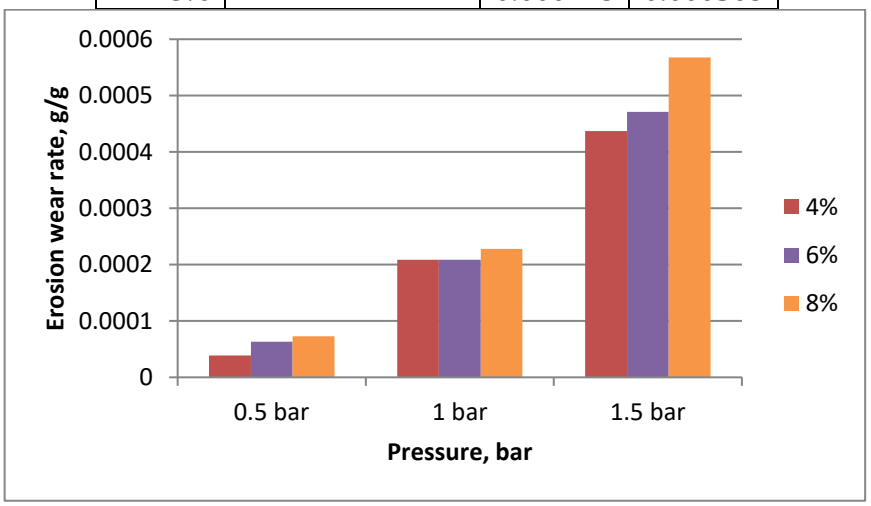

Figure 5.27 Effect of increase in pressure on erosion wear rate for different wt.% addition in the PTFE matrix, at an impingement angle, 45^0

	0.5 bar	1 bar	1.5 bar
4%	3.8835E-06	9.71E-06	6.31E-05
6%	4.85437E-06	1.94E-05	7.77E-05
8%	4.85437E-06	9.71E-06	4.85E-05

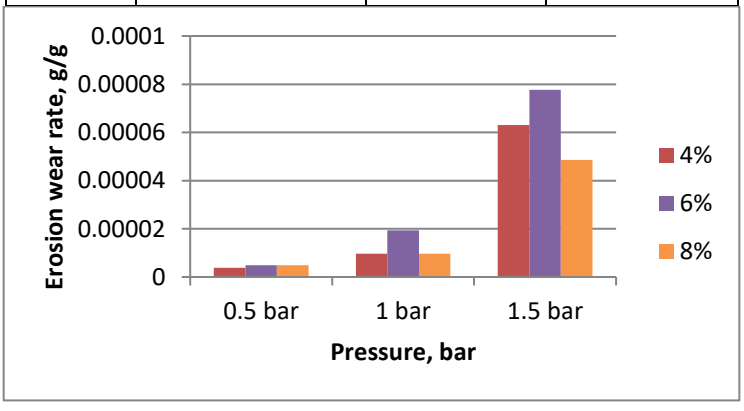

Figure 5.28 Effect of increase in pressure on erosion wear rate for different wt.% addition in the PTFE matrix, at an impingement angle, 90^0

Pressure =0.5 bar	30	45	60	90
4%	4.37E-05	3.88E-05	2.91E-05	3.88E-06
6%	4.85E-05	6.31E-05	3.4E-05	4.85E-06
8%	5.34E-05	7.28E-05	3.4E-05	4.85E-06

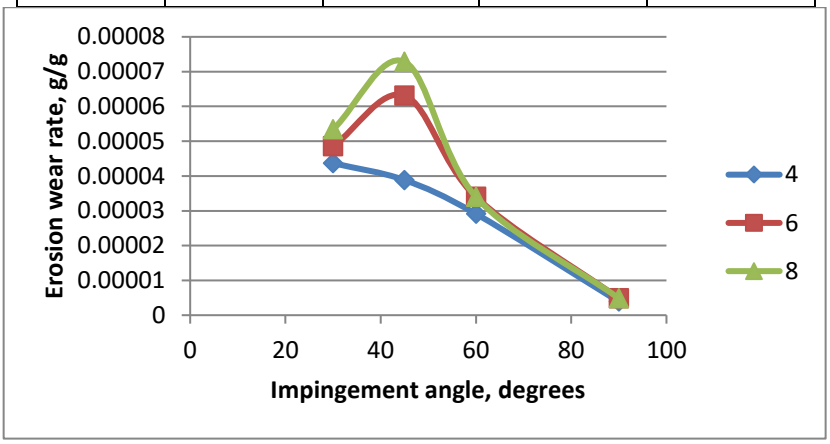

Figure 5.29 Effect of increase in pressure on erosion wear rate of PTFE/HNT nanocomposites for different impingement angles and at a pressure of 0.5 bar

Pressure =1 bar	30	45	60	90
4%	0.000184	0.000209	0.000131	9.71E-06
6%	0.000209	0.000209	0.000155	1.94E-05
8%	0.000272	0.000228	0.000155	9.71E-06

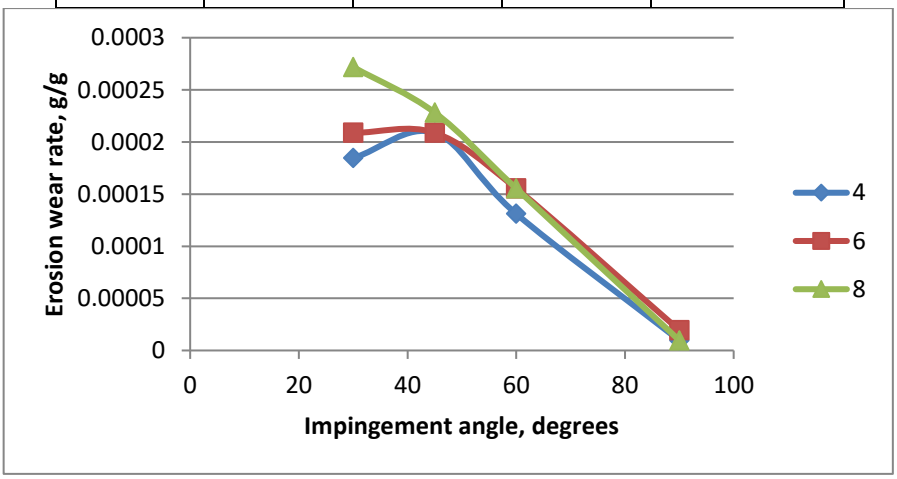

Figure 5.30 Effect of increase in pressure on erosion wear rate of PTFE/HNT nanocomposites for different impingement angles and at a pressure of 1 bar

p=1.5 bar	30	45	60	90
4%	0.000437	0.000437	0.000291	6.31E-05
6%	0.000485	0.000471	0.00035	7.77E-05
8%	0.000665	0.000568	0.000379	4.85E-05

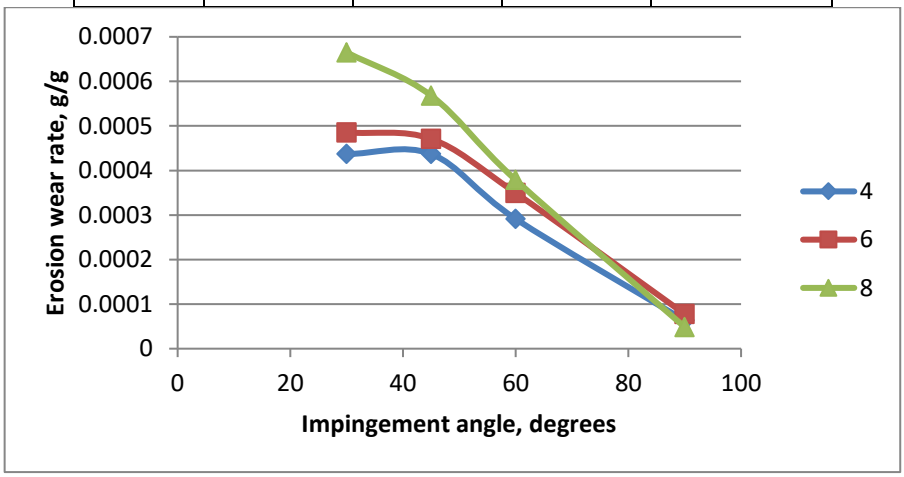

Figure 5.31 Effect of increase in pressure on erosion wear rate of PTFE/HNT nanocomposites for different impingement angles and at a pressure of 1.5 bar

Chapter - 6

CONCLUSIONS & SCOPE OF FUTURE WORK

Morphology, Thermal, and Mechanical Characterization

The neat PTFE was strengthened with natural mineral Halloysite nanotubes. The PTFE nanocomposite sheets of 2%–10% with an increment of 2 wt% HNT loading were fabricated. Subsequently, thermal and mechanical tests were conducted and the following conclusions were drawn:

- The peaks in XRD plots indicated the presence of HNT in the nanocomposites. With the wt.% of HNT increase in the nanocomposites, an increase in the peak size was observed around a 2 theta of 12.3°. A maximum increase in the intensity count was observed for 8 wt.% HNT addition which corresponds to a basal spacing of 7.18.
- From XRD study, degree of crystallinity of PTFE/HNT nanocomposites were estimated from the relative area of intensity of crystalline and halo peaks. The degree of crystallinity of neat PTFE was found to be 51.55 % and a maximum value of 76.34% was found at 4 wt.% HNT addition in the PTFE matrix. The reasons for variation of degree of crystallinity for the PTFE nanocomposites can be stated from the degree of dispersion of HNTs in the PTFE matrix. At low wt.% HNT addition, maximum value of degree of crystallinity was found. i.e., at 4 wt.%
- DSC results has shown that HNT act as hetero nucleating agent. The HNT content in nanocomposites has helped in increasing the degree of crystallinity. The degree of crystallinity of PTFE increased from 57.83% for neat PTFE to 73.5% at 4 wt. % HNT addition.
- DMA results shown increase in storage modulus, loss modulus and tan delta values. The variation in the results indicates that the addition of HNTs has improved the capability of the material to dissipate energy as it indicates an enhanced loss modulus.
- Improved mechanical properties of PTFE/HNT nanocomposites showed an increase in yield tensile strength by 135% and tensile modulus by 250% at 6 wt. % HNT addition in comparison with neat PTFE. Also, an increase in the impact strength by 130% at 4 wt% loading is observed. The maximum Vickers micro-hardness value is observed for sample ‘F’ (10 wt. %), which is increased by 163% compared to neat PTFE. From the mechanical analysis, at higher HNT loading (i.e. >8 wt%), poor dispersion HNT is

realized. Moreover, change in PTFE structure is also observed. The enhancement in mechanical properties can be attributed to increase in degree of crystallinity.

- SEM micrographs are shown for impact as well as tensile fracture surfaces. From SEM micrographs, pull out regions are observed suggesting resistance offered by the HNT in the matrix attributed to good interfacial strength. This is mainly evident at smaller fraction of HNT (4 wt. % to 6 wt. %) where, the dispersion of HNT in PTFE matrix is proper.

Hence, HNTs (4 wt. % to 6 wt. %) can be suggested as a reinforcement material for improving both mechanical and thermal properties of PTFE matrix.

Wear Characterization

Phase I: Abrasive Wear optimization by Designer requisite based hybrid method

Experimental runs are planned as per Taguchi L27 orthogonal array and conducted on pin on disc apparatus. The values of COF, and mass loss are measured and the responses SWR, and EW were estimated. Single response optimization was carried out corresponding to $C_2L_1D_1S_1$, $C_1L_1D_2S_2$, and $C_1L_1D_3S_2$. Later utility approach was used to find the utility index (U) values for all runs. The U values were calculated after calculating the weight factors based on designer's choice of response parameters. RSM was utilized and optimum values of process parameters were found corresponding to maximization of utilization of the sample.

The following conclusions were made from the dry sliding wear behaviour of PTFE/HNT nanocomposites.

- Addition of HNT particles as fillers increases the wear resistance of the material. However, significant improvement in wear resistance is observed at nearly 4 wt% of HNT loading.
- Appreciable increase in wear resistance was found at the cost of slight increase in friction coefficient compared to unfilled PTFE.
- Desirability value corresponding to maximum utilization, the optimum values were found: At Desirability =1: 4 wt. % HNT, 8.5354 N load, 2.0 km distance and at a velocity of 1.0 m/s. The value of utility index observed to be 15.5066 and was within 95% confidence interval (13.01 to 17.99).

From hybrid method as per designer based requirement the value of wt. % HNT was about 4% and from RSM based on same weightage to all factors, the wt. % HNT was about 6.67%.

Hence, the hybrid method suggested optimum wt. % HNT addition to be 4 % and minimum COF, minimum SWR, and maximum EW might be obtained.

Phase II: Abrasive Wear optimization by changing counterface roughness

- The tribological parameters of PTFE/HNT nanocomposites when running against counter surface fitted with several SiC abrasive grade papers were examined by using RSM.
- The optimum input parameters and responses of PTFE/HNT nanocomposites for the abrasive wear study were predicted to be 4 wt. % of HNT addition, 20 N of load, 3.0 km of distance, 3 m/sec of sliding velocity when running against a counter surface roughness of 9.5 microns were 0.1001 and 700×10^{-6} mm^3/N-m for COF and SWR respectively. Since the composite desirability was close to 1, which indicated the responses were reasonably optimized.
- SEM analysis revealed the reduction in coefficient of friction of PTFE/HNT nanocomposites due to the deposition of transfer film. It was also observed the strength of transfer film was found to be optimum at a surface roughness of 9.5 microns under optimum operating conditions of input parameters.

Phase III: Erosion wear

- The experiments on air jet erosion test rig were performed by using Design of Experiments technique and total 36 runs were designed for various controlling factors and levels. The velocity of particles is determined by using double disc method.
- The experimental results were then analyzed by using design of experiments software and a valid model was obtained with an R-squared value of 98.06%.
  The effect of interaction of input parameters on the erosion rate was also studied with the help of surface plots. The erosion wear rate of PTFE/HNT nanocomposites would increase at the high wt. % HNT addition as well as low impingement angles.
- Conforming to the minimization of erosive wear at desirability equal to 1: wt. % HNT addition of 5.14 %, pressure of 0.83 bar, and an impingement angle of 88.42^0 were found. Erosion wear rate corresponding to the optimum input parameters was predicted as $0.349455x10^{-5}$ g/g
- The effect of individual input parameters such as, pressure and impingement angle for all compositions of HNT on erosion rate was also studied from the plots. It was observed from the plots that maximum wear occurs corresponding to low impingement angles

and higher operating pressures. Minimum wear rate was observed for compositions between 4-6% HNT additions in the PTFE matrix material.

From the present research work, it can be concluded that, a novel 'green' and cost effective PTFE/HNT nanocomposites were fabricated and tested. From the characterization study, it was concluded that about 4 wt. % HNT to 6 wt. % HNT addition, the material had shown multi-functional properties such as improved mechanical , thermal, and tribological properties due to better dispersion in the PTFE matrix material. Also, from Fig. 6.1, the PTFE/HNT nanocomposite can be compared with the work done by previous authors. Though, the PTFE/HNT nanocomposite wear performance is moderate compared to the wear performance of other fillers as shown in Fig. 6.1, the coefficient of friction was less affected by the wt. % addition of HNT in the PTFE matrix. These characteristics help in increasing the fatigue life of PTFE/HNT nanocomposite components. Hence, for self-lubrication applications the components can be fabricated with PTFE filled with Halloysite nanotubes.

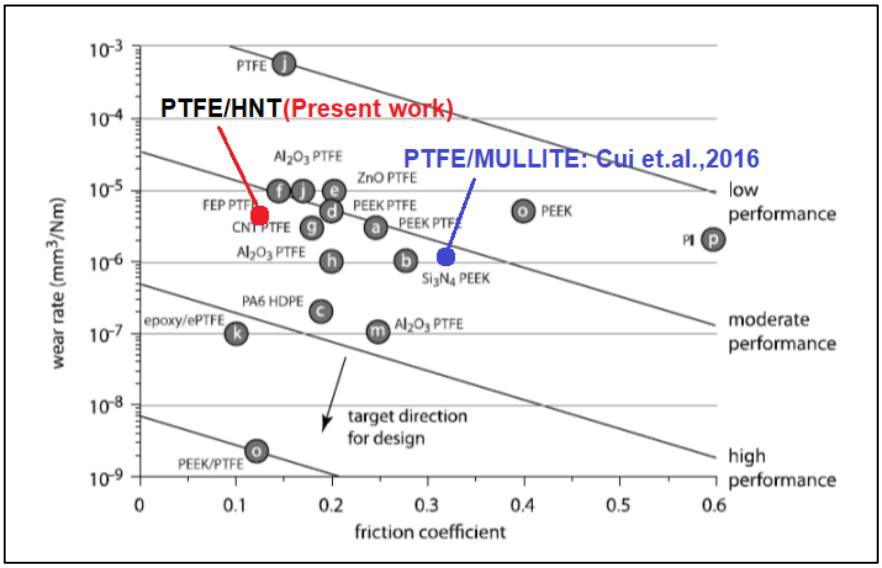

Figure 6.1 Validation of wear results of PTFE/HNT nanocomposites

Scope of future work

- The effect of surface modification of HNTs can be explored
- Determination of best processing temperatures for sintering cycle ramp
- Explore the properties of PTFE/HNT nanocomposites over a range of compression pressures (cold compression)
- Cross linking structure with the use of blends
- More natural fillers can be reinforced to reach the tribological target of PTFE /HNT nanocomposites for wide range of applications as well as environment friendly.
- The developments in nanocomposites lead to the development of tribo-set ups for testing by using unsymmetrical wear paths
- Study of transfer film characteristics of PTFE/HNT nanocomposites
- Numerical simulation of abrasive wear and erosion wear can be explored

VISUAL OUTCOMES OF THE PRESENT WORK

International journal:

1. Suresh Gamini, V Vasu and Suryasarathi Bose, "Tube-like natural halloysite /poly(tetrafluoroethylene) nanocomposites: simultaneous enhancement in thermal and mechanical properties ", Materials Research Express, Vol. 4, pp. 045301-13, 2017. DOI:org/10.1088/2053-1591/aa68b6. [SCI journal]

2. G Suresh, V Vasu, M Venkateswara Rao, "Multi-response optimization of Tribological Parameters of Polytetrafluoroethylene (PTFE) Matrix filled with Halloysite Nanotubes (HNT) material by using a Sandwich (Taguchi-Utility-RSM) Method", Silicon, Springer: [Accepted for publication – SCI journal]

3. G Suresh, V Vasu, G Raghavendra, "Optimization of Input Parameters on Erosion Wear Rate of PTFE/HNT filled nanocomposites", Materials Today Proceedings. [Accepted for publication – SCOPUS journal]

International conference:

1. G Suresh, V Vasu, "Multi-objective optimization of Wear Parameters of Tube-like Clay Mineral Filled Thermoplastic Polymer using Response Surface Methodology", International Journal of Arts & Sciences (IJAS*)* International Conference for Engineering and Technology, May, 22nd -26th, 2017, held at Harvard Medical School, Boston, Massachusetts, USA.

2. Suresh Gamini, Vasu V, Venkateswara Rao M, "Property characterization of Fluorinated Thermoplastic Nano composites for Tribological Applications", Proceedings of the conference Advanced Polymer Materials, February 14th -15th, CIPET, 2014, Bhubaneswar, INDIA.

3. Suresh Gamini, Vasu V, Venkateswara Rao M, " Effect of HNT clay loading on mechanical and thermal properties of PTFE Nano clay composites for solid lubrication", Proceedings of the international conference on Advances in Tribology, February 21st to 24th 2014, NIT, Calicut, INDIA.

National conference:

1. Gamini Suresh, V Vasu, "Optimization of Wear Parameters of HNT Clay Filled PTFE Nanocomposites by Taguchi L27 Orthogonal Model", National Symposium of Mechanical Engineering Research Scholars, October 7th-2016, NIT Warangal, INDIA.

REFERENCES

[1] NATO-RTO, "RTO lecture notes," 2005.

[2] A. Usuki, M. Kawasumi, Y. Kojima, A. Okada, T. Kurauchi, and O. Kamigaito, "Swelling behavior of montmorillonite cation exchanged for ω-amino acids by -caprolactam," *J. Mater. Res.*, vol. 8, no. 5, pp. 1174–1178, May 1993.

[3] A. Polymeric, N. Materials, and P. S. Raleigh, "Review article : Polymer-matrix," vol. 40, no. 17, pp. 27–32, 2006.

[4] F. Hussain, "Polymer-matrix Nanocomposites, Processing, Manufacturing, and Application: An Overview," *J. Compos. Mater.*, vol. 40, no. 17, pp. 1511–1575, 2006.

[5] E. T. Thostenson, C. Li, and T. W. Chou, "Nanocomposites in context," *Compos. Sci. Technol.*, vol. 65, no. 3–4, pp. 491–516, 2005.

[6] L.-Q. Wang, X.-M. Jia, L. Cui, and G.-C. Chen, "Effect of Aramid Fiber and ZnO Nanoparticles on Friction and Wear of PTFE Composites in Dry and LN 2 Conditions," *Tribol. Trans.*, vol. 52, no. 1, pp. 59–65, 2008.

[7] J. H. Koo, *Polymer Nanocomposites: Processing, Characterization and Applications*. 2006.

[8] M. Alexandre and P. Dubois, "Polymer-layered silicate nanocomposites: preparation, properties and uses of a new class of materials," *Mater. Sci. Eng. R Reports*, vol. 28, no. 1–2, pp. 1–63, Jun. 2000.

[9] R. Valapa, S. Loganathan, G. Pugazhenthi, and S. Thomas, "An Overview of Polymer/Clay Nanocomposites," *researchgate.net*.

[10] H. Hu, L. Onyebueke, and A. Abatan, "Characterizing and Modeling Mechanical Properties of Nanocomposites- Review and Evaluation," *J. Miner. Mater. Charact. Eng.*, vol. 9, no. 4, pp. 275–319, 2010.

[11] R. E. Gorga and R. E. Cohen, "Toughness enhancements in poly(methyl methacrylate) by addition of oriented multiwall carbon nanotubes," *J. Polym. Sci. Part B Polym. Phys.*, vol. 42, no. 14, pp. 2690–2702, 2004.

[12] B. Z. Ma, Peng Cheng, Kim, Jang-Kyo, Tang, "Functionalization of carbon nanotubes

using a silane coupling agent," *Carbon N. Y.*, vol. v. 44, no. 15, pp. 3232–3238, 2006.

[13] A. Das, F. R. Costa, U. Wagenknecht, and G. Heinrich, "Nanocomposites based on chloroprene rubber: Effect of chemical nature and organic modification of nanoclay on the vulcanizate properties," *Eur. Polym. J.*, vol. 44, no. 11, pp. 3456–3465, 2008.

[14] H. Chen *et al.*, "Dispersion of carbon nanotubes and polymer nanocomposite fabrication using trifluoroacetic acid as a co-solvent," *Nanotechnology*, vol. 18, no. 41, p. 415606, 2007.

[15] L. N. Carli, T. S. Daitx, G. V. Soares, J. S. Crespo, and R. S. Mauler, "The effects of silane coupling agents on the properties of PHBV/halloysite nanocomposites," *Appl. Clay Sci.*, vol. 87, pp. 311–319, 2014.

[16] Z. L. Wang, *Characterization of nanophase materials*. Wiley-VCH, 2000.

[17] M. Meyyappan, *Carbon nanotubes : science and applications*. CRC Press, 2005.

[18] S. W. Zhang, "State-of-the-art of polymer tribology," *Tribol. Int.*, vol. 31, no. 1–3, pp. 49–60, 1998.

[19] M. Kutz, *Handbook of measurement in science and engineering. Volume 2*. .

[20] Y. Enomoto and T. Yamamoto, "New materials in automotive tribology," *Tribol. Lett.*, vol. 5, pp. 13–24, 1998.

[21] H. Meng C., Ludema K.,C., "Wear Models and Predictive Equations: Their Form and Content," vol. 181–183, pp. 443–457, 1995.

[22] H. Böhm, S. Betz, and A. Ball, "The wear resistance of polymers," *Tribol. Int.*, vol. 23, no. 6, pp. 399–406, 1990.

[23] E. Assenova, V. Majstorovic, A. Vencl, and M. Kandeva, "GREEN TRIBOLOGY AND QUALITY OF LIFE UDC :," *Int. J. Adv. Qual.*, vol. 40, no. 2, pp. 1–6, 2012.

[24] E. Rabinowicz, *Friction and wear of materials*. Wiley, 1995.

[25] O. V. R. and E. G. L. S B Ratner, I I Faberova, *Comparison of the Abrasion of Rubbers and Plastics*. 1967.

[26] B. Briscoe and S. K. Sinha, "Wear of polymers," *Proc. Inst. Mech. Eng. Part J J. Eng.*

Tribol., vol. 216, no. 6, pp. 401–413, 2002.

[27] B. J. Briscoe and S. K. Sinha, “Wear of polymers,” vol. 216, pp. 401–413.

[28] P. A. Mahanwar, S. Bose, and H. Raghu, “Effect of talc and synthetic sodium aluminum silicate (SSAS) on the properties of PC/PMMA blend,” *J. Thermoplast. Compos. Mater.*, vol. 19, no. 5, pp. 491–506, 2006.

[29] X. Shi, G. Zhang, C. Siligardi, G. Ori, and A. Lazzeri, “Comparison of Precipitated Calcium Carbonate / Polylactic Acid and Halloysite / Polylactic Acid Nanocomposites,” vol. 2015, 2015.

[30] M. Vable, “Mechanical Properties of Materials,” *Springer*, vol. 190, p. 645, 2012.

[31] D. L. Burris and W. G. Sawyer, “A low friction and ultra low wear rate PEEK/PTFE composite,” *Wear*, vol. 261, no. 3–4, pp. 410–418, 2006.

[32] G. Straffelini, “Surface Engineering for Tribology,” Springer, Cham, 2015, pp. 201–235.

[33] S.K. Sinha and B.J. Briscoe, *Polymer Tribology*. 2009.

[34] L. Nicolais, E. Milella, and M. Meo, *Composite Materials: A Vision for the Future*. 2011.

[35] T. L. Schmitz, J. E. Action, D. L. Burris, J. C. Ziegert, and W. G. Sawyer, “Wear-Rate Uncertainty Analysis,” *J. Tribol.*, vol. 126, no. 4, p. 802, 2004.

[36] G. Arena, “Solid particle erosion and viscoelastic properties of thermoplastic polyurethanes,” *Express Polym. Lett.*, vol. 9, no. 3, pp. 166–176, 2015.

[37] A. Patnaik, A. Satapathy, N. Chand, N. M. Barkoula, and S. Biswas, “Solid particle erosion wear characteristics of fiber and particulate filled polymer composites: A review,” *Wear*, vol. 268, no. 1, pp. 249–263, 2010.

[38] J. K. Lancaster, “Abrasive Wear of Polymers*,” *Wear*, vol. 14, pp. 223–239, 1969.

[39] K. Friedrich, R. Reinicke, and Z. Zhang, “Wear of polymer composites,” *Proc. Inst. Mech. Eng. Part J J. Eng. Tribol.*, vol. 216, no. 6, pp. 415–426, 2002.

[40] F. Findik, “Latest progress on tribological properties of industrial materials,” *Mater. Des.*, vol. 57, pp. 218–244, 2014.

[41] T. S. Note, *Physical properties of Fluon ® unfilled and filled PTFE*. .

[42] K. Tanaka and S. Kawakami, “Effect of various fillers on the friction and wear of polytetrafluoroethylene-based composites,” *Wear*, vol. 79, no. 2, pp. 221–234, 1982.

[43] T. Makinson, “The friction and transfer of polytetrafluoroethylene,” *Proc. R. Soc. London A Math. Phys. Eng. Sci.*, vol. 281, no. 1384, 1964.

[44] NETZSCH, “Polytetrafluoroethylene (PTFE),” *Technical Information*. p. 1, 2006.

[45] S. K. Biswas and K. Vijayan, “Friction and wear of PTFE,” *Wear*, vol. 158, pp. 193–211, 1992.

[46] G. W. (Gwidon W. . Stachowiak and A. W. (Andrew W. . Batchelor, *Engineering tribology*. Elsevier Butterworth-Heinemann, 2005.

[47] T. A. Blanchet and F. E. Kennedy, “Sliding wear mechanism of polytetrafluoroethylene (PTFE) and PTFE composites,” *Wear*, vol. 153, no. 1, pp. 229–243, 1992.

[48] J. K. Lancaster, “Accelerated wear testing of PTFE composite bearing materials,” *Tribol. Int.*, vol. 12, no. 2, pp. 65–75, 1979.

[49] H. Wang, X. Feng, L. Mu, and X. Lu, “Different Nano-Fillers on the Tribological Properties of PTFE Nanocomposites,” in *Advanced Tribology: Proceedings of CIST2008 {&} ITS-IFToMM2008*, J. Luo, Y. Meng, T. Shao, and Q. Zhao, Eds. Berlin, Heidelberg: Springer Berlin Heidelberg, 2010, pp. 392–395.

[50] J. R. Vail, D. L. Burris, and W. G. Sawyer, “Multifunctionality of single-walled carbon nanotube-polytetrafluoroethylene nanocomposites,” *Wear*, vol. 267, no. 1–4, pp. 619–624, 2009.

[51] J. Loomis *et al.*, “Graphene-nanoplatelet-based photomechanical actuators,” *Nanotechnology*, vol. 23, no. 4, p. 45501, Feb. 2012.

[52] P. Xu, J. Loomis, B. King, and B. Panchapakesan, “Synergy among binary (MWNT, SLG) nano-carbons in polymer nano-composites: a Raman study,” *Nanotechnology*, vol. 23, no. 31, p. 315706, Aug. 2012.

[53] P. Xu, J. Loomis, R. D. Bradshaw, and B. Panchapakesan, “Load transfer and mechanical properties of chemically reduced graphene reinforcements in polymer composites,”

Nanotechnology, vol. 23, no. 50, p. 505713, Dec. 2012.

[54] D. L. Burris and W. G. Sawyer, "Tribological Sensitivity of PTFE/Alumina Nanocomposites to a Range of Traditional Surface Finishes," *Tribol. Trans.*, vol. 48, no. 2, pp. 147–153, 2005.

[55] D. L. Burris and W. G. Sawyer, "Improved wear resistance in alumina-PTFE nanocomposites with irregular shaped nanoparticles," *Wear*, vol. 260, no. 7–8, pp. 915–918, 2006.

[56] D. L. Burris *et al.*, "A route to wear resistant PTFE via trace loadings of functionalized nanofillers," *Wear*, vol. 267, no. 1–4, pp. 653–660, 2009.

[57] M. Conte and A. Igartua, "Study of PTFE composites tribological behavior," *Wear*, vol. 296, pp. 568–574, 2012.

[58] F. hua Su, Z. zhu Zhang, and W. min Liu, "Friction and wear behavior of hybrid glass/PTFE fabric composite reinforced with surface modified nanometer ZnO," *Wear*, vol. 265, no. 3–4, pp. 311–318, Jul. 2008.

[59] Y. Xue and X. Cheng, "Tensile properties of glass fiber reinforced PTFE using a rare-earth surface modifier," *J. Mater. Sci. Lett.*, vol. 20, no. 18, pp. 1729–1731, 2001.

[60] H. Ismail and H. S. Ahmad, "Effect of halloysite nanotubes on curing behavior, mechanical, and microstructural properties of acrylonitrile-butadiene rubber nanocomposites," *J. Elastomers Plast.*, vol. 46, no. 6, pp. 483–498, 2013.

[61] D. Rawtani and Y. K. Agrawal, "Multifarious applications of halloysite nanotubes: A review," *Reviews on Advanced Materials Science*, vol. 30, no. 3. pp. 282–295, 2012.

[62] T. S. Gaaz, A. B. Sulong, M. N. Akhtar, A. A. H. Kadhum, A. B. Mohamad, and A. A. Al-amiery, "Properties and Applications of Polyvinyl Alcohol , Halloysite Nanotubes and Their Nanocomposites," pp. 22833–22847, 2015.

[63] R. C. Daly, C. A. Fleischer, A. L. Wagner, M. Duffy, S. Place, and H. N. Hnt, "Halloysite Nanotubes in Polymers."

[64] K. Prashantha, M. F. Lacrampe, and P. Krawczak, "Processing and characterization of halloysite nanotubes filled polypropylene nanocomposites based on a masterbatch route:

Effect of halloysites treatment on structural and mechanical properties," *Express Polym. Lett.*, vol. 5, no. 4, pp. 295–307, 2011.

[65] P. Kubade and R. Kshirsagar, "Current Research Trends in Modification / Interaction of Halloysite Nanotube Filled Polymer Blends and Its Composites : A Review," vol. 4, no. 12, pp. 1766–1772, 2015.

[66] R. Ramamoorthi and P. S. Sampath, "Experimental Investigations of Influence of Halloysite Nanotube on Mechanical and Chemical Resistance Properties of Glass Fiber Reinforced Epoxy Nano Composites," vol. 74, no. December, pp. 685–689, 2015.

[67] P. Pasbakhsh, H. Ismail, M. N. A. Fauzi, and A. A. Bakar, "EPDM/modified halloysite nanocomposites," *Appl. Clay Sci.*, vol. 48, no. 3, pp. 405–413, 2010.

[68] M. Du, B. Guo, and D. Jia, "Newly emerging applications of halloysite nanotubes: A review," *Polym. Int.*, vol. 59, no. 5, pp. 574–582, 2010.

[69] Z. Jia, Y. Luo, B. Guo, B. Yang, M. Du, and D. Jia, "Reinforcing and Flame-Retardant Effects of Halloysite Nanotubes on LLDPE," *Polym. Plast. Technol. Eng.*, vol. 48, no. 6, pp. 607–613, 2009.

[70] X. XIE, Y. MAI, and X. ZHOU, "Dispersion and alignment of carbon nanotubes in polymer matrix: A review," *Mater. Sci. Eng. R Reports*, vol. 49, no. 4, pp. 89–112, May 2005.

[71] S. Bose and P. A. Mahanwar, "Influence of particle size and particle size distribution on MICA filled nylon 6 composite," *J. Mater. Sci.*, vol. 40, no. 24, pp. 6423–6428, Dec. 2005.

[72] S. Deng, J. Zhang, L. Ye, and J. Wu, "Toughening epoxies with halloysite nanotubes," *Polymer (Guildf).*, vol. 49, no. 23, pp. 5119–5127, Oct. 2008.

[73] K. Prashantha, H. Schmitt, M. F. Lacrampe, and P. Krawczak, "Mechanical behaviour and essential work of fracture of halloysite nanotubes filled polyamide 6 nanocomposites," *Compos. Sci. Technol.*, vol. 71, no. 16, pp. 1859–1866, 2011.

[74] V. A, Ulrich A. Handge, Katrin Hedicke, "Composites of polyamide 6 and silicate nanotubes of the mineral halloysite: Influence of molecular weight on thermal, mechanical and rheological properties," *Polymer (Guildf).*, vol. 51, no. 12, pp. 2690–

2699, 2010.

[75] L. Jiang, C. Zhang, M. Liu, Z. Yang, W. W. Tjiu, and T. Liu, “Simultaneous reinforcement and toughening of polyurethane composites with carbon nanotube/halloysite nanotube hybrids,” *Compos. Sci. Technol.*, vol. 91, pp. 98–103, 2014.

[76] H. Schmitt, K. Prashantha, J. Soulestin, M. F. Lacrampe, and P. Krawczak, “Preparation and properties of novel melt-blended halloysite nanotubes/wheat starch nanocomposites,” *Carbohydr. Polym.*, vol. 89, no. 3, pp. 920–927, 2012.

[77] B. Guo, Q. Zou, Y. Lei, M. Du, M. Liu, and D. Jia, “Crystallization behavior of polyamide 6/halloysite nanotubes nanocomposites,” *Thermochim. Acta*, vol. 484, no. 1–2, pp. 48–56, 2009.

[78] S. Zhang, “Green tribology: Fundamentals and future development,” *Friction*, vol. 1, no. 2, pp. 186–194, Jun. 2013.

[79] J. K. Sutter *et al.*, “Erosion Coatings for Polymer Matrix Composites in Propulsion Applications,” *High Perform. Polym.*, vol. 15, no. 4, pp. 421–440, Dec. 2003.

[80] N. Dalili, A. Edrisy, R. Carriveau, N. Dalili, A. Edrisy, and R. Carriveau, *Renewable & sustainable energy reviews.*, vol. 13, no. 2. Elsevier Science, 1997.

[81] W. B. Goldsworthy, D. Dawson, W. B. Goldsworthy, and D. Dawson, “Composites, Fabrication,” in *Encyclopedia of Polymer Science and Technology*, Hoboken, NJ, USA: John Wiley & Sons, Inc., 2001.

[82] G. W. (Gwidon W. . Stachowiak and A. W. (Andrew W. . Batchelor, *Engineering tribology*. 2006.

[83] D. R. Andrews, “An analysis of solid particle erosion mechanisms,” *J. Phys. D. Appl. Phys.*, vol. 14, no. 11, pp. 1979–1991, Nov. 1981.

[84] A. Suresh, A. P. Harsha, and M. K. Ghosh, “Solid particle erosion of unidirectional fibre reinforced thermoplastic composites,” *Wear*, vol. 267, no. 9–10, pp. 1516–1524, Sep. 2009.

[85] J. Zahavi and G. F. Schmitt, “Solid particle erosion of reinforced composite materials,”

Wear, vol. 71, no. 2, pp. 179–190, Sep. 1981.

[86] P. J. Mathias, W. Wu, K. C. Goretta, J. L. Routbort, D. P. Groppi, and K. R. Karasek, "Solid particle erosion of a graphite-fiber-reinforced bismaleimide polymer composite," *Wear*, vol. 135, no. 1, pp. 161–169, Dec. 1989.

[87] A. Brandstädter, K. C. Goretta, J. L. Routbort, D. P. Groppi, and K. R. Karasek, "Solid-particle erosion of bismaleimide polymers," *Wear*, vol. 147, no. 1, pp. 155–164, Jul. 1991.

[88] N.-M. Barkoula and J. Karger-Kocsis, "Solid Particle Erosion of Unidirectional GF Reinforced EP Composites with Different Fiber/Matrix Adhesion," *J. Reinf. Plast. Compos.*, vol. 21, no. 15, pp. 1377–1388, Oct. 2002.

[89] U. . Tewari, A. . Harsha, A. . Häger, and K. Friedrich, "Solid particle erosion of carbon fibre– and glass fibre–epoxy composites," *Compos. Sci. Technol.*, vol. 63, no. 3–4, pp. 549–557, Feb. 2003.

[90] A. Rout, A. Satapathy, S. Mantry, A. Sahoo, and T. Mohanty, "Erosion Wear Performance Analysis of Polyester-GF-Granite Hybrid Composites using the Taguchi Method," *Procedia Eng.*, vol. 38, pp. 1863–1882, 2012.

[91] G. Drensky, A. Hamed, W. Tabakoff, and J. Abot, "Experimental investigation of polymer matrix reinforced composite erosion characteristics," *Wear*, vol. 270, no. 3–4, pp. 146–151, Jan. 2011.

[92] L. BAO, D. QIAN, G. WANG, and K. KEMMOCHI, "Solid Particle Erosion Characteristics of Composites Filled with Nano Carbon Fibers," *J. Text. Eng.*, vol. 58, no. 2, pp. 13–19, Apr. 2012.

[93] M. P. Journal, K. V. Subbaiah, and K. D. Devi, "Optimization Studies on Mechanical Properties of Montmorillonite (Mmt) Clay Filled Epoxy / Polyester," vol. 8, no. 2, pp. 34–40, 2013.

[94] I. Ghasemi, M. Karrabi, M. Mohammadi, and H. Azizi, "Evaluating the effect of processing conditions and organoclay content on the properties of styrene-butadiene rubber/organoclay nanocomposites by response surface methodology," *Express Polym. Lett.*, vol. 4, no. 2, pp. 62–70, 2010.

[95] S. E. Yalc and C. Ayla, “Preparation of polystyrene / montmorillonite nanocomposites : optimization by response surface methodology (RSM),” vol. 34, pp. 581–592, 2010.

[96] N. Mohan, S. Natarajan, and S. P. Kumareshbabu, “Investigation on Two-Body Abrasive Wear Behavior of Silicon Carbide Filled Glass Fabric-Epoxy Composites,” *Wear*, vol. 9, no. 3, pp. 231–246, 2010.

[97] T. Rajmohan, K. Palanikumar, J. Davim, and A. A. Premnath, “Modeling and optimization in tribological parameters of polyether ether ketone matrix composites using D-optimal design,” *J. Thermoplast. Compos. Mater.*, p. 0892705713518790-, 2014.

[98] O. S. Raghavendra G, Samantarai SP, Acharya SK, “Modeling of Abrasive Wear Behaviour of Natural Fiber (Rice Husk Ceramic) Epoxy Composite Using Response Surface Methodology.,” *Casp. J. Appl. Sci. Res.*, vol. 1, no. 13, pp. 182–189, 2012.

[99] GFL, “PROCESSING GUIDE - Fine cut Granular PTFE,” pp. 1–8.

[100] M. Liu, Z. Jia, F. Liu, D. Jia, and B. Guo, “Tailoring the wettability of polypropylene surfaces with halloysite nanotubes,” *J. Colloid Interface Sci.*, vol. 350, no. 1, pp. 186–193, 2010.

[101] L. D. K. & G. N. M. Dibyendu S Bag, Bhanu Nandan, Sarfaraz Alam, “density measurement.pdf,” *Indian Journal of Chemical Technology*, pp. 561–563, 2003.

[102] T. H. H. Lee, F. Y. C. Y. C. Boey, and K. A. A. Khor, “X-Ray Diffraction Analysis Technique for Determining the Polymer Crystallinity in a Polyphenylene Sulfide Composite,” *Polym. Compos.*, vol. 16, no. 6, pp. 461–488, 1995.

[103] D. B. GW Becker, Ludwig Bottenbruch, Rudolf Binsack, *Engineering Thermoplastics. Polyamides.* 1998.

[104] H. Chan, “Standard Operating Procedure Differential Scanning Calorimeter (DSC) in POWER Laboratory Model TA Q-20.” 2014.

[105] P. Rae and E. Brown, “The properties of poly (tetrafluoroethylene)(PTFE) in tension,” *Polymer (Guildf).*, vol. 46, no. February, pp. 8128–8140, 2005.

[106] Hevin P. Menard, “Dynamic Mechanical Analysis A practical introduction,” *Tissue*

Eng., 2008.

[107] T. M. Nair, M. G. Kumaran, G. Unnikrishnan, and V. B. Pillai, "Dynamic mechanical analysis of ethylene-propylene-diene monomer rubber and styrene-butadiene rubber blends," *J. Appl. Polym. Sci.*, vol. 112, no. 1, pp. 72–81, Apr. 2009.

[108] J. D. Ferry, *Viscoelastic properties of polymers*. 1980.

[109] E. Manias, G. Polizos, H. Nakajima, and M. J. Heidecker, "Chapter 2 Fundamentals of Polymer," pp. 1–38, 2006.

[110] N. Ning, Q. Yin, F. Luo, Q. Zhang, R. Du, and Q. Fu, "Crystallization behavior and mechanical properties of polypropylene/halloysite composites," *Polymer (Guildf).*, vol. 48, no. 25, pp. 7374–7384, 2007.

[111] Y. Yan, Z. Jia, and Y. Yang, "Preparation and mechanical properties of PTFE/nano-EG composites reinforced with nanoparticles," *Procedia Environ. Sci.*, vol. 10, no. PART B, pp. 929–935, 2011.

[112] S. Bazhenov, "Mechanical Behavior of Filled Thermoplastic Polymers," *Met. Ceram. Polym. Compos. Var. Uses*, pp. 171–194, 2011.

[113] G. I. Lawal, S. A. Balogun, and E. I. Akpan, "Review of Green Polymer Nanocomposites," vol. 11, no. 4, pp. 385–416, 2012.

[114] Y. X. Gan, "Effect of Interface Structure on Mechanical Properties of Advanced Composite Materials," pp. 5115–5134, 2009.

[115] M. Liu, Z. Jia, D. Jia, and C. Zhou, "Recent advance in research on halloysite nanotubes-polymer nanocomposite," *Prog. Polym. Sci.*, vol. 39, no. 8, pp. 1498–1525, 2014.

[116] M. Naffakh and A. Díez-Pascual, "Thermoplastic Polymer Nanocomposites Based on Inorganic Fullerene-like Nanoparticles and Inorganic Nanotubes," *Inorganics*, vol. 2, no. 2, pp. 291–312, 2014.

[117] Y. Sahin, "Analysis of abrasive wear behavior of PTFE composite using Taguchi's technique," *Cogent Eng.*, vol. l, pp. 1–15, 2015.

[118] M. S. Cheema, A. Dvivedi, and A. K. Sharma, "A hybrid approach to multi-criteria optimization based on user's preference rating," *Proc. Inst. Mech. Eng. Part B J. Eng.*

Manuf., vol. 227, no. 11, pp. 1733–1742, 2013.

[119] P. J. Blau, *Friction Science and Technology*. CRC Press, 2009.

[120] M. Conte and A. Igartua, "Study of PTFE composites tribological behavior," *Wear*, vol. 296, no. 1–2, pp. 568–574, 2012.

[121] R. H. Myers, D. C. Montgomery, and C. Anderson-Cook, "Response Surface Methodology: Process and Product Optimization Using Designed Experiments ," *Wiley Ser. Probab. Stat.*, no. June 2015, p. 704, 2009.

[122] N. Draper and J. John, "Response-surface designs for quantitative and qualitative variables," *Technometrics*, vol. 30, no. 4. pp. 423–428, 1988.

[123] R. S. Design, "Multifactor RSM Tutorial," no. Ccd, pp. 1–56, 2005.

[124] R. Zenasni, a. Hebbar, and J. V. Olay, "Modeling the tribological abrasive wear behavior of woven composite materials using the planning design experimentation approach," *J. Thermoplast. Compos. Mater.*, pp. 93–105, 2012.

[125] G. Derringer, "Simultaneous optimization of several response variables," *J. Qual. Technol.*, 1980.

[126] J. Ye, D. Burris, and T. Xie, "A Review of Transfer Films and Their Role in Ultra-Low-Wear Sliding of Polymers," *Lubricants*, vol. 4, no. 1, p. 4, 2016.

[127] P. S. Centre *et al.*, "POLYMER SCIENCE Thermal Transitions in Polymers," vol. c, 2006.

[128] C. P. Koshy, P. K. Rajendrakumar, and M. V. Thottackkad, "Evaluation of the tribological and thermo-physical properties of coconut oil added with MoS2 nanoparticles at elevated temperatures," *Wear*, vol. 330–331, no. June, pp. 288–308, 2015.

[129] H. Li, Z. Yin, D. Jiang, L. Jin, and Y. Cui, "A study of the tribological behavior of transfer fi lms of PTFE composites formed under different loads , speeds and morphologies of the counterface," vol. 329, pp. 17–27, 2015.

[130] S. Mantry, A. Satapathy, A. K. Jha, S. K. Singh, and A. Patnaik, "Preparation, characterization and erosion response of jute-epoxy composites reinforced with SiC

derived from rice husk," *Int. J. Plast. Technol.*, vol. 15, no. 1, pp. 69–76, 2011.

[131] Jeffery S. Smith, S.V. Swaminathan, and M. D. Gandy, "High-temperature erosion testing standard and round robin testing," *Sixth Int. Conf. Adv. Mater. Technol. Foss. Power Plants; St. Fe, NM. August 31st – Sept. 3rd, 2010*, pp. 0–17, 2010.

[132] S. Walley and J. Field, "The erosion and deformation of polyethylene by solid-particle impact," *Philos. Trans.*, 1987.